WAD
(Return)

NATIONAL ACADEMIES OF SCIENCES AND ENGINEERING

NATIONAL RESEARCH COUNCIL

of the

UNITED STATES OF AMERICA

UNITED STATES NATIONAL COMMITTEE

International Union of Radio Science

National Radio Science Meeting

9 – 12 January 2002

Sponsored by USNC/URSI

University of Colorado at Boulder
Boulder, Colorado
USA

United States National Committee
International Union of Radio Science

ABSTRACTS

National Radio Science Meeting
9-12 January 2002
University of Colorado, Boulder

Sponsored by USNC/URSI

Table of Contents

Membership

United States National Committee
INTERNATIONAL UNION OF RADIO SCIENCE

Chair:	Gary S. Brown*
Secretary & Chair-Elect:	Umran S. Inan*
Immediate Past Chair:	Susan K. Avery*

Members Representing Societies, Groups, and Institutes:

American Astronomical Society:	Thomas G. Phillips
American Geophysical Union:	Donald T. Farley
American Meteorological Society:	Vacant
IEEE Antennas and Propagation Society:	Linda P.B. Katehi
IEEE Geosciences and Remote Sensing Society:	Roger Lang
IEEE Microwave Theory and Techniques Society:	Arthur A. Oliner

Members-at-Large	Amalia Barrios
	J. Richard Fisher
	Anthony C. Frasier-Smith
	Michael S. Shur
	Yahya Rahmit-Samii
	Richard Ziolkowski

Chairs of the USNC-URSI Commissions:

Commission A	Samir El-Ghazaly
Commission B	Piergiorgio L. E. Uslenghi
Commission C	Alfred O. Hero
Commission D	Alan Mickelson
Commission E	Jon Schoenberg
Commission F	Edgeworth R. Westwater
Commission G	John C. Foster
Commission H	Min-Chang Lee
Commission J	Peter Napier
Commission K	Frank S. Barnes

Officers, Chairs and Vice Chairs of Commissions of URSI residing in the United States

Past President	Thomas B. A. Senior
Chair, Commission E	Robert L. Gardner
Chair, Commission J	Jackie N. Hewitt
Vice Chair, Commission A	Quirino Balzano
Vice Chair, Commission H	Umran S. Inan

*Member of USNC/URSI Executive Committee

Description of the International Union of Radio Science

The International Union of Radio Science is one of the world scientific unions organized under the International Council of Scientific Unions (ICSU). It is commonly designated as URSI from its French name, Union Radio Scientifique Internationale). Its aims are (1) to promote the scientific study of radio communications, (2) to aid and organize radio research requiring cooperation on an international scale and to encourage the discussion and publication of the results, (3) to facilitate agreement upon common methods of measurement and the standardization of measuring instruments, and (4) to stimulate and to coordinate studies of the scientific aspects of telecommunications using electromagnetic waves, guided and unguided. The International Union itself is an organizational framework to aid in promoting these objectives. The actual technical work is largely done by the National Committee in the various countries.

The new officers of the International Union are:

President:	Hiroshi Matsumoto (Japan)
Past President:	Thomas B.A. Senior (USA)
Vice Presidents:	Kristian Schlegel (Germany)
	Joseph Shapira (Israel)
	Andrzej W. Wernik (Poland)
	Paul H. Wittke (Canada)
Secretary-General:	Paul Lagasse (Belgium)
Assistant Secretary-General:	Peter Van Daele
Administrative Assistant:	Inge Heleu

The Secretary-General's office and the headquarters of the organization are located at Avenue Albert Lancaster, 32, B-1180 Brussels, Belgium. The Union is supported by contributions (dues) from 38 member countries. Additional funds for symposia and other scientific activities of the Union are provided by ICSU from contributions received for this purpose from UNESCO.

The International Union, as of the XXVth General Assembly held in Toronto, Canada, August 13-21, 1999, has ten bodies called Commissions for centralizing studies in principal fields.

Every three years the International Union holds a meeting called the General Assembly. The next is the XXVIth, to be held in August 2002, in Maastricht, the Netherlands. The Secretariat prepares and distributes the Proceedings of the General Assemblies. The International Union arranges international symposia on specific subjects pertaining to the work of one or several Commissions and also cooperates with other Unions in international symposia on subjects of joint interest.

Radio is unique among the fields of scientific work in having a specific adaptability to large-scale international research programs, since many of the phenomena that must be studied are worldwide in extent and yet are in a measure subject to control by experimenters. Exploration of space and the extension of scientific observations to the space environment are dependent on radio for their research. One branch, radio astronomy, involves cosmic phenomena, URSI thus has a distinct field of usefulness in furnishing a meeting ground for the numerous workers in the manifold aspects of radio research; its meetings and committee activities furnish valuable means of promoting research through exchange of ideas.

Steering Committee:

R. Frehlich, Cooperative Institute for Research in Environmental Sciences, Univ. of Colorado
K. Grosland, Office of Conference Services, Univ. of Colorado
J. McKie, Cooperative Institute for Research in Environmental Sciences, Univ. of Colorado
S. Palo, Department of Aerospace Engineering, Univ. of Colorado
K. Zellers, Cooperative Institute for Research in Environmental Sciences, Univ. of Colorado

Technical Program Committee:

G.S. Brown, Chair
U. Inan, Secretary
A. Gasiewski, Student Paper Competition

(A) W. Davis
(B) P. Uslenghi
(C) A. Hero
(D) A. Mickelson
(E) J. Schoenberg
(E) J. Murray
(F) E. Westwater
(G) J. Foster
(H) M.-C. Lee
(J) P. Napier
(K) F. Barnes with S.K. Avery

Session, 9:00-Thurs.

PLENARY

Chairpersons: G. Brown and A. Gasiewski

SETI: PULLING SIGNALS OUT OF COSMIC NOISE

J. Tarter
SETI Institute
2035 Landings Drive
Mountain View, CA 94043

A recent series of workshops has laid out a roadmap for SETI research for the next few decades. Three different approaches were identified. 1) Continue the radio search; build an affordable array from consumer market components, expand the search in frequency, and increase the target list to 100,000 stars. This array will also serve as a technology demonstration and perhaps enable the international radio astronomy community to realize an array that is a hundred times larger and capable (among other things) of searching a million stars. 2) Begin searches for very fast optical and infrared pulses from a million stars. 3) As Moores Law delivers increased computational capacity, build an omni-directional sky survey array capable of detecting strong, transient, radio signals from billions of stars.

SETI could succeed tomorrow, or it may be an endeavor for multiple generations. We are, after all, a very young technology in a very old galaxy. While our own leakage radiation continues to outshine the Sun at many frequencies, we remain detectable to others. When our use of the spectrum becomes more efficient, it will be time to consider deliberate transmissions and the really tough questions: Who will speak for Earth? What will they say? Maybe by then we will be old and wise enough to find some answers.

THE NATIONAL SCIENCE FOUNDATION AND TETHER-FREE WORLD AND WIRELESS TECHNOLOGY

J.W. Mink and J.Cousins
National Science Foundation
Arlington, VA 22230

This presentation will first overview The National Science Foundation (NSF), its Foundation wide programs and initiatives. However, the primary focus will be upon engineering and communications technology. The discussion will place emphasis upon planned programs by the Directorate for Engineering and the Directorate for Computer and Information Science Engineering of the National Science Foundation addressing the Tether-Free World and Wireless Technology. Wireless technology breaks the physical tethers that support our current communications infrastructure. As one envisions a tether free world of the future: one sees the monitoring and control of processes being done from anywhere, seamless information transmission and reception from anywhere to anywhere, work and personal tasks being done anywhere, materials, structures, vehicles, and even humans, signaling when they need attention. It is expected that this research program will result in non-traditional approaches, and applications that will leap-frog current wireless technology to a much broader concept of the tether-free environment. One envisions future generations of wireless technology will shift to broadband techniques along with a shift from current voice dominated wireless systems to information dominated wireless systems.

Session A1, 8:55-Fri.

TRANSIENT AND FREQUENCY-DOMAIN MODELING

Chairperson: W. Davis

IMPULSE RADAR

Sairam k.v.s.s.s.s.s.*
professor, ECE Department, Dr.M.G.R. Engg.College,
Chennai - 602 102, Tamilnadu state.

RADAR has wide applications in the field of communication, signal processing, image extraction etc. In this paper we have delved about JOINT TIME FREQUENCY (JTF) ANALYSIS for Digital Radar Imaging. The radar usually transmits a sequence of pulses or other signal waveforms with Pulse Repetition Frequency (PRF) required for maximum range of detection.

The target information may be examined from the radar-range or from its frequency spectrum by applying the Fourier transform. The Fourier transform is based on the assumption that the frequency contents of analyzed signals are time-invariant. In reality for a moving target, the Doppler frequency shifts are time varying which causes image-blurring problems. But the JTF representation of a signal is a 2-D feature space that facilitates the interpretation of complex electromagnetic phenomenology. The paper shows that, the displaying of discrete-time events using JTF leads to more insight into scattering mechanisms than the information available from either time or frequency domain representation. The paper also gives a special emphasis on JTF-ISAR (Inverse Synthetic Aperture Radar) processing applied to cross range (or Doppler frequency). In this standard Range Tracking and Doppler Tracking are done and then, time frequency transform is applied to range profiles, which results in Range Doppler Time-Frequency cube.

The paper shows that, by replacing the Fourier Transform with a high resolution JTF Transform, the image blurring caused by the time varying Doppler frequency shift can be mitigated easily.

Apart from the above discussion, the data collected at the Advancement RCS measurement Range at WRIGHT-PATTERNSON AFB in co-operation with MRC (Mission Research Corporation) has also been submitted to illustrate ISAR processing. This study has shown that JTF representation is highly effective for radar imaging. These images will be displayed during our presentation. We have also made an EXPERT SYSTEM ALGORITHM to classify between Fourier Transform and Time-Frequency Transform. This simulation will be executed at the time of our presentation.

SYMMETRY IN SINGLE-POLARIZATION REFLECTOR IMPULSE-RADIATING ANTENNAS

Carl E. Baum
AFRL/DEHE
3550 Aberdeen Ave SE
Kirtland AFB, NM 87117-5776

Impulse-radiating antennas (IRA) have many applications and a large literature has developed. There are various construction details for reflector impulse-radiating antennas (IRAs) which limit the achievement of the ideal performance characteristics. For some applications (e.g., polarimetry) a controlled frequency-independent polarization is important. An important technique for polarization control is symmetry in the antenna geometry. Here our attention is directed to polarization on the beam center which can be a symmetry axis for the antenna.

The present paper can be considered an extension of previous papers where various features (including symmetry) of the TEM feed of a reflector IRA are considered. Symmetry planes are important for polarization purity in the direction of the main beam. This involves details of the feed cables, possible inclusion of a ground plane perpendicular to the ideal electric field, and location of perturbations in low-field regions. Besides the general overall geometry of the IRA, now smaller pieces are considered for their effects on the symmetry. These include especially the signal cables including their locations relative to the other conductors. Inevitably some small asymmetries will be present, but the effects of these can be minimized by judicious positioning of the signal cables, and by the positioning of conductors at locations which minimize interaction with undesirable field components.

Note that here we are not considering high-voltage operation with, say, a spark gap at the focal point. Rather we are considering a low-voltage type with two 100 Ω feed cables from a single 50 Ω cable as discussed in previous papers. (See, e.g., Sensor and Simulation Note 327.) In this paper we refer to 50 Ω and 100 Ω coaxes. While these are convenient choices they can, in principle, take on other values. For present purposes, these numbers are labels.

Another symmetry considered is that of duality (in the Maxwell equations) as applied to the low-frequency electric- and magnetic-dipole moments so as to better achieve the desirable balance between these two. This concerns the balancing of the low-frequency electric and magnetic dipoles by including special structures connected to the feed arms.

SOME SIMPLE FORMULAE FOR TRANSIENT SCATTERING

Carl E. Baum
AFRL/DEHE
3550 Aberdeen Ave SE
Kirtland AFB, NM 87117-5776

In transient scattering measurements one needs an adequate received signal to successfully detect and perhaps identify the scatterer. This depends on the properties of the scattering dyadic and the transmit and receive antennas. For the case of backscattering received signals are estimated with choice of some kind of impulse radiating antenna with a large band ratio. Over the years much calculations and measurements of electromagnetic scattering have been performed. While these are performed primarily in the frequency domain, they can be applied in time domain as well by inverse Laplace/Fourier transformation provided phase is retained (which is not the case for radar cross sections). For transient remote sensing, one has some transmitting and receiving antennas which send out a pulse and receive the pulse scattered by some object of interest. Such antennas also need to be characterized and optimized for their transient performance. Various types of impulse radiating antennas (IRAs) are suitable for this purpose. One needs to know what are the characteristics and amplitudes of the received voltage as a function of the transmitter voltage waveform and amplitude and the scattering dyadic operator for the object of interest. In the present paper, some simple canonical scatterers are considered for this purpose: disk (normal incidence), curved surface, circular cone on axis, and thin wire at broadside. In addition to the antennas and scatterer, one may need to consider the properties of the intervening media. A common example concerns the interface between air and soil for the case of buried targets.

Hopefully this compilation of simple scattering formulae and combination of these with antenna characteristics will prove useful in estimating signal strengths for detection of various scatterers both in the air and buried. One could add various other canonical scatterers, but this should help one bound the problem. The antennas are of the IRA variety with their wideband ratio, and for which the formulae in time domain simplify somewhat. Alternately one can deconvolve the response of other types of antennas (if they have sufficient bandwidth) to obtain similar results.

FREQUENCY-DOMAIN MODELS FOR NONLINEAR CIRCUITS BASED ON LARGE-SIGNAL MEASUREMENTS

Jargon, J.A., Remley K.A., DeGroot, D.C., NIST
Schreurs, D., K. U. Leuven
Gupta, K.C., University of Colorado at Boulder
Email: jargon@boulder.nist.gov

In this presentation, we describe a method of generating models for nonlinear devices and circuits, based upon measurements of travelling-wave voltages at a periodic large-signal excitation and its harmonics using a nonlinear vector network analyzer (NVNA). Utilizing a second source, we use multiple measurements of a nonlinear device to train artificial neural network models that yield portable, nonlinear large-signal scattering parameters. We obtain an independent check by comparing an example diode-circuit model generated by means of this methodology to a compact, equivalent-circuit model simulated in commercial harmonic-balance software, and show that the two methods agree well.

An NVNA excites a nonlinear device under test with a signal comprised of one or more sine-wave signals and detects the amplitude and phase of a number of spectral components of both the complex incident and reflected travelling voltage waves. Assuming the device exhibits neither sub-harmonic nor chaotic behavior, the input and output signals will be combinations of sine-wave signals, due to the nonlinearity of the device in conjunction with impedance mismatches between the system and the device. If a single excitation frequency is present, new frequency components will appear at harmonics of the excitation frequency.

Like commonly used linear scattering parameters, nonlinear large-signal scattering parameters can also be defined as ratios of incident and reflected wave variables. However, unlike linear scattering parameters, which can be directly calculated from vector network analyzer measurements, nonlinear large-signal scattering parameters depend upon the signal magnitude and must take into account the harmonic content of the input and output signals since energy can be transferred to other frequencies in a nonlinear device. They cannot be directly determined from available instrumentation since impedance mismatches effects from the measured device response and harmonics from the source cannot be eliminated in these instruments.

We conclude by showing possible applications of nonlinear large-signal scattering parameters, such as determining the source impedance required for conjugate match (maximum power transfer) at the excitation frequency of a nonlinear device. They can also be used for selecting the optimum output load impedance at the fundamental frequency in a power amplifier or at specified harmonics for a frequency multiplier.

Session A2, 10:35-Fri.

BURIED OBJECTS AND DIELECTRIC MEASUREMENTS

Chairperson: W. Davis

SCATTERING FROM A BURIED CONDUCTING DISK

K.F. Casey
SRI International
Engineering and Systems Division, G-202
333 Ravenswood Avenue
Menlo Park, CA 94025

We consider the problem of electromagnetic scattering from a perfectly conducting disk that is situated in a lossy dielectric half-space (ground) and illuminated from the region above the half-space (air). The disk is oriented parallel to the interface. This problem geometry is representative of those encountered in the detection of buried metal mines using forward-looking ground penetrating radar. Its exact solution is useful as a check against solutions obtained by approximate analytical methods such as physical optics, or by numerical methods such as general-purpose body of revolution codes; and it is also of interest in its own right.

The electromagnetic field is decomposed into two sets of angular eigenfunction modes that are TE and TM with respect to the direction normal to the disk and the interface. Obtaining the solution for any modal field requires that one solve a mixed boundary-value problem that can be expressed in terms of a pair of dual integral equations with Hankel kernel. The problem of solving the dual integral equations and thereby obtaining the scattered field can be reduced to that of solving a single inhomogeneous Fredholm integral equation of the second kind (I. N. Sneddon, *Mixed Boundary Value Problems in Potential Theory*, North-Holland, Amsterdam 1966). The natural resonances of the buried disk for a given eigenfunction mode can be investigated by determining the solutions to the corresponding homogeneous integral equation.

We present numerical results for the backscattering cross-section of the buried disk as a function of frequency and compare these results with the physical-optics expressions of the same quantity. The low-frequency behavior of the solution, and its interpretation in terms of scattering from a buried polarizable object, is also discussed; and we present some results showing the behavior of the natural resonance frequencies as the ground conductivity and burial depth are varied. Finally, we indicate how the solution approach can be applied to a more general scatterer such as a resistive sheet or a thin void.

INDUCTION SCATTERING FROM METALLIC OBJECTS: VALIDITY ANALYSIS AND APPLICATIONS

Dr. Keli Sun
Thayer School of Engineering at Dartmouth
Hanover, NH 03755
Prof. Kevin O'Neill
Thayer School of Engineering at Dartmouth
Hanover NH 03755
Dr. Fridon Shubitidze
Thayer School of Engineering at Dartmouth
Hanover, NH 03755
Prof. Keith Paulsen
Thayer School of Engineering at Dartmouth
Hanover, NH 03755

The problem of numerical modeling of electromagnetic induction (EMI) scattering by metallic objects is complicated by the fact that transmitted ("primary") fields typically penetrate the target, but will often only do so slightly. Resolving this essential but small active layer near the target surface challenges established modeling methods. We approach the problem using the Thin Skin Depth Approximation (TSA), designed particularly for relatively high frequency cases where the skin depth is small relative to the scatterer dimensions. Computational experience suggests that the formulation based on TSA gives better results for higher relative permeability. When the relative permeability of the scatterer material is high enough (e.g. as for steel), the TSA results are accurate across the entire EMI frequency band, although TSA itself is not accurate at low frequency and its accuracy depends on relative permeability only through induction number. This counter-intuitive result is explained by theoretical analysis based on analytical solutions for scattering from spheres and cylinders. The analysis shows that, the accuracy of ultimate TSA solution depends not only on the accuracy of TSA approximation, but also its significance in the whole system of equations. As example applications of high frequency analysis, we consider cases involving multiple buried targets. Simulations produce scattered field data for a distribution of source location and observation points. Based on this data, one can determine a best fit to the directional scattering characteristics of the individual contributing objects, even though their scattered fields overlap spatially. In the least, one can evaluate the fit of alternative assumptions that there is a single object or multiple objects.

CLASSIFICATION OF SCATTERER'S MAJOR AXIS ASPECT RATIO USING BROADBAND EMI RESPONSES

F. Shubitidze, K.Sun, K. Paulsen
Thayer School of Engineering,
Dartmouth College,
Hanover, NH, 03755, USA
K. O'Neill
USA ERDC Cold Regions,
Research and Engineering Laboratory,
Hanover, NH, 03755, USA

Recently, electromagnetic induction sensors have been used for identification and classification of subsurface metallic objects, particularly unexploded ordinance (UXO). When EMI methods are applied for the detection and identification of UXO, one is confronted with the problem of discriminating between UXO and widespread pieces of metallic clutter. Ability to infer basic object shape is needed, over this very broad and very low frequency band (at least 30 Hz to 20 kHz). The EMI responses are typically characterized by in phase and quadrature components, which arise due to surface and volume current distributions respectively. Numerical and the experimental investigation shows that responses from metallic objects strongly depend on their principal axis sizes. Particularly for elongated magnetic targets, we see a dramatic upward shift in the frequency of the peak in the quadrature component when the object is rotated from axial to transverse orientation, relative to the primary field.

The specific motivation of this work is detailed investigation of characteristic electromagnetic field distributions inside metallic targets, to understand the underlying physics and apply it to target classification purposes. To analysis EM field distribution inside objects we have apply the method of auxiliary sources (MAS). Numerical study has shown that elongation of permeable cylinders with fixed diameter shifts the frequency peak of the quadrature component into a lower frequency range, under axial orientation of the primary magnetic field. Our studies also show that the frequency peak in the quadrature component does not change as elongation increases with fixed diameter under transverse excitation. Physical consideration of EM field structure inside magnetic targets in terms of resonating magnetic current elements suggests that the frequency location of the quadrature peak should be inversely related to the depth of the target along the axis facing the transmitter.

In this paper we will explore a detailed picture of EM distribution inside of canonical target shapes, and will demonstrate how low frequency EMI responses are related to the targets major axis dimensions. Finally, we show how these results could be used to infer aspect ratios of several targets, such as cylinders and spheroids, given multi-orientation scattering data.

PROGRESS TOWARD AN ELECTROMAGNETIC INDUCTION MINE DISCRIMINATION SYSTEM

Riggs L.S., Cash S.,Sulzberger G.,Bryant C.,Stucker L.
ECE Department 200 Broun Hall
Auburn Universtiy, Alabama 36849

This paper describes recent progress toward developing an electromagnetic induction (EMI) based real time mine discrimination system. Earlier versions of our hardware borrowed heavily from technology germane to the current U.S. Army's standard issue hand-held pulse-induction detector the AN/PSS-12. Now however, the fiberglass wand is the only component of the old AN/PSS-12 system that we still use in our new discrimination system.

We have gained new insights into EMI system performance through the development and analysis of a magnetically coupled circuit composed of transmitter, receiver, and buried object loops. We show that the frequency domain transfer function for receiver output current divided by transmitter input current is composed of a product of first order high-pass terms with distinct break frequencies. The break frequencies are specified by the resistance-inductance ratios of the transmitter and the object loops. In general it is desirable to have the break frequency of the receiver loop occur at a much lower frequency than that of the object loop so that the object's response can be measured with maximum fidelity. The circuit model also points to other trade-offs in coil design. For example, the strength of the response is proportional to the product of the mutual coupling between the transmitter and object and between the object and receiver coil (MTO MOR). Increasing the number or turns on the transmitter and receiver loops will of course increase MTO MOR but will also change the break frequency of the receiver loop and the bandwidth of the transmitter loop. These and other tradeoffs will be discussed in greater detail during the presentation.

In the not distant future we plan to collect data with our new discrimination system at the JUXOCO blind and calibration grids at Fort A. P. Hill, VA. The performance of our system will be presented in term of probability of detection versus probability of false alarm (receiver operating characteristics (ROC)). Real time operating issues with the "user in the loop" will also be addressed.

COMPLEX PERMITTIVITY MEASUREMENTS OF DIELECTRIC SUBSTRATES USING SPLIT-CYLINDER AND SPLIT-POST RESONATORS

M. D. Janezic, J. Baker-Jarvis
National Institute of Standards and Technology
Boulder, CO USA
E.F. Kuester
University of Colorado
Boulder, CO USA
J. Krupka
Warsaw University of Technology
Warsaw, Poland

When the permittivity and loss tangent of a dielectric material are measured, many traditional resonator measurement methods such as the cylindrical cavity or dielectric post resonator are available. Although usually limited to a single frequency, these resonant methods provide the high accuracy and sensitivity that broadband methods lack. Unfortunately, these techniques usually require machining the samples into a precise geometry such as a cylinder. Since such machining of the sample is destructive, time-consuming and relatively expensive, conventional resonator methods are rarely used for large-scale quality-control purposes.

We present the split-cylinder and split-post resonators as two methods that possess the accuracy of traditional resonator methods but require no sample machining. These methods require a planar sample of uniform thickness, making it ideal for the measurement of dielectric substrates. The nondestructive nature of these two methods comes at a cost, however, as the theoretical models are more complicated than those for conventional resonator methods.

We overview the split-cylinder and split-post resonator methods and describe their advantages and disadvantages. Using the mode-matching method, we present a theoretical model for both the split-cylinder and split-post resonators for determining the permittivity and loss tangent of low-loss dielectric materials. To verify the performance of both methods we compare measurements of several dielectric substrates using the split-cylinder and split-post resonator resonators at 10 GHz to measurements made in a cylindrical cavity resonator. In addition, using various split-post and split-cylinder resonators we present permittivity and loss tangent data for several dielectric materials over a frequency range of 2 to 20 GHz.

Session A/B/D1, 9:15-Wed.

ACTIVE INTEGRATED ANTENNAS FOR COMMERCIAL APPLICATIONS

Chairpersons: V. Nair and R.G. Rojas

RECONFIGURABLE GPS ANTENNAS

R.G. Rojas* , K.W. Lee , N. Surittikul
The Ohio State University
Dept. Electrical Engineering, ElectroScience Laboratory
Columbus, Ohio 43212-1191, USA

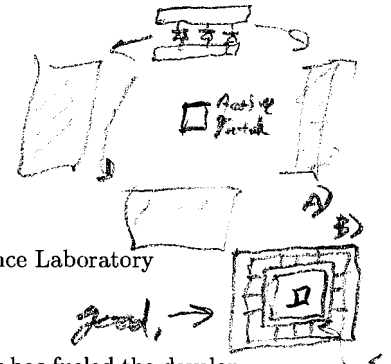

The rapid growth of a variety of wireless systems has fueled the development of new concepts for high performance antennas/arrays. A well designed antenna/array can help improve the overall system performance and relax system requirements. For example, at the receiving end of the Global Positioning System (GPS), the desired signals coming from GPS satellites can be interfered by unwanted signals from other sources. This presents a serious threat to the performance of a GPS receiver and requires an antenna/array system that can handle such a hostile environment.

Typical GPS receiving antennas have several requirements (N. Padros *et al., IEEE Trans. Antennas Propagat.*, **45**, 698-706, 1997). Dual band antennas are often required since GPS transmitters/receivers can operate at two frequency bands, namely, L1 (1.575 GHz) and L2 (1.227 GHz). Besides, right-hand circularly polarized (RHCP) antennas are necessary to avoid polarization loss, because GPS systems transmit RHCP signals. In addition, a hemispherical coverage in the upper-half space is needed to receive signals from the satellites. Printed antennas are often employed as receiving GPS antennas because their capabilities to meet the above needs. However, the potential interference from signals arriving along the horizon still remains. Therefore, there is a need for antenna elements that have the ability to modify their radiation patterns to mitigate the effects of these interfering signals without a significant decrease in coverage.

In this paper, reconfigurable printed antenna elements for GPS applications will be presented. A typical element consists of a circularly polarized rectangular microstrip patch antenna surrounded by parasitic metallic rings loaded with switches. The switches can be implemented with diodes, transistors or RF MEMs. The radiation patterns of these antenna elements can be modified in real time by controlling the operation states (on/off) of the switches. Principles of operation and some design procedures of the reconfigurable elements will be discussed. In addition, the antenna performance in the presence of unwanted signals will be presented.

Note that a 3-D finite difference time domain (FDTD) computer code developed at the Ohio State University is employed to calculate the antenna characteristics.

HIGH EFFICIENCY RF FRONT-ENDS AND RETRODIRECTIVE ARRAYS

Cynthia Y. Hang, Tatsuo Itoh
Electrical Engineering Dept.
University of California, Los Angeles

Active Integrated Antennas (AIA) has been a growing area of research interest. It has shown much promise in designing high performance, lower cost, and compact size modern communication systems. This paper reviews the recent research activities of AIA applications in designing high efficiency RF front-ends as well as retrodirective arrays.

In any wireless communication system, power amplifiers must be designed as efficient as possible to extend battery lifetime as well as to reduce the size of heat sink. One promising approach to design a highly efficient PA is by employing the AIA concept, where the antenna provides reactive terminations at the higher harmonics, in addition to its original role as a radiating element at the fundamental frequency. Improvements in PAE and output power using the AIA concept were first demonstrated through several single-ended PA designs. More recently, this concept has been extended into push-pull power amplifier designs, where the power of two anti-phase driven class-B power amplifiers are directly combined through a dual feed planar antenna to allow the antenna to serve as a power combiner and a harmonically tuned load, in addition to its original role as a radiating element, thus minimizing circuit size and insertion loss. In the most recent push-pull PA design, the amplifier is integrated with a modified Quasi-Yagi antenna, which is capable of reactively terminating the second harmonic. A peak PAE of 60.9% at the output power of 28.2 dBm has been achieved at 4.15 GHz.

Improving communication links between the transponder and base station is another key point in the design of model communication systems. Retrodirective arrays can be used to achieve that goal by effectively tracking the interrogator position. Unlike the "smart antenna" approach, retrodirective arrays do not rely on the sophisticated digital signal processing algorithms to reflect any incident signal back toward the source without prior knowledge of the source location. Instead, retrodirectivity can be realized through phase conjugation. One way to achieve phase conjugation is by heterodyne mixing using an LO that has twice the RF frequency. In this scheme, the lower sideband product has the same frequency as the RF, but the phase is conjugated. When combined with an antenna and placed in an array, the phase-conjugated signal from each antenna element will be radiated towards the source direction. More recently, an active retrodirective array circuit topology was demonstrated. The use of MESFETs in phase-conjugated circuitry can provide conversion gain in addition to the mixing operation. The experimental results of have shown excellent retrodirective performance, and can find uses in wide range of applications in wireless communication systems.

QUASI-OPTICAL ACTIVE ARRAYS FOR MILLIMETER-WAVE COMMUNICATIONS

W. A. Shiroma* and M. P. De Lisio
Hawaii Center for Advanced Communications
University of Hawaii at Manoa
2540 Dole Street, Holmes Hall 483
Honolulu, HI 96822

A serious obstacle in developing millimeter-wave circuits for wireless communications is the limited power-handling capability of semiconductor devices. One solution is to use a quasi-optical power combiner, in which the power from individual devices embedded in a radiating structure is combined in free space. While the output power is proportional to the number of elements, the driving-point impedance of the device is determined by the unit cell. This allows optimization for gain or low-noise performance through the unit cell while independently selecting the array size to meet power requirements.

Recent research in quasi-optical active arrays at the University of Hawaii has concentrated on developing key components for quasi-optical transmitter and receiver subsystems: amplifiers, linearizers, mixers, oscillators, and retrodirective arrays. Although the motivation for developing these arrays is for millimeter-wave applications, the prototypes were demonstrated at microwave frequencies.

A high-dynamic-range 100-element mixer grid achieved an input third-order intercept of 11 W and an associated conversion loss of 5.1 dB; this power is 100 times higher than that of a microstrip mixer using a single element, with comparable conversion loss. To compensate for the AM-AM and AM-PM distortion in amplifiers, a linearizer array having 2.5 dB of gain expansion and 25° of phase compensation was developed. Omnidirectional transistor grids functioning as an oscillator in transmission mode and a self-oscillating mixer in receive mode have been demonstrated at C-band for multipoint communications. Retrodirective arrays in various forms have also been developed: a 96-element self-oscillating mixer grid with retrodirectivity over 360°, and a planar array with a free-space local-oscillator feed.

ACTIVE AMPLIFIER ANTENNAS AND ARRAYS

Zoya Popovic
Department of Electrical and Computer Eng.
University of Colorado
Boulder, CO 80309, USA
Phone: (303) 492-0374, zoya@colorado.edu

An overview of recent work at the University of Colorado in active amplifier antenna arrays is presented. When an antenna element is integrated directly with an active circuit, we refer to it as an active integrated antenna (AIA). Such AIAs have been demonstrated with oscillators, amplifiers, multipliers, VCOs, switches, a good review is, e.g., (R.A. York, Z. Popovic, eds., *Active and Quasi-Optical Arrays for Solid-State Power Combining*, Wiley, 1997).

When designing an integrated circuit and antenna, the otherwise stadard 50-ohm environment is often not optimal (K.C. Gupta, P. Hall, eds., *Analysis and Design of Integrated Antenna Circuit Modules*, Wiley, 2001). For example, the optimal output load for high efficiency power amplifiers (PAs) is not 50 Ω and an integrated PA and antenna overall size can be reduced by a factor of 2 if the antenna is designed to be nonresonant with the optimal load impedance for the PA. When such antennas are integrated in arrays, efficient biasing and coupling between active elements become part of the design. For example, in a 6 by 6 MMIC amplifier array, the bias variation depends on the internal MMIC biasing circuit and if care is not taken in the bias design, there can be a 70% variation in gain over the entire array.

In this paper, the design method for the antenna element, amplifier circuit, array topology, bias distribution, and thermal stability is discussed on several example active antenna elements and arrays. The following specific examples are given: (1) X-band high-efficiency integrated antennas and switched-mode amplifiers with over 70% efficiency at 10GHz; (2) Ka-band watt-level power combining arrays; (3)full and half-duplex transmit-receive amplifier arrays at X, K and Ka bands; (4) multibeam Ka-band active arrays; and (5) energy-efficient optically-controlled X-band half-duplex array with fast (nanosecond) switching between transmit and receive. It is also shown how some of these arrays can perform front-end processing and relieve the load in smart (adaptive) arrays.

ACTIVE ANTENNA ARRAYS USING HETEROSTRUCTURE INTERBAND TUNNEL DIODES

K. Liu, S. M. El-Ghazaly
Telecommunication Research Center
Arizona State University
Tempe, AZ 85287-7206, USA

V. Nair, H. Goronkin
PSRL, Motorola Labs, Motorola Inc
7700 S. River Parkway, M/D ML34
Tempe, AZ 85284, USA

The Heterostructure Interband Tunnel Diode (HITD) is receiving increased research interests for it's enhanced functionalities and low supply voltage than other diodes. The device, when appropriately biased, exhibits negative resistance and has been used in VCO, mixer and active antenna circuits [Kai Liu, et al in URSI 2000, 2001]. In this talk, various issues related to active antennas, such as diode RF properties, instability, antenna characterization, array synchronization and beam steering, are addressed in order to find application of the tunnel diode in wireless communication through reliable and feasible design and simulation schemes.

In this research, RF characterizations of HITD diodes are achieved through extraction scheme embedded in wafer measurements. Antennas are fully characterized through the Spectral Domain Approach (SDA). Designs of active antennas are based on above data and are incorporated in HP ADS software for device circuit simulations, and FDTD for validation of active antenna designs. The simulation, design and circuit techniques developed in this research are applied to applications incorporating HITD's. Nevertheless, the techniques are also applicable to other negative resistance devices.

The DC stability issues, which are typical for negative resistance devices, have to be carefully addressed, not only in the DC measurement set up, but also in implementations of RF circuits. To overcome the instability, we use chip capacitors to force individual diode bias in active antenna arrays. Moreover, the injection-locking scheme is adopted for single- and array-antenna circuits. After injection locking, the active antennas exhibited very stable oscillation conditions, while having comparable and smooth phase noise, relative to Gunn-type active antennas.

Experimental results of single antennas at the L band and array antennas at the C band are presented and compared with simulations. High frequency applications above 10.0 GHz are feasible as demonstrated in the RF characterizations.

ADVANCES IN MONOLITHIC GRID AMPLIFIERS

DeLisio, M.P., Deckman, B.C., Rosenberg, J.J.
Wavestrean Wireless Technologies
100 N. Barranca St.; Suite 980
W. Covina, CA 91791
Cheung, C.-T., Rutledge, D.B.
California Institute of Technology
Mail Stop 136-93
Pasadena, CA 91125

High-power millimeter-wave transmitters can improve the quality of a wireless communications link by enabling smaller antenna sizes, higher bit rates, longer link distances, or greater immunity to rain fade. In order to realize solid-state components with higher power, spatial or quasi-optical techniques have been developed. Quasi-optical power combining provides greater output power or efficiency by coupling many active components to large-diameter guided beams or waveguide modes, rather than the planar transmission lines used in circuit combining structures. Since all of the elements are operating in parallel, the loss is roughly independent of the number of amplifiers. The output power will scale in direct proportion to the number of devices combined. Ohmic losses in these systems are minimal since the energy is distributed and combined in air via low-loss waveguides or Gaussian beams. Most of the losses in these systems are associated with coupling from the active devices to the propagating beam and/or coupling to a power collection port, both of which can be minimized through careful design.

A quasi-optical grid amplifier is a dense periodic array of closely spaced differential transistor pairs. The input and outputs are cross-polarized, and off-chip polarizers are used for tuning. The drawback of grids is that the small cell sizes limit the gain and power per cell to that available from a single differential pair. Because the active devices are very dense, however, the grid amplifier can be monolithically fabricated; this makes grids a very attractive technology for moderate gain and power applications that demand a single-chip mass-producible solution.

This talk will detail recent advances in monolithic millimeter-wave grid amplifier arrays. Results from a 5-W Ka-band amplifier will be presented. The designs of monolithic grids for operation from 60 to 94 GHz will also be discussed. In addition, the most recent modeling and packaging techniques will be reported. These recent advances make quasi-optical grid amplifiers a compelling candidate for low-cost millimeter-wave sources with Watt-level outputs. These sources could, in turn, enable an entirely new generation of radar and communications transmitters.

A COMPACT, MULTILAYER UHF PRE-AMPLIFIER

N. K. Higuchi*, P. Li, E. Quach, M. P. De Lisio, and W. A. Shiroma
Department of Electrical Engineering
University of Hawaii at Manoa
2540 Dole Street, Holmes 483
Honolulu, HI 96822

L. C. Howard and H. M. Aumann
MIT Lincoln Labs
244 Wood Street
Lexington, MA 02420

A 450-MHz pre-amplifier for a 96-element UHF linear array has been designed and fabricated. The unit integrates a single-pole double-throw (SPDT) switch, tapped-line interdigital filter, balanced low-noise amplifier, and gain stage in a compact, multilayer package. Design considerations include low noise figure, high third-order intercept (IP3), compact size, and low cost.

Two cascaded M/A-COM SW-279 SPDT switches are used to toggle between the input RF signal and a calibration signal. This cascade configuration results in 67 dB of isolation, 20 dB return loss, and 1 dB insertion loss. Implementing a filter at UHF typically results in a large circuit size. A fifth-order tapped-line interdigital filter was selected for its compact size compared with stepped-impedance and coupled-line topologies, and for its reproducibility compared with that of a lumped-element design. Implemented in stripline, the filter exhibits 0.8 dB of insertion loss in a 107-MHz 3-dB bandwidth. The low-noise amplifier uses two Agilent ATF-34143 pseudomorphic high-electron mobility transistors in a balanced configuration to provide good return loss, using Anaren Xinger 11303-3 hybrid couplers. The amplifier exhibits 20 dB of gain and 0.7 dB noise figure. This is followed by a Watkins-Johnson AH1 14.2-dB gain stage with an output IP3 of 36 dBm.

The switch and amplification stages are realized on one layer, and the stripline filter is realized on a second layer. Rogers *Duroid* 6006 ($\epsilon_r = 6$, thickness 1.27 mm) is used as the substrate for each layer. The entire package measures 10 cm $\times$ 3.175 cm $\times$ 0.305 cm. One-hundred-eight units were manufactured. The preamplifier has a 3-dB bandwidth of 100 MHz, 31 dB gain, 3 dB noise figure, and 30.6 dBm output third-order intercept.

Session B1, 8:55-Wed.

RANDOM MEDIA AND ROUGH SURFACES

Chairperson: V.I. Tatarskii and A.A. Maradudin

FRESNEL APPROXIMATION FOR THE WAVE SCATTERING IN RANDOM MEDIUM

V.I. Tatarskii
Zel Technologies
and NOAA/ETL
Boulder, CO 80305

We consider the single scattering of waves in a medium containing weak inhomogeneities of refractive index using Fresnel diffraction approximation. We do not introduce the scattering volume but consider the transmitting antenna with the Gaussian distribution of current and receiving antenna with Gaussian distribution of attenuation across the aperture. The results obtained are valid both in the near and far zones of antenna. The known contradiction between the applicability of Fraunhofer diffraction approach and the size of scattering volume formed by intersection of directivity diagrams is resolved. Similarly to the Fraunhofer zone approach, the scattering intensity obtained is proportional to the Bragg component of the inhomogeneities that are averaged in Fourier space with some specific weighting function depending on antenna size and pulse duration.

In the case considered in this paper, we deal with the scattering of Gaussian beam. The incident wave has different energy flux in different parts of the scattering volume, and receiving antenna summarizes scattered fields from different parts of scattering volume coherently. In such conditions we are unable to determine the scattering cross-section using common definition. To describe the relative scattering intensity, we use the ratio of the mean square of the electric field at the antennas horn to the integrated square of incident field across the beam. This ratio has the same dimension as scattering cross-section and substitutes the scattering cross-section.

In the far zone of antenna the result obtained is similar to the conventional result, expressed in terms of scattering cross-section. In the near zone, the scattering intensity does not depend on the distance from antenna to the scattering slab.

PSEUDO-NONDIFFRACTING BEAMS FROM ROUGH SURFACE SCATTERING

T. A. Leskova, A. A. Maradudin
Department of Physics and Astronomy
University of California
Irvine, CA 92697 USA

The nondiffracting beam introduced by Durnin is a solution of the free-space wave equation of the form $E(r, x_3) = \exp(i\beta x_3)J_0(\alpha r)$, in which $\alpha^2 + \beta^2 = k^2$, where k is the wave number, $J_0(x)$ is the zero-order Bessel function, and $r = (x_1^2 + x_2^2)^{\frac{1}{2}}$. This beam has an infinite extent in the transverse plane, and is incapable of propagating to infinity in the x_3-direction without spreading. Such an ideal nondiffracting beam contains an infinite amount of energy, and is impossible to realize in practice. Consequently, most recent studies of nondiffracting beams have focused on pseudo-nondiffracting beams. Such beams have a finite propagation range, have variations in transverse beam profiles, and intensity peaks in the direction of propagation. The propagation length, although finite, can extend to many tens of centimeters, long enough for many applications.

In this work we consider a system consisting of vacuum in the region $x_3 < -D$; a dielectric film characterized by a dielectric constant ϵ in the region $-D < x_3 < \zeta(x_1)$; and vacuum in the region $x_3 > \zeta(x_1)$. The surface profile function $\zeta(x_1)$ is assumed to be a single-valued function of x_1. This structure is illuminated at normal incidence from the vacuum region $x_3 < -D$ by an s-polarized plane electromagnetic wave of frequency ω, whose plane of incidence is the x_1x_3-plane. The amplitude of the transmitted field is calculated by the use of phase perturbation theory. On the basis of this result the surface profile function $\zeta(x_1)$ is designed in such a way that the resulting structure acts as an optical element that produces a transmitted field that is a two-dimensional pseudo-nondiffracting beam. Such a beam is characterized by a constant intensity along the direction of its propagation over a finite propagation length, and a beam-like shape in one of its transverse directions, in this case the x_1-direction. Numerical calculations show that this structure indeed produces a two-dimensional pseudo-nondiffracting beam.

RADAR IMAGE STUDIES OF A LAYERED MEDIUM WITH ROUGH INTERFACE

H. Kim*, J.T. Johnson
ElectroScience Laboratory
The Ohio State University
1320 Kinnear Rd, Columbus, OH 43212

Electromagnetic scattering problems from a layered medium with rough interfaces have gained wide interest in the area of remote sensing, particularly in the area of subsurface sensing. Several approximate solutions have been developed to assist in predicting scattering from a single rough interface. For a rough surface with subsurface boundaries, however, derivation of a general analytical solution is much more complicated. Though efficient numerical methods based on iterative technique can provide accurate predictions for scattering results, exact solution requires a huge computation when applied to a large scale surface or a high permittivity medium.

Recent studies have used the small perturbation method (SPM) for a layered medium with a slightly rough interface. However, the SPM solution predicts scattering results accurately only for surfaces with small height variations. Improved solution for very rough interface can be achieved by using the small slope approximation (SSA), avoiding this limitation as long as the surface slope is small. In this study a lowest order SSA solution for a layered medium is considered. A rather simpler form of the modified SSA formula is employed by assuming the boundary of sublayers are flat, but without restricting the number of layers. In addition, only a single bounce mechanism (transmission-reflection-transmission) between rough interface and sublayers is considered, along with a single scattering process from the rough interface.

Backscattering from a layered medium will be described by means of radar imaging based on back-projection tomography. High resolution radar images formed from frequency and angle swept backscatter data are investigated under various surface and wave parameters. Interpretations of scattering features observed from the images are provided in detail, and the effects of surface roughness, medium property, depth and size of the layer, polarization and incident angle will also be discussed.

RADAR BACKSCATTERING FROM GERSTNER'S WAVE

Fuks, I.M., ZelTech,LLC/ETL NOAA, Boulder, CO 80305, USA
Voronovich, A.G., ETL NOAA, Boulder, CO 80305, USA

Microwave band radio wave backscattering by non-linear surface waves is considered within framework of two-scale model (F.G. Bass and I.M. Fuks, itWave Scattering from Statistically Rough Surfaces, International Series in Natural Philosophy, bf93, edited by C.B.Vesecky and J.F.Vesecky, Oxford: Pergamon, 1979). Large scale (undulating) surface roughness is modeled by 2-D Gerstner's wave, which is an exact solution of hydrodynamics equations. The profile $z(x)$ of Gerstner's wave is given by trochoid's equation: $x = t/K - a\sin t$; $z = a\cos t$, where $K = 2\pi/\Lambda$, Λ is a wavelength and a is a surface wave amplitude. The shape of these waves is characterized by the more sharpen crests and extended troughs as compared to the corresponding sinusoidal wave. For small values of steepness parameter aK the wave shape is very close to sinusoid, and for $aK = 1$ it takes the cycloid's form.

The zero-order field is calculated in the geometrical optics approximation (with shadowing effects taken into account) and by exact numerical solution of the appropriate diffraction problem. The diffuse scattering by small-scale ripples is considered in the first-order (Bragg) approximation. Spatial distribution of the specific backscattering cross section over the Gerstner's profile is obtained for both polarizations of the incident wave. It is shown that the radar backscattering cross-section at horizontal polarization is modulated by the Gerstner's wave slopes more effectively than at the vertical one. Backscattering cross-section averaged over period Λ of large-scale wave at moderate and near grazing angles is also more sensitive to the surface slope aK in the case of horizontal polarization.

The Doppler frequency spectra of radar signal are not symmetrical and have the opposite skewness for HH and VV polarizations. The mean Doppler frequency shifts strongly depend on the incidence angle: for grazing angles they are approaching the limit determined by the value of orbital velocity of liquid particles plus phase velocity of small ripples and tend to zero at steep incidence. At moderate angles the mean Doppler shift for horizontal polarization exceeds essentially that one for vertical polarization, and the difference between them increases strongly with steepness parameter aK increasing. The exact account for diffraction effects reduces this difference as compared to the Kirchhoff approximation. The cause and qualitative explanation of this effect is discussed.

SCATTERING SIMULATIONS FROM AN ENSEMBLE OF NUMERICALLY GENERATED 10-CM SPILLING BREAKERS

J.V. Toporkov*, SFA, Inc., Largo, MD
R. Leighton, M.A. Sletten, Naval Research Lab, Washington DC

Recent numerical studies of scattering from the ocean-like surfaces (e.g. J. V. Toporkov and G. S. Brown, Numerical simulations of scattering from time-varying, randomly rough surfaces, *IEEE TGRS*, **38**, no. 4, 2000) found that the shapes of the Doppler spectra depend strongly on the model for ocean surface temporal evolution. However, at present there seems to be a general lack of practical hydrodynamic models that adequately describe surface dynamics on a short-wave scale. Also, the few available surface representations such as Creamer and Watson-West models do not capture wave-breaking events that have been shown to have a significant effect on the HH scattering.

The present investigation is a further step to incorporate more rigorous hydrodynamic models in the studies of sea-surface scattering. The one-dimensional surface profiles representing temporal evolution of a short-scale spilling breaker were generated through direct numerical solution of Navier-Stokes equation with full non-linear boundary condition (R. Leighton and G. B. Smith, Vorticity generation in a 10-cm spilling breaker, *Phys. of Fluids*, **13**, 2001). The growth of water wave leading to breaking is achieved by applying a propagating air pressure wave. For Monte Carlo studies, an ensemble of such breakers is obtained by perturbing the initial water surface. When generating time-evolving surface profiles, the hydrodynamic code also supplies a wealth of additional information such as kinetic and potential energy of the developing wave. Those parameters were found to be reliable and convenient indicators of various breaking stages, which facilitates analysis and interpretation of the scattering results.

Backscattering from this set of waves was calculated at three electromagnetic wavelengths: 3 cm, 1 cm, and 0.5 cm, for the grazing angles of 30 and 10 degrees. Both up-wave and down-wave radar looks were considered. Significant differences are observed in radar cross-sections and Doppler spectra for up-wave and down-wave geometries. A substantial enhancement in HH/VV return ratio occurs for the up-wave look around the time of the breaking event. Doppler spectra appear to be multi-modal, and time sub-domain analysis can be used to relate the different spectral bands to the stages of wave breaking. Comparisons to analytical models such as Small Perturbation Method and first-order Small Slope Approximation further help to clarify the dominant scattering mechanisms.

Computational costs will also be addressed, as the direct hydrodynamic solution method becomes a major time and resource-consuming factor in the simulations.

GENERALIZED FOURIER TRANSFORM FOR IRREGULAR STRATIFIED CHIRAL MEDIA

Crittenden*, P.E.,Dept of Mathematics and Center for Electro-Optics, Univ. of Nebraska-Lincoln, NE
Bahar, E., Dept. of Elect. Eng. and Center for Electro-Optics, Univ. of Nebraska-Lincoln, NE

An electromagnetic scattering problem involving two semi-infinite chiral materials with a rough interface at $y = h(x)$ is considered.

The Drude-Born-Fedorov constitutive relations for chiral materials are

$$\begin{aligned} D &= \epsilon(E + \beta \nabla \times E) \\ B &= \mu(H + \beta \nabla \times H). \end{aligned} \tag{1}$$

On substituting (1) into the time harmonic form ($e^{j\omega t}$) of Maxwell's Equations assuming a magnetic line source, $\mathcal{K} = K\delta(x - x')\delta(y - y')e_z$, (where e_z is the unit vector in the z-direction,) yields, after considerable manipulation, the following coupled scalar equations for the (transverse) z-components of the electric and magnetic fields:

$$\begin{aligned} \nabla^2 E_z + \frac{\gamma^4}{k^2}\left(1 + k^2\beta^2\right) E_z - 2j\omega\mu\beta\frac{\gamma^4}{k^2} H_z &= 2\beta\frac{\gamma^4}{k^2}\mathcal{K} \cdot e_z \\ \nabla^2 H_z + \frac{\gamma^4}{k^2}\left(1 + k^2\beta^2\right) H_z + 2j\omega\epsilon\beta\frac{\gamma^4}{k^2} E_z &= j\omega\epsilon\frac{\gamma^4}{k^4}\left(1 + k^2\beta^2\right)\mathcal{K} \cdot e_z \end{aligned} \tag{2}$$

where $k = \omega\sqrt{\epsilon\mu}$ and $\gamma = \frac{k^2}{1-k^2\beta^2}$. It should be noted that here k does not denote the characteristic values for the chiral media (wavenumbers).

The standard Fourier transform of both equations (2) is found with respect to x followed by the Laplace transform with respect to y above and below the interface. The resulting algebraic equations are solved for the Laplace-Fourier Transforms of H_z and E_z. The Laplace transforms are inverted and the exact boundary conditions for horizontally stratified media are applied to yield the Fourier transforms of H_z and E_z. The inverse Fourier transforms are found by deforming the path of integration in the complex plane to obtain a transform pair that can be applied to problems in which the interface and electromagnetic parameters vary along the (lateral) x-axis. The other components of the electromagnetic fields can be found using Maxwell's equations. The fields above and below the interface are expressed as left and right circularly polarized characteristic waves with wavenumbers $\gamma_1 = \frac{k}{1-k\beta}$ and $\gamma_2 = \frac{k}{1+k\beta}$. Terms corresponding to the direct, reflected, refracted, lateral, and surface waves are identified. The solution to a problem with an electric line source can be found by using the standard duality relationships in electromagnetic theory.

CONICAL PROPAGATION OF A SURFACE POLARITON ACROSS A GRATING

M.Kretschmann*, T. A. Leskova, A. A. Maradudin
Department of Physics and Astronomy
University of California
Irvine, CA 92697

In the only previous studies of the propagation of surface polaritons across a classical diffraction grating, when the plane of incidence is not perpendicular to the generators of the surface (D. L. Mills, Phys. Rev. B**15**, 3097 (1977); S. R. Seshadri, J. Appl. Phys. **58**, 1733 (1985)), the emphasis was on the dependence of the dispersion relation of these surface electromagnetic waves in the vicinity of the gap in the surface polariton dispersion curve on the angle the wave vector of the surface polariton wave vector $\mathbf{k}_{\|}$ makes with the generators of the surface. In the present paper by the use of the homogeneous form for the reduced Rayleigh equation for the electric field above and on a two-dimensional rough surface, we obtain the dispersion relation for a surface polariton propagating across a classical grating when the plane of incidence is not perpendicular to the generators of the surface. We refer to this as the conical propagation of surface polaritons across a grating by analogy with the conical scattering of light from a classical grating. This dispersion relation obtained is exact within the domain of validity of the Rayleigh hypothesis upon which it is based. It is solved numerically, and dispersion curves are obtained for several directions of propagation of the surface polariton, throughout the entire non-radiative region of the $(\omega, \mathbf{k}_{\|})$-plane. Particular attention is paid to the dependence on the direction of propagation of the position and width of the gap in the surface polariton dispersion curve that occurs at the boundary of the first Brillouin zone defined by the periodicity of the grating.

SURFACE PLASMON POLARITON PROPAGATION NEAR AN INDEX STEP

T. A. Leskova, A. A. Maradudin*
Department of Physics and Astronomy
University of California
Irvine, CA 92697
W. Zierau
Institute of Condensed Matter Theory
University of Muenster
Wilhelm Klemmstrasse 10
D48149 Muenster, Germany

In this work we study theoretically the scattering of p-polarized light of frequency ω from a system consisting of a dielectric medium (prism) characterized by a dielectric constant ϵ_0 in the region $x_3 > D$; a metal film characterized by a complex, frequency-dependent dielectric function $\epsilon_1(\omega)$ in the region $0 < x_3 < D$; a dielectric film characterized by a dielectric constant ϵ_2 in the region $\zeta(x_1) < x_3 < 0$; and vacuum ($\epsilon_3 = 1$) in the region $x_3 < \zeta(x_1)$. The light, whose plane of incidence is the x_1x_3-plane, is incident through the prism. For the surface profile function $\zeta(x_1)$ we take the form $\zeta(x_1) = -d\theta(x_1)$ or $\zeta(x_1) = -d\theta(x_1)\theta(L - x_1)$, where $\theta(x_1)$ is the Heaviside unit step function. Thus, we have a dielectric film of thickness d and dielectric constant ϵ_2 covering the half of the lower surface ($x_3 = 0$) of the metal film defined by $x_1 > 0$, or a dielectric film of thickness d and dielectric constant ϵ_2 covering the part of the lower surface ($x_3 = 0$) of the metal film defined by $0 < x_1 < L$. The reduced Rayleigh integral equation for the amplitude of the light scattered back into the prism, $R(q|k)$, is obtained, and solved numerically by converting it into a matrix equation. The result is used to calculate the intensity of the scattered field in the far-field region as a function of x_1 for a fixed value of x_3 for several values of the wavelength of the incident light. The results provide information about the scatteirng of the surface plasmon polariton at the metal-vacuum interface, excited by the incident light, by an index step on that interface.

THEORETICAL STUDY OF A MODEL SCATTER-PROBE OPTICAL MICROSCOPE

C. I. Valencia, E. R. Mendez
Division de Fisica Aplicada
Centro de investigacion Cientifica y de
Educacion Superior de Ensenada
Ensenada, Baja California 22800, Mexico
A. A. Maradudin, T. A. Leskova*
Department of Physics and Astronomy
University of California
Irvine, California 92697

We study theoretically the scattering of light from a model scatter-probe optical microscope consisting of a thin dielectric wire of square cross section, centered at the point (x_0, d) above a rough metal surface defined by $x_3 = \zeta(x_1)$. The dielectric constant of the wire is ϵ_0, and the dielectric function of the metal is $\epsilon(\omega)$. This structure is invariant along the x_2-axis. It is illuminated from the vacuum region $(x_3 > \zeta(x_1))$ by s-polarized light whose wavelength λ is much larger than the edge of the cross section of the wire. It is also assumed that $\zeta(x_1)_{max} < d < \lambda$. The presence of the wire within a wavelength of the surface creates a scattered field with an evanescent component that interacts with the rough surface to generate a field whose evanescent component is converted by the wire into a propagating field that can be detected in the far field. In this way structure on the surface with sub-wavelength dimensions contributes to the scattered intensity in the far field. To extract information about this structure from the far field signal the scattering amplitude is calculated in zero and first order in the surface profile function $\zeta(x_1)$ by the analytic solution of an integral equation of scattering theory. The intensity of the scattered light is calculated from this result, also through terms of first order in $\zeta(x_1)$, at a point of observation (x_1, x_3) in the far field as a function of the position of the wire x_0 for a fixed value of d. From this result $\zeta(x_1)$ can be obtained by Fourier analysis from experimental data for the field intensity. For the experimental values of the intensity we use the results of an exact numerical solution of the scattering equations based on Green's second integral identity in the plane. It is found that $\zeta(x_1)$ can indeed be reconstructed from far-field scattering data with sub-wavelength resolution.

Session B2, 13:35-Wed.

ELECTROMAGNETIC INTERACTIONS WITH COMPLEX PLATFORMS

Chairpersons: C.E. Baum and R. Gardner

RADIATION, PENETRATION AND SCATTERING FOR A SLOTTED SEMIELLIPTICAL CHANNEL FILLED WITH ISOREFRACTIVE MATERIAL - I. EXACT SOLUTIONS

Uslenghi, P.L.E.
Department of Electrical and Computer Engineering
University of Illinois at Chicago
851 South Morgan Street
Chicago, IL 60607, USA

A novel canonical solution to a boundary-value problem is presented. The geometry under consideration consists of a metallic semielliptical channel slotted along the interfocal distance and flush-mounted under a metallic plane. The channel is filled with a material that is isorefractive to the medium occupying the half-space above the channel (e.g., air); in particular, the material filling the channel may be identical to that filling the half-space above it. The field scattered by such a structure was exactly determined by the author for plane wave incidence from the half-space above the channel and either E- or H-polarization, by utilizing field expansions in terms of Mathieu functions (Digest of the IEEE-APS/URSI/NEM International Symposium, Chicago, IL, July 1992).

In this work, the exact solution is determined for the cases of a line source or a dipole parallel to the direction of the channel. The line source and the dipole may be either electric or magnetic, and may be located inside the channel, in the free half-space above it, or on the interfocal slit separating the interior and exterior regions. The solution is determined by expanding the primary and secondary fields in infinite series of eigenfunctions involving the products of radial and angular Mathieu functions, and by imposing the boundary and radiation conditions. This process leads to an analytic determination of the modal coefficients in the eigenfunction expansions, hence the obtained solutions are exact and constitute new canonical solutions of boundary-value problems.

The geometry considered herein is important for two reasons: it contains sharp metallic edges, and it involves two different penetrable materials. Thus, the problem whose exact solution is presented herein is of sufficient complexity to represent a challenging validation case for general computer codes developed for studying radiation and scattering from complicated structures.

RADIATION, PENETRATION AND SCATTERING FOR A SLOTTED SEMIELLIPTICAL CHANNEL FILLED WITH ISOREFRACTIVE MATERIAL - II. NUMERICAL RESULTS BASED ON EIGENFUNCTION EXPANSIONS

Erricolo, D., Greenenwald, K. A.(*), Uslenghi, P.L.E.
Department of Electrical and Computer Engineering
University of Illinois at Chicago
851 South Morgan Street
Chicago, IL 60607, USA

A semielliptical channel flush-mounted on an infinite metallic plane and slotted along its interfocal strip is considered. The channel is filled with a material isorefractive to the material filling the half-space above it. In particular, the two materials may be the same, e. g. air. The primary source may be a plane wave obliquely incident on the structure from the half-space above it and either E- or H-polarized, or an electric or magnetic line source parallel to the channel axis and located inside or outside the channel, or an arbitrarily located electric or magnetic Hertzian dipole parallel to the channel axis. Exact solutions for all these boundary-value problems have been developed in terms of expansions in series of products of radial and angular Mathieu functions (P. L. E. Uslenghi, this Digest). The purpose of this work is to present and discuss numerical results based on the evaluation of the infinite series of eigenfunctions representing the exact solutions.

The notation adopted for the Mathieu functions is that of Stratton (Electromagnetic Theory. New York: McGraw-Hill, 1941), also adopted by Bowman, Senior and Uslenghi (Electromagnetic and Acoustic Scattering by Simple Shapes. New York: Hemisphere, 1987) and many others. The volume Tables Related to Mathieu Functions (National Bureau of Standards, Applied Mathematics Series No. 59. Washington, DC: U.S. Government Printing Office, August 1967) contains the relations and formulas used in obtaining our numerical results. We calculate the surface current density on the semielliptical walls of the channel and on the thin metal baffles separating the channel from the upper half-space; the fields at the interface between the two isorefractive media on the interfocal strip connecting the channel to the upper half-space; and the far field in the upper half-space. Special attention is devoted to the case of a narrow interfocal strip, when the channel and the half-space above it are electromagnetically connected via a gap whose width is small compared to the wavelength

PENETRATION INTO AND RADIATION FROM A SLOTTED SEMIELLIPTICAL CHANNEL FILLED WITH AN ISOREFRACTIVE MATERIAL - INTEGRAL EQUATION FORMULATION AND SOLUTION

Chalmers M. Butler* and Michael D. Lockard
Holcombe Department of Electrical and Computer Engineering
336 Fluor Daniel EIB
Clemson University, Clemson, SC 29634-0915 USA

A solution to the boundary-value problem of a slotted ground plane backed by a semielliptical channel and illuminated by a specified source is now available (P. L. E. Uslenghi, this digest) for use as a source of data against which one may compare numerical solutions to this problem. The slot in the ground plane coincides with the interfocal distance of the ellipse, and the semielliptical channel is filled with material which is isorefractive to that of the half space on the other side of the ground plane, including, of course, the case in which both the channel and the half space are filled with the same material. The excitation is taken to be either an electric or a magnetic line source parallel to the slot axis and located in the open half space or in the channel. The field scattered by this structure and that which penetrates the slot into the channel are computed by methods based upon integral equations and their numerical solutions, and these data are compared with those obtained from a method based upon Mathieu function expansions (D. Erricolo, K. A. Greenenwald, P. L. E. Uslenghi this digest). Several sets of valid integral equations are formulated for each polarization and each is solved by an appropriate numerical method. Not only are the numerical results obtained compared with those from the canonial solution but, also, data for a given structure and excitation obtained from one integral equation are compared with those from a different integral equation, allowing one to deduce the conditions under which the various integral equation methods are inaccurate. When the excitation is TM to the slot axis and the source is close to the slot, the penetrated field differs very little from that found when the ground plane is of finite but large width. However, if the slot is very narrow, the penetrated field determined as if the structure (finite-width but large ground plane) were a scatterer is very, very inaccurate.

ANALYSIS OF SIGNALS IN COUPLED COAXIAL AND CYLINDRICAL CAVITIES

Michael G. Harrison
Air Force Research Laboratory (DEHE)
3550 Aberdeen Avenue
Kirtland AFB, NM 87117-5776 USA
Chalmers M. Butler*, John C. Young
Holcombe Department of Electrical and Computer Engineering
336 Fluor Daniel EIB
Clemson University, Clemson, SC 29634-0915 USA

Knowledge of the influence of transmission paths on the magnitudes and phases of signals as they pass through a structure is of paramount importance in any investigation of the effects that an interfering signal might have on electronic components deeply embedded in a system. If a signal of specified properties enters a system at a given point, what are its properties at some other location in the system where a susceptible circuit might be located? Are these properties primarily those peculiar to the entering signal or are they influenced significantly by the "system transfer function" of the transmission path? Complex systems might be difficult to model accurately but usually one can identify features common to most: guiding mechanisms, scattering, resonances, attenuation and reflection, and shielding. By investigating transmission paths which incorporate, in varying degrees and combinations, the features of a typical system, one can acquire an appreciation of the range of effects that transmission paths might exert on interfering signals. In this paper we attempt to address some of the above questions about the influence of typical transmission paths on the properties of signals by investigating signal transmission through simple cascaded coaxial and cylindrical cavities whose properties can be adjusted at will. The structures considered are ordinary cascaded coaxial and cylindrical cavities in various configurations.

Apertures common to adjacent cascaded cavities are identified and coupled integral equations are formulated for the electric field in these apertures. The integral equation kernels contain series of eigenfunctions characteristic of the precise cavity configurations and sizes. Techniques for computing eigenvalues as solutions of transcendental equations and for efficiently summing slowly converging series are discussed. The integral equations are solved numerically and, from the aperture field components obtained therefrom, one can compute all other field components and currents of interest in the cavernous structure. Models have been fabricated and experiments are conducted for a number of cavity configurations. Data collected allows one to corroborate values of quantities of interest determined from computations. Computed and measured results are presented

ON THE EFFECTS OF PROPAGATION PATH ON RF SIGNALS IN SYSTEMS

A. Q. Martin*
Holcombe Department of Electrical Computer Engineering
333 Fluor Daniel EIB
Clemson University
Clemson, SC 29634-0915, USA

The influence of the transmission path on the shape and magnitude of a RF signal as it passes through a system is of importance in an investigation to discover how the performance or output of digital circuits might be altered as a result of electromagnetic energy being incident upon, and propagating through, a system. If an RF signal of a specified form enters a system at a given point, it is desirable to determine the salient features of the signal at some other location within the system, where a susceptible digital circuit might be located. Moreover, it is useful to know if these features are primarily those peculiar to the entering signal, or if they are greatly influenced by the properties of the transmission path. Addressing these issues should help one gain some appreciation for the nature of a spurious signal arriving at the input of a digital chip deeply embedded in a complex system that is subjected to high-power RF excitation originating from outside the system proper.

Questions about the influence of the transmission path on the waveshape and magnitude of possibly deleterious signals can be answered by determining the nature of signals which propagate through cascaded coupled cavities that *electromagnetically* replicate the various component configurations found in a typical complex system, such as an aircraft, a missile, a command post blockhouse, a personal computer, or a piece of electronic test equipment.

In the present talk the issue of the influence of the propagation path will be addressed by reporting results from an inchoate study of RF signal propagation through cascaded coupled rectangular cavities. In particular, attention will be devoted to the problem of a transient signal incident upon a narrow slot in an infinite conducting screen that is backed by a rectangular cavity having in its interior a conducting thin-wire probe. The analysis will involve the numerical solution of coupled integral equations in the frequency domain. Transient waveforms of interest will be obtained from the frequency domain results and the known time history of the excitation by means of the FFT. The investigation will consider variations in cavity size and depth, slot length, probe depth and height within the cavity, and the time history of a transient, candidate waveform. The study will involve transient signals whose spectra span a frequency range from nearly DC to 2 or 3 GHz.

EXTENSION OF THE BLT EQUATION TO INCORPORATE ELECTROMAGNETIC FIELD PROPAGATION

Tesche, F.M., Butler, C.M., Dept. of Elec. and Computer Engin.
Clemson University, Clemson, SC, 29634-0915 USA

A key concept in the analysis of the response of a complex electrical system to an external electromagnetic (EM) field excitation is its representation in terms of a topological model. In this approach, the entire system is viewed as several concentric layers, or surfaces, through which energy must pass to penetrate into the system. Usually, such surfaces are highly conducting shields and they effectively isolate one volume of the system from another. However, in most real systems, there are imperfections in these shields and EM energy is able to enter the system, possibly causing upset or damage to electrical components. This view of shielding has been referred to as the "onion" concept (L. W. Ricketts, J. E. Bridges and J. Miletta, *EMP Radiation and Protective Techniques*, John Wiley and Sons, New York, 1976.). It was initially proposed by Baum (C. E. Baum, "Electromagnetic Topology for the Analysis and Design of Complex Electromagnetic Systems", *Fast Electrical and Optical Measurements, Vol I*, I.E. Thompson and L.H. Luessen, eds., Martinus Nijhoff, Dordrecht, 467-547, 1986.) and later formalized in the literature, (F. M. Tesche, *IEEE Trans. AP*, **vol. 26, no. 1**, 60-64, 1978.).

As a result of this topological view of a system, a transmission line network model has been developed for computing the EM-field induced responses within a complex system. This model uses the Baum-Liu-Tesche (BLT) equation [Baum 1986], which is a concise matrix representation of voltage and current responses on a distributed transmission line network. The formulation of the BLT equation involves the propagating voltage or current waves along conductors, together with a description of how these waves are reflected at the junction of the network.

It is apparent that similar propagation and scattering relationships exist for electromagnetic fields produced by localized sources, interacting with the system exterior, and penetrating into the interior. This suggests that it is possible to develop an extended BLT-type equation containing both traveling waves of EM fields and conductor voltage/current.

In this paper, the derivation of the conventional BLT equation for transmission line networks is reviewed, and then the extension of this analysis formalism to add EM field coupling paths is described. This approach uses additional system details for an internal interaction calculation, such as aperture penetration of the EM field and its effect on the response of a near-by transmission line. The hope is that, with this new approach, the effects of internal cavity resonances can also be incorporated into such system-level models of EM field interaction.

SOME DIFFICULTIES IN APERTURE THEORY

Chalmers M. Butler
Holcombe Department of Electrical and Computer Engineering
336 Fluor Daniel EIB
Clemson University, Clemson, SC 29634-0915 USA

Penetration of electromagnetic fields into enclosures or cavities through apertures in the cavity walls has been of interest for many years, yet there are aspects of this important subject which apparently are not widely understood. And there are several fundamentally different methods which researchers have employed over the years to determine interior fields when an aperture-perforated structure is illuminated by radiation from a known exterior source, though the advantages and disadvantages of available methods are rarely delineated. For the simple structure of a perfectly conducting, vanishingly thin shell which possesses an aperture and which encloses a volume region filled with homogeneous material, computation of the interior field caused by a known exterior source can be quite problematic: some methods yield highly inaccurate interior fields, especially when the penetration is weak, and some methods which might otherwise lead to accurate data fail at cavity "resonances" even though the interior is not completely enclosed by the cavity walls there is an aperture present. In this paper, "problems with aperture theory" are addressed. Several methods for solving aperture problems are outlined in general and the solution accuracies that one might expect from them are discussed. Why some methods are more accurate than others is explained. It is pointed out why some methods fail at cavity "resonances," though there is no physical basis for this failure when the cavity shell is perforated by an aperture. Moreover, it is demonstrated by means of simple examples that the interior fields can be determined and expressed in forms free of the singularities inherent in the expressions for these fields arrived at by means of "aperture theory." For the most part, difficulties that one might encounter in aperture theory and how they can be circumvented are illustrated by solutions of simple aperture problems for which closed-form expressions for interior fields can be found.

EM COUPLING THROUGH SLOTS INTO OVERMODED CAVITIES AND LARGE SCALED COMPLEX PLATFORMS USING THE MULTILEVEL FAST MULTIPOLE METHOD.

E. Siah
University of Michigan
K. Sertel
University of Michigan
J. L. Volakis
University of Michigan
V. Liepa
University of Michigan

With the increasing use of wireless devices and sensors, there is a need for an understanding of electromagnetic coupling (EMC) and interference (EMI). Previous studies in this area have mostly concentrated on approximate or small-scale models for EMC analysis. Here, we employ the multilevel fast multipole methods for EMC analysis of structures which may incorporate various shape apertures, wire lines and a variety of other details and features. Because the MLFMM has O(NlogN) CPU and memory requirements, and employs curvilinear elements, large-scale structures with many features can be considered. Moreover, multispectral responses can be generated for better characterization of coupling effects as a function of different geometrical and material parameters. In the case of materials, the MLFMM is combined with the finite element-boundary integral method.

To begin with, we first consider the characterization of coupling into rectangular and non-rectangular cavities. These geometries are chosen because they can be readily constructed and measured, and can thus serve as validation examples. The effect of aperture shape on shielding is carefully examined and conclusions are drawn on the coupling characteristics for the various apertures placed on over-moded cavities. Differences among purely rectangular, non-rectangular and loaded or corrugated cavities will be discussed. In particular, it will be noted that coupling is significantly increased near the slot and/or cavity resonances by several tens of dBs. The shielding characteristics of the structure are strongly affected by the location of these resonances.

We will further discuss the effects and significance of wire traces (though apertures) on coupling. Such wire traces can be responsible for significant increases in coupling. Finally, we will show coupling simulations for entire complex vehicles and platforms in the presence of radiating devices.

COUPLING OF ELECTROMAGNETIC FIELDS TO A WIRE IN A CAVITY

D.R. Wilton, D.R. Jackson, C. Lertsirimit
Department of ECE, University of Houston
Houston, TX 77204-4005
N.J. Champagne
Lawrence Livermore National Laboratory
Livermore, CA 94550

In this presentation we examine a canonical EMC/EMI problem–the excitation of a wire inside a rectangular cavity oriented parallel to one of the cavity axes. A number of excitations and configurations are of interest. These include excitations by one or more slots in the cavity walls coupling to the exterior, by a delta gap voltage generator located somewhere on the wire, or by an external field that is incident on the wire when it penetrates the cavity through an aperture. Either end of the wire can be open-circuited or terminated on a cavity wall, possibly through a load. This simple structure serves as a canonical problem for studying EM field penetration into electronic components such as computers.

Both full-wave computational methods and several analytical methods can be conceived to treat the problem. In either case, a careful selection of the problem formulation is required to ensure that one can accurately model low-level fields penetrating the cavity. Preliminary considerations suggest that simplified analytical models can be developed to predict the currents induced on the wire and the fields within the cavity. Such models can be used both to validate the full-wave numerical calculations and to provide reduced-order representations of the associated coupling mechanisms.

Validation of the computer code, which is primarily based on integral equation formulations, is crucial because the full-wave method employed involves a variety of complex numerical techniques to reduce the computational burden, and a sophisticated object-oriented design to increase the code's generality and maintainability. For example, wire, surface, and aperture modeling, symmetry methods, and parallel processing are all used, along with cavity Green's function representations employing advanced acceleration techniques to sum the associated series. Once validated, however, the code can, in principle, treat essentially arbitrary cavities, coupling apertures, and wire configurations. Furthermore, the code can treat multilayered media inside a cavity that might, for example, represent a simple model of a printed-circuit board inside a computer box. The code can also be used in a hybrid FEM/integral equation mode to treat more general conductive and dielectric inhomogeneities. This could be useful for more realistic modeling of interiors of complicated devices such as computers or other electronic equipment.

FAST TIME DOMAIN ANALYSIS OF NONLINEARLY LOADED PRINTED CIRCUIT BOARD STRUCTURES

K. Aygun*, B. Fischer, A. Cangellaris, E. Michielssen
Center for Computational Electromagnetics
Deparment of Electrical and Computer Engineering
University of Illinois at Urbana-Champaign
Urbana, IL 61801, USA

Modern day electronic systems pose significant challenges to the electromagnetic modeler. Ever-increasing clock rates and circuit density call for the full wave modeling of printed circuit boards (PCBs) with fine geometric features, finite (and possibly inhomogeneous) dielectrics, and nonlinear loads and circuits. Here, a new time domain integral equation solver that achieves such functionality is described. Specifically, a marching-on-time (MOT) algorithm for solving a time domain electric field integral equation pertinent to the analysis of PCBs with conducting surfaces/wires/junctions and (potentially inhomogeneous) finite dielectrics is constructed. Given a bandlimited excitation, the MOT algorithm solves for induced surface currents on conducting elements and polarization currents in dielectric regions. For a geometry modeled using N_s surface/wire and N_v volumetric unknowns, the computational complexity of this solver scales as $O(N_t(N_s + N_v)^2)$ where N_t denotes the number of simulation time steps. To reduce this complexity, the scheme is accelerated by the multilevel plane wave time domain algorithm (A. A. Ergin, B. Shanker, and E. Michielssen, IEEE Antennas and Propagat. Mag., 41, 39-52, 1999). The computational complexity of the resulting solver scales as $O(N_t(Ns + Nv)log^2(Ns + Nv))$ when applied to the analysis of typical PCBs. Any lumped circuits are modeled by coupling modified nodal analysis equations to the MOT system of equations. A nonlinear Newton-based solver is used at each time step to solve a nonlinear system of equations the size of which is equal to the total number of nonlinear circuit elements in the system. Hence, the unknown currents and voltages in both the electromagnetic model and the circuit are solved for in a consistent way at each time step of the simulation. The proposed method has been applied to a number of structures including a shielded active microwave amplifier with a MESFET transistor. We expect this method to find extensive use in the EMC/EMI and signal integrity analysis of PCB devices with realistic complexity.

ASSESSMENT OF SEMICONDUCTOR NON-LINEAR LOADS VIA SINGLE-SHOT HIGH VOLTAGE TIME DOMAIN REFLECTOMETRY

M. A. Bridgwood*
ECE Department
Clemson University
Clemson, SC 29634, USA

For many years Time Domain Reflectometry (TDR) has been recognized as a valuable method for evaluating faults and mismatches in cables or interfaces between conducting media. The technique is also widely used in determining load characteristics in terms of impedance deduced from injected and reflected voltage or current waveforms. For current state-of-the-art commercial TDR's, the injected signal is usually a continuously pulsed waveform with voltage edge transitions no greater than 1 volt and occurring in 30 ps or less. Build up of the response to either positive or negative pulse edges, but not both, is obtained via sampling.

As a method for investigating mechanisms associated with the injection of wide band signals into semiconductor devices the established TDR technique is known to be severely limited in several respects. The paper examines these limitations from the perspective of digital devices subjected to high power microwave rings which may lead to either disruption of system function or local catastrophic failure.

A bipolar TDR system is described which uses high voltage single shot pulses both as disruptive stimulus and also as a characterization tool. Advantages are that digital thresholds may easily be breached and that time dependent non-linear mechanisms may be examined in real time.

The paper describes work that has been undertaken using this TDR approach to cause catastrophic damage in MOS capacitors where separation and characterization of the non-linearity associated with oxide breakdown was a prime goal. The presentation concludes with a comparison of the modeling aspects of this non-linear breakdown process with disruption of a digital circuit input.

EVALUATION OF PROCESSOR FAULTS DUE TO TO EM INTERFERENCE—CONCEPTS AND SIMULATION ENVIRONMENT

Shantanu Dutt, Hasan Arslan
Dept. of Electrical and Computer Engr.
University of Illinois at Chicago

The goal of our work is to determine the extent and categorize the type of processor faults due to EM interference on various modules of a computer system; in this presentation we will focus on EM interference on memory address and data lines and how it affects processor functioning. We will present the conceptual framework for detecting errors in processor functioning and classifying them as either (1) "data errors" or (2) "control errors". Algorithm-based fault tolerance (ABFT) techniques will be used for detecting data errors, while control-flow checking (CFC) using a watchdog processor will be used for detecting control errors. ABFT techniques work by encoding the inputs using schemes like checksums and verifying that the output produced is also correctly encoded data. For example, in matrix multiplication, the two input matrices A, B can have a checksum row and column, respectively, in which case the product matrix C should have both a checksum row and column (i.e., the sum of all data rows of C should be equal to its checksum row, and the sum of all data columns of C should be equal to its checksum column). CFC techniques work by constructing an instruction flow graph of a program and producing an error-detecting function f of the set of instruction bit patterns on each subpath and storing them in intermediate NOP (no operation) instructions at the ends of the subpaths. The sequence of instructions executed is then checked on-line by a watchdog processor that "snoops" on the address and data buses of the main processor to determine if f(subpath of instructions actually executed) matches the stored function value at the end of the subpath. These ABFT and CFC methods will be presented. On the implementation side, a processor will be described in VHDL and fault injection logic will be introduced for the memory buses that can be turned on and off individually and in clusters to simulate the type of fault patterns caused by EM interference. The status of this part of the implementation will be discussed.

Session B3, 13:35-Thurs.

ELECTROMAGNETIC COMPLEX MEDIA AND METAMATERIALS

Chairpersons: N. Engheta and J.M. Arnold

ON A SPECIAL BIANISOTROPIC MEDIUM

F. Olyslager*
Department of Information Technology
Ghent University
Sint-Pietersnieuwstraat 41
B-9000 Ghent, Belgium
I.V. Lindell
Electromagnetics Laboratory
Helsinki University of Technology
PO BOX 3000
FIN-02015 HUT, Espoo, Finland

It is well-known that electromagnetic field problems in uniaxial anisotropic media can be solved almost as easely as in isotropic media because the fields can be split in TE and TM components that each experience the uniaxial medium as an isotropic medium. During the years the present authors have been wondering how far this idea could be generalised to bianisotropic media. This resulted in a very general bianisotropic medium of the form

$$\overline{\overline{\epsilon}} = \alpha(\mathbf{z} \times \overline{\overline{I}} + \mathbf{a}_1\mathbf{b}_1 + \mathbf{b}_1\mathbf{a}_1) + \eta(-\overline{\overline{B}}^T + \mathbf{a}_2\mathbf{b}_1 + \mathbf{b}_2\mathbf{a}_1), \tag{1}$$

$$\overline{\overline{\xi}} = \eta(\mathbf{x} \times \overline{\overline{I}} + \mathbf{a}_2\mathbf{b}_2 + \mathbf{b}_2\mathbf{a}_2) + \alpha(\overline{\overline{B}} + \mathbf{a}_1\mathbf{b}_2 + \mathbf{b}_1\mathbf{a}_2), \tag{2}$$

$$\overline{\overline{\zeta}} = \tau(\mathbf{z} \times \overline{\overline{I}} + \mathbf{a}_1\mathbf{b}_1 + \mathbf{b}_1\mathbf{a}_1) - \alpha(-\overline{\overline{B}}^T + \mathbf{a}_2\mathbf{b}_1 + \mathbf{b}_2\mathbf{a}_1), \tag{3}$$

$$\overline{\overline{\mu}} = -\alpha(\mathbf{x} \times \overline{\overline{I}} + \mathbf{a}_2\mathbf{b}_2 + \mathbf{b}_2\mathbf{a}_2) + \tau(\overline{\overline{B}} + \mathbf{a}_1\mathbf{b}_2 + \mathbf{b}_1\mathbf{a}_2), \tag{4}$$

with α, η, τ scalars, with $\mathbf{a}_1$, $\mathbf{a}_2$, $\mathbf{b}_1$, $\mathbf{b}_2$, $\mathbf{x}$ and $\mathbf{z}$ vectors and with $\overline{\overline{B}}$ a dyadic. This medium has particular properties: 1. This is the most general medium for which the electromagnetic fields can be split in two components. These components experience the medium as simpler bianisotropic media, also called equivalent media. 2. The Green dyadics for the equivalent media can be written in closed form. This is the most complicated medium for which this can be done up to now. 3. The Helmholtz determinant operator for this medium can be factorized. 4. The slowness surface of this medium consists of two second order surfaces, i.e. two quadrics. 5. The slowness surface of the equivalent media consists of two coinciding second order surfaces. 6. In this medium the electromagnetic fields can be derived from two potentials that satisfy decoupled second order partial differential equations. These are generalized Hertz potentials. 7. Also the sources can be decomposed in two parts in this medium. 8. This medium cannot be generalized further using duality transformations.

EXACT SCATTERING FROM METALLIC WEDGES EDGE-COATED WITH ANISOTROPIC MATERIALS

D. Erricolo and P.L.E. Uslenghi*
Department of Electrical and Computer Engineering
University of Illinois at Chicago
Chicago, IL 60607, USA

The coating of metallic edges is used to modify the scattering behavior of the edges, e. g. by means of lossy dielectrics, ferrites, or other absorbing materials. When the coating is cylindrically symmetric and centered at the edge of the wedge, the boundary-value problem may be exactly solvable by separation of variables. This technique was previously employed in the case of line sources parallel to the edge of the wedge (see e. g. M. A. K. Hamid and S. J. Towaij, IEEE Trans. Antennas Propagat., vol. 25, no. 5, pp. 663-665, Sept. 1972), by using a technique expounded by Harrington in his book "Time-Harmonic Electromagnetic Fields" (New York: McGraw-Hill, 1961). The case of anisotropic coating of the edge of a metallic half-plane was considered by Uslenghi, Floreani and Zich (URSI Symposium on Electromagnetic Waves, Victoria, Canada, May 2001), by employing a modification of the method introduced by MacDonald in his book "Electric Waves" (Cambridge: University Press, 1902).

In the present work, the technique of MacDonald is modified for the case of a metallic wedge of arbitrary angle, whose wedge is capped by a metallic cylinder with axis coincident with the edge of the wedge. The cylindrical cap is in turn coated with one or more coaxial layers made of anisotropic materials. The incident field is a plane wave with arbitrary direction of incidence and arbitrary polarization. If the anisotropic layers are biaxial in a circular cylindrical coordinate system whose symmetry axis coincides with the edge of the wedge, then the scattering problem is solvable exactly, in terms of Bessel and Hankel functions with certain arguments and orders. Thus, a novel canonical solution to a rather complicated scattering problem is obtained. Several numerical results are presented for different geometrical dimensions and material properties, and the results are compared to those for an uncoated edge and an edge with an uncoated cylindrical metallic cap. The effectiveness of penetrable coating layers in modifying the scattering characteristics of the wedge is discussed.

UPPER LIMIT FOR THE LOSS FACTOR OF THE CHIRALITY PARAMETER IN ISOTROPIC MEDIA

Ari Sihvola
Helsinki University of Technology
Electromagnetics Laboratory
P.O. Box 3000
FIN-02015 HUT, Finland

The laws of physics pose restrictions on the magnitude of the electromagnetic material parameter values. This happens in particular if we are analyzing materials belonging to certain subclasses. Restricting conditions can be dictated, for example, by the requirements of reciprocity, linearity, or dissipativity. Let us consider homogeneous and isotropic chiral medium with the relative material parameters ϵ (permittivity), μ (permeability), and κ (chirality), as in the following constitutive relations

$$D = \epsilon E - \mathrm{j}\kappa H \qquad B = \mathrm{j}\kappa E + \mu H \tag{1}$$

with the electric and magnetic fields (E, H) and flux densities (D, B).

Most often when limitations for chiral materials are presented, the focus is on the real part of the chirality parameter κ. It is fairly unproblematic, and the generally accepted result in regions outside strong dispersion is that κ (as a real number for lossless media) should not exceed the refractive index of the medium. However, for the imaginary part, there are different limits, some stricter than others. For lossy media, the material parameters are often written in frequency domain as

$$\epsilon = \epsilon' - \mathrm{j}\epsilon'', \quad \mu = \mu' - \mathrm{j}\mu'', \quad \kappa = \kappa' - \mathrm{j}\kappa'' \tag{2}$$

It is known that for passive isotropic dielectric materials, the imaginary part of the permittivity ϵ should be non-positive (meaning that $\epsilon'' \geq 0$).

The strict limit for the imaginary part of the chirality parameter for isotropic, lossy, chiral medium is

$$|\kappa''| < \sqrt{\epsilon''\mu''} \tag{3}$$

This condition is concluded in [I.V. Lindell: *Methods for electromagnetic field analysis*, IEEE Press and Oxford University Press, 1995] by considering the eigenvalues of the bi-isotropic material matrix that is contained in the electromagnetic energy functional. However, absence of a direct physical interpretation to the condition may have been the cause that this condition is not appreciated very much in the literature. In this presentation, physical reasons, based on material modelling and polarizabilities of particles, are given to support the limiting condition (4).

LONGITUDINALLY SYMMETRIC ARTIFICIAL MATERIALS ISOREFRACTIVE WITH FREE SPACE

J. S. Tyo
EECE Department
University of New Mexico
Albuquerque, NM 87131-1356

Isorefractive materials are materials that share the same speed of light, but with different wave impedences, i.e.

$$\sqrt{\mu_1\epsilon_1} = \sqrt{\mu_2\epsilon_2}, \quad \sqrt{\mu_1/\epsilon_1} \neq \sqrt{\mu_2/\epsilon_2}. \tag{1}$$

Isorefractive materials are important in scattering theory because there are many canonical problems that can be solved in closed form when an interface is between two isorefractive materials that cannot be solved in other circumstances (see for example Uslenghi, *IEEE Trans. Antennas Propagat.*, **45** 1382–1385). For time-domain applications, isorefractive materials would be beneficial because TEM modes can travel parallel to material boundaries thereby eliminating dispersion.

When designing an impulse radiating antenna, aperture efficiency is lost due to field energy that travels on the TEM feed structure that is not captured by the focusing optic. One method for mitigating this problem is to use isorefractive materials to construct the IRA (Tyo, *et al.*, *IEEE Trans. Antennas Propagat.* **46** 1114–1115). By filling the interior region with a lower-impedance material, the fraction of power inside the aperture is increased, improving the aperture efficiency. Ideally, one would have the medium outside the feed structure be air (for ease of construction), but then the material inside the feed would have to be isorefractive with free space.

In this paper, a class of longitudinally symmetric artificial materials is presented that are isorefractive with free space. These materials are essentially multi-conductor transmission lines with multiple undriven electrodes. Filling the space inside the TEM transmission line with a lattice of perfectly conducting rods introduces a transverse polarization that serves to raise the effective dielectric constant of the medium. Because of the longitudinal symmetry, the phase velocity is $1/\sqrt{\mu\epsilon}$ for all frequencies, making the artificial materials non-dispersive. Calculations were performed that predict the effective impedance of the artificial materials. The longitudinally symmetric materials can be easily generalized to a conically symmetric medium for IRA applications.

One of the principal problems with such an approach is skin loss on the surface of the conducting rods. As the inclusions get smaller and smaller, these losses increase, and can lead to dispersion in their own right (Baum and Tyo, *Measurement Note #47*, (AFRL, Kirtland AFB, NM, 1996)). Loss mechanisms are addressed, and the effect on material risetime are discussed.

QUASI-PHASE-MATCHING SECOND-ORDER NONLINEAR OPTICS BY QUANTUM-WELL SUPERLATTICE INTERMIXING

J. M. Arnold*, D. C. Hutchings, University of Glasgow, Glasgow, UK

Parametric nonlinear optical interactions such as second-harmonic generation in a guided wave environment generally require some form of phase-matching in order to maximise the efficiency of parametric wave interaction processes. This requirement arises because the phase velocities of two waves at different harmonic frequencies may not be the same in a dispersive medium. The semiconductor gallium-arsenide is highly dispersive, and leads to a significant difference between the phase velocities of the fundamental and second harmonic waves, which is enhanced when the second harmonic photon energy $\hbar\Omega_2$ is slightly below the bandgap of the semiconductor due to optical resonance.

When the material is formed from a superlattice of coupled quantum wells it is possible to alter the second-harmonic generation coefficients in a spatially controllable manner, by using the technology of semiconductor quantum-well intermixing (QWI). Intermixed regions have a higher bandgap than nonintermixed regions, so have smaller nonlinear coefficients because the light is further from resonance with the bandedge. In addition it is possible, by symmetry breaking, for quantum wells to have tensor susceptibility components which vanish in the bulk medium.

By means of QWI it is possible to form an effective phase-matching grating in the second-order nonlinear susceptibility tensor $\chi^{(2)}$ of the material, and hence to phase-match the SHG. This principle has been demonstrated experimentally in a fabricated planar waveguide device (A. Saher Helmy *et al.*, *Optics Letters*, **25**,1370–1372, 2000), exhibiting phase-matched generation of 775 nm light from a fundamental pump source at 1550 nm.

A full description of the electromagnetic theory involved in this process ranges from microscopic description of the underlying electronic bandstructure of the superlattice subject to intermixing, *via* effective medium calculations of the macroscopic nonlinear susceptibilities (D. C. Hutchings, *App. Phys. Lett.*, **76**, 1362–1364, 2000), to 3-D BPM modelling of the parametric interactions between the modes at the fundamental and second-harmonic frequencies. These theoretical considerations will be described in the paper.

SIMULATION AND CHARACTERIZATION OF LEFT-HANDED METAMATERIALS

D. R. Smith*, D. C. Vier, R. A. Shelby, N. Kroll, S. Schultz
Department of Physics, 0319
University of California, San Diego
9500 Gilman Drive
La Jolla, CA 92093-0319

We discuss several issues associated with simulating and characterizing left-handed metamaterials (LHMs). LHMs are materials that exhibit at least one frequency band over which the electric permittivity and the magnetic permeability are simultaneously negative. No naturally occurring material or composite has such a property, although it had been previously shown in an early paper by Veselago (V. G. Veselago, *Sov. Phys. Usp.*, **10**, 509-513, 1968) that a left-handed material would not be precluded by other physical laws.

In order to demonstrate a left-handed medium, we have combined two arrays of conducting, nonmagnetic scattering elements. The first medium, a square array of conducting wires with lattice spacing much less than the wavelengths of interest, responds to electromagnetic waves with an effective permittivity that is negative below a cutoff frequency. The second medium, a square array of conducting dual split ring resonators, responds to electromagnetic waves with an effective permeability that is negative over a bandwidth that is roughly ten percent of the operating frequency. By carefully interlacing these two effective media, each having the same sized unit cell, a composite medium results that has a frequency band in which both the permittivity and the permeability are simultaneously negative. In the absence of losses, the index of refraction for this composite medium, determined by taking the square root of the product of the permittivity and permeability, is real; thus, electromagnetic waves propagate in the left-handed frequency band. However, the negative root for the refractive index must be taken when the material is left-handed, leading to the unusual and remarkable properties first hypothesized by Veselago.

In designing left-handed metamaterials, we have relied on standard computational techniques such as finite-difference frequency domain (FDFD), finite-difference time domain (FDTD), and finite element methods. We will describe our computational approach to metamaterials, including the averaging method we use to extract the effective permittivity and permeability from the electric and magnetic fields computed by FDFD codes.

MACROSCOPING MODELING OF ELECTROMAGNETIC FIELDS IN NEGATIVE REFRACTION INDEX METAMATERIALS

S.A. Cummer
Electrical and Computer Engineering Department
Duke University
Durham, NC 27708, USA

Recent papers have explored the fascinating theoretical properties of electromagnetic materials with a negative index of refraction. More importantly, materials with a negative refraction index in a limited frequency range have actually been manufactured using metallic inclusions, and some properties of these materials have been verified experimentally. These structures are typically periodic, and detailed numerical simulations of a unit cell of these metallic inclusions have also demonstrated their LH properties.

These microscale simulations are too detailed to easily simulate the fields in a larger region of space like one might encounter in an actual application of these materials. The bulk dielectric properties of these materials have been experimentally verified and are well-understood, making analytical simulation an option. But in strongly dispersive materials like these, non-sinusoidal solutions are not easy to derive, and they are typically only analytically tractable for very simple material geometries and inhomogeneities. A numerical method for simulating the macroscopic fields in a relatively large region of LH materials would be valuable for simulating applications and including effects like losses that are not easy to treat analytically.

Thus far the physically realizable LH materials are simply a combination of an electric cutoff (such as a plasma) and a magnetic cutoff or Lorentz resonance. The combination of these material effects leaves a linear, isotropic, and temporally dispersive medium that can be simulated with finite difference techniques. We derive such a technique and investigate some of the important properties of these materials, including the exponential growth of waves with imaginary wave number and associated subwavelength focusing. Absorbing boundary conditions for this material present an interesting problem. Ordinarily, the perfectly matched layer (PML) is straightfowardly adaptable to dispersive materials, but we show analytically and numerically that the opposite directions of phase and energy velocity cause the fields in the negative index band to grow exponentially in the PML.

DESIGN AND MODELING OF NEGATIVE PERMITTIVITY AND PERMEABILITY METAMATERIALS

Richard W. Ziolkowski
Department of Electrical and Computer Engineering
The University of Arizona
1230 E. Speedway Blvd.
Tucson, AZ 85721, USA

In the past few years, there has been a renewed interest in using structures to develop materials that mimic known material responses or that qualitatively have new response functions that do not occur in nature. Artificial dielectrics were explored, for example, in the 1950's and 1960's for light-weight microwave antenna lenses. Artificial chiral materials were investigated in the 1980's and 1990's for microwave radar absorber applications. Recent examples of these artificial material activities include photonic band gap structured materials, artificial electric and magnetic molecules, and artificial electric and magnetic materials which, like many of the chiral materials, can exhibit positive or negative permittivity or permeability properties. Very recent experiments involving artificial materials with simultaneous negative permittivity and permeability, here called Double Negative (DNG) media, have captured the public's attention.

The qualitatively new response functions of these metamaterials are often generated by artificially fabricated, extrinsic, low dimensional inhomogeneities. For instance, the artificial molecules are based upon the introduction of arrays of electrically small, loaded antennas into in a host substrate. Design rules for obtaining the molecule metamaterials that exhibit the common Debye and Lorentz material model responses and their generalizations have been given for both electric and magnetic properties. More recently, a number of electromagnetic structures that exhibit effective DNG permittivity and permeability properties have been designed and experiments have been performed.

A basic review of these metamaterials and their ability to achieve negative permittivity and permeability values will be reviewed. Both FEM and FDTD simulations will be presented to demonstrate the behavior of a DNG metamaterial slab. Paraxial focusing of a cylindrical wave with a Drude model DNG slab will be presented. It will also be demonstrated how reflection and transmission data from these simulations can be used to determine the actual permittivity and permeability values of the DNG slab. Some applications of DNG metamaterials will be discussed.

META-MATERIALS AND SHEETS WITH WIDE-BAND NEGATIVE MATERIAL PARAMETERS

S.A. Tretyakov
Helsinki University of Technology
P.O. 3000, HUT, Finland

Recently, electromagnetic materials with negative permittivity and permeability values (sometime called "media with negative refraction index") have been given much attention in literature. Probably the most interesting feature of these media is that the directions of the phase velocity and that of the Poynting vector of a plane wave are the opposite, in other words, plane waves are backward waves. This results in anomalous refraction on interfaces with usual media.

Realization of negative media parameters implies the use of resonant inclusions, such as broken ring resonators. The required response is reached in a narrow frequency band near the resonance, where the material is highly dispersive (the media parameters quickly vary with the frequency). As is obvious from the Kramers-Kronig relations, the parameters in such composites are complex functions, and materials are absorptive. This means that it is actually not possible to realize media with *real* and negative values of the permittivity and permeability as composite materials with passive linear inclusions.

Here we show that this causality restriction can be relaxed in composite materials with active inclusions. It is proven that using small dipole and loop antennas loaded by certain simple electronic circuits as composite inclusions, the material behaves as an effective medium with real negative parameters in wide frequency bands. In this case, we allow inclusions (artificial molecules) to contain electronic circuits, possibly with transistor amplifies etc., which also include local DC power supplies. Similarly, thin sheets of negative materials can be simulated by strip or patch arrays loaded by active circuits.

It turns out that simple impedance inverter circuits are sufficient to create appropriate loads for small metal inclusions forming the composites. It is well known that such circuits are easy to realize and they are stable in wide frequency bands.

GUIDED WAVES IN PAIRED DIELECTRIC-METAMATERIAL WITH NEGATIVE PERMITTIVITY AND PERMEABILITY LAYERS

N. Engheta
University of Pennsylvania
Department of Electrical Engineering
200 South 33rd Street
Philadelphia, PA 19104-6390, U.S.A.

Study of electromagnetic properties of complex media has been the subject of research interests in the past several decades. Recently, the concept of complex materials in which both permittivity and permeability possess negative values at some frequencies has gained considerable attention [see e.g., D. R. Smith et al., Phys. Rev. Lett., vol. 84, no. 18, pp. 4184-4187, 1 May 2000]. This idea dates back to Veselago, who in 1967 theoretically investigated plane wave propagation in a material whose permittivity and permeability were assumed to be simultaneously negative [V. G. Veselago, Soviet Physics Uspekhi, vol. 10, no. 4, pp. 509-514, 1968. (Usp. Fiz. Nauk, vol. 92, pp. 517-526, 1967)]. Shelby, Smith, and Schultz constructed such a composite medium for the microwave regime, and demonstrated experimentally the presence of anomalous refraction in this medium [R. A. Shelby et al., Science, vol. 292, no. 5514, pp. 77-79, 6 April 2001]. Previous theoretical study of electromagnetic wave interaction with omega media has also revealed the possibility of having negative permittivity and permeability in omega media for certain range of frequencies [M. M. I. Saadoun and N. Engheta, chapter 15 in Progress in Electromagnetic Research (PIER) Monograph series, vol. 9, A. Priou, (Guest Editor), 1994, pp. 351-397].

Since for monochromatic plane wave propagation in the medium with negative permittivity and permeability the direction of the Poynting vector is antiparallel with the direction of phase velocity, this can lead us to interesting possibilities/ideas. One such idea is guided wave propagation in paired dielectric-metamaterial with negative permittivity and permeability layers. Recently we introduced and studied the idea of the compact cavity resonators using such a paired layer [N. Engheta, Proceedings of International Conference on Electromagnetics in Advanced Applications (ICEAA'01), Torino, Italy, September 101-4, 2001] In our present study we have explored the properties of guided waves in a structure in which a combination of a regular dielectric and a metamaterial possessing negative permittivity and permeability has been inserted. We have analyzed dispersion relations for such guided waves, and have obtained interesting features unique for such paired layers as waveguides. In this talk, we will present the results of our theoretical studies on these guided wave structures, and we will discuss physical intuitions and potential applications of our findings.

Session B4, 8:35-Fri.

ANTENNAS AND ARRAYS

Chairperson: A.W. Glisson and M.K. Karkkainen

EQUIVALENT CURRENT EXCITATION FOR AN APERTURE ANTENNA EMBEDDED IN AN ARBITRARILY SHAPED IMPEDANCE SURFACE

Glisson, A. W.
Dept. of Electrical Engineering
The University of Mississippi
University, MS 38677-1848, USA

The problem of computing the radiation from an aperture in an infinite, perfectly conducting ground plane can be modeled by shorting the aperture with a perfect electric conductor, placing an equivalent magnetic current on the shorted aperture to bring the electric field back to its correct value in the aperture, and then applying image theory to obtain a situation that is equivalent to the original problem in the open half-space of interest. The procedure provides an exact representation of the radiated fields if the true aperture fields are known. The same procedure is often used to compute an approximate radiation field by using an estimate of the aperture electric field; for example, for a waveguide opening into a half-space, the aperture electric field may be approximated by the electric field distribution of the waveguide mode at the aperture location.

Apertures in finite, perfectly conducting structures may be modeled by a slightly more complex procedure in which the "aperture," whose shape is defined for convenience, is again shorted with a perfect electric conductor, and a magnetic current of appropriate strength is placed just outside the shorted aperture. If the aperture electric field is known, the equivalent magnetic current distribution is easily determined. In this case, however, the equivalent magnetic surface current radiates in the presence of the shorted conductor surface to produce the correct radiated fields everywhere external to the surface.

In this paper it is demonstrated via the equivalence principle that if the aperture fields are known, one can also explicitly obtain the equivalent current excitation required for modeling an aperture in an arbitrarily shaped impedance surface when the aperture surface is closed by replacing it with an impedance surface. It is also demonstrated that the impedance condition over the antenna body and the closed aperture can be non-uniform and anisotropic, and that different choices are possible for the value of the surface impedance of the surface that closes the aperture. It is expected that the procedures described will be most useful in approximately modeling aperture antennas embedded in non-planar impedance surfaces where the aperture electric field is known or can be reasonably approximated.

NOVEL ANTENNAS WITH ARTIFICIAL SURFACES: 2D-FDTD MODELLING

M.K. Karkkainen*
Helsinki University of Technology
Radiolaboratory, P.O. Box 3000, FIN-02015 HUT
Finland
S.A. Tretyakov
Helsinki University of Technology
Radiolaboratory, P.O. Box 3000, FIN-02015 HUT
Finland

The use of an artificial impedance surface to reduce the near field of an antenna in regions where absorptive bodies may be positioned has been introduced in the literature. The impedance layer should be located between the antenna and the bodies which can absorb or disturb the antenna field, thus degrading the antenna performance. The goal is to preserve sufficiently high radiated field in the far zone and still have good screening in the near zone.

We study the radiation of a wire antenna in the vicinity of an impedance surface. The problem arises when considering the radiation of antennas in the vicinity of an artificial impedance sheet used to improve the antenna performance. The antenna support is modelled as a perfect electric conductor rod with quadrilateral cross-sectional shape. For simplicity, we assume uniform structure in the third dimension. One side of the support is covered by a composite layer, which can be modelled with a surface impedance.

To calculate the radiation patterns of the antenna, we construct a 2-dimensional FDTD-model. We embed the quadrilateral PEC-object into the computational zone and cover one side of it. A sinusoidal line-source excitation is located just above the impedance boundary. An efficient and robust update scheme for the field components on the covered surface is developed, and near-field radiation patterns are calculated. In specific applications, some estimates about a suitable size and properties of the screen can be made based on the simulations.

In the special case of an infinite impedance surface, an exact solution can be calculated using the image theory. To validate the model, we increase the screen size and truncate the computational zone with perfectly matching layer boundary conditions, thus enabling comparison to the exact results.

USE OF A CIRCULAR WAVEGUIDE LENS FOR PHASE RETRIEVAL MICROWAVE HOLOGRAPHY AND EMPIRICAL ERROR ANALYSIS

W. Chalodhorn*, D. R. DeBoer
School of Electrical and Computer Engineering
Georgia Institute of Technology
Atlanta, GA

The Misell phase retrieval algorithm for microwave holography requires the capability to axially move an antennas subreflector or feed to obtain a defocused far-field magnitude pattern (Morris, *IEEE A&P Trans.*, **AP-33**, 749-755, 1985). A microwave lens may be used as an alternative method of defocusing an antenna for the situation where the subreflector and feed may not be displaced (Chalodhorn and DeBoer, *URSI abstract*, 24, 2000). A metal-plate lens of quadratic surface shape has been designed and implemented at the Georgia Tech Woodbury Research Facility for such purpose (Chalodhorn and DeBoer, *IEEE A&P Trans.*, in press, June 2002). Even with some artifacts, important signatures of the antenna were successfully revealed, and the results were in good agreement with that obtained from the previously measured phase coherent holography. Limitations however were discovered for this new technique partly due to the polarization dependence of the metal-plate lens.

A circular waveguide lens has therefore been designed and constructed. This lens has no polarization dependence; thus eliminating alignment errors as well as depolarization effects, which occurred when the metal-plate lens was used. Furthermore, to investigate the use of different phase variation profiles, this lens is designed to possess a three-stepped spatial distribution. Even though the phase variation profile of this lens differs from the quadratic profile of traditional defocusing, the measurement shows the results to be comparable with that of phase coherent holography. In addition to the measurements, an empirical error analysis has been performed. The Misell phase retrieval algorithm was performed under different simulated conditions, and the results were compared with the model to obtain retrieval errors. The effects of measurement noise, lens transfer function error, and the amount and spatial distribution of the phase variation on the phase retrieval have been obtained. Preliminary study also indicates that a better retrieval may be achieved using a non-quadratic phase variation profile.

MUTUAL COUPLING OF TWO COLLOCATED DIFFERENTLY ORIENTED LOOP ANTENNAS

Gary Fridman
University of Illinois at Chicago
ECE Department (M/C 154)
851 South Morgan Street
Chicago,Il.,60607

The mutual coupling of two identical thin wire loop antennas with arbitrary orientations and with a common center is analyzed. The main motivation for this work is design of a complete polarization diversity antenna which has three differently oriented collocated circular loops. In this work, for the sake of simplicity, we consider only two loops each driven by a delta function generator. The classical theory of thin wire loop antennas is used to form two integral equations for the currents on the surface of the loops, which are then solved by a conventional Fourier series expansion method. The Fourier coefficients are easily computed using modern computational tools such as MathCAD. Input admittances of each loop are obtained as functions of electrical size of the loops and of the relative orientation angles. This work is limited to electrical sizes of the loops being smaller that half the wavelength. In this case only the first two terms of the Fourier coefficients of the currents remain significant. Using the admittance matrix derived in the above fashion, self-admittance of the loops is compared with their mutual admittance to evaluate the relative importance of the loop coupling. Two special cases of the coupling currents in the loops are discussed. Firstly, in the mutual coupling of two orthogonal loop antennas only unbalanced coupling currents are found to occur. Secondly, in the mutual coupling of the two loop antennas the angles between which is slightly smaller than 90 degree, the induced current is the result of the first case plus an additional term which is proportional to the tilt angle.

A PHASED ARRAY USING OSCILLATORS COUPLED ON A TRIANGULAR GRID

R.J. Pogorzelski
Jet Propulsion Laboratory
California Institute of Technology
4800 Oak Grove Drive
Pasadena, CA 91109-8099

During the past few years it has been demonstrated by several authors that an array of mutually injection locked oscillators coupled to nearest neighbors on a Cartesian grid can be used to control the aperture phase of a phased array antenna. [R. A. York, IEEE Trans., MTT-41, pp.1799-1809] [P. Liao and R. A. York, IEEE Trans., MTT-41, pp. 1810-1815] [R. Ispir, S. Nogi, M. Sanagi, and K. Fukui, IECE Trans. Electron., E80-C, 1211-1220, Sept. 1997] [R. J. Pogorzelski, Microwave and Guided Wave Letters, 10, pp. 478-480.] [J. Shen and L. W. Pearson, 2001 Nat. Radio Sci. Mtg, Boston, MA] A linear phase distribution can be established in which the rate of phase progression is controllable via adjustment of the tuning (free running frequency) of the oscillators on the perimeter of the array. The set of oscillator output signals is suitable for excitation of an array of radiating elements equally spaced on a Cartesian grid thus producing a steerable radiated beam.

In this paper a triangular array based on this principle is proposed. The oscillators are coupled to nearest neighbors on a triangular grid rather than a Cartesian one. This implies that each oscillator is directly coupled to six others instead of four. The boundary of the array is an equilateral triangle. (Rhombic and hexagonal boundaries are also possible but are much less convenient to analyze in the manner presented herein.) Analysis of the dynamic behavior of the proposed array is carried out using a linearized continuum model. [R. J. Pogorzelski, P. F. Maccarini, and R. A. York, IEEE Trans., MTT-47, 463-470, April 1999] Solution of the resulting partial differential equation over the triangular region is facilitated by the use of the eigenfunctions of a triangular waveguide. [P. L. Overfelt and D. J. White, IEEE Trans. MTT-34, 161-167, Jan. 1986] It is shown that the array behavior is isotropic and that, while the response of the array is slower than that of the corresponding Cartesian array, individual oscillators in a triangular array may be tuned further from the ensemble frequency without losing lock than is the case in a Cartesian array. The detuning of the oscillators necessary to effect beam steering is shown to be constant along the edges of the array as is the case in the Cartesian array.

A POYNTING-VECTOR APPROACH TO DETERMINE WHERE RADIATION ORIGINATES FROM THE SURFACE OF A PERFECT CONDUCTOR

E.K. Miller
Consultant
Santa Fe, NM 87506-1213

If one asks, "Where, and in what amount, does far-field power originate from over the surface of a perfect electric conductor (PEC) on a per-unit-length or -area basis?," the usual reaction ranges over responses like: "This is not a sensible question to ask," or "Why would we need to know?," or "This is an interesting question but it is probably not answerable.

It's ironic, given the revolution in problem-solving capability brought about by the computer, that ever larger and more-complex problems are being routinely modeled, and yet one of the most fundamental aspects of electromagnetic fields seems to resist resolution. The author has reported previously on a procedure called FARS (Farfield Analysis of Radiation Sources) (E.K. Miller, *IEEE AP-S Magazine*, **41**, 82-86, 1999), which seems to provide a physically plausible answer to the above question. Although no analytical proof has been developed to confirm its validity, results from FARS have been found to be in agreement with earlier, very different work (S.A. Schelkunoff and C.B.Friedman, *Proceedings of the IRE*, **30**, 511-516, 1942).

An alternative to FARS, which incorporates the tangential divergence of the Poynting vector at the surface of a PEC and is denoted as PVRAD, is demonstrated here. While the Poynting vector at the surface of a PEC is derivable from the normal electric field and tangential magnetic field, these fields can be more simply expressed in terms of the current and charge densities on that surface. PVRAD is described and results presented for several wire objects for comparison with FARS. For a straight wire dipole 10 wavelengths long, the surface Poynting vector is found to exhibit a monotonic decrease from the feedpoint, the normalized divergence of which is found to be graphically indistinguishable from the FARS results except in the near-vicinity of the feedpoint. The feedpoint difference can be attributed to the fact that PVRAD automatically incorporates the influence of the exciting field through the latter's effect on the current and charge while FARS does not. Generally similar agreement, to within a few per cent, if found for a straight wire excited by a plane wave incident at various angles. For a bent dipole and circular- and square-loop antennas, the results are qualitatively similar to FARS, but there are significant differences, whose cause is speculated to be due to near-field coupling effects. The implications of these results concerning the question "Where does radiation come from?" are considered.

TRANSIENT ELECTROMAGNETIC FIELDS OF A LINEAR ANTENNA

Mattos, M.A.F. *
Okime Eletromagnetismo Aplicado
rua Vicente Stancato 590, Baro Geraldo
13085-121,Campinas, SP, Brazil
Ramirez,F.F.
FEEC,UNICAMP
Cidade Universitria,Campinas, SP,Brazil

It has been a major problem to predict the electric and magnetic fields generated by transients on transmission lines. These lines can be an antenna, a lightning channel, structures, grounding meshes, power transmission lines, etc. Traditionally, the way to obtain these fields are on frequency domain which is practical for many purposes on EMC, however, for transient pulses the time domain equations are needed.

The time domain electromagnetic fields integral-differential equations are obtained for a dipole antenna. The integral-differential equations were derived from the Maxwell Equations and the general formulation from the Electric Potential and the Magnetic Potential Vector. The development of these equations is shown on this paper. Some comparison were done with experimental results, and with very traditional and well known analytical results.

Measurements of the electromagnetic fields generated by a transmission line were performed and compared with numerical calculations based on these equations discretised using finite difference on time domain. The transmission line simulation was performed with TLM (Transmission Line Method).

Measurements were done with a wire over a conducting ground plane. A generator at one end fed the wire transmission line. That line was parallel to the ground plane with one meter long and 0.205m height. The generator had out put impedance of 50 W and was connected to the line with a 50 W coaxial cable. At a distance of 0.374m from the input a linear antenna was fixed for measuring the vertical field. Two results were obtained for comparison, one for the line short-circuited and the other for the line matched.

The integral-differential equations in this work are also compared to well known analytical solutions.

COMPUTER AIDED CALIBRATION OF FAR-FIELD OF THE OFF-SET OPTICAL CASSEGARIAN ANTENNA

C. Dasgupta
Department of Electrical Engineering
Indian Institute of Technology
Kanpur, India 208016

Successful calibration of the computer aided measurement of the far field with the help of x-band horn with 150 mw output klystron tube tuned to mode at 9 GHz by means of A/D Card 207 along with PC 486 had been reported at the recent 2001 IEEE/URSI International Symposium at Boston by the author.

A fan beam type of Cassegarian unit with planar metal-dielectric feeder has been synthesized semi-empirically, which shows multimode response at 11 GHz and 17 GHz. But due to non-availability of the high powered Klystrons particularly at these frequencies direct measurement of radiation pattern of the far-field could not be done for the Cassegarian structure.

Computer-calibration of the set-up had been done earlier with PC 486 with lower speed A/D Card 207 which is being planned to be up-graded for IBM Pentium III with higher speed card.

High power optical source whether at 850 nm and 1550 nm are already in the Department. Corresponding computer aided calibration of the set-up at optical range has already been done in the laboratory.

The work is being planned to study the far-field of the off-set optical Cassegarian antenna, which by virtue of its small size can be demonstrated at the time of presentation.

If high powered 11 GHz and 17.5 GHz Klystron sources are available (or with the help of IIT Delhi, BEL Ghaziabad), the radiation patterns of Fan-beam Cassegarian-Antenna Unit with planar metal-dielectric feeder will also be presented.

INPUT IMPEDANCE OF MICROSTRIP PATCH ANTENNAS USING NEURO-COMPUTING

Pattnaik, S.S Panda D.C
Electronics and Communication Engineering
NERIST, Nirjuli-791109, India.
Devi, S.
Computer Science and Engineering
NERIST, Nirjuli-791109, India.

A new method of using Artificial Neural Networks (ANNS) for the accurate determination of input impedances of microstrip patch antennas has been adopted in this paper. The results using ANNs are compared with the experimental findings, theoretical values and with the simulated results obtained using IE3D. The ANNs results are more in agreement with the experimental findings. Input impedances of rectangular microstrip patch antenna and circular microstrip antenna are considered for different modes.

The Current focus on electronics packaging and interconnects in wireless technology has led to design of efficient, wide band, low cost, low SAR and small volume antennas which can readily be incorporated into a broad spectrum of systems. The calculation of exact feed point impedance i.e input impedance for best matching is extremely difficult for coax fed small volume microstrip antennas specially when the size is drastically small. The ability and adaptability to learn, generalizability small information requirement, fast real time operation and ease of implementation features of ANNs have been exploited in this paper for accurate determination of input impedance of microstrip antennas. 20 patterns each in (1,0) mode and (0,1) mode have been tested to see the accuracy of the model incase of rectangular microstrip patch antenna where as 29 patterns in (2,1) mode and 19 patterns in (1,1) mode are tested incase of circular microstrip patch antennas. The testing time is less than a second for all the patterns where as the training time is below 3 minutes in P-III (833 Mhz) HP Brio Pc. For (1,0) mode the average error is 1.57 ohms per pattern and that for (0,1) mode is 0.8 ohm per pattern. Incase of circular microstrip antenna for (1,1) mode the average error is 0.62 ohm per pattern and for (2,1) mode it is 1.46 ohms per pattern.

Application of ANNs for the calculation of input impedance of microstrip antennas is a simple, inexpensive and accurate method having a very good agreement with the experimental results. Acknowledgement: Thanks are due to MHRD, Govt. of India for sponsoring the project.

ANTENNA SYSTEMS FOR FOCUSING ELECTROMAGNETIC ENERGY IN A POINT.

Vasilchenko S.D.
02217 Kiev, Zakrevskij str. 13, 255
Kiev, 02217 Ukraine

The new class of aerials is offered - aperture-focusing systems. These are dual-reflector and reflector-lenses antennas systems of a microwave-range. The feature of such antennas is ability to focus electromagnetic energy in a point of space, which is on small (tens lengths of waves) distance from the aperture. The number of the electrical circuits (schemes) multifunctional antennas systems with improved electrical and operating performances was developed. Such structures allow to work simultaneously on several frequencies and in a wide range of lengths of waves (from 10 up to 2 sm), and also to realise angular scanning in two mutually perpendicular planes without noticeable increase aberration.

The parameters are considered and the technique of their measurements allowing to describe a feature of new sorts antennas systems and them to estimate objectively is offered. For such antennas systems the new parameters are entered: geometrical resolution (diameter focal stain and depth of sharpness) and focusing coefficient. The techniques of account based on principles of radial optics, allowing to synthesise of dual-reflector antenna systems with various configurations are developed.

Aperture focusing antenna system can be applied to receive (or transmission) and space processing of signals in remote monitoring kits and equipment of radiovision. These kits are intended for solution of the specific tasks of electromagnetic compatibility, control of electrotightness of the equipment, medical diagnostics and destruction of electronic devices of a unauthorised control and number others. The offered technical solutions and circuits of antenna systems, which were developed, have not known analogues.

Session B5 8:35-Fri.

NUMERICAL STUDIES

Chairpersons: D.V. Thiel and R.D. Nevels

ABSORBING BOUNDARY CONDITIONS IN LOSSY MEDIA FOR THE IMPEDANCE METHOD

Professor David V. Thiel
Radio Science Laboratory
Griffith University
TEN 3:12 Nathan
Qld Australia 4111
Glenn Wilson
Radio Science Laboratory
Griffith University
Nathan
Qld Australia 4111

A self-consistent impedance method has been developed for the numerical solution of Maxwell's equations in media (Thiel Mittra, Radio Science, 2000). A single cell absorbing boundary condition was developed for one dimensional modelling in air (Thiel Mittra, Asia Pacific Microwave Conference, 2000). This boundary condition achieved reflection coefficients of less than -50 dB at the frequency of interest. The application of the impedance method to numerical modelling of electromagnetic surface impedance has now been developed, however, to date, an absorbing boundary condition (ABC) at the bottom of a lossy earth layer has not been successful. In this paper, the use of a single cell layer to provide accurate surface impedance data over inhomogeneous horizontal layers overlying an infinitely deep basement is presented.

The impedance method of numerical modelling requires the discretization of the solution space with rectangular or triangular cells bounded by elements with a lumped impedance element on each side related to both the electromagnetic properties of the medium and the size of the cell. The modelling is performed in the frequency domain and the bandwidth of the impedance boundary condition is quite narrow. Despite this, very high absorption rates can be achieved at the precise frequency of interest. The success of the ABC, even at normal incidence, allows successful surface impedance modelling for geophysical exploration applications.

In this paper, the self-consistant impedance method for surface impedance determination will be reviewed. The single cell width ABC will be presented for both air and lossy media. Various applications of the impedance method to both forward and inverse modelling of surface impedance measurements will be discussed.

NUMERICAL IMPLEMENTATION OF THE MODIFIED ELECTRIC FIELD INTEGRAL EQUATION FOR INFINITE AND LARGE, FINITE ARRAYS

F. Capolino, D. R. Wilton
Dept. of Electrical and Comp. Engineering
University of Houston
4800 Calhoun Rd.
Houston, TX 77004-4005
R. J. Adams
Dept. of Electrical and Comp. Engineering
University of Kentucky
Lexington, KY 40506-0046

A new regularization method, the modified electric field integral equation (MEFIE), obtained by successively applying the standard EFIE operator (R. J. Adams and G. S. Brown, *Electronics Lett.*, **35**, 2015-2016, 1999) is investigated for its application to array problems. The new integral operator possesses the important property of being stable with respect to discretization, and is generally well-conditioned for both the high- and low-frequency limits.

Some numerical issues will be discussed pertaining to the numerical discretization of the MEFIE in the 2D case. These include the choice of basis and test functions, computation of the composite MEFIE operator, analysis of the condition number with increasing discretization and decreasing frequency, and combining the MEFIE with the magnetic field integral equation to eliminate internal resonances. The algorithm for the evaluation of the discretized operator is particularly crucial since one would like to reuse the discretization and evaluation schemes already developed for the standard EFIE without compromising accuracy. A few possibilities will be discussed and compared.

It will be shown that the principal numerical advantages of the MEFIE as applied to finite scattering bodies are still preserved when dealing with infinite arrays. Indeed, when the array elements are closed bodies, the MEFIE operator is compact.

When the new MEFIE is applied to the analysis of large bodies, it naturally incorporates high-frequency effects. Truncation effects in 2D large arrays are well-described by localized cylindrical waves arising from the array edges; the MEFIE numerically recovers this trend since its forcing term incorporates diffraction from the array edges. Furthermore, a new way to precondition the finite array problem is shown, based on combining the solution of the infinite array with the MEFIE. The new composite operator is compact and tends to the identity operator for interior array elements.

AN ITERATIVE PROCEDURE FOR CONSTRUCTING INVERSE OPERATORS FOR BOUNDARY INTEGRAL EQUATIONS

R. J. Adams*
University of Kentucky
B. A. Davis
Virginia Tech

It is possible to represent many scalar and vector field problems via formulations akin to second kind integral equations (SKIEs). An important consequence for numerical simulations is a reduced iteration count. This can be attributed to the determination of problem formulations that directly incorporate the physics of a scattering problem. However, such formulations are not sufficient to address several remaining problems, including multiple right-hand sides and nearly resonant geometries. In this presentation we address these problems by iteratively constructing the inverse operator.

Consider the 3-D SKIE parameterized by the complex constant α: $\psi(x;\alpha) = \psi^i(x) + \alpha P\psi(x;\alpha)$. The free-space bounary operator P is independent of α. Denote the eigenvalues of P by λ_P. We seek the inverse $(I-\alpha P)^{-1}$ at $\alpha = 1$. A straightforward method for obtaining the desired inverse is via an analytic continuation from $\alpha = 0$ to $\alpha = 1$. The appropriate continuation path in the α-plane is determined by the zeros of $(I-\alpha P)$. These are located at the inverses of the eigenvalues of P, $\alpha = \lambda_P^{-1}$. Hence, the use of an appropriate integral formulation is essential to the efficiency of this approach. This will be demonstrated by considering various boundary integral equations. It will also be shown that the proposed continuation method allows for the exponential summation of multiple-scattering interactions.

To be practically useful, an efficient representation must be used for the operator at each point along the continuation path. However, many "fast" algorithms (such as FMM) rely on the specific properties of the free-space Green function. It appears somewhat difficult to modify these algorithms in order to efficiently represent $(I - \alpha P)^{-1}$ when $\alpha \neq 0$. We introduce an alternate compression algorithm that can be used for all α and does not rely on the separation of the operator into near and far regions. When combined with the preceding continuation algorithm, this yields a single-level inversion algorithm requiring $O(N^2)$ floating point operations and $O(N^{1.5})$ storage. Each application of the inverse to an incident vector requires $O(N^{1.5})$ operations. A multilevel implementation is expected to yield additional savings.

3-D CAD-BASED MESH GENERATOR FOR A LOCALLY CONFORMAL FDTD ALGORITHM

G.W. Waldschmidt*, A. Taflove
Northwstern University
Evanston, IL 60208

The finite-difference time-domain (FDTD) method is a second-order accurate method for solving Maxwells equations. However, it is well known that due to its regular orthogonal grid, it is subject to error in geometry generation due to staircasing that may be significant for certain structures. Various techniques have been proposed to reduce this error, but locally conformal algorithms have been shown to be the most accurate and stable. This paper will focus on one such method, the Dey-Mittra FDTD (D-FDTD) method. Dey-Mittra (and independently other authors) showed that the D-FDTD method exhibits significant improvement relative to the standard FDTD algorithm. Since locally conformal methods are based on a standard FDTD grid, they require minimal alteration of existing FDTD codes. Their additional complexity lies solely in the geometry generation and the calculation of edge lengths and cell areas.

In a 2000 article in the IEEE Antennas and Propagation Society Magazine, Dey-Mittra reported the formulation of a mesh generator for this purpose. In this paper, we present the formulation and validation of an alternative mesh generator which may be more robust than that reported by Dey-Mittra for arbitrary 3-D PEC geometries. Our mesh generator is capable of importing 3-D geometries from AutoCad and ProE. It models either scattering or resonating structures and is built on a finite-element (FE) mesh generator. The FE mesh is an irregular, non-orthogonal grid consisting of planar facets created to model the geometry. This mesh is imported into the D-FDTD mesh generator and is then superimposed onto a Cartesian FDTD grid. The intersection points of the FE geometry with the FDTD grid are evaluated and the appropriate edge lengths and areas are modified. Care is taken to distinguish between the wide variety of potential intersections of the faceted FE surface and the local FDTD grid cells.

The accuracy of this D-FDTD mesh generator has been determined via comparison with published results by Railton and Schneider (IEEE Trans. Microwave Theory and Techniques, 1999 pp. 56-66) for the resonant frequencies of cylindrical and spherical cavities. It is shown that the new mesh generator yields an accuracy comparable to that reported in this article. Current work involves applying this tool to microwave devices for use in particle accelerators.

A METHOD FOR IMPLEMENTING INTERLEAVING IN THE NUMERICAL SOLUTION OF PROPAGATOR EQUATIONS

R.D. Nevels* and C-S Shin
Department of Electrical Engineering
Texas AM University
College Station, Texas

A full wave Feynman path integral solution for the electromagnetic field based on the time domain form of Maxwells differential equations has recently been published (R. D. Nevels, J. A. Miller, and R. E. Miller, A Path Integral Time Domain Method (PITD) for Electromagnetic Scattering, IEEE Trans. Antennas Propagat., April, 2000). The path integral is a propagator method. That is, the field evolves through one time step in space when convolved with the propagator, an expression closely related to the time domain Greens function.

The PITD has potential as a new scattering technique, but as yet it can only be applied to dielectric scatterers, not perfect conductors. Difficulties in handling perfect conductors can be traced to the fact that its solution is in a form known as a phase space path integral. A numerical method for evaluating the phase space path integral is easily devised. In fact one can simply select a fixed time step, determined by the size and physical complexity of the scattering object, and replace the forward and inverse Fourier transforms with discrete Fourier transforms. However, with this method all of the electromagnetic field components must be computed at each point in the numerical space. This can be an advantage because contours of scattering objects can be modeled with a high degree of accuracy. On the other hand, the drawback of this method as compared to techniques in which the field is interleaved, is that both the tangential magnetic field and the normal electric field must be computed on the surface of perfect conductors. In order to satisfy boundary conditions, these field components require knowledge of the present time current and charge, which can only be found by the tedious procedure of solving an integral equation.

In this presentation we will describe how to derive the finite-difference time-domain method (FDTD) equation set using the propagator method. We will then show how to improve the accuracy of the FDTD equation set from the standpoint of the propagator formulation. Finally we will show how the PITD method can be reformulated to incorporate spatial interleaving, thereby allowing wave scattering from perfect conductors. Results will be given for scattering from a conducting plate and cylinder and compared with those obtained by the FDTD method.

INVESTIGATION OF GENETIC ALGORITHM GENERATION OF WAVELETS FOR SPHERIC CLASSIFICATION.

Y. Hill, S.G. O'Keefe, D.V. Thiel
Radio Science Laboratory
Microelectronic Engineering
Griffith University, Nathan, QLD, 4111
AUSTRALIA

The wavelet transform (WT) is an accepted transient identification technique in many diverse areas. The difficulty faced by potential users of the WT, particularly in the field of identification, is the selection of the original wavelet function or mother wavelet. Apart from generalised suggestions relating a recognised group of wavelets for compression and another group for analysis, there are no guidelines for selection in order to obtain optimal performance in discrimination. Wavelet selection is vital for good frequency and time resolution, in addition to signal identification.

This paper describes the development of a far field lightning stroke identification wavelet required for a surface impedance measurement device, known as the Lightning Surface Impedance Meter (LSIM). A Genetic Algorithm (GA), using real valued chromosomes, for efficiency, was used to generate populations of wavelets. The chromosomes represent the phase, frequency and amplitude of Blackman windowed trigonometric functions. Various numbers of dilations of each wavelet were used in the wavelet transform. Great care must be taken when allowing a GA to generate wavelets to ensure the rules of design are obeyed. Normalisation and windowing functions have been employed in the GA. The GA was implemented using the Genetic Algorithms for Optimisation Toolbox (GAOT) in Matlab developed by Houch, Joines and Kay.

These wavelets were trialed against a large number of pre-recorded spherics. The spherics were recorded on the earths'surface at various sites exhibiting different surface impedance. The fitness of each member of the population was calculated by the integral of the square of the wavelet transform coefficients. Results showed that successful wavelets mimicked the high power frequency components of the spheric, with the most successful wavelets homing in on harmonic relationships in the spherics. Using this technique we hope that more suitable wavelets can be bred to optimise classification and maximise the identification of spherics.

Session B6, 13:35-Fri.

FAST METHODS IN ELECTROMAGNETICS

Chairpersons: E. Michielssen and J.L. Volakis

FAST PLANE WAVE TIME DOMAIN ALGORITHMS FOR QUASI-PLANAR STRUCTURES

E. Michielssen, Department of Electrical and Computer Engineering, University of Illinois at Urbana-Champaign
A. Boag, Department of Electronic Engineering, Tel-Aviv University
B. Shanker, Department of Electrical and Computer Engineering, Iowa State University

The recently developed plane wave time domain (PWTD) scheme (A. A. Ergin, B. Shanker, and E. Michielssen, Journal of Computational Physics, vol. 146, no. 1, pp. 157-180, 1998) permits the fast marching on in time (MOT) based solution of time domain integral equations (TDIEs) pertinent to the analysis of scattering from arbitrarily shaped scatterers. The PWTD scheme is the extension of the frequency domain fast multipole algorithm to the time domain. Not unlike the fast multipole method, the PWTD scheme assumes that the scatterer is subdivided into subscatterers and accounts for interactions between subscatterers that are far removed from one another through plane wave expansions that cover all 4 Pi directions. PWTD enhanced MOT solvers permit the analysis of scattering from three-dimensional surface structures in $O(N_t N_s log^2(N_s))$ operations (here N_t and N_s denote the total number of time steps and spatial unknowns in the problem) as opposed to $O(N_t N_s^2)$ operations for classical MOT solvers.

Because PWTD algorithms apply to arbitrarily shaped scatterers, they are suboptimal for analyzing scattering from quasi-planar structures, viz. structures whose transverse dimensions far exceed their height (rough surfaces, microstrip antennas on a finite ground plane, etc.). Indeed, it is intuitively clear that for such scatterers knowledge of the far-field behavior in a narrow cone surrounding the transverse plane suffices to account for interactions between far removed subscatterers and that processing full radiation patterns is wasteful. Here, an algorithm that formalizes these ideas is presented. In essence, the proposed scheme is an extension of the steepest descent fast multipole scheme (V. Jandhyala et al., IEEE Trans. Geoscience and Remote Sensing, vol. 36, No. 3, pp. 738-749, 1998) to the time domain. Unlike the latter scheme, which expands fields radiated by subscatterers comprising a quasi-planar structure along a steepest descent path, the time domain scheme represents transient fields radiated by quasi-planar sources in terms of windowed Whittaker-type expansions of the propagator in homogeneous plane waves. It is demonstrated that no single window function can cover the range from DC to the highest frequency of interest; hence the temporal signature of the sources is described in terms of a multiresolution basis comprised of approximate prolate interpolants that are devoid of DC components. The computational complexity of the new PWTD scheme scales as $O(N_t N_s log(N_s))$.

MULTILEVEL FAST MULTIPOLE METHOD FOR VOLUMETRIC STRUCTURES

Kubilay Sertel
University of Michigan
John L. Volakis
University of Michigan

The fast multipole method and its multilevel versions have been shown to reduce memory and CPU requirements down to O(NlogN) and have therefore been extensively applied for solving full scale aircraft, large finite arrays in minutes and hours as compared to hours and several days in the past. A 200,000 unknown matrix solution can now be carried out in 2-3 minutes (per iteration) on a desktop, and millions of unknowns can be solved on processors that can be purchased for a few thousand dollars. These speed-ups have been demonstrated for mostly metallic structures.

In this paper we describe the development of MLFMM for dielectric and composite structures using a volumetric formulation. A volumetric, equivalent current formulation is utilized to construct the integral operators and curvilinear hexahedral elements are introduced to reduce the degrees of freedom for accurate modeling. Two different basis functions are employed in the context of this volumetric formulation and these are compared in terms of accuracy and efficiency. We also describe the achievable speed-up before and after parallelization of the MLFMM algorithm. Issues relating to element grouping for MLFMM application, converge of iterative solvers and improvement of these for speed-up are also discussed.

The hybrid finite element-boundary integral (FE-BI) method is another approach for modeling composite structures, and it is therefore important to compare it with corresponding volume integral equation (VIE) simulations. For a selected set of geometry the FE-BI and VIE methods (both with MLFMM implementations) will be compared and discussed in terms of accuracy and speed-ups when identical discrete geometry models are used.

FAST TIME DOMAIN INTEGRAL EQUATION ALGORITHM

Bleszynski, E.H., Bleszynski, M.K., Jaroszewicz, T.
Monopole Research
Thousand Oaks, CA

We propose a fast time domain integral equation based solution technique which utilizes a simultaneous impedance matrix compression in space and time.

Our problem is to solve a time domain integral equation which can be written, in a generic form, as:

$\int$

Discretization in time and space leads to a matrix equation

Σ

where $\alpha, \beta = 1, ..., N_s$ denote the spatial and $\mu, \nu = 1, ..., N_t$ the temporal indices. It follows from causality, from the translational invariance of the Green's function and from the uniform and nonoverlapping discretization in time, that the matrix A is block lower-triangular and block-Toeplitz in time indices.

Fractal pattern-application of a recursive scheme.

On each level of recursion k, matrix $A_s w$ can be alternatively represented as composed of $N_s \times N_s$ blocks of size $\nu_k \times \nu_k$, $\nu_k = N_t/2^k$, each of them Toeplitz and lower triangular.

Application of the FFT type compression in spatial indices, analogical to that described in (E. H. Bleszynski, M. K. Bleszynski, T. Jaroszewicz, *Radio Science*, **31**, 1225-1251, 1996, O. P. Bruno, L. E. Kunyansky, *Caltech preprint*, 2000) but on the block level, and utilizing temporal Toeplitz properties and lower triangularity of every block result in the the total operational count of $O(N_t N_s log^2 N_t log N_s)$ and $O(N_t N_s^{4/3} log^2 N_t log N_s)$ for surface and volume problems respectively.

We stress that the proposed method relies only on the *translational invariance* of the Green's function, and not on its specific analytic form. Therefore, it is applicable directly and at no additional cost to *dispersive* media and to such *layered* media for which the Green's function is translationally invariant. Also, since the proposed algorithm does not depend on a specific analytic form of the Green's function, it is free of the anti-casual ghost signal effect and no subdivision of the source signal into subsignals to gate out the ghost signal is required.

FAST TIME DOMAIN INTEGRAL EQUATION ALGORITHM FOR DISPERSIVE MEDIA

Bleszynski, E.H., Bleszynski, M.K., Jaroszewicz, T.
Monopole Research
Thousand Oaks, CA 91360

We discuss aspects of the implementation and applications of a new *superfast* time-domain integral equation solution technique reported recently in (E. H. Bleszynski, M. K. Bleszynski, T. Jaroszewicz, *2001 IEEE APS Symposium*, **4**, 176-179, 2001). The essential element of the algorithm is the Fast Fourier Transform (FFT)-type impedance matrix compression carried out *simultaneously* in space and time. Realization of the FFT-type compression relies exclusively on the *translational invariance* of Green's function and not on its specific analytic form. Therefore the resulting computational complexity of the solution, $O(N_t\,N_s\,\log N_t\,\log(N_t\,N_s))$ and $O(N_t\,N_s^{4/3}\,\log N_t\,\log(N_t\,N_s))$ for surface and volume problems respectively, is independent of the degree of dispersion (N_t and N_s are the numbers of temporal and spatial sampling points). The spatial compression technique used in the approach is analogous to that described in (E. H. Bleszynski, M. K. Bleszynski, T. Jaroszewicz, *Radio Science*, **31**, 1225-1251, 1996) as well as that of (O. P. Bruno, L. E. Kunyansky, *J. Comp. Phys.*, **169**, 80-110, 2001) which employs an improved choice of auxiliary, far-field equivalent sources. The method is therefore applicable to arbitrarily shaped 3-d geometries and is particularly advantageous for dispersive media.

The time domain integral equation we aim to solve can be written in a generic form as $\int dt'\,d\mathbf{r}'\,K(t-t',\mathbf{r}-\mathbf{r}')\,x(t',\mathbf{r}') = b(t,\mathbf{r})$, where K is the integral operator, x the solution (e.g. the unknown currents), and b the incident field. Discretization in time and space leads to a matrix equation $\sum_{\nu=1}^{\mu}\sum_{\beta=1}^{N_s} A^{\mu\nu}_{\alpha\beta}\,x^{\nu}_{\beta} = b^{\mu}_{\alpha}$, where $\alpha,\beta = 1,\ldots,N_s$ denote the spatial and $\mu,\nu = 1,\ldots,N_t$ the temporal indices. Causality, translational invariance of Green's function, and the uniform temporal discretization with nonoverlapping basis functions imply that the matrix A is block lower-triangular and block-Toeplitz in time indices (the blocks $A^{\mu\nu}$ depend only on the difference of time indices, $\mu-\nu$). In contrast to the conventional Marching-on-in-Time (MOT) scheme which is based on block forward substitution, our approach uses the "divide and conquer" solution strategy relying on both the block lower triangularity of the impedance matrix and its block Toeplitz property. Implementation of simultaneous temporal and spatial compression is possible by utilizing two alternative representations of the impedance matrix. The first is a block Toeplitz structure with blocks labeled by temporal indices, and the second is a matrix composed of Toeplitz blocks labeled by spatial indices. Spatial compression is then carried out as a time-independent transformation of the far-field component of the impedance matrix to its Toeplitz form.

Applications of the proposed method to different integral equation formulations and different discretizations will be discussed.

This work was partially supported by the AFOSR, Contract F49620-01-1-0504.

FAST MULTIPOLE METHOD AND MICROLOCAL DISCRETIZATION FOR THE 3-D WAVES EQUATIONS

E. Darrigrand*
CEA/CESTA - DEV/SIS
BP 2, 33114 Le Barp, FRANCE
Eric.Darrigrand@math.u-bordeaux.fr

We are concerned with integral methods applied to the solution of the waves equations where the linear system is solved using an iterative method. We need to perform matrix-vector products whose time and memory requirements are increasing as a function of the wave number κ. A lot of methods have been developed in order to speed up the matrix-vector product calculation or to reduce the size of the system. Microlocal discretization methods enable one to consider new systems with reduced size. The version of this kind of methods according to T. Abboud, J.-C. Ndlec and B. Zhou enables one to consider a new system whose size is of order $\kappa^{2/3} \times \kappa^{2/3}$ instead of $\kappa^2 \times \kappa^2$ ([1]). However, in their method, due to the geometrical approximation of the surface, the fine mesh of the standard case is still considered. Another method, the fast multipole method introduced by V. Rokhlin ([2]), is one of the most efficient and robust methods used to speed up the calculation of matrix-vector products. It enables one to obtain a calculation of matrix-vector products of complexity $\mathcal{O}(\kappa^3)$ using the one-level method and $\mathcal{O}(\kappa^2 \ln^2(\kappa))$ using the multilevel one. We have studied a coupling of these two recent methods for the 3-D Helmholtz equation. It enables one to reduce the CPU time very efficiently for large wave numbers. Satisfactory numerical tests have also been obtained to confirm the theoretical study within a new integral formulation written by B. Després ([3]). Results was obtained for a sphere with a size of 26λ by a resolution based on a mesh with an average edge length about 2λ where λ is the wavelength. Results was also obtained for an industrial test case. We now study the coupling for Maxwell's equations and we will be able to give results for the Maxwell's equations. Perpectives also concern another microlocal discretization method due to A. de La Bourdonnaye.

[1] T. Abboud and J.-C. Nédélec and B. Zhou, *Improvement of the Integral Equation Method for High Frequency Problems* , 3rd international conf. on math. aspects of wave propag. phen., SIAM, 1995.

[2] R. Coifman and V. Rokhlin and S. Wandzura, *The Fast Multipole Method for the Wave Equation: A Pedestrian Prescription* , IEEE Ant. and Prop. Mag., June 1993.

[3] B. Stupfel and B. Després, *A Domain Decomposition Method for the Solution of Large Electromagnetic Scattering Problems* , J. Elect. Waves and Appl., 1999.

Session B7, 9:15-Sat.

ELECTROMAGNETIC THEORY AND EXPERIMENTS

Chairperson: R.M. Jones and W.A. Imbriale

IMAGINARY PART OF THE GROUP REFRACTIVE INDEX

R. Michael Jones
CIRES
University of Colorado
Boulder, CO 80309-0216, USA

The group refractive index $n' = d/d\omega(n\omega)$ can be complex if the complex phase refractive index n is complex, as it would be for propagation in an absorbing medium. The real part of the group refractive index is known to be proportional to the travel time of a pulse. The imaginary part can be shown (NOAA Tech. Memo. ERL WPL-80, 1981. PB82161977) to be proportional to the frequency derivative of the absorption coefficient.

$$\Im(n') = -c\frac{d\alpha}{d\omega},$$

where c is the free-space speed of light, and α is the absorption coefficient for a wave whose amplitude varies as $\exp(-\alpha z)$.

A pulse will have its peak frequency shifted by an amount proportional to $\Im(n')$ and the distance traveled, and inversely proportional to the curvature of the frequency transform of the pulse peak. For a Gaussian-shaped pulse $\exp[-(t/\tau)^2]$, the frequency shift will be given by

$$\delta\omega = \frac{2z\Im(n')}{c\tau^2},$$

where z is the distance traveled and τ is the pulse length.

For an inhomogeneous medium, the frequency shift is

$$\delta\omega = \frac{2\Im(P')}{c\tau^2},$$

where

$$P' = \frac{d}{d\omega}[\omega P(\omega)]$$

is the complex group path,

$$P = \int_{raypath} \mathbf{n} \cdot \mathbf{ds}$$

is the complex phase path, $\mathbf{n}$ is a vector pointing in the wave normal direction whose magnitude equals the complex phase refractive index, and $\mathbf{ds}$ is a vector pointing in the ray direction.

NEW NONUNIFORM TRANSMISSION LINE EQUATION

Yaowu Liu*, K. K. Mei
Dept. of Electronic Engineering
City University of Hong Kong
Kowloon, Hong Kong

Nonuniform transmission line is widely used in MMIC and microwave devices. The applications of the nonuniform transmission line, such as filters, power dividers, directional couplers and resonators, have been studied for decades by many authors. Most of investigations have paid great attention to wave interaction with the transmission lines. The nonuniform transmission line, including continuously varying transmission line, can be generally treated as a cascading of many short uniform transmission lines, so the discontinuities produced by any two neighbouring segments in the nonuniform transmission line should be considered. Although the radiation generated by the discontinuities is observed for a long time (Naishadham, et al.,IEEE Trans. Elctromagn. Compat., 35, 159-169, 1993), no one has given us any circuit model to take account of the radiation from the discontinuities of the nonuniform transmission line itself. Thus, the conventional nonuniform transmission line equation could describe reflection only, but not for the radiation. This is one of deficiencies for the conventional nonuniform transmission line equation. Another deficiency is that the parameters extracted from the conventional equation will change with the transmission line loads and per unit length inductance and capacitance become complex numbers at high frequencies. In order to solve the above problems, the novel nonuniform transmission line equation is derived by circuit theory in this paper for the first time, and the parameters of the new equation are numerically determined by the full wave solutions of the method of moments (MoM). The difference from the conventional nonuniform transmission line equation is that the new equation has two new terms, dependent series voltage and dependent shunt current sources, which are relative to the radiation effects generated by the discontinuities of the nonuniform transmission line itself. As a result, all the extracted transmission line parameters from the new equation are always independent on the loads. The extracted per unit length inductance and capacitance are kept in real numbers and change slowly with frequency. However, the extracted radiation parameters represented by two dependant sources are greatly varied with frequency.

THE PHYSICAL-OPTICS APPROXIMATION AND EARLY-TIME SCATTERING

Carl E. Baum
AFRL/DEHE
3550 Aberdeen Ave SE
Kirtland AFB, NM 87117-5776

The physical optics (PO) approximation is often used to describe the scattering from perfectly conducting targets before information from the shadow boundary can reach the observer. In some cases, including bodies of resvolution, it seems often to be a good approximation for axial backscattering. However, for other target shapes, it is sometimes a (very) bad approximation. The validity is discussed in the context of several selected scatterers.

After considering the PO approximation in frequency and time domains, specific examples are considered for the case of axial backscattering, thereby avoiding the shadow-boundary limitation. First we consider bodies of revolution. For the paraboloid PO gives the known exact solution. For the circular cone the PO solution agrees with the known asymptotic solution for large and small interior semivertex angles. The ratotaion symmetry of course guarantees no depolarization in the exact solution, in agreement with PO.

A counterexample to this agreement is that of a perfectly conducting angular sector in axial backscattering. Simple symmetry considerations show that there is scattering with the incident electric field parallel to the plane of the angular sector, but no scattering for this field perpendicular to this plane. The PO approximation gives zero backscatterring for both polarizations. The reader might be concerned about the case of zero thickness conductors and the shadow boundary. However, consider a cone of elliptic cross section. This should also depolarize in axial backscattering. As the minor radius of the ellipse shrinks toward zero the area function becomes arbitrarily small, as does the PO backscattering. The angular sector is but a limiting case of the cone with elliptical cross section.

The PO scattering dyadic appears to be a useful approximation in some cases, but not others. We need to understand just when it can be used and when not. We need to extend the list of canonical targets with exact solutions. Using modern numerical methods one may obtain "semianalytic" results for which some exact properties are known, but some parameters are caluclated numerically (tabulated). An example is the class of cones for which a constant dyadic coefficient multiplies the simple frequency/temporal behavior. The perfectly conducting angular sector is a good example of this. Thereby one may establish a library of quasi-canonical scatterers.

THICK DICHROIC PLATES WITH ARBITRARILY SHAPED HOLES - EXPERIMENTAL RESULTS

Imbriale, W. A., Reilly, H. F., Cirillo, R.
Jet Propulsion Laboratory
California Institute of Technology
Pasadena, CA 91109, USA

A thick dichroic plate acts as a frequency selective surface (FSS) in that it is transparent at one frequency while at the same time reflective to other frequencies. It is used in the Deep Space Network (DSN) to enable simultaneous multiple-frequency operation. Most of the plates currently in use were designed with programs that analyzed only the simple geometries, such as circular or rectangular holes. Since it is too expensive to experimentally determine the FSS parameters, only designs that could be accurately analyzed were chosen, and it is the primary reason why the recent FSS designs use rectangular holes. To achieve the sharp corners of the rectangular holes, it was necessary to use a relatively expensive electrical discharge machining (EDM) manufacturing technique.

Using an end milling process could reduce the cost by 75 percent. However, plates manufactured using an end milling process would have rounded corners. Consequently, an analysis was formulated and a computer program written to accurately characterize the effects of the rounded corners. A plate that passed Ka-band (31.7-32.2 GHz) and reflects X-Band (7.145-8.5 GHz) was manufactured using end milling. The performance of the plate was very similar to the more expensive EDM plate currently in use in the DSN. Several other test plates were manufactured that demonstrated that plates could be manufactured with walls as thin as 0.3 mm.

The arbitrarily shaped holes analysis is accomplished by combining the Finite-element method (FEM) for determining the waveguide modes of arbitrarily shaped guides with the method of moments and Floquet mode theory for periodic structures. The software was verified by comparison with previously measured and computed dichroic plates.

MEASUREMENTS IN ANECHOIC CHAMBER TO VALIDATE EM PROPAGATION MODELS. A TUTORIAL OVERVIEW

U. G. Crovella, G. D'Elia, D. Erricolo
University of Illinois at Chicago
Department of ECE (M/C154)
1020 SEO
851South Morgan St, Chicago, IL 60607, USA.

Until recently, anechoic chambers were used to perform EMC and EMI measurements and to characterize antenna directivity mainly. On the other hand, EM propagation models were usually compared to field measurements in order to be validated. Unfortunately, 3G systems need efficient management of network resources in order to accomplish reliable data transmission at an acceptable velocity (2 Mb/s and beyond). Therefore, new and more complex propagation models need to be developed, and new ways of validating them need to be investigated.

Accurate network planning can be achieved by using deterministic models which, given the precise topography and morphology of an area, can compute the exact fields in each single point of the considered area. The major drawback of these models is that the complexity of the algorithm increases exponentially with the size of the scenario and therefore can be used to plan micro-cell coverage only. Moreover, the accuracy of the output derives from an accurate input data set, which might be difficult to obtain in open space.

In this work, the authors introduce a new step in validating propagation models, which allow the verification of the theoretical method within a controlled environment. Inside the anechoic chamber, measurements can be performed more easily and more configurations can be examined. In this case, the uncertainties of the measurements can be reduced to a much lower degree with respect to field measurements, thus pointing more evidently out the possible weaknesses of the model. Also, many theoretical assumptions can be verified separately one from each other, analyzing their contributions to the output.

This tutorial presentation includes: 1) An overview of some existing propagation prediction techniques 2) A case study of measurements in a controlled environment 3) Comparisons between different methods to validate propagation models.

AN UNDERGRADUATE WIRELESS TRANSCEIVER

D. S. Goshi*, A. T. Ohta*, M. A. Tamamoto*, K. S. Ching, H. L. Caraang, Jr., N. H. Phan, G. S. Shiroma, M. C. Binonwangan, and W. A. Shiroma
Hawaii Center for Advanced Communications
University of Hawaii at Manoa, Honolulu, HI 96822

We present a 5-GHz RF front end for a wireless transceiver, designed and built by a ten-student team consisting of three seniors, three juniors, two sophomores, and two high school students. The purpose of this far-reaching project is to: (a) stimulate interest in RF/wireless topics at the undergraduate and high school levels, (b) provide students with hands-on microwave measurement experience beyond that of traditional undergraduate engineering labs, and (c) expose students to real-life engineering issues such as budgeting, scheduling, and team dynamics. While the performance of this transceiver is admittedly not state-of-the-art, it does demonstrate that undergraduates are capable of nontrivial wireless circuit design. One senior served as the overall project leader, while another senior single-handedly secured 20 licenses of *Microwave Office* from Applied Wave Research, a donation worth $560,000.

The team selected a 5-GHz operating frequency, as this is where personal communication systems are anticipated to migrate as the 2.4-GHz range becomes congested. The 5-GHz transmitter subsystem consisted of a dual-output local oscillator, BPSK modulator, and power amplifier. The transistor-based modulator demonstrated an amplitude imbalance of 1.2 dB and a phase imbalance of less than 1°. The three-stage power amplifier exhibited 27 dBm of output power, 23.6 dB of gain, and a power-added efficiency of 24%. The 5.1-GHz receiver subsystem consisted of a two-stage low-noise amplifier, a stripline image-reject filter, and a single-balanced mixer. The filter achieved 26.3 dB of rejection at the image frequency of 4.9 GHz, and the mixer had an RF-LO isolation of 19.4 dB. A transmit/receive switch was designed using eight HEMTs, and achieved 23 dB of isolation. To allow high-frequency switching, chip inductors were used to compensate for the parasitic transistor capacitances. Using copper tape, two high school students empirically determined the relationship between the patch dimensions and operating frequency, and between the feed position and input return loss of a microstrip patch antenna. The final antenna design was optimized using CAD, resulting in an input return loss of 37 dB and a cross-polarization ratio of 15 dB.

A future goal of this project is to integrate undergraduates with interests in digital and baseband electronics (for the demodulation), signal processing and software (for implementing channel-coding algorithms), and mechanical engineering (for packaging), resulting in a truly cross-disciplinary undergraduate project experience.

Session C1, 8:55-Wed.

MIMO WIRELESS COMMUNICATION

Chairperson: M. Andrews

CAPACITY OF TIME AND FREQUENCY SELECTIVE CHANNELS

Andrew Brzezinski, Rohit U. Nabar, Arogyaswami J. Paulraj
Information Systems Laboratory
Department of Electrical Engineering
Stanford University
Stanford, CA 94305

Multiple-input multiple-output (MIMO) systems enable significant increases in wireless channel capacity, and have attracted a great deal of recent interest. Wireless links are impaired by random fluctuations in signal power (fading) across frequency/time/space. Therefore, the capacity of a wireless link also fluctuates and must be modeled as a random variable. Classically, the discrete-time MIMO channel is modeled by a random matrix consisting of independent and identically distributed (i.i.d.) random elements, with the assumption of frequency and time flat fading. This case has been studied extensively for ergodic and outage capacity, and asymptotic properties.

In this paper, we introduce simple channel models that reflect time and frequency selectivity in MIMO channels, with i.i.d. properties extended to allow for more general correlations between channel elements. The capacity of these time and frequency selective channels is studied analytically and through simulation. After establishing comparable channel models, we show that the ergodic capacity of the simple time and frequency selective channels is identical to the ergodic capacity of the non-selective channel. Analysis of the time selective channel demonstrates that the random capacity approaches ergodic capacity as the channel coherence time becomes arbitrarily small. Conditions are derived under which the frequency selective channel has random capacity approaching ergodic capacity, given an exponentially decaying power-delay profile of channel taps. Simulations are conducted to demonstrate evolution of outage and ergodic capacity towards these limiting cases. Capacity cumulative density functions show the effects of frequency and time selectivity on random capacity values, as well as the impact on outage properties.

COMMUNICATING OVER MULTI-ANTENNA WIRELESS CHANNELS WITH BOTH TEMPORAL AND SPECTRAL FLUCTUATIONS

Sigloch, K.*, Univ. Karlsruhe & Bell Labs, Lucent Technologies
Mitra, P.P., Thomson, D.J., Andrews, M.R.,
Bell Labs, Lucent Technologies

In this paper we consider new ways of communicating in the presence of both temporal (i.e., over time) and spectral fluctuations (i.e., over frequency) of the multi-antenna (MIMO) channel. The fundamental problem, or approximation, is that spectral variations take time to measure properly, for instance with so-called "pilot signals", whereas during the time-course of those measurements themselves, the channel itself is not a constant. A first solution is to artificially assume that one can treat the channel to be constant over short enough intervals of either time or frequency, and measure the fluctuations of the complementary variable, i.e., frequency or time respectively, in one interval after the other. This is what is typically done in wireless communication systems, but unfortunately, it sacrifices either time or frequency resolution at the expense of frequency or time resolution, respectively. What we examine is a new scheme that treats both time and frequency on equal footing, and rather than assuming "piecewise constant", or a zeroth order approximation to the fluctuations, makes the first order corrections by assuming linear complex amplitude variations across both the spectral and temporal domains. A set of pulse shaping functions, and a computationally simple decoding algorithm well suited to the new scheme will be discussed. We also present experimental results for various fluctuating MIMO wireless channels and compare to other schemes.

OPPORTUNISTIC BEAMFORMING: DUMB ANTENNAS AND SIMPLE SCHEDULING

Viswanath, P.*
Department of ECE
University of Illinois, Urbana-Champaign
IL 61801
Tse, D.
Department of EECS
University of California, Berkeley.
Laroia, R.
Flarion Technologies,
Bedminster, NJ

Abstract: *Multiuser diversity* is a form of diversity inherent in a wireless network, provided by independent varying channels across the different users. The diversity benefit is exploited by tracking the channel fluctuations of the users and scheduling transmissions to users when their instantaneous channel quality is near the peak. The diversity gain increases with the dynamic range of the fluctuations and is thus limited in environments with little scattering and/or slow fading. In such environments, we propose the use of multiple transmit antennas to artificially induce large and fast channel fluctuations so that multiuser diversity can still be exploited. The scheme can be interpreted as *opportunistic beamforming* and we show that *true* beamforming gains can be achieved when there are sufficient users, even though very limited channel feedback is needed. Furthermore, in a cellular system, the scheme plays an additional role of *opportunistic nulling* of the interference created on users of adjacent cells.

In contrast, traditionally, channel fading is viewed as a source of *unreliability* that has to be *mitigated.*. In the context of multiuser diversity, however, fading can instead be considered as a source of *randomization* that can be *exploited.* This is done by scheduling transmissions to users only when their channels are near their peaks. The larger the dynamic range of the channel fluctuations, the higher the peaks and the larger the multiuser diversity gain. In practice, such gains are limited in two ways. First, there may be a line-of-sight path and little scattering in the enviroment, and hence there is a small dynamic range of channel fluctuations. Second, the channel may fade very slowly compared to the delay constraints of the application so that transmissions cannot wait until the channel reaches its peak. Effectively, the dynamic range of channel fluctuations is small within the timescale of interest. Both are important sources of hindrance to implementing multiuser diversity in a real system. In this paper, we propose a scheme which artificially induces random fading when the environment has little scattering and/or the fading is slow

MULTIUSER PRECODING STRATEGIES USING TRANSMIT ANTENNA DIVERSITY

M. J. Lopez, G. W. Wornell
Massachusetts Institute of Technology
Cambridge, MA 02139

Consider transmitting distinct messages to a number of receivers from an array of antennas. When channel state information is available at the transmitter, strategies have recently appeared (G. Caire and S. Shamai, *IEEE ISIT*, 147, 2001 and G. Ginis and J. M. Cioffi, *Proc. Asilomar*, 1627-1631, 2000) that, rather than using beamforming to null out all interference, instead embed information in the known interference. We provide a matrix-algebraic interpretation of this type of approach and place it in the context of other methods of transmitter- or receiver-based interference rejection. We go on to investigate implementation issues with a focus on building low-complexity, practical systems.

Assume independent, flat fading channels from each transmit antenna to each receiver. Knowing the fading coefficients, the transmitter can manipulate the different messages in any way such that a power constraint is maintained. Several effective strategies from the literature can be written in terms of combinations of two types of manipulations: (i) a linear (beamforming) step that can be written as a matrix multiplication, and (ii) an interference cancellation step that consists of a matrix multiplication intertwined in a simple way with slicer and/or modulo operations. For the precoding system of interest, the users are ordered and the the first step is used to avoid interference to later users, while the second step cancels interference to earlier ones. We show how this corresponds to a QR factorization of the channel matrix. Alternatively, depending on the assumptions of channel knowledge and receiver communication, this or other factorizations can be performed at either the transmitter, receivers, or mix of both, resulting in a rich class of possible strategies. The precoding system in particular is notable for its high performance without requiring communication among receivers.

In principle, it is known how to achieve the capacity of the precoding system asymptotically. For the design of practical systems, however, it is also desirable to have robust, low-complexity transmitters and receivers. We consider the effect of discrete constellations for both the host (interference) and embedding signals, and how to optimize the embedding function to take this into account. The resulting operations bear a resemblance to the distortion-compensated quantization index modulation (DC-QIM) embedding method of (B. Chen and G. W. Wornell, *IEEE Trans. Info. Th.*, **4**, 1423-1443, 2001) but differ in important ways due to the different types of constraints.

USING PHASE AND AMPLITUDE CONTROL ACROSS NETWORKS TO INCREASE CAPACITY UP TO FOURFOLD

Chow, C.*, MIT & Bell Labs, Lucent Technologies
Shraiman, B.I., Sengupta, A.M., Andrews, M.R.,
Bell Labs, Lucent Technologies

We propose a novel scheme for suppressing co-channel interference, which employs phase coherent and cooperative transmissions from the cellular base network and utilizes continuous channel estimation. Feasibility of this scheme crucially depends on the ability to measure complex-valued amplitudes of received pilots accurately. The fundamental limit on estimating and forecasting these amplitudes requires that the coherence time and flat fading bandwidth product be large enough, on the order of 1000. Propagation studies of indoor environments suggest that this constraint can be satisfied, and simulations indicate that the new scheme may do better than standard frequency or code reuse in terms of the number of users it can serve. Real-time networking experiments designed to demonstrate these concepts are underway.

CODING FOR MIMO SYSTEMS WITH ANTENNA SELECTION

Ghrayeb, A.
The American University
United Arab Emirates
Duman, T. M.
Arizona State University

Wireless communications systems with multiple antennas at the transmitter and at the receiver have been receiving a lot of attention in the recent years, mainly, due to the recent information theoretical results that prove that the capacity of the system increases linearly with the number of transmit antennas under certain fading channel assumptions. Based on this promised capacity, Tarokh et. al. and many others have developed practical space-time coding techniques. More recently, motivated by the practical implementations of the receivers Molisch, Win and Winters have derived bounds on the capacity of multiple antenna systems with antenna selection at the receveir.

In this paper, we consider receiver antenna selection as well, however we take a different approach dealing with the performance of practical coding schemes under this scneario. In particular, we analyze the performance of the multiple input/multiple output (MIMO) systems with antenna selection over quasi-static Rayleigh fading channels. The basic idea is that, for a given number of receive antennas M, the receiver uses the best L out of M where, typically, L less than M. We examine the effects of the antenna selection on the coding and diversity gains, and we show that regardless of the specific space-time code used, the diversity gain provided by the code is maintained, while the coding gain deteriorates. We also give a (somewhat loose) upper bound on the amount of this loss. We present a practical (near optimal) antenna selection schemeand provide semi-analytical and simulation results that support our analysis for several examples.

TRANSMIT SITE DIVERSITY FOR OFDM MULTI-CELL WIRELESS COMMUNICATION NETWORK

T. Fujii, M. Inoue, M. Nakagawa
Dept. of ICS, Keio University
3-14-1, Hiyoshi, Kohoku-ku, Yokohama 223-8522, Japan

Orthogonal frequency division multiplexing (OFDM) has brought significant attention for using in the fourth generation mobile communication systems and wireless local area networks (LANs). OFDM system allows all cells to transmit the packets in the same frequency simultaneously by making use of the characteristic of a guard interval. This method, known as single frequency network (SFN), was originally proposed in digital terrestrial broadcasting. This technique can improve the performance of the edge of the cell and can be used for a site diversity of OFDM, however the signals cannot be coherently combined.

In this paper, in order to improve the performance of forward link channel with diversity gain around the edge of a cell, we propose a novel transmit site diversity for OFDM using a space time transmit diversity (STTD) technique. In general transmit diversity, elements are set on a transmit antenna and used for improving the performance in the cell. In this paper, in order to improve the performance of multi-cell communications, these elements are separated to multiple base stations (BSs), as a result each BS is regarded as an element of a transmit diversity. We use STTD for site diversity, because this technique does not require the channel condition at the transmitter and the mobile terminals of all the area can achieve the diversity gain. The transmitter system consists of a central control unit (CCU) and two sets of BSs. In the CCU, the transmitting signal of each set of BSs is generated according to the STTD signal generation rule. First, two continuous data signals, S_1, S_2 are converted to two STTD transmit patterns as follows, STTD pattern 1: $t = S_1, t+1 = -S_2^*$ and STTD pattern 2: $t = S_2, t+1 = S_1^*$, where $(\cdot)^*$ is complex conjugate. Each pattern is assign to each set of BSs. If we can know the channel response α and β at the receiver, S_1, S_2 are demodulated with diversity gain as follows, S_1 demodulation : $\alpha^* r_t + \beta r_{t+1}^* = (\alpha^2+\beta^2)S_1 + n_1'$ and S_2 demodulation : $\beta^* r_t - \alpha r_{t+1}^* = (\alpha^2+\beta^2)S_2 + n_2'$, where r_t, r_{t+1} is the received signal of $t, t+1$, respectively, and n_1', n_2' is noise. By using above signals, the data are recovered with diversity gain with coherent signals combining.

This technique can use in following applications. (1) Performance improvement around the edge of the cell, (2) Broadcast and multicast packet transmission with high quality, (3) Performance improvement of terrestrial digital broadcasting, (4) Road-to-vehicle communications, etc. We evaluate the performance of the proposed system using computer simulation and confirm the effectiveness of the proposed system.

MULTIPLE ANTENNAE, MULTIPOLE RADIATION, AND BEAM FORMATION: COUNTING ELECTROMAGNETIC DEGREES OF FREEDOM

Polyakov, A.S., New York University
Mitra, P.P., Andrews, M.R., Bell Labs, Lucent Technologies

We propose an algorithm to design localized multi-antennae capable of directed beams with multiple degrees of freedom by studying an appropriate concentration problem. We describe electromagnetic waves emerging from a localized region of space in terms of the electric and magnetic multipole moments of the source. Maximizing the concentration, defined as the normalized radiated energy within a solid angle, leads to an eigenvalue equation analogous to that studied earlier by Slepian, Landau, and Pollak in the context of the spectral concentration problem. This approach allows us to define a principled measure of the number of electromagnetic degree of freedom in a given solid angle. The number of degrees of freedom is related to the channel capacity for multiple antennae concentrated in a small volume, and helps us to design directed multi-antennae. In particular, by combining electric and magnetic multipole elements we can double the number of radiated degrees of freedom compared to electric-only or magnetic-only designs.

Session C2, 15:35-Wed.

RADAR SIGNAL PROCESSING

Chairperson: Jeff Krolick

INFERRING ATMOSPHERIC REFRACTIVITY FROM SEA CLUTTER USING A GENETIC ALGORITHM

P. Gerstoft
Marine Physical Laboratory
University of California
San Diego, La Jolla, CA 92093-0238 USA
L.T. Rogers
Space and Naval Warfare Systems Center
Atmospheric Propagation Branch (D858)
San Diego, CA 92152-5001

This paper describes the estimation of low-altitude atmospheric refractivity from observations of radar sea clutter. The vertical structure of the refractive environment is described using five parameters and the horizontal structure of one of the parameters (the inversion base height), is modeled using six parameters corresponding to the principal components eigenfunction of a Markov process with respect to range. An electromagnetic propagation model maps the refractivity structure into a replica field. Replica fields are compared to the observed clutter using a squared-error objective function. A global search for the 11 environmental parameters is performed using a Genetic Algorithm general purpose inversion code. The inversion algorithm is implemented on S-band radar sea clutter data from a propagation experiment at Wallops Island Virginia. Ground truth data are range-dependent refractivity profiles obtained with a helicopter.

The goodness of the inversion method is assessed by comparing (a) the propagation predicted by the radar-inferred refractivity profiles to that predicted using the helicopter profiles, (b) refractivity parameters diagnosed from the helicopter soundings to those estimated via the inversion algorithm, and (c) examining the goodness of fit between the observed clutter and the optimal replica field.

The intended use of the technique is to provide near-real-time estimation of ducting effects for naval forces. In real-world circumstances, it is unlikely that naval forces would have range-dependent soundings; rather having a single representative sounding would be a best-case scenario. We use the goodness of a single sounding as the benchmark for evaluating the goodness of the radar inferred environmental parameters. The overall result is that the "refractivity-from-clutter" technique approaches the goodness of our benchmark for prediction of propagation, however, it is not as good an estimator of the refractivity structures themselves.

PERFORMANCE BOUNDS ON ALTITUDE ESTIMATION USING OVER-THE-HORIZON RADAR

M. A. Papazoglou*
Naval Research Laboratory
Washington, DC 20375, USA

Refraction of over-the-horizon (OTH) sky-wave radar signals through the ionosphere facilitates wide-area surveillance. Historically, OTH radar systems have been used for aircraft tracking and have been capable of estimating target ground range, azimuth, and velocity (Headrick and Skolnik, *IEEE Proc.*, **62**, 664-673, June 1974). However, a recent interest in the ability to estimate target altitude using OTH radar has emerged (Papazoglou and Krolik, *IEEE Trans. Signal Proc.*, **47**(4), 966-976, April 1999). A maximum likelihood algorithm for OTH radar altitude estimation has been developed that exploits multipath propagation due to radar ground reflections local to the aircraft. This multipath results in a single target producing multiple returns that are typically unresolvable in a single radar dwell, but which produce altitude-dependent dwell-to-dwell phase changes in the received signal.

The Cramer-Rao lower bound (CRLB) for altitude estimation is presented for OTH altitude estimation using multiple radar revisits. The CRLB illustrates the dependence of altitude estimation accuracy on radar signal processing parameters (bandwidth and coherent integration time) and uncertainty. Two sources of uncertainty are investigated. They are (1) uncertainty in the range-dependent environmental model, (specifically ionospheric tilt) and (2) uncertainty in the dwell-to-dwell signal coherence.

The CRLB bound suggests that altitude estimation accuracy to within 5,000 ft can be achieved using multiple radar revisits using reasonable bandwidth and coherent integration time, even at moderate levels of dwell-to-dwell signal coherence. The bound results also illustrate the sensitivity of altitude estimation to uncertainty in range-dependent environmental parameters. This is in contrast to earlier work which found that altitude estimation is robust to uncertainty in range-independent environmental uncertainty (Papazoglou and Krolik, *ICASSP Trans.*, 559-562, 1997).

MULTISTATIC PASSIVE RADAR IMAGING OF AIRCRAFT: A FEASIBILITY STUDY USING FISC

Y. Wu, D. C. Munson, Jr.
Coordinated Science Laboratory
University of Illinois
1308 W. Main St.
Urbana, IL 61801, USA
A. Lanterman
School of Electrical and Computer Engineering
Georgia Institute of Technology
Mail Code 0250
Atlanta, GA 30318

We are studying the feasibilty of imaging aircraft using reflected radio and television signals. Unlike conventional X-band synthetic aperture radar (SAR), which operates around 10 GHZ and can use a small synthetic aperture (e.g. 3 degrees), the frequencies in the passive case are in the 100 - 800 MHz band, necessitating a much wider aperture. In addition, the bandwidth of any individual signal is practically zero, necessitating the use of many transmitters and/or receivers.

We have considered an imaging scenario in the Gaithersburg, MD area, where we assumed a single receiver, and multiple transmitters at 211.25 MHz and below. The transmitters were assigned to have the actual frequencies and locations of a set of television stations near Gaithersburg. As the aircraft traverses an assumed flight path, the receiver collects signals reflected from the aircraft, as well as direct copies of the television transmissions for use in the demodulator. Ignoring aspect dependence of the aircraft reflectivity, the bistatic radar principle states that the demodulated, reflected signal from any particular television frequency provides samples of the Fourier transform of the reflectivity of the target. The samples lie on a circular arc, with multiple transmitters providing data on multiple arcs.

We investigated feasibility of image formation by simulating radar returns from a Falcon-100 aircraft, using the Fast Illinois Solver Code (FISC), which is more accurate than XPATCH for the low frequencies of interest. Our simulations show that by selecting a good receiver location, one can obtain a recognizable image of the aircraft. However, a poor receiver location can provide Fourier data that is too sparse, making imaging difficult. Our study suggests that, depending on the flight path and transmitter-receiver geometry, it is possible to produce recognizable aircraft images, using about 20 or fewer television stations. The number of transmitters could be reduced by using multiple receivers, or perhaps by using stations operating at higher frequencies in the UHF band (up to 800 MHz).

MULTIDIMENSIONAL NONLINEAR INVERSE SCATTERING FOR SUBSURFACE SENSING AND BIOMEDICAL IMAGING

Qing H. Liu and Zhong Qing Zhang
Department of Electrical Engineering
Duke University
Box 90291
Durham, NC 27708-0291

Numerous applications of electromagnetic waves in subsurface sensing and biomedical imaging require the inversion of electrical properties of the anomalous objects in a generally heterogeneous background. In such environments, multiple scattering effects are typically very strong and cannot be neglected in the processing of scattering data. Many simplifying inversion schemes, such as the Born approximation, ignore the nonlinear multiple scattering effects, leading to significantly reduced accuracy and resolution.

In this presentation, we will report our recent progress in nonlinear inverse scattering in both two and three dimensions. Issues important to subsurface sensing and biomedical imaging will be addressed, including solution nonuniqueness, resolution, and computational efficiency. Two methods recently developed in our group are fast inversion techniques based on the extended Born approximation and contrast source. These methods do not require forward solutions during the inversion iterations, and are very attractive for multidimensional inverse scattering. Fast Fourier and Hankel transform asignal processing will also be discussed.lgorithms are effectively incorporated in these algorithms to accelerate the Green's function operations. For subsurface sensing, we have applied these algorithms for both surface electromagnetic induction (EMI) and borehole induction measurements (Z. Q. Zhang and Q. H. Liu, Inverse Problems, vol. 16, no. 5, pp. 1281-1296, 2000; Z. Q. Zhang and Q. H. Liu, IEEE Trans. Geosci. Remote Sensing, vol. 39, no. 6, pp. 1331-1339, June 2001). For biomedical imaging, we have developed these algorithms for microwave imaging for breast cancer detection (Q. H. Liu et al., IEEE Trans. Microwave Theory Tech., in press). Both synthetic and laboratory data have been successfully inverted for high-contrast media. These algorithms can be applied to other applications involving electromagnetic scattering. Potential applications of such algorithms to radar signal processing will also be discussed.

RECURSIVE BAYESIAN ESTIMATION OF TROPOSPHERIC REFRACTIVITY FROM RADAR CLUTTER

R.H. Anderson, S. Vasudevan, J.L. Krolik
Department of Electrical and Computer Engineering
Duke University
Durham, NC 27708-0291

This paper addresses the problem of estimating range-varying parameters of the height-dependent index of refraction over the sea surface in order to predict ducted microwave propagation loss. In previous refractivity from clutter (RFC) work, a "black-box" parabolic equation propagation model has been used to find the best fit between predictions of the two-way propagation loss near the sea surface and the observed radar clutter return. The difficulty with such an approach is that a high dimensional non-linear optimization is required, which is computationally intensive and sometimes ambiguous. In this paper, refractivity estimation is performed using a Markov model for the microwave radar clutter returns. Specifically, the split-step Fourier solution to the parabolic equation is exploited to formulate the problem as a non-linear recursive Bayesian state estimation problem. This results in some state-equation components which march the field out in range and others which impose a smoothness constraint on the range variation of height-dependent refractivity parameters. The non-linear observation equation in this framework consists of pulse-averaged log-amplitude radar clutter returns versus range whose statistics are approximately independent and Gaussian given the refractivity parameters. This non-linear state-space framework lends itself to efficient solution by sequential importance sampling (SIS) methods. Solution for the maximum a posteriori (MAP) sequence of range-varying refractivity parameters is achieved using a particle filtering technique based on the Viterbi algorithm. Simulation and real data results based on experiments performed off Wallops Island, Virginia are presented which quantify the technique's ability to predict propagation loss at 3 Ghz. Propagation loss estimates made using RFC estimates compare favorably to those predicted using helicopter-borne refractivity measurements.

SIFTER: SIGNAL INVERSION FOR TARGET EXTRACTION AND REGISTRATION

Sergey V. Fridman*, L. J. Nickisch
Mission Research Corporation
10 ragsdale Dr., Suite 201, Monterey, CA 93940-5776

Signal inversion for target extraction and registration (SIFTER) is a new technique for enhanced radar target detection and coordinate registration (CR). The technique is currently being developed for over-the-horizon radar (OTHR), however its transition to any other type of radar is straightforward.

Electromagnetic returns received by OTHR are comprised of waves backscattered by objects located in the area illuminated by the radar. The received power as a function of slant coordinates and Doppler may be expressed as an integral operator applied to the field of backscatter cross section (FBC) per unit area of the earths surface. In general, the FBC is a function of the geographic position and the velocity vector of the scattering point. Targets appear in the FBC as delta-function-like peaks. The kernel of the integral operator is treated as a known function that is determined entirely by the model of the propagation channel, antenna patterns, and the radar signal processing parameters. The relationship between the FBC and the received power is treated as an integral equation that needs to be resolved (inverted) with respect to the FBC. This inversion is accomplished using special techniques for ill-posed problems (such as Tikhonovs method). The obtained FBC is subsequently analyzed on peaks. The location of a peak provides an estimate for actual ground coordinates and velocity vector of the target. This processing provides a gain in sensitivity and CR accuracy because of the effective combining of target returns from different propagation modes, overlapping antenna beams, etc.

Further gain in sensitivity and CR is achieved with our developed SIFTER time evolution algorithm. We introduce a continuity equation for the FBC. The equation is based on most general assumptions regarding the behavior of potential targets. This equation evolves the FBC between radar revisit cycles. The data from each subsequent revisit is utilized to correct the FBC evolved from previous cycles. That helps the SIFTER inversion to recover targets that experience irregular fading and at the same time minimizes effects from spurious noise-related peaks. Two versions of the SIFTER time evolution algorithm are presented. One is based on Tikhonovs method, and the other on the Kalman filter method.

SIFTER concepts and performance are demonstrated using modeled as well as real OTHR data.

Session C3, 13:55-Thurs.

IMAGE MODELING AND INVERSE PROBLEMS

Chairperson: R. Nowak

ON MODELING LOCATION UNCERTAINTY IN IMAGES

Michael Orchard
Electrical and Computer Engineering
Rice University
Houston, Texas

The focus of this session is mathematical methods in imaging science. In the past several decades image processing and analysis has developed into a mature science. This has been fueled by the increase in computing capabilities which have helped to make very sophisticated and advanced mathematical algorithms practical. Modern image processing and analysis research can be roughly categorized into (i) image modeling, (ii) algorithm development, and (iii) analysis of algorithms. In fact, these three tasks are intimately related. Algorithms are usually derived from image modeling considerations and the analysis of algorithms (which includes deriving performance bounds) involves a careful study of the relationship between algorithms and models. In keeping with the interdisciplinary scientific spirit of the URSI meeting, the objective of this session is to bring together a diverse group of researchers from engineering, statistics, and allied sciences who are interested in image modeling and analysis. Aspects of the three tasks above are examined in this work.

Almost all image coding algorithms model the uncertainty in images as probability distributions of random coefficients of some linear expansion of the image. The encoded bitstream then consists of a specification of unknown coefficient values. Humans, however, typically use a very different type of representation in verbally encoding the contents of images either in written or spoken form (in a book or telephone conversation). Verbal descriptions of images often do not specify the value of any coefficient, relying instead on specifying the location or parameters derived from the location of features in the image. For example, locations of features, smoothness of contours, curvature and directions of contours, are much more common in spoken image descriptions than the brightness or intensity of any region or group of regions of the image. This talk suggests that the human verbal encoding of images is a better match to the true uncertainty of most classes of images, and describes efforts to develop efficient image models that directly model location-based parameters in images.

WAVELET DOMAIN EDGE GRAMMARS

Justin Romberg and Richard Baranuik
Rice University
6100 Main Street
Houston, TX 77005 USA

Wavelet domain algorithms have risen to the forefront of image processing. The power of these algorithms is derived from the fact that the wavelet transform restructures the image in a way that makes statistical modeling easier. Since the edge singularities in an image account for the most important information, understanding how edges behave in the wavelet domain is the key to modeling. In the past, wavelet-domain statistical models (such as the hidden Markov tree), using the "wavelet basis function as a local edge detector" heuristic, have codified the behavior of edges in the wavelet domain using chains of large magnitude coefficients across scale. Algorithms based on these models have enjoyed success, particularly for image restoration and segmentation, but still leave something to be desired in their treatment of edges.

In this paper, we deal more directly with edges in the wavelet domain. We examine the "multiscale edge grammar": a set of deterministic rules that describe the inter-relationships required of the wavelet coefficients to make up a "valid" edge. The set of wavelet coefficients that make up a valid edge form a low dimensional manifold in the space of all possible wavelet coefficients. Using these rules, we can project observed wavelet coefficients onto this manifold to get local information about edge behavior in images.

In the complex wavelet domain, the multiscale edge grammar can be simplified into two key components: persistence of magnitudes and coherence of phase across scale. This simplification allows us to incorporate the edge grammars into existing models, resulting in algorithms that yield images with cleaner edges.

STOCHASTIC MULTIRESOLUTION MODELS FOR TURBULENCE

Brandon Whitcher
Geophysical Statistics Project
Climate and Global Dynamics Division
National Center for Atmospheric Research
P.O. Box 3000, Boulder, Colorado 80307

The efficient and accurate representation of two-dimensional turbulent fields is of interest in the geosciences because the fundamental equations that describe turbulence are difficult to handle directly. Rather than extract the coherent portion of the image from the background variation, as in the classical signal plus noise model, we present a statistical model for individual vortices using the non-decimated discrete wavelet transform (MODWT). Unlike the orthonormal two-dimensional discrete wavelet transform (2D DWT), the 2D MODWT produces a redundant non-orthogonal transform. The main reason for this discrepancy is that the 2D MODWT does not downsample after convolving the wavelet filters with the input field. Hence, each wavelet field will have the same dimension as the original field. A template image, supplied by the user, provides the features we want to extract from the observed field. By transforming the vortex template into the wavelet domain specific characteristics present in the template, such as size and symmetry, are broken down into components associated with spatial frequencies. Multivariate multiple linear regression is used to fit the vortex template to the observed vorticity field in the wavelet domain. Framing the regression model in the wavelet domain, through the multiresolution analysis, a template function that is idealized and simplistic in nature provides the foundation of a semi-parametric fit. For example, the template may be a two-dimensional Gaussian bump of fixed size. This is reasonable as an intuitive description of the coherent structures seen in the simulations of interest, but does not allow for the full range of vortices observed; e.g., different sizes, distorted shapes, etc. The multiresolution analysis of the template separates features of the idealized vortex by direction (horizontal, vertical and diagonal) and size (ranges of spatial frequency) through the use of a collection of basis functions (wavelets). Thus, fitting the template function via a multiresolution-based regression to an observed vortex results in a distinctly non-Gaussian shaped model. Application to a vortex census algorithm that tracks quantities of interest (such as size, peak amplitude, circulation, etc.) as the vorticity field evolves is given. Extensions to three dimensions are also provided.

A STATISTICAL MULTISCALE FRAMEWORK FOR INVERSE IMAGING PROBLEMS

Robert Nowak and Eric Kolaczyk
ECE Dept
Rice University
Houston, TX 77005

The focus of this session is mathematical methods in imaging science. In the past several decades image processing and analysis has developed into a mature science. This has been fueled by the increase in computing capabilities which have helped to make very sophisticated and advanced mathematical algorithms practical. Modern image processing and analysis research can be roughly categorized into (i) image modeling, (ii) algorithm development, and (iii) analysis of algorithms. In fact, these three tasks are intimately related. Algorithms are usually derived from image modeling considerations and the analysis of algorithms (which includes deriving performance bounds) involves a careful study of the relationship between algorithms and models. In keeping with the interdisciplinary scientific spirit of the URSI meeting, the objective of this session is to bring together a diverse group of researchers from engineering, statistics, and allied sciences who are interested in image modeling and analysis. Aspects of the three tasks above are examined in this work.

Probabilistic multiscale image models often yield very powerful image processing and analysis algorithms requiring minimal computational resources. However, in many (perhaps most) applications of interest, the object we wish to recover is subjected to a transformation or distortion during data acquisition (e.g., tomographic projections, atmospheric distortions, blurring). In such cases, image recovery requires the solution of an inverse problem. Multiscale image models have proved to be tremendously useful in image denoising, segmentation, and texture synthesis, but less is understood about their utility in solving inverse problems in imaging. The goal of this work is to propose a unified multiscale framework for image reconstruction and restoration problems involving transformed or distorted data, treating both Gaussian and Poisson observation models.

WAVELET BASED ESTIMATION OF A SEMI PARAMETRIC

Francios Meyer
University of Colorado at Boulder

Most of the current methods of analysis of fMRI data rely on an experimental paradigm consisting of ON (active) and OFF (rest) periodic stimulations of the subject. A commonly employed method to estimate the effect of the stimulus at a given voxel M in the brain relies on the linear model associated with the two sided Student's t-test, and assumes that the fMRI signal $\mathbf{y_M}$ at M is given by

$$y_{i,\mathbf{M}} = \beta_{\mathbf{M}}\, x_i + \sigma^2 \nu_{i,\mathbf{M}} \quad , \quad i = 0, \cdots, N-1 \tag{1}$$

where $\mathbf{x} = [x_0, \cdots, x_{N-1}]^t$ is the stimulus time course, composed of -1s (OFF) and 1s (ON). $\beta_{\mathbf{M}}$ is a scalar that measures the strength of the response to the stimulus induced by neuronal activation. $\nu_{\mathbf{M}} = [\nu_{0,\mathbf{M}}, \cdots, \nu_{N-1,\mathbf{M}}]^t$ is a white noise process caused by thermal and quantum noise. Unfortunately, the detection of significant changes in the fMRI signal is further complicated by the presence of long term physiological drifts and instrumental instability that contribute to a systematic increase or decrease in the signal with time. It is obvious that if such baseline drifts are not removed, any analysis based on the model (??) will be tracking the large variation in the signal instead of the effects of the stimulus. In this work we propose to replace the model (??) with the following model :

$$y_{i,\mathbf{M}} = \theta_{i,\mathbf{M}} + \beta_{\mathbf{M}}\, x_i + \sigma^2 \nu_{i,\mathbf{M}} \;,\; i = 0, \cdots, N-1 \tag{2}$$

where $\theta_{\mathbf{M}} = [\theta_{0,\mathbf{M}}, \cdots, \theta_{N-1,\mathbf{M}}]^t$ is a baseline drift. Our assumption is that an appropriate model for the trend is provided by a linear combination of large scale wavelets :

$$\theta(t) = s\theta_0^J \Phi(2^{-J}t) + \sum_{j=J_0}^{J} \sum_{k=0}^{2^{-j}N-1} d\theta_k^j \psi(2^{-j}t - k). \tag{3}$$

The first contribution of this work is a new model of the drift that belongs to a subspace spanned by large scale wavelets. The second contribution of the work is a new method to estimate the drift θ and to test for the significance of the response β to the stimulus. The method performs a scale space regression in the wavelet domain with the scales of the drift being omitted. Experiments with fMRI data demonstrate that our approach can infer and remove drifts that cannot be adequately represented with low degree polynomials. Our approach results in a noticeable improvement by reducing the false positive rate and increasing the true positive rate.

POISSON EMISSION TOMOGRAPHY USING COMPRESSED LIST MODE DATA

T.J. Kragh, A.O. Hero
Dept. of Electrical Engineering and Computer Science
University of Michigan, Ann Arbor

This work concerns acceleration of image reconstruction for Poisson emission tomographic modalities such as SPECT and PET where uniform detector binning is impractical due to the high dimensional observation space yet the modality generates massive amounts of counts. This is becoming a problem of great relevance as fully 3D modalities are developed to increase sensitivity. In listmode reconstruction multiple attributes such as position, energy, scatter angle, etc., are recorded for each detected photon as a point in a multi-dimension detector space. Each photon then contributes to the likelihood function and the maximum-likelihood solution can be found using expectation-maximization or other algorithms. However the computational complexity per iteration is proportional to the total number of counts. The basic idea behind our approach is that different regions of the detector space yield different amounts of information about the emission source and therefore one can get away with coarse quantization of the observation space in regions of low information. This suggests the use of adaptive data compression techniques to compress the observations to a low dimensional subspace with minimal loss of information about the source. We will present a technique which combines optimal asymptotic vector quantization to minimize loss in the Fisher information, Lloyd's algorithm for constructing virtual detector bins "on-the-fly" from list mode data, and subsequent image reconstruction algorithms operating on compressed data. We will show that this framework can reduce computation time by a factor of 2 or more in practical tomographic scenarios with little increase in mean-square reconstruction error. This work has been funded under NIH for development of an electronically collimated Compton camera for SPECT medical image reconstruction.

ALPHA DIVERGENCE FOR FEATURE PRUNING AND INDEXING OF LARGE BIOLOGICAL DATABASES

John D. Gorman, Cytoprint, Inc.
3900 Paseo del Sol, Santa Fe, NM 87507
Alfred O. Hero, III, Department of EECS
University of Michigan, Ann Arbor, MI 48109-2122

We present recent results on the application of alpha-divergence via minimal graph methods to the problem of feature selection and indexing of very large, high-dimensional biologically-based datasets. We provide an overview of some emerging image-based techniques in biotechnology and discuss our approach to "datamining" biological signatures by use of alpha-divergence and related statistical measure for signature matching and dimension reduction. We also compare the classification accuracy and computational efficiency of minimal graph approaches to alternate classification and feature pruning methods such as greedy data partitioning and principal-components analysis (PCA) methods.

Emerging drug discovery technologies in the pharmaceutical industry are generating large volumes of very high-dimensional data and there is a critical need for computationally efficient search and indexing algorithms. Two such technologies are gene microarray assays and high-content screening (HCS) via cell-based fluorescent microscopy. In these two examples, feature vectors are extracted from large sequences of multi-band imagery and the goal is to infer biological function from the extracted feature vectors by classifying or clustering feature vectors according to their statistical similarity. With HCS, for instance, the object is to group drug-like compounds based on how they affect cell phenotype (i.e., biological and physical characteristics of the cell).

In this paper we discuss the use of recently developed minimal-graph techniques for estimating alpha-divergence and their application to dimension reduction and classification of HCS data. In particular, we compare the relative classification accuracy and computational complexity of minimal graph methods to more conventional approaches such as PCA and greedy data partioning algorithms such as CART or C4.5. Attractive attributes of the minimal graph techniques are their lower computational complexity and superior convergence rates as compared to more conventional kernel-density based divergence estimation methods.

ESTIMATION OF NOISE AND BLUR PARAMETERS FOR BLIND DECONVOLUTION OF NATURAL IMAGES

Andre Jalobeanu
CNRS/INRIA/UNSA
University of Nice-Sophia Antipolis
BP 93, 2004 Route des Lucioles
06902 Sophia-Antipolis Cedex, FRANCE
Laure Blanc-Feraud
CNRS
University of Nice-Sophia Antipolis
BP 93, 2004 Route des Lucioles
06902 Sophia-Antipolis Cedex, FRANCE
Josiane Zerubia
CNRS/INRIA/UNSA
University of Nice-Sophia Antipolis
BP 93, 2004 Route des Lucioles
06902 Sophia-Antipolis Cedex, FRANCE

In this work, a new method is proposed to estimate the parameters of the noise of the sensor and the impulse response of an optical system, from blurred and noisy images, for instance remote sensing data. The modulation transfer function is parametrized, and modeled taking into account the physics of the imaging system (including atmosphere, optics and sensor). We assume the noise is Gaussian, white and stationary, whith an unknown variance. The natural scene is described by a fractal model, which is known to efficiently model a large range of natural phenomena. The scene is modeled by a 2D fractional gaussian noise, which captures the scale invariant properties of natural scenes. This enables us to build a stochastic model of the observed (blurred and noisy) image, by using a Bayesian approach.

The parameter estimation is performed automatically, by maximizing the marginalized likelihood, which is achieved by a fast deterministic algorithm. The method used is robust: the optimization is performed over a small number of parameters, since the joint likelihood is integrated over the nuisance parameters (the image model parameters).

The method can be applied to satellite, aerial or ground-based imaging, but also to planetary imaging in Astronomy. The estimated parameters can be used as they are, or in a deconvolution algorithm to restore the observed data. The method has been tested on simulations provided by the French Space Agency - CNES (SPOT5 and Pleiades satellites planned from 2002 to 2012). The proposed algorithm could also be used in natural signal processing (1D) or in confocal microscopy (3D).

Patent deposit request at INPI (France) no 0110189 - July 30, 2001.

Session C/F1, 13:55-Wed.

PROPAGATION AND SCATTERING IN VEGETATION

Chairpersons: R. Lang and B. Sadler

SOME FUNDAMENTAL ISSUES IN FOLIAGE PENETRATION

G.S. Brown
EMIL, Bradley Dept. of ECE
Virginia Tech
Blacksburg, VA 24061-0111

Wave propagation and scattering in foliage represents a challenge for many reasons; some of these are obvious and some are subtler. The dielectric properties of the material comprising foliage give rise to both strong absorption and scattering. In addition, it is difficult to identify the "components" of the foliage that can be taken as representative of the electrophysical properties and structure of the foliage. Clearly, these are issues that on-going numerical modeling will resolve in the future. However, decisions must be made now relative to systems designs and this forces to investigate the penetration problem at a more basic but perhaps less rigorous level of study. Such is the purpose of this paper. The specific problem to be addressed is that of a synthetic aperture radar (SAR) viewing a ground-based target obscured by a relatively thick layer of foliage comprising trees and bushes. We first point out the obvious limitation of a 2-D imager such as SAR when viewing a penetrable volume, e.g., the radar has no ability to resolve scatterers in the look angle coordinate. We next use some simple results obtained by Ishimaru for the scattering of a Gaussian beam incident upon a absorbing and multiple scattering medium in which the scattering is strongly in the forward direction. We discuss the justification of this forward scattering approximation when the frequency of the incident field is low. We then compute the target signal-to-clutter ratio (SCR) when there is a target located at some depth into the foliage Assuming negligible ground clutter, we show that the SCR result can be expressed as the product of three distinct factors. First, there is the SCR in the absence of any intervening attenuation by the foliage; it is simply the ratio of the target radar cross section to the product of the foliage scattering cross section per unit volume and the radar resolution volume. The next factor represents the effect of the double passage multiple scattering in an absorptive medium; this is the factor that is highly dependent upon the absorption that takes place in the medium. Finally, the last factor represents the effect of enhanced backscattering in a multiple scattering absorptive medium. As Ishimaru notes, when there is multiple scattering present, it is absorption that most affects the "free-space" SCR. That is, when multiple scattering is included, the expression for the "in the medium" SCR is dominated by the absorption. This apparent paradox is explained by noting that when multiple scattering is present, there is a non- zero probability that incident energy will be scattered back to the receiver. We also discuss the implications of this result and its frequency dependence relative to radar design.

MAPPING FOREST BIOMASS IN PANAMA USING VHF SAR

Imhoff, M. L.
Biospheric Sciences Branch/Code 923
NASA's Goddard Space Flight Center
Greenbelt, MD 20771, USA
Johnson, P., Carson, S., Hyer, J., Holford, W.
Zimmerman Associates Inc./American Electronics, Inc.
Vienna, VA 22182-2623, USA
Lawrence, W., Stutzer, D.
Bowie State University
Bowie, MD 20715, USA

In 1998 a VHF (80-116 MHz) synthetic aperture radar (BioSAR) mounted on NASA's C-130 aircraft collected data over a series of Smithsonian Tropical Research Institute (STRI) test sites along the Panama Canal Zone in the Republic of Panama. The data for each ground cell were collected in a downward looking mode using 6 frequency bands separated into 5 degree incidence angle bins (+/- 45 degrees) fore and aft of the flight line. Ground resolution for a data cell is 30m x 300m (azimuth and cross-track direction respectively). The nadir pulses were discarded. The SAR was calibrated at the airstrip using a tone generator at the beginning and end of the flight. Fourteen flight lines were made over tropical rain forests in the Panama Canal watershed. Best results for S/N were achieved when the data were averaged over the full frequency range and range of incidence angles. The radar signal was adjusted for terrain variation by calculating the local slope and aspect for each data cell from DTED and using that information to refine the estimate of the true incidence angle for each cell relative to the ground surface. An equation relating biomass to the return signal was applied and a biomass surface map of the area was generated by interpolating between BioSAR measurement points for a set of parallel flight lines. Signal averaging over incidence angle appears to best suit the downward looking mode of the instrument and seemed to improve the relationship between the radar signal and total biomass by enhancing sensitivity to volume over structure. Comparison to field data showed good agreement (+/- 10 percent) between the sensor-derived estimates of above ground biomass and ground-based measurements.

PASSIVE L-BAND MODELS AND MEASUREMENTS OVER CONIFER FORESTS

R.H. Lang*, C. Utku
Dept. of Electrical and Computer Engineering
The George Washington University
Phillips Hall, Washington, DC 20052
D. Le Vine
Goddard Space Flight Center, NASA
Greenbelt, MD 20771
N. Chauhan
NPOESS Integrated Program Office
Silver Spring, MD 20910

Airborne L-band radiometer sensitivity to forest biomass and soil moisture has been a topic of recent investigation. Flights over conifer stands in southern Virginia by ESTAR, a 1.43 GHz horizontally polarized synthetic aperture radiometer, have been made as part of this study. The data from these flights have shown that the brightness temperature is sensitive to forest biomass, as well as, to forest floor soil moisture. A field team that recorded soil moisture and stand parameters in selected forest stands has accompanied the over-flights, which occurred in the summer and fall of 1999.

The imaged area, which is owned by International Paper Inc, consists of even aged loblolly pine stands of approximately one to two kilometers on a side. The stands range in biomass from 20 to 200 tons/ha and are located on mostly flat terrain. Ground truth measurements of the stands included dbh, trunk density, branch size distribution and needle density. The forest floor soil consists of a layer of litter (organic matter) overlying a sandy loam soil. During the over-flights moisture measurements of both the litter and the soil were made. In addition, litter thickness at selected sites within the stands was also recorded.

A passive distorted Born model for predicting the brightness temperature from stand and ground parameters has been constructed. This model uses a previously developed radar backscatter model in conjunction with Peak's principle which relates active and passive microwave signatures. A two layer model of the ground has been incorporated in the modeling procedure so that changes in litter and soil moisture can be related to changes in brightness temperature. Model and experimental results will be compared.

ANALYSIS OF VEGETATION MICROWAVE PARAMETERS DEPENDENCY ON VIEW ANGLE AND POLARIZATION (SMOS MISSION)

M. Parde, A. Chanzy
INRA-Unite CSE (Climat-Sol-Environnement)
Site Agroparc - Domaine Saint Paul
84914 - Avignon Cedex 9 FRANCE
J.-P. Wigneron
INRA-Unite bioclimatologie
BP 81
33 883 Villenave D'ornon FRANCE
T. Schmugge *
USDA/ARS Hydrology Lab
Bldg 007 - BARC West
Beltsville, MD 20705-2350 USA

The main objective of the Soil Moisture and Ocean Salinity (SMOS) mission is to deliver crucial variables of the land surfaces: soil moisture. Soil moisture, and its spatio-temporal evolution as such, is a key variable in the hydrologic cycle, for numerical weather and climate models, and should be accounted for in vegetation monitoring. The only direct way to access to soil moisture is through the use of L-band (1.4 GHz) microwave radiometer systems. The SMOS mission will make multiple measurements of the brightness temperature at many view angles and two polarizations. To model the soil first layer water content, we have to account for the effect of the vegetation on soil emission and for the vegetation emission itself. Very few studies have investigated to date the vegetation microwave signature, including the angular and the polarization dependence. Because of the SMOS measurements configuration, view angle, time, polarization and vegetation species dependences of the vegetation microwave signature, have to be studied. The model we used for simulating the vegetation emission is the $\tau - \omega$ model. In this model, the single scattering albedo,ω, accounts for scattering effects and the optical depth τ accounts for attenuation effects within the canopy. In order to model accurately the crop microwave signature, it is thus necessary to compute the dependence of ω and τ as a function of view angle, polarization and canopy type. To perform this study, we used the BARC (Wang et al.,1981) and PORTOS (Wigneron et al.,1995) data sets over corn, wheat, alfalfa, grass and soybean. A simple approach was used to calculate the microwave parameters b and ω for each crop canopy. Results showed that for corn, the angular and polarization dependence of b and ω are significant. For the alfalfa and grass canopies, this dependence is lower. Moreover, we pointed out the fact that the values of b are higher for grass and alfalfa than for corn vegetation. It seems that scattering effects are lower within the stem-dominated canopy (corn) than within the low and leafy grass cover.

RELATING SURFACE AERODYNAMIC ROUGHNESS TO INTERFEROOMETRIC SAR DATA

Ernestor Rodriguez
Jet Propulsion Laboratory
Scott Denning
University of Colorado
Ralph Dubayah
University of Maryland

The aerodynamic parameters of vegetation are important to determine the vertical gradients of mean wind speed and the conditions for momentum transfer. In modeling the wind profile and drag over a canopy, the height where the wind speed becomes zero is referred as the aerodynamic roughness length of the vegetation. This roughness length is equivalent to the rms height variation of the vegetation at the top of the canopy. Once this roughness length is determined for a certain canopy, it does not change with the wind speed, stability or stress. However, the roughness length can change if the canopy structure and density change. In this paper, we investigate the feasibility of estimating this parameter from interferometric SAR (INSAR) measurements. It has been shown that the phase difference calculated from the cross product of two complex images obtained by INSAR is sensitive to surface height which is defined as the distance between the scattering phase center and a reference line. Over vegetated surfaces, the scattering centers are shifted within the canopy and their relative location depends on the vegetation height, density and type, and the radar wavelength. A scattering model based on wave theory has been developed to simulate the INSAR measurements over forest canopies. In this model the vegetation layer is treated as a discrete random medium where the canopy components are represented as three dimensional canonical geometries. The model simulation shows that the cross-correlation phase and amplitude when averaged over an ensemble of pixels are accurately related to the rms height of the vegetation or the aerodynamic roughness length. The relation between the correlation and the rms height of the surface is presented analytically. Model simulations performed over realistic canopy parameters obtained from field measurements in boreal forest environment demonstrate the capability of the INSAR measurements for estimating and mapping surface roughness lengths over forests and/or other vegetation types.

ISSUES IN FOLIAGE PROPAGATION IN ARMY MOBILE COMMUNICATIONS

Perlman, B., US Army Communications-Electronics Command, Ft. Monmouth, NJ
Sadler, B.M., Army Research Laboratory, Adelphi, MD

In this talk we discuss some of the issues associated with the multi-user wireless communications problem, focusing on Army mobile ad hoc networks and electronic sensors that must operate in and out of foliage. Future mobile Army systems must operate in dense foliage, with both ground-to-ground and air-to-ground links, on the move, and with wide bandwidths. We address Army requirements in the context of current foliage propagation and transceiver signal processing efforts.

RF propagation modeling in foliage, up to MMW frequencies, will allow rapid evaluation of notional communications infrastructure and associated technology offerings. To achieve this goal, enhanced higher fidelity RF propagation models are being developed with a physics based approach used to model foliage and asymptotic techniques (ray tracing methods) used to handle multipath effects. Appropriate terrain and foliage sensitive tools are being developed, to be interfaced with network models to realize accurate representation of the wireless channels. Both gross and fine models are needed. Gross models provide for reduced complexity scalable network simulations, with fast run times that can accommodate hundreds to thousands of mobile heterogeneous nodes. Fine models allow simulation and study of channel impulse response statistics in a variety of specific scenarios. These may lead to new statistical channel models for optimal statistical signal processing in future transceivers.

The study of spatial statistics of foliage channels will help with the development of new smart antenna receiver algorithms. Fundamental questions surround the use of spatial beamforming versus diversity combining. The optimality of this choice depends critically on the expected spatial coherence. In addition, space-time methods that exploit multiple antennas on transmit and receive may derive significant benefits from the dense scattering environment, with enhanced capacity and throughput.

MILLIMETER WAVE ATTENUATION PREDICTIONS THROUGH TREE FOLIAGE

S. A. Torrico*
Comsearch
Ashburn, VA 20147
R. H. Lang
Electrical and Computer Engineering Department
The George Washington University
Washington, DC 20052

Motivated by the development of modern broadband wireless communication systems, there is a need to better understand the propagation channel for millimeter waves in vegetated residential environments. Path lengths for millimeter wave links are relatively short. Consequently, the Fresnel zones between the transmitter and the receiver are also small - much smaller than at lower frequencies. It is therefore quite practical in most cases to avoid blockage of the first Fresnel zone. This is not the case for systems located at the rooftop of domestic houses where tree foliage can be important. Here foliage may completely or partially block the transmission path. Therefore, it is of practical interest to find out the attenuation effects of trees on the propagation at these frequencies.

This work describes the use of the radiative transfer equation to understand the attenuation effects of trees on the propagation for millimeter waves. The vegetation canopy is modeled by a random collection of branches and leaves, which are replaced by cylinders and discs respectively. At millimeter wave frequencies, the wavelength is small compared to the size of the scatterers and, as a result, a forward scattering approximation can be employed to simplify the transport analysis. In this analysis, the specific intensity is split into two parts: the coherent and the incoherent intensity. The wave scattering from foliage generates the incoherent waves traversing the foliage in addition to the attenuated coherent wave. We will show how the ratio between the incoherent and coherent intensity varies with penetration depth for different foliage parameters and frequencies.

FOLIAGE PENETRATION, PROPAGATION AND SCATTERING MEASUREMENTS FOR BLAST

A. Pidwerbetsky*, D.M. Romain, A.D. Tubbs
Bell Laboratories/Lucent Technologies
Whippany, NJ 07981, USA

BLAST (Bell Labs LAyered Space-Time processing) can provide an order of magnitude greater spectral efficiency (more bits/sec per Hz) for wireless communications than traditional techniques. It exploits multi-path propagation through the use of multiple transmit and receive antennae and space-time signal processing. This exploitation requires understanding the nature of multi-path propagation in different environments as well as BLAST processing and array design. To better understand and apply BLAST we have conducted a number of experiments in outdoor environments with several array designs and have calculated the data-rate capacities BLAST could provide in those environments.

Propagation measurements for BLAST differ from traditional propagation measurements in that not only is the signal level important, but also the transfer function from each of the multiple transmit elements to each of the multiple receive elements in terms of both amplitude and phase. To make these measurements, we have constructed specialized data collection equipment supporting 16 simultaneous transmit and receive channels and the development of new analysis techniques. These have been used to explore a number of geometries and environments. In particular, recent experiments have focused on various foliage environments, where the scattering by foliage provides a significant opportunity for greater BLAST capacity by using the resulting multi-path propagation.

Results from a number of experiments with both fixed and mobile geometries (including foliage obstructed air-to-ground and ground-to-ground links) will be presented. These results show the enhanced data-rate capacity that BLAST can provide in foliage environments.

Acknowledgement: This research was performed in connection with Contract/Cooperative agreement DAAD19-01-C-0022 with the US Army Research Laboratory under DARPA's FCS-Communications program.

MIMO CAPACITY FOR RICIAN FADING CHANNELS

Mahesh Godavarti
Altra Broadband, Inc
Irvine, CA 92618.
Alfred Hero
Univ. of Michigan
Ann Arbor, MI 48109-2122

The demand for high date rates over wireless channels has led many to investigate deployment of multiple antennas at the transmitter and the receiver to increase link capacity. The channel capacity for such multiple input multiple output (MIMO) systems has been investigated under the Rayleigh fading assumption by Telatar (1995), Marzetta and Hochwald (1999), and Zheng and Tse (2001). Very significant gains in capacity have been observed when the transmitter can take advantage of the random independent fades intrinsic to the Rayleigh channel model. However, for many practical channels the Rayleigh channel assumption is not valid due to the presence of one or more specular multipath components. For such cases the Rician model, which accounts for both diffuse multipath (Rayleigh fading) and specular multipath components, is more appropriate. Capacity for the Rician MIMO model with a time varying isotropically random specular component has been recently investigated by Godavarti, Marzetta and Schitz (2001). The min-capacity for a persistent static specular component has been investigated by Godavarti and Hero (2001). These results apply to the restricted case of equally likely angles of incidence of the specular component on the receiver array.

In this paper, we analyze MIMO channel capacity under an unrestricted Rician fading model subject to an average transmitted energy constraint. We assume that the specular component of the Rician model is known to both transmitter and receiver while the Rayleigh component is known to the receiver but not known to the transmitter. This we call the informed receiver scenario. We also consider the uninformed Rician MIMO channel capacity when pilot symbols are used in a training sequence to aid the receiver in estimating the channel. We obtain asymptotic closed form expressions for the capacity in various limiting situations including: large and small SNR and specular/diffuse power ratio, and large Rayleigh coherence interval. In particular, we establish that for low SNR the specular component of the channel completely determines the form of the optimum capacity attaining signal whereas for high SNR the Rayleigh component completely determines optimum signal structure. We conclude that beamforming at the transmitter is the optimum signaling strategy for low SNR. Finally, we establish a SNR threshold effect on the effectioveness of training in terms of achieving the channel capacity of the informed receiver. In particular. while training can be used to acheive the informed MIMO capacity in high SNR, it is not effective at low SNR.

AN INTERFERENCE-BLOCKING RAKE RECEIVER FOR WIRELESS COMMUNICATIONS SYSTEMS

T.T. Lin
National Lien-Ho Institute of Technology
1 Lien Kung, Kung Ching Li,
Miaoli, Taiwan, R.O.C. 360

A major challenge for wireless communications systems is the limited capacity, mainly determined by the interference rejection capability, due to sparse radio frequency spectrum. In CDMA systems, signals from other users, termed as interference, can be significantly attenuated by means of lower cross-correlation among users spreading codes. However, strong narrowband interference cannot be completely suppressed because of insufficient processing gain and will result in certain performance degradation. In addition, multipaths introduced by the environment will deteriorate the performance. As a remedy, the RAKE receiver is proposed for the purpose of coherently combining of the multipath signals.

In this paper, a space-time RAKE (ST-RAKE) with an interference-blocking (IB) scheme is proposed for combating the strong interference in CDMA communications systems over multipath fading channels. Specifically, a scheme is developed firstly to construct an IB transformation for removing the strong interference. From the fact that the power level of the signal is well below that of the strong interference, the interference term can be approximately expressed in terms of the dominate eigenvectors corresponding to the larger eigenvalues of the received data correlation matrix. The complementary (orthogonal) subspace, referred to IB subspace, can be utilized for suppressing the strong interference. An optimum beamforming is then performed based on the IB transformed data to produce effective reception of signals of interest (SOIs) and suppression of strong interference.

The overall procedure of the proposed interference-blocking RAKE (IB-RAKE) receiver can be summarized as below: (1) Compute the IB transformation based on the received data correlation matrix. (2) Compute the optimal beamforming weights based on the transformed data, which consists only of the SOIs and noise. (3) Apply RAKE technique to the beamformer outputs to produce constructive combining of SOIs. (4) Obtain the estimated data by using a hard decision processor.

Numerical results obtained via a W-CDMA system, a third generation cellular system, demonstrate that the proposed IB-RAKE receiver exhibits robustness against strong interference and a significant performance enhancement as compared with the conventional RAKE receivers.

Session D1, 13:35-Thurs.

NANOTECHNOLOGY

Chairpersons: P. Ajayan

NANOSTRUCTURED MATERIALS AND NANOTECHNOLOGY

Richard W. Siegel
Materials Science and Engineering
Rensselaer Polytechnic Institute
Troy, NY 12180

The past decade has seen explosive growth worldwide in the synthesis and study of a wide range of nanostructured materials, the building blocks of nanotechnology. A wide variety of scientifically and technologically interesting nanostructured materials have been synthesized and investigated. These have included metals, ceramics, and composites made by means of a number of experimental methods. While these new materials have been synthesized most elegantly from either atomic or molecular precursors, those made from bulk precursors have yielded important results as well. The structures and properties of nanostructured materials have now been elucidated in a number of important areas and a fundamental understanding of the relationships among these areas is beginning to unfold. Most important among these is an understanding of the atomic-scale structures of the nanocale building blocks and their interfaces and the important role of spatial confinement on material properties in general, when the sizes of the nanoscale building blocks become smaller than the critical length scale for any particular property. Investigations of mechanical, chemical, electrical, magnetic, and optical behavior of nanostructured materials have demonstrated the possibilities to engineer the properties of these new materials through control of the sizes of their constituent building blocks and the manner in which these constituents are assembled. It is now very clear that through nanostructuring we can access novel material properties.

In this talk, an overview of nanoscience and nanotechnology and their relationship to nanoscale materials will be presented within the framework of the 2001 U. S. National Nanotechnology Initiative (http://www.nano.gov). Several examples from our own research results will be discussed. A variety of useful nanostructured composite materials with novel properties using polymer, ceramic, and carbon nanoscale building blocks have been created. The properties of these nanocomposites are quite different from the corresponding matrix material and they can be engineered by means of careful control of nanoscale filler dispersion. For example, ceramic/polymer nanocomposites can exhibit superior scratch resistance, increased values of modulus combined with increased strain-to-failure, enhanced dimensional stability, and novel interactions with biological cells. On the other hand, carbon-nanotube/ceramic nanocomposites can exhibit significantly increased fracture toughness while maintaining high hardness values.

CARBON NANOTUBES IN NANOELECTRONICS AND SENSORS

Meyya Meyyappan
NASA Ames Research Center
Center for Nanotechnology
Moffett Field, CA 94035

Carbon nanotubes (CNTs) are at the crossroads of micron size traditional carbon fibers and well defined carbon molecules. A host of remarkable properties has provided carbon nanotubes, the status to be considered as the ultimate one dimensional structure (fiber) ever made. The uniqueness of the nanotube structure arises from what is known as helicity in the arrangement of hexagonal arrays on their surface layer honeycomb lattices. This helicity (local symmetry), along with diameter (which determines the size of the repeating structural unit) introduces significant changes in the electron density of states and provides the unique electronic character of nanotubes. Carbon nanotubes hence exhibit unique electrical and extraordinary mechanical properties and offer remarkable potential for revolutionary applications in nanocomposites, electronics devices, computing and data storage technology, sensors, instrumentation, and as a tip in scanning probe microscopy (SPM) for imaging and nanolithography. Thus the CNT synthesis, characterization and applications touch upon all disciplines of science and engineering. Chemical vapor deposition (CVD) and plasma-enhanced CVD have been used to grow vertical arrays of nanotubes needed for many applications. Chemical functionalization of the tips in the array with probe molecules is in progress, which is critical for the biosensor development for astrobiology and biomedical applications. We have made significant demonstrations in the use of nanotube tips in AFM in semiconductor metrology, profilometry and imaging of biological samples. A nanotube based inverter has been demonstrated which will be a building-block for nanoscale integrated circuits. This talk will provide an overview and progress report on CNT growth, chemical functionalization, application development in device and sensor technologies along with the current barriers to realization of the complete potential of CNTs.

PATTERN DEFINITION IN SELF-ASSEMBLED PHOTONIC BAND GAP MATERIALS

Paul Braun
Department of Materials Science and Engineering
University of Illinois at Urbana-Champaign
Urbana, IL 61801

The formation of low dielectric contrast three-dimensional nano- and microperiodic structures through colloidal templating is relatively straightforward, but fabrication of high dielectric contrast structures as required for formation of a three-dimensional photonic band gap material remains quite challenging. Furthermore, for most applications, the functionality of self-assembled photonic crystals will be greatly enhanced if complex nanoscale features including wave guides and optical cavities are defined within the interior of the photonic crystal. We have discovered routes to address both these issues. First, we developed a range of materials chemistry routes which operate within the three dimensional void space of a colloidal template to form essentially infinite, high dielectric contrast three dimensionally periodic structures. These strategies included imbibing of nanocrystalline titania, melt imbibing of chalcogenide glasses, and electrodeposition of II-VI semiconductors and conducting polymers. Second, we developed several promising approaches based on multiphoton polymerization of monomers contained within the interstitial space of the precursor colloidal crystal to write buried polymer wave guides and optical cavities with nanoscale precision within the self-assembled photonic crystals. Both 2- and 3-photon polymerization strategies were found to be effective for urethane and acrylate based systems respectively. The colloidal templates containing the polymerized features were then imbibed with a high dielectric constant material following the above procedure, which should result in integrated photonic band gap waveguides and optical cavities. The high dielectric constant material fills the interstitial space of the colloidal crystal everywhere except where the polymerized feature had been formed. Preliminary results on the optical properties of these patterned nano- and microscale structures will also be discussed.

CARBON NANOTUBES AS ROBUST ELECTRON FIELD EMITTERS FOR VACUUM ELECTRONICS

Otto Zhou
Department of Physics and Astronomy
University of North Carolina
Chapel Hill, NC 27599

Materials comprising nanostructured building blocks often have novel properties that are not shared by their conventional counterparts in bulk forms. Interests in basic science at nanometer-scale and nanotechnology have led to synthesis and fabrication of a growing number of new nanostructures including the recently discovered carbon nanotubes (CNTs). Only a decade after their discovery, the new knowledge available in this field indicates that nanotubes may be used in several practical applications. There have been great improvements in synthesis techniques, which can now produce reasonably pure nanotubes in gram quantities as well as in pre-selected orientations on planar substrates. In addition to being an ideal system to investigate the fundamental science at the nanometer scale, the carbon nanotubes are shown to have a wide range of potential technological applications, for example as probes for high resolution microscope, electrode materials for high energy density rechargeable batteries, electron field emitters in vacuum electronics including flat-panel displays, telecommunication devices and medical imaging. Compared to the conventional emitters such as the Spindt-type tips formed by lithography, the CNTs have a significantly lower threshold field for emission (1V/mm), and enhanced high current capability (A/cm2). In this talk we will give a brief overview of the basic emission characteristics of the CNTs and discuss the effects of structure, morphology and higher-level architecture of the CNT materials on their macroscopic emission properties. Techniques developed to fabricate CNTs and incorporate them into device structures will be reviewed. The performance to the CNT emitters in device environments will be presented. In addition we will demonstrate some prototype CNT based cold-cathodes devices for over-voltage protection, amplifier and for imaging applications. The work presented here was supported by an Office of Naval Research MURI program at UNC and by Applied Nanotechnologies, Inc.

PHOTONIC DEVICES BASED ON CARBON NANOTUBE - ORGANIC MATRIX COMPOSITES

David L. Carroll
Department of Physics and Astronomy
Clemson University
Clemson, SC 29634-1911

Advances in the field of composite formation using organic and organic/inorganic nano-particles and nano-architectures, have created exciting new possibilities for realizing organic based optical circuitry. This includes active optical sources, light gathering, sensing, and computational networks based on recent demonstrations of tailored hole mobility in organic light emitting diodes, enhanced pyroelectric and piezoelectric response of PVDF nanocomposites, and enhanced photovoltaic efficiencies from carbon nanotube - organic composites. Within the last few years, increasing attention has been focussed on the optical properties of multi-walled and single walled carbon nanotubes. Specifically, nanotube-polymer composites have been shown to have exceedingly good optical limiting properties, pyro electric response, and enhanced quantum yield in luminescence devices (LEDs). Recent work has suggested that there are two regimes of optical response; far-field nonlinearities and near-field interactions that must be considered in the optics of a nanotube aggregate. While generally these considerations offer only small corrections to the optical properties of a composite, there are several examples (such as mentioned above) in which they play an important role. In this discussion, the role of nanotube optics, coupled with their unusual electrical transport properties, will be presented for several matrix composite based devices. In particular, organic light emitting diodes (OLEDs), organic photo voltaic cells (OPV), and organically based pyro-electric detectors will be shown to exhibit substantial performance increases with the insertion of the nanocomposite into the device design. In each of these cases, performance augmentation is quantified as a function of nanotube loading, type of nanotube (doped/undoped, SWNT/MWNT), and nanotube length. A model for the modification of nanotube-photon interactions due to the host will be presented that gives a general framework to device function with nanocomposites.

NOISE ASPECTS OF NANOTECHNOLOGY DRIVEN ELECTRONICS

L.B. Kish
Texas AM University
Department of Electrical Enginering
College Station, TX 77843-3128, USA

In this talk, we will discuss various aspects of the noise in nanometer size devices. Approaching nanometer length scale with electronic device sizes has serious implications on performance and noise properties. By shrinking to the mesoscopic size range, not only the parameters but also the governing physical phenomena can change. One well-known example is the Coulomb-blockade effect which reduces the shot noise of junctions. However, the effect of shrinking is not always so beneficial, because the new parameters set new limits for device performance. From classical knowledge on device noise an increased 1/f noise and increased effective thermal noise voltage is expected which imply performance limitations at the low frequency and high frequency ends, respectively. The result is a reduced long-term stability and increase false-bit-switching or false alarm events. From the research-and-development side, the origin and engineering of conductance noise (1/f noise) is often an unsolved problem. For example, in carbon nanotubes, the published experimental results are contradictory and it is not possible to draw a final conclusion about the nature and possible ways of engineering this crucial kind of noise source. It is important to realize that more active noise sources do not always mean limitation of performance. In chemical sensing applications, the measurement of noise can be used to detect chemical agents and their composition with a great selectivity and sensitivity, because the chemical fragments dynamically interact with the current transport in the device. This is the situation when the noise in nano-sensors has a great advantage as compared to the noise in classical devices. The increased specific surface of nanostructures and the large number of possible structural combinations have a great potential for both gas and fluid sensing applications via noise analysis.

Session D2, 8:35-Fri.

WIDE BANDGAP SEMICONDUCTOR DEVICES

Chairpersons: J. Sewell and R. Fitch

A HISTORICAL BACKGROUND OF WIDE BANDGAP SEMICONDUCTORS FOR RADIO AND TELECOMMUNICATIONS

Stutz, C.E.
Air Force Research Laboratory
AFRL/MLPS Bldg 620
2241 Avionics Circle
WPAFB, OH 45433

The area of Wide Bandgap Semiconductors, which includes semiconductors with a bandgap greater than 2 eV, has been dramatically growing since the late eighties due to enhanced growth capabilities. Materials such as SiC and the nitrides have dominated this area for high power RF, high power switches, and optical devices. The ability of SiC to easily conduct heat (thermal conductivity of 4.9 W/cm-K) away from a device is very useful for high power and RF applications. Its large critical field (2.0e6 V/cm) allows for a very high energy density, which allows for a smaller footprint and hopefully a cheaper device. However, GaN has an even bigger critical field (3.3 V/cm) and has the potential for an even higher power density. Unfortunately, the thermal conductivity of GaN is significantly lower (1.3 W/cm-K) than SiC. This has caused people to grow GaN on SiC substrates hoping for the best of both worlds. However, the lattice constants are significantly different (about 2 percent) which causes copious amounts of extended defects (greater than 1xe8 cm-2). Nitride based light emitting diodes grown on sapphire substrates (whose lattice constant difference is 13 percent) have been shown to have their lifetimes dramatically increased using novel epitaxial growth techniques, like epitaxial layer overgrowth (ELO), by reducing the number of defects. It has not been confirmed, but these defects are expected to cause reduced device reliability in RF devices, also. The ELO-like techniques however have produced very conductive layers. For RF based applications this is not acceptable due to transmission losses. Alternative based substrates have been suggested like ZnO, LiGaO, AlN and GaN.

CHARACTERIZATION OF ALGAN/GAN DEVICE LAYERS AND OHMIC CONTACTS USING LEEN SPECTROSCOPY

Jessen, G.H., Bradley, P., Smith, P., Brillson, L.J.
The Ohio State University, 205 Dreese Laboratory
2015 Neil Avenue, Columbus, OH 43210
Van Nostrand, J., Fitch, R., Gillespie, J., Via, D., Dettmer, R., Sewell, J.
Air Force Research Laboratory
WPAFB, OH 45433

Cathodoluminescence spectroscopy (CLS) performed at low incident electron beam energies can yield information about the electronic properties of semiconductor surfaces and interfaces of device material that can affect device performance. By varying the incident beam energy, we can probe the device layers as a function of depth. We call this form of CLS Low Energy Electron Nanoscale luminescence (LEEN) spectroscopy. We have fabricated ohmic contacts on AlGaN/GaN High Electron Mobility Transistor (HEMT) structures grown by MBE and used LEEN spectroscopy to characterize the active and semi-insulating (SI) layers and ohmic contacts of the devices.

Ohmic contacts to n-GaN were made with Ti/Al/Ni/Au annealed at 800 (C for 30 seconds. Ohmic values from 5x10-7 to 5x10-5 (cm2 were obtained and measured via TLM. The presence of spatially localized midgap states observed by LEEN spectroscopy correlates with higher values of contact resistance in the TLM structures. Luminescence measurements also show variation in the quality of the SI layers. In some SI layers, the near bandedge emission of GaN is the only discernible feature. In other SI layers, we either observe no near bandedge emission at all, or weak, broad near bandedge emission accompanied by a continuum of midgap states directly below the bandedge. In HEMT active layers, the localized layer of higher defect density associated with the yellow luminescence normally observed in n-GaN may occur near the AlGaN/GaN interface with the 2-DEG or on the bulk GaN side of this interface. We are also able to spectroscopically detect changes in material quality due to processing. Unprocessed material shows low near bandedge to yellow emission ratios. During formation of the ohmic contacts, the sample processing increased the near bandedge to yellow emission ratio on all samples.

Our measurements can detect features that may be present in materials prior to device fabrication and could manifest themselves in completed devices. The results presented here show that CLS can help identify regions of poor device performance. This information helps to understand atomic scale electronic properties that can be used as feedback in processing improvements. Additional studies to correlate gate structure performance with LEEN spectroscopy are in progress to correlate CLS signatures with Schottky barriers and frequency performance.

NOVEL GALLIUM NITRIDE BASED HETEROJUNCTION FIELD EFFECT TRANSISTOR

Simin, G., Kahn, A.
University of South Carolina
Dept. of Electrical Engineering
301 S. Main St.
Columbia, SC 29208
Gaska, R.
Sensor Electronics Technology Inc.
Lantham, NY 12100
Shur, M.S.
Rensselaer Polytechnic Institute
Troy, NY 12180

Unique properties of GaN and related semiconductors make them superior for high-power applications. The maximum density of the two-dimensional electron gas at the GaN/AlGaN heterointerface or in GaN/AlGaN quantum well structures can reach 1 to 5x1013 cm-2, which is an order of magnitude higher than for traditional GaAs/AlGaAs heterostructures. The mobility-sheet carrier concentration product for these two dimensional systems might also exceed that for GaAs/AlGaAs heterostructures. High current values in GaN/AlGaN devices can be combined with very high breakdown voltages. Self-heating, which is unavoidable in power devices, raises operating temperatures of power devices well above the ambient temperature. For GaN-based devices, the use of SiC substrates having high thermal conductivity is essential for ensuring effective heat dissipation. In this talk, we will review the novel designs of AlGaInN/GaN and AlGaInN/InGaN Heterostructure Field Effect Transistors. These innovations include the use of Strain Energy Band Engineering approach (in order to independently control strain and strain related polarization charges and band gap offsets), MOSHFET and MISHFET designs using silicon dioxide and silicon nitride layers, the use of silicon dioxide bridging (instead of air bridging) in multi finger power devices, and the use of quantum well AlGaInN/InGaN HFETs for the elimination of so-called current collapse effects therefore increasing the output power.

GaN-based HEMTs are being developed for several commercial and military applications including cellular/satellite communications and radar. Target frequencies range from L-band to Ku-band. In addition to high-power operation, these devices have potential to offer high efficiency, high linearity, as well as improved robustness.These devices will soon be available for system insertion.

GAN-BASED ELECTRONIC DEVICES FOR HIGH FREQUENCY , HIGH TEMPERATURE, AND HIGH POWER

J.W. Johnson, B. Luo, B.P. Gila, A.P. Zhang, R. Mehandru, S.J. Pearton, C.R. Abernathy, F. Ren
Dept. of Chem. Eng., Dept. of Mat. Sci. and Eng.
University of Florida, Gainesville, FL 32611, USA
A.G. Baca
Sandia National Laboratories, Albuquerque, NM 87185, USA

Increasing performance demands (e.g. bandwidth, operation temperature, voltage rating) are fueling the demand for wide bandgap electronic device development. Satellite and radar communication systems, wireless base stations, high temperature electronics, and high power solid state switching are only a few examples of the numerous areas of potential for appropriately designed wide bandgap devices and components. GaN and related alloys are one of the most attractive material systems for such applications.

AlGaN/GaN HEMTs have been grown by MOCVD on sapphire and SiC substrates. Drain current density approached 1 A/mm and extrinsic transconductance exceeded 200 mS/mm for small gate periphery devices. Devices fabricated on the high thermal conductivity SiC substrates exhibited superior high temperature performance and a reduced density of threading dislocations. Initial investigations of the proton and gamma-ray radiation tolerance of these HEMTs has demonstrated their potential for space-borne, nuclear, and/or military applications.

Gd2O3 and ScO were grown by gas source molecular beam epitaxy as candidate gate dielectrics for GaN MOS devices. MOSFETs with a stacked gate dielectric of SiO2/Gd2O3 were operational at a drain-source bias of 80 V and a forward gate bias of 7 V. Effective passivation of the (Al)GaN surface with these novel dielectric materials may prove useful in reducing the DC-to-RF dispersion effects currently limiting the large signal performance of AlGaN/GaN HEMTs.

Bulk GaN templates grown by hydride vapor phase epitaxy were used to fabricate vertical geometry Schottky rectifiers. These vertical geometry devices show significant improvements in forward turn-on voltage, on-state resistance, and reverse recovery characteristics relative to previously reported lateral devices fabricated on heteroepitaxial GaN. A major short-term target for such wide bandgap switches is 13.8 kV, a common residential distribution mode. Future goals are 25 kV blocking voltage, 2 kA forward current, on-resistance less than 2 percent of the rated voltage, and switching speeds of 50 kHz. Other applications include control circuitry for electronic motor drives, hybrid-electric automobiles and military vehicles, and more-electric airplanes and nautical vessels.

Session D3, 13:35-Fri.

PHOTONIC NETWORKS, DEVICES AND APPLICATIONS

Chairperson: A. Mickelson

FUTURE PHOTONIC NETWORKS

Sairam k.v.s.s.s.s.*
Prof. ECE Dept. , Dr. M.G.R. Engg. College,
Affiliated to University of Madras, Maduravoyal,
Chennai 602 102, Tamilnadu State, INDIA

The recent explosion in internet traffic implies the dawn of the multimedia age.It is expected that volume of data traffic on the Globe will exceed to unhitherto unimagined Quantities of voice data. Foremost requirement of the future networks is the large bandwidth Transport capability and a much smaller transfer Delay. Optical layer enables quantum leaps in both transmission capacity and transport node Throughput simultaneously by exploiting wavelength-division multiplexing routing. Key Technologies such as WDM transmission networks, fiber amplifiers, network node interface, Network protection and restoration strategies are Discussed. The envisaged future photonic networks with high reliability and integrity are highlighted in detail. Our network will support the paradigm shift from voice to data-centric network.

Optical fiber transmission has led to a dramatic cost reduction over the last two decades. Basic concept of photonic transport Network in comparison with the existing network is depicted. In existing networks electrical processing is done at every node; optical technologies are only utilized for point to point Transmission.Photonic networks on the other hand will use direct optical connections without Electrical processing.

The photonic network consists of the core transport network and the edge network. The core network should provide abundant Transmission capacity with large throughput optical nodes. Electrical processing,if required is performed only in the edge network. In photonic networks, cell by cell or packet by packet electrical processing is not performed in transit nodes, Which minimizes transfer delay. The removal of electrical processing and introduction of wavelength routing will yield a core transport node with vast throughput.

Photonic networks are sure to become a pillar of the future information society.

DESIGN OF THE SMART OPTOELECTRONIC EXCLUSIVE OR GATE BASED ON MULTIMODE INTERFERENCE STRUCTURE

Wen-Ching Chang, Hsueh-Hui Lin, Hung-Jen Wang, and Shih-Wan Weng
Department of Electrical Engineering, Tamkang University
Tamsui, Taipei Hsien, Taiwan 25137, R. O. C.

AbstractXA novel smart optoelectronic XOR gate based on multimode interference structure has been proposed for the first time. Different from conventional methods, the multimode interference structure is employed to realize the XOR logic function. It takes advantages of the linear operation and the easy-to-implement logic function. In this paper, the detailed investigations such as configuration of the logic gate, and design rules of MMI structure have been considered.

In this paper, a novel smart XOR gate based on MMI structure has been proposed for the first time. The XOR logic function can be realized by partial index modulation in the middle of the MMI. The major components of the optoelectronic XOR gate are including MMI switches, optoelectronic converters, 90:10 optical couplers, and delay lines. The input power from input A or B is applied 90waveguide of MMI and coupled 10partial input phase. Besides, the input power will pass to the output waveguide if there is only one input light injected, and the light will dissipate on wafer if input A and B injects at the same time. Furthermore, the purpose of the delay lines is to synchronize the optical and electrical signal in the MMI.

The theory of a general MMI with at most N possible input and N output guides is reporded by [1]. The coupler length L is given as follows: $L=3Lc/N$ (1) where Lc is the beat length of the two lowest-order modes[1], can be written as $Lc=4nW/3\lambda$ (2) Compared to conventional methods, the structure takes advantages of the linear operation, being easy to realize logic functions, and large fabrication tolerance. Through the design of the smart exclusive OR gate, it is believed that logic gates based on MMI should be of great interest in the future.

(1.L.B.Soldano and E.C.M.Penning,*J. Lightwave Technol.*,**13**,615-627, 1995)

OPTICAL INTEGRATED CIRCUITS APPLICATIONS IN MEDICINE

sairam k.v.s.s.s.s.*
Prof. ECE Dept, Dr. M.G.R. Engg. College
Maduravoyal, Chennai 601 102, Tamilnadu State, INDIA.

ASIC is the "mantra" among today's electronics engineers. To make a major impact in the integrated circuit arena, it is essential to find a way to add functionality to silicon devices. Such is the aim of the Optical Application Specific Integrated circuit (OASIC) research. The photosensitive property of silicon is used in advance imaging technology through "smart pixel" sensors. The heart of an OASIC chip is poly-Si because it is a wavelength-sensitive reflector, absorber, and transmitter of light.

A chip on your fingertip can measure and transmit data on your body temperature, pressure, oxygen level, and impulse rate. These medical telesensors are for the military troops in combat zones. These when attached externally at various points on a solider, send physiological data by wireless to an intelligent monitor on another solider's helmet. The monitor alerts medics if the data showed that the soldier's condition fits one of five levels of trauma. It would also receive and tansmit global satellite positioning data to locate the wounded solider.

Oxygen level detector OASIC with a light source and detector can measure changes in the haemoglobin, due to oxygen level variations.

Since very early in the semiconductor revolution, silicon has been the workhorse in our electronic devices.,because of Silicon grows a stable oxide, which protects silicon from environmental degradation and creates an insulating layer, allowing the development of three dimensional structures needed for electronics devices. Electrical properties of silicon enable the creation of two types of complementary transistors, while other semiconductor materials. Silicon is an inexpensive and readily available material.

Silica makes the tremendous financial investement in the silicon processing infrastructure used by computer, electronics, and telecommunications industries worldwide. So , to make a major impact in the integrated circuit arena, it is essential to find a way to add functionality to silicon devices manufactured using standard process.

Such is the aim of Optical application-specific Integrated Circuit (OASIC) r esearch.

Session E1, 13:35-Thurs.

HIGH POWER ELECTROMAGNETICS

Chairperson: L.H. Bowen

EFFECT OF UNWANTED ELECTROMAGNETIC SIGNALS ON MESSAGE SIGNALING

R. Boling*, I. Kohlberg
Institute for Defense Analyses
Alexandria, VA 22311

In the last few years there has been increasing attention given to the proposition that bit errors caused by unwanted electromagnetic signals are responsible for upset in some systems. The plausibility for this conjecture is based on a combination of theoretical studies, and experiments conducted for a variety of electromagnetic sources. This paper is an extension of earlier theoretical studies; it includes in more detail the specific effects that unwanted wide-band (impulse), pulsed radar-type signals, and CW waveforms have on bit-by-bit and block-orthogonal signaling. Of particular interest is the performance of data networks in the presence of Intentional EMI (IEMI). This is especially illuminating, because the performance of virtually all data networks currently employed in the non-military infrastructure and in military systems is designed and based on signal-to-noise ratios computed for Gaussian noise.

Electromagnetic interference caused by IEMI signals is not readily characterized by Gaussian noise. It is not obvious nor is it always useful to attempt to represent IEMI signals as Gaussian equivalent noise sources. Nevertheless, the probability of signal detection error (and resulting possibility of system upset) can be estimated from statistical decision theory using a bank of matched filters and deterministic or stochastic IEMI signals.

Calculations of probability of bit error and probability of message error are carried out for several combinations of signaling schemes and unwanted waveforms. The results elucidate the importance of matching the unwanted waveform to the system architecture and protocols in order to achieve the most adverse effect, given fixed operational constraints such as average power and PRF. Conversely, insights into hardening systems against unwanted signals using coding schemes are also examined.

APPLICATION OF COMPUTATIONAL ELECTROMAGNETICS TO EMI EFFECTS ANALYSIS

B.J.Hankla*,C.A.Ropiak
NSWCDD, Code B20
17320 Dahlgren Rd.
Dahlgren VA, 22448-5100
P.Hayes
Envisioneering Inc.
Dahlgren VA, 22485

The presence of electromagnetic (EM) interference can result in undesirable effects on exposed electronic devices. The characterization of these electronic effects is of interest to many communities. Our work has focused on the development of robust methods that will allow for the forecast of effects in complex environments.

In general, electronic systems are located within structures that are complicated by geometry, material, and contents. Categorical effects threshold information obtained through testing of systems in such a complicated environment is often difficult to extrapolate to even similar configurations. This difficultly is due to the large number of variables that influence the effects in a manner that is not obvious. Even so, a common approach is to simplify the parameterization of the problem to a few easily measured quantities. In the case of EM interference, one such quantity is often a point field measurement. Such a measurement is generally very sensitive to exact placement in the environment and changes in the structure. A robust analysis depends on a measurement or variable that is well correlated to the more general EM environment. This is only the case for well-controlled experiments. Further difficulty lies in the sensitivity of the conclusion of the analysis to the location of the system of interest. What is sought is a more general prediction of the effect probability. The method described in this paper explores the use of descriptors of the field environment as determined by computational EM. The distribution of the descriptors is accumulated in a region of interest. This information is then combined with statistical regression techniques to form the basis of the effects analysis method.

To introduce the method, a simple example of an induced threshold condition is presented. The utility of the method is then explored by expanding to a more complex system that could not be readily estimated without computational EM.

APPLICATION OF MULTIVARIATE LOGISTIC REGRESSION TO THE PROBLEM OF EMI EFFECTS ANALYSIS

C.A.Ropiak*
Naval Surface Warfare Center
Code B20
17320 Dahlgren Road
Dahlgren, VA 22448-5100, USA
T. W. Larkin
Metatech Corporation
2309 Renard Place, S.E.
Suite 401
Albuquerque, New Mexico 87176-7378
R.L. Gardner
Consultant, JPO-STC
Naval Surface Warfare Center, Code B20
17320 Dahlgren Road
Dahlgren, VA 22448-5100, USA

For a number of electromagnetic interference (EMI) and high power microwave (HPM) problems one is interested in determining the conditions for upset of complex electronic systems. In particular, the identification of highly sensitive configurations or parameter sets is of interest. To accomplish this goal one must develop the tools necessary to predict the outcome of an illumination of that complex electronic system. Usually, these systems are much too complex to use deterministic analysis techniques so that one is forced to add information from empirical approaches. When utilizing an empirical approach the experiment must be planned beginning with a determination of the required parameters for investigation. In this paper an analytic solution for the problem of aperture excitation of a wire in a rectangular cavity is considered. The parameters of interest are the frequency of illumination, two angles, and range between source and target. For this data set, upset thresholds are defined in terms of the induced current on the wire. It should be noted that in general upsets are convoluted functions of the incident fields and the operating state of the system, but that type of data is not available for this study.

Upset data is categorical in nature, i.e., pass-fail. To describe this data multivariate logistic regression is used to fit the available parameters with the associated upset data. Once a successful fit is found, one has in hand a function that allows for the prediction of the outcome of future experiments provided the conditions remain within the limits of the initial data set. Although extrapolation outside the bounds of the initial data set is possible, its validity must be carefully scrutinized.

CHAOTIC COMMUNICATIONS THROUGH ARBITRARY ATTENUATION: A HARDWARE DEMONSTRATION

Arthur Fleming-Dahl*
Southwest Research Institute
PO Drawer 28510
San Antonio, Texas 78228-0510

A chaotic communications baseband system has been designed and implemented in hardware that transmits, synchronizes, and recovers a data message over arbitrary amounts of attenuation in the presence of noise. The primary result is that general nonlinear dynamical chaos-based signals can propagate through physical channels across arbitrary distances and achieve successful communication if the link budget is satisfied. This solution of the chaotic "distance problem" enables chaos to shed its status as a laboratory curiosity and move into the realm of realizable communications technology.

The hardware demonstration system encodes a user-defined message in chaos, and drives the corresponding analog signal into a 50-ohm channel and through an RF step attenuator. A maximum demonstrated attenuation of 70 dB is limited by the link budget limitations of the D/A voltage driven into the channel, A/D noise floor, and quantizer minimum voltage capability. Communication through arbitrary attenuation in 1 dB steps demonstrates that arbitrary distance has been achieved.

The Signal Amplitude Restorer (SAR) exploits the transmit probability density function to correct received amplitude to within tenths of a dB of a desired level. This digital algorithm has a verified instantaneous dynamic range of over 400 dB (+/-200 dB), leaving the typical 80-90 dB dynamic range physical front end as the limiting factor. Operation as low as 0 dB signal-to-noise ratio (SNR) has been developed to date. Fundamentally different and more accurate than automatic gain control (AGC), the SAR can operate on generic chaotic processes.

Key to the SAR are a direct SNR estimator, and the fact that scaling a received waveform leaves the SNR unaltered. The incoming waveform is first processed for raw received signal power, yielding an estimate of signal-plus-noise. It is then scaled by a factor that is controlled by the algorithm. Using knowledge of the transmit pdf, the maximum likelihood SNR causing the current observed value can be determined. Continuously making these instantaneous SNR estimates for every received value, a running weighted average can be defined that accurately reflects the received SNR (signal-over-noise). Feeding the SNR estimate back to the received power estimate, the received signal power can be isolated. A scaling factor is calculated to very accurately place the signal portion of the scaled received signal-plus-noise waveform at the desired receiver operating power level.

EFFECT OF PROPAGATION ON A LIGHTNING STANDARD CURRENT WAVEFORM

R. L. Gardner
Consultant
6152 Manchester Park Circle
Alexandria, VA 22310, USA

The lightning community has derived a standard current waveform for use in EMC and related applications in system hardening. That waveform was derived from a large number of electric field measurements that are then converted to current waveforms through a specialized free field electric dipole model. The model is restrictive in that it only includes the vertical component of the channel and requires that the current waveform propagate at the speed of light. These waveforms were then used in a curve fit that is the standard current waveform.

The environment for propagation of the lightning generated electromagnetic fields is more complex than a free field model and includes such things as lossy ground. The lossy ground tends to distort the waveform and preferentially attenuate higher frequencies. The transition frequency and the degree of attenuation depend on the ground parameters and the range but are significant at 1 MHz and 10s of kilometers. This set of parameters is important in the lightning measurement process.

In this paper, we will use an existing model [Gardner, R. L., Science, 16, 1981] to determine a range of attenuation for interesting propagation parameters. Since the ground attenuation is preferential for high frequency the result of this calculation is the enhancement of the high frequency content of the standard current pulse. The actual conditions of the propagation are not known so reasonable estimates are used and a recommended range of corrections are given.

While the frequency range and degree of enhancement to the waveform are not large, the impact on hardening systems can be significant since increased frequency content can demand treatment of apertures and other penetrations that would not otherwise be excited.

ZEUS: THE WORLD'S LARGEST MAN-MADE ELF TRANSMITTER

A.C. Fraser-Smith*
STAR Laboratory
David Packard Electrical Engineering Bldg., Rm 358
Stanford University
Stanford, CA 94305-9515, USA
P.R. Bannister
154 Nebraska Circle
Sebastian, FL 32958, USA

Several years ago we drew attention to some strong 82-Hz radio signals being generated by a Russian extremely-low frequency (ELF; 3 Hz – 3 kHz) transmitter located on the Kola Peninsula [Fraser-Smith and Bannister, *Radio Science*, *33*, 83–88, 1998]. We now describe this remarkable transmitter, the world's largest, in greater detail (it is now named "Zeus" after the lightning-tossing Greek god) and we point out some of its important possible non-communication applications.

The antenna for the Zeus transmitter is an electric power line about 60 km long, oriented in the EW direction, and grounded at its ends. It is located in the northern part of the Kola Peninsula on ancient rock of very low electrical conductivity, which makes grounding difficult. In this case a low grounding resistance is ensured by the use of specially arranged steel lattices buried at a depth of 0.5 m over an area of about 1 km^2. The current flowing in the antenna is typically in the range 200–300 A and its magnetic moment can reach a level of about 1.5×10^{11} Am^2. At present, Zeus can generate ELF signals in the range 30–200 Hz range and it is planned to extend this range down to 0.1 Hz. It therefore has greater frequency flexibility than the US's dual antenna ELF transmitting system located in Wisconsin and Michigan and it is roughly 5–10 dB more powerful.

The choice of name for the transmitter is significant because radio noise in the ELF range consists predominantly of radio signals (called sferics) radiated by the lightning occurring in thunderstorms. Interpretation of the characteristics of this noise is difficult due to the large number ($\sim$ 2000) and variety of these source regions in existence around the world at any time and controlled transmissions from Zeus would make possible, for the first time, a number of studies that would help explain the propagation and other properties of the noise. Since the ELF signals penetrate with comparatively little attenuation to depths in the range 100 m to 5 km in the ground (depending on the local electrical conductivity), the Zeus transmissions could have important geophysical applications, including the monitoring of earthquake fault regions for conductivity changes that might precede earthquakes.

RELATIONSHIPS BETWEEN TIME- AND FREQUENCY-DOMAIN NORMS OF SCALAR FUNCTIONS

Carl E. Baum
AFRL/DEHE
3550 Aberdeen Ave SE
Kirtland AFB, NM 87117-5776

Norms have been introduced to reduce the number of parameters characterizing transient waveforms to a few nonnegative numbers, which can be used in some kind of bounding sense. This applies to both excitation and response waveforms and the transfer operators that relate them. Such transfer operators model the properties of electromagnetic systems. The present paper is concerned only with waveforms.

As it is common to consider the Laplace/Fourier transform of waveforms for their (complex-) frequency spectra, one can also consider such norms of these frequency-domain functions. This raises the question of the relation between the various norms in time and frequency domains, the subject of this paper.

This paper addresses the relationship between time-domain waveforms and their Fourier transforms in terms of various norms of the two, specifically the 1-, 2-, and ∞-norms. As one might expect, norms in time domain can be used to provide some bounds concerning the norms in frequency domain, and conversely.

The results includeed here are quite general, and provide some simple bounds for norms one may not wish to calculate in terms of other norms one may have already obtained. In a previous paper we have considered window norms for a time interval $t_1 \leq t \leq t_2$. Since this is equivalent to the norm of a waveform function $f(t)[u(u-t_1)-u(t-t_2)]$, then the present results apply to such functions as well. However, the Fourier transform of such a window function does not have the same form as a window in frequency domain. Of course the p-norm of such a windowed function is bounded by the p-norm of the (unwindowed) function.

PROGRESS IN THE OPTIMIZATION OF IMPULSE RADIATING ANTENNAS

L.H. Bowen, E.G. Farr
Farr Research, Inc.
614 Paseo Del Mar NE
Albuquerque, NM 87123
T.C. Tran
Air Force Research Laboratory / Directed Energy Directorate
3550 Aberdeen Ave. SE
Kirtland AFB, NM 87117-5776

Over the last several years we have made a number of improvements to the basic design of the reflector Impulse Radiating Antenna (IRA). The first modification improved the gain and the cross polarization rejection of the IRA by relocating the feed arms from the traditional +/-45deg. from the vertical to +/-30deg. from the vertical (L.H. Bowen, et al, Experimental Results of Optimizing the Location of Feed Arms in a Collapsible IRA and a Solid IRA, Sensor and Simulation Note 450, 2000). This modification was based on efficiency calculations for the IRA (J. S. Tyo, Optimization of the Feed Impedance for an Arbitrary Crossed-Feed-Arm Impulse Radiating Antenna, Sensor and Simulation Note 438, 1999). However, the most significant improvement (¿12dB) was in the cross polarization rejection of the antenna. The 18in. diameter antennas used for this work have been designated FRI-IRA-1 for the traditional arrangement and FRI-IRA-2 for the optimized version.

Next we added a ground plane on the horizontal plane of symmetry. The ground plane effectively shorted out the horizontal E field and reduced the cross polarization coupling by an additional 6dB. This antenna is referred to as a FRI-IRA-3.

For radar applications, it is highly desirable that the TDR of an antenna be as flat as possible, to reduce late time ringing. However, in the case of an IRA, a large dip occurs in the TDR when the wave initially strikes the closest point of the reflector. By modifying the feed arm design and/or the resistor configuration, it is possible to further optimize the IRA performance to reduce reflections. After many experiments, we have found that a distributed resistance works best for the IRA-1 case and a load with a small amount of inductance works best for the IRA-3. Use of two resistor strings made up of carbon film resistors seemed to work well in this case.

This work was funded in part by the Air Force Office of Scientific Research, Alexandria, VA, and in part by the Air Force Research Laboratory, Directed Energy Directorate, under contract number F29601-99-C-0050.

ANTENNAS FOR THE SWITCHED-OSCILLATOR SOURCE

Carl E. Baum
AFRL/DEHE
Kirtland AFB, NM 87117-5776

A recent paper has considered the design of a switched oscillator as a way of generating a resonant waveform to be radiated by some antenna. Thereby one can increase the interaction with some electronic system. This type of source can be thought of as a medium bandwidth source, with bandwidth somewhere between narrowband sources (microwave tubes) and hyperband sources such as impulse radiating antennas (IRAs) which have typically two decades of *band ratio*. This paper introduces some concepts for antennas appropriate to be used with switched oscillators to effectively radiate the oscillating waveform.

The first kind is a dipole-fed reflector in which the quarter-wave (in the dielectric medium) oscillator is connected to an antenna of approximately a half-wave long (in air or SF_6). The half wavelenth makes the antenna element resonant at the same frequency as the oscillator. In a simple (but approximate) transmission-line model the characteristic impedance Z_c of the oscillator section is much less than Z_a of the antenna section. The oscillating antenna element might be of circular cylindrical shape from the oscillator. To better avoid electrical breakdown, this might look like an equivalent asymptotic conical dipole (ACD). In addition near the connection to the source there might be some special insulating dielectric medium (e.g., oil, polyethylene) to handle the high electric fields there. For greater fields at a distance one needs some significant antenna gain. This is efficiently accomplished by a paraboloidal reflector with focus at the dipole-like element. Noting the polarization of electric-dipole fields the reflector should not extend past the dipole element, at least above the dipole.

The second kind of antenna is a TEM-fed reflector with blocking capacitor. It has a TEM feed of characteristic impedance Z_f, typically using two feed arms giving an impedance in the 100 Ω ballpark for a half reflector with ground plane. Since we are considering concentrating the operation around some radian frequency $\omega_0 = 2\pi\ f_0$ we can revisit the choice of the terminating impedance $Z_t(s)$ for optimum results. Near the output of the switched oscillator there is a blocking capacitance C (parallel combination of two in the arms). This has the function of isolating the high voltage source from the antenna. Of course the source must now charge C_0 + C where C_0 is the oscillator capacitance. So we need to choose C carefully. The charging current through C returns through the feed arms and reflector to the ground plane so Z_t must be finite at low frequencies (perhaps even a short circuit). The presences of C can be compensated to some extent by adding a series inductance L to tune the combination to the oscillator frequency.

USE OF APERTURE TRIMMING TO IMPROVE PROMPT RADIATED RESPONSE FROM AN IRA

J. S. Tyo
EECE Department
University of New Mexico
Albuquerque, NM 87131-1356
M. J. Baretela
ECE Department
US Naval Postgraduate School
Monterey, CA 93943

Recent advances in the design and construction of impulse radiating antenna (IRA) apertures have led to increases in the prompt radiated fields possible from these devices. It is a well known property of IRAs that the radiated far-field on boresight is given by

$$E_{rad} = \frac{1}{2\pi r c}\frac{d}{dt}\left(\int\int_A E_y(x,y,t-r/c)\right)dxdy, \tag{1}$$

where r is the distance and E_y is the principal component of the electric field in the aperture defined by A. Ideally, one would want all of the energy from the feed structure to impinge on the aperture A with uniform amplitude and polarization. Such a configuration would maximize the prompt radiated fields. With IRAs it is necessary to use a TEM transmission line to feed the aperture in order to minimize dispersion. TEM transmission lines have open modes, and there are two distinct loss mechanisms that must be dealt with: 1) energy in the TEM mode that passes outside the aperture and 2) non-uniformity of the TEM mode in amplitude and polarization (Buchenauer, *et al.*, *IEEE Trans. Antennas Propagat.*, **49** 1155–1165). For typical reflector IRAs, as much as 50% of the mode energy passes outside the aperture. Even if the aperture were extended to encompass this additional area, much of the field is oriented in the wrong direction and will contribute destructively to the integral in (??).

In this paper, calculations and experimental results are presented that demonstrate a method to increase the prompt radiated response from IRAs by eliminating portions of the aperture that have the fields oriented in the wrong direction and expanding other portions of the aperture to capture beneficial fields. For 4-arm IRAs with feeds oriented at 45° or more from the vertical, the increase in the prompt resonse can be 10% or more. TEM geometries and aperture shapes are presented that optimize the prompt response for circular and rectangular apertures, and the relative size of the feed electrodes and the aperture dimension are altered to provide additional increase. Optimum orientations of the feed arms for a circular aperture are at approximately 30° from the vertical with the maximum radius of the aperture 1.15 times larger than the circle of symmetry of the TEM feed electrodes.

EXPERIMENTAL VERIFICATION OF ULTRA-WIDEBAND ANTENNA ELEMENTS EMBEDDED IN A PLANAR ARRAY

Schoenberg, J.S.H.*, Krueger, R.M.
Department of Electrical Engineering
U.S. Air Force Academy, CO 80840 USA

Planar ultra-wideband antenna arrays have been the subject of theoretical and simulation studies undertaken at the Air Force Research Laboratory [1,2]. In these studies, arrays of planar bicones were determined to have a flat frequency response up to the frequency corresponding to the full wave periodicity of the array elements, thereby showing promise for use as ultra-wideband antenna arrays. We report the results of an undergraduate capstone engineering project with the goal of experimental verification of these studies. First, planar bicone arrays were simulated using a commercially available finite element method (FEM) software package which confirmed McGrath's hybrid-FEM results [2]. Next, a planar bicone array with approximately 1 ns of clear time across its span was fabricated, with the center element of the array driven by a 50 ps risetime step generator and the remaining elements terminated. The response of the element embedded in the array was measured by a small B-dot sensor and a Tektronix 11801B digitizing oscilloscope. Data correction techniques were applied and the radiated impulsive waveform shows a risetime of 70 ps and full-width half-maximum (FWHM) pulse width of about 150 ps, yielding a bandwidth of about 2.5 GHz. The driven element's return loss was measured using a HP 8510C network analyzer, and had a VSWR of under 2:1 from 2.4 GHz to 10.6 GHz. Next, an planar exponential flare array was simulated, fabricated and tested in the same manner. The exponential flare element exhibited a risetime of 50 ps and a FWHM pulse width of just over 100 ps, yielding a bandwidth of about 4.5 GHz. The driven element's VSWR was under 3:1 from 1.5 GHz to 20 GHz. Further experimental studies whereby several elements are driven are contemplated.

[1] C.E. Baum, "Self-Complementary Array Antennas," Sensor and Simulation Note 374, USAF Phillips Laboratory, Kirtland AFB, NM, 27 October 1994.

[2] D.T. McGrath and C.E. Baum, "Scanning and Impedance Properties of TEM Horn Arrays for Transiet Radiation," IEEE Transactions on Antennas and Propagation, Vol. 47, No. 3, pp 469-473.

FAST TRIGATRON AND FERRATRON MEASUREMENTS

E.G. Farr, D.E. Ellibee
Farr Research, Inc.
614 Paseo Del Mar, NE
Albuquerque, NM 87123
J.M. Elizondo
Electromagnetic Technologies Corporation
716 Montclaire Dr. NE
Albuquerque, NM 87110
J.M. Lehr
AFRL / DE
3550 Aberdeen Ave. SE
Kirtland AFB, NM 87117-5776

This paper documents our ongoing work on trigatron and ferratrons. The goal of this research is to develop an integrated high-voltage source with low jitter and high reliability.

In the past year, we have achieved higher voltages, using a charge voltage as high as 40 kV, and trigger voltages as high as 20 kV. This has led to output waveforms with somewhat slower risetimes than previously reported, but with higher output voltages. Currently, we are achieving risetimes of approximately 500 ps.

We have experimented with a flattened main gap electrode design, and we have compared it to the double-cone design that was previously used. We present results for the two configurations, showing that the waveforms are comparable.

We have built a dc block at the output of our switch, thereby converting the switch to an independent source. A 100-pF capacitor was used in the center conductor of the coaxial output line. After the capacitor, the output line tapers down to a high-voltage connector. The output is fed into a high-voltage attenuator, and can be measured directly into an oscilloscope. Results for the new configuration will be provided.

Finally, we will have results comparing the output of the switch when used in both a trigatron and a ferratron configuration. Recall that a ferratron uses a ferroelectric material to trigger the breakdown of the switch. It is hoped that the ferratron configuration will have less jitter and will be more reliable than comparable trigatrons. It is also hoped that ferratrons will exhibit less erosion in the trigger electrodes.

Session E/F/J1 8:55-Wed.

RFI MITIGATION FOR REMOTE SENSING AND RADIO ASTRONOMY

Chairpersons: M. Davis, A. Gasiewski and E. Smith

CURRENT ISSUES IN DOMESTIC SPECTRUM MANAGEMENT AFFECTING RADIO ASTRONOMY AND REMOTE SENSING

P.G. Steffes*
School of Electrical and Computer Engineering
Georgia Institute of Technology
Atlanta, GA 30332-0250 USA
D.C. Backer
Department of Astronomy
University of California at Berkeley
Berkeley, CA 94720-3411 USA

The National Research Council Committee on Radio Frequencies (NRC/CORF) serves to coordinate and define the U.S. research community's needs for passive radio frequency allocations in research areas such as space science, radio astronomy, meteorology, oceanography, agriculture, and remote sensing. Over the past year, the National Academies, through CORF, has filed comments with the FCC on several Notices of Proposed Rulemaking having direct impact on the interests of the passive services.

In early 2001, the FCC received comments on a Notice of Proposed Rulemaking (NPRM) involving the transfer of a host of bands in the range from 216 to 2390 MHz from governmental to non-governmental usage. The proximity of many of these bands to the 1.4 GHz and 1.6 GHz bands used heavily in radio astronomy, and also in passive earth sensing, resulted in CORF supporting allocation plans which placed more compatible services in the adjacent or shared bands, whose out-of-band (OOB) emissions would present a significantly lower risk of harmful interference to the passive services. Both in this NPRM, and in other proceedings, a recurring issue involves the effects of out-of-band (OOB) and spurious emissions from satellites whose downlinks lie adjacent to radio astronomy allocations.

In Summer 2001, the FCC received comments on a NPRM involving modifications to band plan for the 36.0-51.4 Ghz band, in response to the actions of WRC-2000. Since the proposal involved allocation and operational rules for satellite downlinks in the proximity of the 42.5-43.5 GHz radio astronomy allocation, a significant technical response was developed, strongly supporting the Commission's stated desire to protect that allocation. Additionally, CORF asked for protection zones around observatories active in this band, since sharing with non-governmental fixed and mobile services was also proposed.

In addition to these activities, CORF has worked to educate those involved in frequency allocation activities in the government on the concerns of those involved in passive scientific uses of the spectrum.

CANCELLATION OF TV INTERFERENCE

D. Anish Roshi
NRAO, Box 2, Green Bank, WV 24944

I present results of attempts to suppress Television signals using different RFI cancellation techniques. A considerable fraction of the radio frequency spectrum in the VHF (54 – 88 and 174 – 216 MHz) and the UHF (470 – 890 MHz) bands are allocated for TV transmission. These frequency ranges can be of potential importance for Astronomy for a variety of observations. For example, the signature of the reionization of the Universe is expected as a sharp step in the spectrum of the sky due to redshifted HI 21-cm line emission anywhere in the frequency range $\sim$ 70 to 240 MHz (Shaver et al 1999).

A parametric interference cancellation technique was first tried for suppressing TV signals in the telescope output. This technique is based on parametric modeling of the interfering signal. The TV signal is a composite signal consisting of horizontal and vertical synchronization and blanking pulses and chrominance synchronization signal in addition to the monochrome and chrominance signal of the picture itself. A reference antenna output, which receives the TV signal, is used to model the synchronization signals and a noise-free copy is synthesized. I used two methods to incorporate the picture signal in the synthesized TV signal – (a) the detected monochrome and chrominance signal from the the reference antenna output; (b) an autoregressive modeling of the monochrome and chrominance signal. The synthesized copy of the TV signal is then subtracted from the telescope output to achieve suppression.

This paper presents the performance of parametric interference cancellation on the suppression of TV interference. A second suppression technique which makes use of the non-quadrature modulation of the monochrome signal will also be discussed. A comparative study of the two methods will be presented.

A RADIO FREQUENCY INTERFERENCE MITIGATION STRATEGY FOR THE ALLEN TELESCOPE ARRAY

G.C. Bower*
601 Campbell Hall
Radio Astronomy Laboratory
UC Berkeley
Berkeley CA 94720

We describe a multi-layered strategy for the mitigation of radio frequency interference (RFI) at the Allen Telescope Array (ATA). Because of the unique broadband nature of the ATA, RFI is a greater problem than for existing arrays. Accordingly, RFI mitigation is a subject of planning at all levels: site selection, antenna design, array configuration, building layout and design, RF design, digital design and post-processing architecture. An RFI survey is providing detailed information on the nature of interferers at Hat Creek from 300 MHz to 11 GHz.

Many techniques are newly available to radio astronomy because of the large number of antennas that will be a part of the ATA. This permits the use of multiple high gain reference antennas and significant flexibility in the formation of phased-array signals. Many of these issues will also be pertinent for the design of the Square Kilometer Array.

We describe in detail a design for a phased-array reference signal canceller employing a Wiener filter. This technique has been extensively studied with data from the Rapid Prototyping Array. We have shown that it is effective in eliminating GPS and Glonass signals at a level of 30 dB, or greater. This technique naturally handles multipath problems. We discuss the relative merits of using individual antennas or phased-array beams as reference sources. We also consider the relative merits of pre- and post-correlation cancellation techniques.

We also describe potential schemes for nulling interferers. Up to N-2 narrow band (approximately 100 kHz) nulls can be placed at any location on the sky without significant deformation of the main beam. These nulls have a typical width of 10 arcseconds at a depth of 40 dB. This size can be widened significantly with the placement of multiple nulls in the same region. We discuss implementation issues including the effects of delay resolution, gain stability, and update rates.

EFFICIENT MULTIBEAM SYNTHESIS WITH INTERFERENCE NULLING FOR LARGE ARRAYS

S.W. Ellingson, The Ohio State University, USA
W. Cazemier, Astron, The Netherlands

A class of FFT-based multibeam synthesis algorithms has been developed that are useful for large arrays when interference nulling is also desired. These algorithms have a computational cost per output which is only a little greater than that of the FFT with no interference nulling; and orders of magnitude less than conventional (non-FFT) beamforming, with or without nulling. These algorithms are well-suited to the task of forming "station beams" for future radio telescopes and other large arrays where it is desired to form multiple beams while simultaneously nulling interference.

The basic technique, which we now call "Beamspace Interference Projection" (BIP), was described at a previous conference (S.W. Ellingson, *US SKA Consortium Open Meeting*, Arecibo, 2000) and involves "projecting out the interference subspace". BIP is simple to use but has the disadvantage of causing distortion of the Fourier beam patterns. This distortion is small and deterministic, but nevertheless unconstrained. We have since developed some enhanced algorithms (S.W. Ellingson and W. Cazemier, *IEEE Trans. Ant & Prop*, submitted; preprint available at `http://esl.eng.ohio-state.edu/people/researchers/ellingson.html`). One of these improved methods is "Interference Beam Subtraction" (IBS), which allows a subset of the Fourier beams to be protected against distortion by constraining the patterns at one point in the main lobe and reducing the variation elsewhere by windowing the subtracted beam. An alternative approach, called Fourier Beam Subtraction (FBS), allows *all* Fourier beams to be constrained at one point, albeit at the cost of increased distortion away from the constrained point. The disadvantage of IBS and FBS with respect to BIP is that the coefficient updates are more difficult to compute; although once updated, the number of operations per output is the same.

These algorithms require that the interference directions-of-arrival (DOAs) be known in advance and that the array be well-calibrated before beamforming. Thus, this approach is best suited to dealing with RFI from satellites, as opposed to mobile radios or internally-generated RFI. We are currently investigating extensions of these algorithms to systems with large fractional bandwidths and methods for relaxing the restrictions associated with use of the spatial FFT.

INTERFERENCE FROM THE ROBLEDO DSN TRANSMITTERS TO CENTRAL MADRID IMT-2000/UMTS SYSTEM THROUGH TERRAIN DIFFRACTION AT S-BAND

Christian M. Ho, Miles K. Sue, Ted K. Peng
Jet Propulsion Laboratory
4800 Oak Grove Dr.
Pasadena, CA 91109-8099
Ernest K. Smith
Department of Electrical and Computer Engineering
University of Colorado at Boulder
Campus Box 425
Boulder CO 80309-0425

This study evaluates the possible interference from DSN Robledo 70-m transmitter with Madrid IMT-2000/UMTS wireless users in Spain as both systems will share the same frequency band. Using effective earth radius, the 50 km terrain profile between Robledo and Madrid is modified and reconstructed. The diffraction propagation losses by mountain peaks are calculated relative to the receivers in the Madrid urban area. The mountains along the path are simplified into a single knife-edge and a rounded obstacle. The results show that for a near surface receiver (1.5 m above the ground) in Madrid, interference signal powers received are less than -129 dBm, which is much below the -109 dBm, the IMT-2000 wireless phone threshold. When a receiver is located at 40 m above the ground, diffraction will generate the interference power about -110 dBm. We have also compared our calculations with those from the Longley-Rice model using a low resolution terrain profile. Both results are basically consistent, even though the latter has higher interference powers because the less mountain peaks are included. In comparison with measurements, we find that normalized interference levels of -120 dBm at the top of the Clock tower of Cibeles Palace, about 40 m above the ground, is in the range of the estimation. At some high buildings within Madrid city, which are less shaded from the mountain peaks, the interference powers may slightly exceeds the wireless phone threshold. However, in the almost all areas of Madrid at the surface levels, interference through the diffraction will not cause any problem to IMT-2000/UMTS users.

DETECTING AND FILTERING LOW LEVEL RFI WITH A DIGITIZING MICROWAVE RADIOMETER

C.S. Ruf, J. Li*, S.A. Rogacki
Department of Atmospheric, Oceanic and Space Sciences
University of Michigan
Ann Arbor, MI 48109, USA

Radio frequency interference (RFI) is a common and growing problem in microwave radiometry. This is especially true on airborne and spaceborne platforms where the area of interest is highly variable and can include urban areas with a plethora of manmade emitters. Very high levels of RFI can usually be reliably detected because their effect on the data is sudden and extreme and differs in a clearly recognizable way from natural phenomena. The presence of low level RFI can be much more difficult to differentiate from natural variability. Persistent low level RFI will tend to bias the affected brightness temperatures high (RFI cannot lower a radiometer's brightness temperature). If passed undetected into downstream data products, this has the potential to introduce troubling biases there as well.

A digitizing microwave radiometer samples its signal prior to square law detection. This approach is often used to perform cross-correlations between signals. Examples include polarimetric radiometers, spatial interferometers and autocorrelation spectrometers. In each of these cases, two signals are digitally multiplied and their product is averaged in time. The 10s to 100s of MHz clock speeds available with current programmable gate array digital logic devices permit these operations to be performed in an environment where additional bandpass filtering and statistical analysis of the pre-detected signals are readily accommodated. For example, the signal can be subdivided into narrow spectral sub-bands that cover the full bandwidth of the original signal. Each sub-band can then be individually processed and the results averaged to reproduce the total power present in the incoming signal. If RFI is detected in one or more of the sub-bands, it can be deleted from the average to prevent corruption of the data. This presupposes that the RFI can be detected. Access to the raw pre-detected signal also permits low level RFI to be detected even when its effect on the detected power is not distinguishable from typical natural variability. This is possible because the pre-detected signal originating from natural microwave emission possesses a purely gaussian statistical distribution whereas most sources of RFI have some other (often narrowband and deterministic) distribution. Functions of certain statistical moments of the pre-detected signal are particularly adept at detecting the presence of even a very small level of non-gaussian distributed signal. This detection scheme will be described and examples of the performance of such a radiometer will be presented.

Session F1, 8:55-Wed.

PROPAGATION MODELING AND MEASUREMENTS I

Chairperson: J. Goldhirsh and Daniel Dockery

SIMULATION OF PATH RAIN ATTENUATION TIME SERIES AND STATISTICS AT VARIABLE FREQUENCIES, ELEVATION ANGLES AND RAIN RATE ZONES

J. Goldhirsh
The Johns Hopkins University
Applied Physics Laboratory
11100 Johns Hopkins Road
Laurel, Maryland 20723-6099

A methodology is reviewed for the simulation of two-dimensional rain rate fields based on past radar measurements and point rain rate distributions [Goldhirsh, J., "Two-dimension visualization of rain cell structures," Radio Science, Vol. 35, No. 3, pp 713-729, May-June, 2000]. The visualization is represented by a number of randomly located two-dimension rain cells whose rain rates exponential decay with distance from their peak levels. The formulation for generating this array requires a three-parameter fit of a logarithmic function describing the conditional rain rate distribution for the particular rain rate zone. The above visualization provides a tool for the estimation of radar clutter levels, terrestrial and earth-satellite attenuation at variable frequencies, elevation angles and azimuth directions. Databases of rain attenuation statistics, hitherto not measured, may be constructed from such visualizations for frequencies, elevation angles and rain rate zones. The rain field is dependent on the geographic location (e.g., ITU-R rain rate zone) and may be considered a snapshot frozen in time showing the variability of rain rate intensity along the x and y directions of a rectangular grid. By advecting the "frozen" rain rate field with an assumed steering wind past a fixed communications path, cumulative fade and fade duration distributions are derived at example frequencies and elevation angles. Also shown are examples of rain attenuation versus variable elevation angles resulting from communications between a fixed earth site and a moving aircraft or an orbiting satellite. Effects on the above results are presented for different ITU-R rain rate zones. Comparisons are presented between simulated and measured time-series and fade distributions.

PROPAGATION MODELING IN A STABLE MARINE ATMOSPHERIC SURFACE LAYER

R.A. Paulus*, K.D. Anderson
Space and Naval Warfare Systems Center D858
49170 Propagation Path
San Diego, CA 92152

A parameter called the evaporation duct height can be used to characterize the typical refractive structure of the marine atmospheric surface layer at microwave frequencies. The evaporation duct height is taken to be the height of the minimum in the profile of modified refractivity. Under certain meteorological conditions, the surface layer is subrefractive and the modified refractivity profile increases monotonically through the surface layer. The minimum in the modified refractivity profile is at the surface resulting in a zero evaporation duct height. Under these same conditions, the refractivity profile initially increases with altitude, reaches a maximum, and then decreases with altitude. Analogous to the evaporation duct height, a parameter called subrefractive layer height can be used to characterize surface layer subrefraction. The subrefractive layer height is the height of the maximum in the refractivity profile.

Goldhirsh *et al.* (*Radio Sci.*, **29**, 1994) showed subrefraction can have significant effects on a propagation link. Christophe *et al.* (AGARD CP-567, 1995) reported on a NATO Research Study Group 8 multi-frequency propagation experiment off the coast of Lorient, France. This experiment collected both propagation and meteorological data from mid-September to mid-November 1989. Propagation measurements were made in S-, C-, X-, Ku-, Ka-, and W-bands on a 27.7 km path. Transmitter and receiver heights were nominally 8-9 and 10-11 meters above mean sea level. Meteorological data were recorded every 10 minutes on a buoy located near mid-point of the propagation path. Using air-sea temperature difference as an indicator of stability, the surface layer was stable approximately 72% of the time for this experiment. Of this portion of the data, approximately 63% were evaporation ducting and 37% were subrefractive.

This paper compares modeled to measured propagation loss during the Lorient 89 experiment for S- through Ku-bands with emphasis on the stable atmospheric conditions and possible ocean surface roughness effects.

EVAPORATION DUCT HEIGHT CALCULATION USING HELICOPTER-COLLECTED BULK METEOROLOGICAL MEASUREMENTS

G.D. Dockery, J.Z. Gehman, A.K. Kochhar, M.H. Newkirk*, J.R. Rottier, J.R. Rowland
JHU/APL
11100 Johns Hopkins Road
Laurel, MD 20723, USA

It is well known that the near-sea surface environment can have a dramatic effect on radar and communication systems performance. The various conditions are generally categorized by the shape of the altitude-dependent refractivity profile. The class of refractive conditions described as evaporation ducting is traditionally quantified by collecting bulk measurements of air and sea temperature, relative humidity, atmospheric pressure and wind speed from a shipboard or buoy platform. These measurements are fed into one of several models to provide the duct height, and for some models a profile of refractive index as a function of altitude. This presentation discusses use of helicopter instrumentation to collect the necessary bulk measurements to drive the evaporation duct models. The motivation for such a capability is presented, along with a description of the instrumentation and measurement procedure. The data collected with this unique system are applied fed to a number of evaporation duct models, including the Liu-Katsaros-Businger (LKB), Constant Virtual Temperature (CVT) and Paulus-Jeske models.

The helicopter inferred evaporation duct heights and refractivity profiles are compared to those obtained by using more conventional ship-based meteorological data collection systems when these data are relatively coincident in time and location. These near-surface measurement systems include the environmental assessment portion of the Shipboard Environmental Assessment Weapons System Performance (SEAWASP) prototype system that was deployed on the USS Anzio (CG-68) and USS Cape St. George (CG-72), as well as the similar system deployed on the JHU/APL-owned R/V Chessie. From these systems, data are available for the Puerto Rico and Virginia Capes (Wallops Island) areas. Conditions in these areas provide considerable variation in duct heights, and therefore a wide range of conditions under which the two measurement methods can be compared.

AN UPDATE ON THE PERFORMANCE OF REFRACTIVITY-FROM-CLUTTER FOR EVAPORATION DUCTS

L.J. Wagner, L.T. Rogers
Space and Naval Warfare Systems Center, San Diego
Code D858
San Diego, CA 92152-7385

In the 2001 presentation of this same name, four questions were posed regarding the ability of a refractivity-from-clutter (RFC) algorithm to estimate evaporation duct height from radar sea echo. Data from the space range radar (SPANDAR) at Wallops Island, VA, and data from at-sea demonstrations of Lockheed-Martin's Tactical Environmental Processor (TEP) onboard the USS O'Kane (DDG-77) and the USS Normandy (CG-60) were used to answer two of the four questions: 1) to what degree the spatial variability of the sea clutter cross section contaminated measurements and 2) the effect of the grazing angle dependency.

This presentation will look at the remaining two questions.

1. What is the minimum clutter-to-noise ratio that is needed to obtain reliable results? The RFC algorithm for evaporation ducting works by comparing the slope of the observed clutter power to the slope of the modeled clutter power over the interval $\Delta r = r_f$ - r_0, where r_f and r_0 are the final and initial ranges respectively. A minimum value for Δr of 4 km has been established from experience, and if the clutter power is not above a threshold value at $r_f = r_0 + \Delta r$, then those data are declared non-available. In earlier work, r_0 was set to 8 km to avoid closer ranges where the grazing angle (ψ) is changing more rapidly; the assumed ψ-dependence significantly changes the expected slope of the modeled clutter power for a given evaporation duct height. In this test, r_0 has been moved to 5 km and the clutter power is assumed to be independent of ψ. It is found that the availability is improved while not adversely affecting the accuracy of the algorithm. This result can be considered weak support for the argument that $\sigma^\circ \propto \psi^0$ for vertical polarization.

2. How effective are methods for eliminating rain and point target contamination? An algorithm was developed to classify the spatial behavior of the clutter power as to whether it could or could not be explained by evaporation ducting. Features that are flagged as "non-evaporative ducting" are then sub-classified as point targets or non-point targets. Non-point targets are then further tested classified as returns and being associated with multiple elevations. In the long term, the methods will complement classification schemes being developed within the weather radar community for "anomalous propagation" (AP) clutter mitigation.

A RAY TRACE APPROACH FOR ESTIMATION OF REFRACTIVITY FROM LAND CLUTTER

A. Barrios
SPAWARSYSCEN SAN DIEGO, D858
49170 Propagation Path
San Diego, CA 92152-7385

Two methods of estimating refractivity from land clutter were investigated in a previous report where one of the methods used a parabolic equation (PE) algorithm combined with a least squares technique, and the other used a ray trace algorithm combined with a rank correlation scheme (A.E. Barrios, *AP 2000 Millenium Conf.*, Apr. 2000). Based on simulations alone, both of these methods were fairly successful in estimating a tri-linear representation of a radiosonde-measured refractivity profile over two mixed land-sea paths. However, it is the ray trace/rank correlation method which offers a more attractive alternative to the conventional least-squares technique because of its execution speed and simplicity, therefore this presentation will focus on a more extensive look at this technique.

This method relies purely on geometrical ray tracing and uses a rank, or nonparametric, correlation scheme between the observed clutter power and ray density at the surface to determine the maximum likelihood estimate of the duct parameters. Results from initial simulations showed promise in the ability to estimate duct parameters based on the simple assumption that the strongest clutter returns arise from regions most illuminated by radar, which can be determined easily via ray trace. However, it did perform poorly over land paths that were sharply varying in terrain elevation. In initial studies, we looked primarily at *only* range variation of received, or simulated observed, clutter. Land clutter, however, varies not only in range, but in height as well. Height information along any particular path can be easily obtained from widely available terrain elevation databases such as DTED. By also considering the height interval or "spread" over which rays strike the surface one can lessen the ambiguity inherent in this inversion method, thereby improving refractivity estimates.

Results from simulations will be presented as well as results from observed land clutter combined with available refractivity soundings.

A STREAMLINED APPROACH FOR COLLECTING SIGNAL STRENGTH DATA TO VALIDATE A GROUND-TO-GROUND PROPAGATION MODEL

K. Chamberlin
Dept. of Electrical Computer Engineering
Kingsbury Hall
Univ. of New Hampshire
Durham, NH 03824-3591

One major problem in developing propagation models in the past has been obtaining quality measured signal strength data with which to validate those models. As a result, there are many propagation models whose accuracy and limitations are not well understood or documented. To remedy this problem, a portable data collection package has been developed that facilitates an almost seamless collection of measured data and subsequent comparison with modeled data. Signal strength is measured using a calibrated, computer-controlled WiNRADiO, and position information is logged using GPS. The data collection package is self powered and can be installed in a vehicle in a matter of minutes using magnetic-mount antennas.

Once the measured data have been collected, they are read by a validation program into which the user can enter transmitter and receiver data (antenna heights and gains, effective radiated power, and the coordinates of the transmitting antenna). For each data collection point, and there may be thousands of them, the validation model queries a terrain database to create a two-dimensional profile between the transmitter and the measurement location. The program then creates a piecewise-linear representation of that terrain profile, and finally runs a ray-tracing propagation model to estimate received signal strength. Both the measured and modeled signal strength values are placed in a file for analysis.

This paper overviews the data collection hardware and software and then focuses on some of the results obtained, both measured and modeled. Pertinent topics, such as small-scale fading, averaging and statistical techniques, measurement repeatability, model accuracy, and computer execution times are addressed.

AN EVALUATION OF REFRACTIVITY FROM CLUTTER USING MPME WALLOPS 2000 DATA

T. Nguyen*, V.R. Wiss
Naval Surface Warfare Center Dahlgren Division

To better understand propagation in the low altitude region, the concept of estimating the refractivity profile characterizing the environment directly from measured sea surface radar clutter is studied. This concept is known as refractivity from clutter (RFC), which has principally been developed by Ted Rogers of SPAWAR Systems Center-San Diego (SSC-SD). It is applicable to evaporation ducting and surface based ducting propagation environments where extended sea surface clutter can be measured. Using the measured clutter with some basic assumptions of sea surface conditions, radar performance, and normalization techniques, it may be possible to estimate the refractive profile of the atmosphere above the ocean surface.

The approach consists of creating a set of modeled refractivity profiles, calculating the modeled clutter powers, normalizing the modeled clutter to a clutter measurement, and implementing an objective function for comparison of the measured and modeled clutter. A two-parameter model of refractivity, including mixing layer height and transitional layer modified refractivity (M) deficit with fixed slopes for the mixing, transitional, and standard atmosphere segments is used. The slopes were derived from the John Hopkins University Applied Physics Laboratory (JHU/APL) helicopter meteorological measurements. The measured clutter data is from the National Aeronautics and Space Administration (NASA) Space Range Radar (SPANDAR) atmospheric research radar on Wallops Island, VA. The normalization process of the modeled clutter is based on equivalent total measured clutter power. A least squared error function is used to compare measured verses modeled clutter.

The RFC technique is evaluated by comparing measured and resultant RFC refractivity profiles and the respective coverage diagrams, which show propagation factor verses range and height. The results are compared qualitatively and quantitatively against ground truth propagation measurements from the Naval Surface Warfare Center Dahlgren Division (NSWCDD) Microwave Propagation Measurement System (MPMSII), and refractivity profiles that were collected by JHU/APL meteorological helicopter or profiles from rocketsondes. The data set for this study comes from the Ship Based Defense Demonstration for Interactive Adaptation of Fire Control Sensors to the Environment, Microwave Propagation Measurements Experiment (MPME) Wallops 2000. An Office of Naval Research ONR351/322MM cooperative effort provided funding for this analysis. This evaluation was coordinated with Ted Rogers of SSC-SD as an independent analysis for this RFC technique.

EVALUATION OF HELICOPTER AND ROCKETSONDE REFRACTIVITY PROFILES WITH AND WITHOUT APPENDED LKB OR PAULUS/JESKE EVAPORATION DUCTS

W. Thornton, T. Brown Lockheed Martin Tactical Systems, P.O. Box 1570, Dahlgren VA 22448
J.Stapleton, E. Burgess, D. Shanklin, Naval Surface Warfare Center Dahlgren Division, Dalhgren VA, 22448

During the spring of 2000, the ONR351 Air and Surface Weaponry Technology Program conducted a Ship Based Defense Demonstration at Wallops Island, VA. A series of experiments designed to show how environmental knowledge could be used to improve shipboard radar performance against cruise missile threats were conducted. A variety of sensors were simultaneously used to collect pertinent data. These included multiple refractivity sounding systems, several bulk meteorological measurement systems including boats and buoys, a direct propagation measurement system operated at three radar frequencies of interest, and sea surface backscatter measurements from both the SPANDAR atmospheric research radar and the AN/SPY-1A radar. The simultaneous measurement of all of these data allowed for a number of studies to be conducted. This work presents the portion examining the performance of the Johns Hopkins Applied Physics Laboratory (JHU/APL) helicopter sounding system and a rocketsonde sounding system as two data sources for refractive structures such as surface based ducts and subrefractive layers. As part of this study the importance of including an evaporation duct profile with these helicopter or rocketsonde data is examined. Both the Paulus/Jeske and Liu-Katsaros-Businger (LKB) evaporation duct height models are included. All of the refractive profile combinations (helicopter, rocketsonde, with and without Paulus/Jeske and LKB evaporation duct profiles appended) are used as input to the JHU/APL propagation model, TEMPER (Tropospheric Electro-Magnetic Parabolic Equation Routine), and results compared to the directly measured propagation loss, which was measured simultaneously with the refractivity and bulk meteorological data. A statistical representation of all of the applicable data from the test period is presented and conclusions stated with regard to the best performance versus data source and model used and the general environmental conditions under which various levels of performance are achieved.

PROPAGATION MODELING EVALUATION IN NEAR STANDARD, SUPERREFRACTIVE, TRAPPING, AND MULTIMODAL ENVIRONMENT TYPES

D. M. Shanklin*, J. K. Stapleton
Naval Surface Warfare Center, Dahlgren Division
W. D. Thornton
Lockheed Martin Tactical Systems, Dahlgren, VA

During the spring of 2000, the ONR351 Air and Surface Weaponry Technology Program conducted a Ship Based Defense Demonstration at Wallops Island, VA. A series of experiments designed to show how environmental knowledge could be used to improve shipboard radar performance against cruise missile threats were conducted. A variety of sensors were simultaneously used to collect pertinent data. These included multiple refractivity sounding systems, several bulk meteorological measurement systems including boats and buoys, a direct propagation measurement system operated at three radar frequencies of interest, and sea surface backscatter measurements from both the SPANDAR atmospheric research radar and the AN/SPY-1A radar. The simultaneous measurement of all of these data allowed for a number of studies to be conducted.

This paper presents the work of examining the performance of propagation modeling based on environmental types observed, using the Microwave Propagation Measurement System II (MPMS II) coverage diagrams, during this experiment. All of the data collected during the experiment can be characterized by at least one of the following four environment types, Near Standard, Superrefractive, Trapping, and Multimodal. Statistical comparisons of modeled propagation coverage diagrams with those simultaneously measured using the MPMS II are presented. General trends will be noted and summarized using the statistical results for each of the four environment types.

Over the past 10 years at NSWCDD, a capability has been developed to assess, through direct measurements at radar operating frequencies, the impact of the natural propagation environment. This capability has been used to support land based radar testing, development of radar environmental adaptation techniques and to increase fundamental understanding of temporal and spatial variability of phenomena affecting the performance of radars. Many of the field measurements that have been undertaken by this group have included radar clutter data collection, meteorological data collection from a number of platforms for refractivity assessment, and direct measurement of the microwave pathloss.

Session F2, 13:55-Thurs.

PROPAGATION MODELING AND MEASUREMENTS: II

Chairperson: K. Anderson

MID-PATH NEAR-SURFACE ATMOSPHERE PROPERTIES IN ROUGHNESS AND EVAPORATION DUCT (RED) EXPERIMENT

K. L. Davidson, P. A. Frederickson
Department of Meteorology
Naval Postgraduate School
Monterey, CA 93943, USA

Near-surface properties (profiles and turbulence) affecting Rf and EO propagation seem to be inadequately described by bulk models. Partially for this reason, NPS performed EO mid-path buoy collection during RED to relate EO propagation phenomena scintillation, refraction and loss) to descriptions of turbulent airflow and 2-dimensional surface waves as well as mean airflow profiles and surface temperature properties. These same near-surface properties will be related to properties and processes occurring on the Rf propagation path. NPS Interpretations are being based on empirical scaling (Monin-Obukhov) of flux-profile relationships. Since wind speed variations occurred during RED, examinations can also be made of departures from Charnock-type surface roughness parameterizations that work reasonably well for fully developed,equilibrium wind-wave states. Failure of a motion sensor along one-axis, caused direct covariance fluxes, and one- and two-dimensional wave spectra (from which relevant wave quantities are derived) not to be available for about a week of the four-week period. However, wave data were being collected nearby, near surface were collected and inertial dissipation methods are being used to estimate the structure function parameters and surface fluxes. The in situ buoy obtained direct or near-direct values are compared to existing bulk-derived values as well as to kite-borne sonde obtained profiles extending up to 100 meters. The same properties described in RED were measured from the NPS buoy at mid-point locations in past San Diego vicinity EO propagation (EOPACE) and Wallops Island Rf Wallops'98&'00)experiments. The distinct properties of the RED data set, compared to these existing results, are the higher sustained winds ($>$ 10-12 m/s) and wave steepness associated with combined swell and wind waves. A primary initial objective in these initial interpretations is to compare with the previous results and relate to different stability and wind-wave regimes.

USING INSTRUMENTED KITES TO QUANTIFY ATMOSPHERIC CONDITIONS DURING THE RED

Guest, P., Davidson, K. , Frederickson, P. , Mabey, D
Department of Meteorology
Naval Postgraduate School
Monterey, CA

This paper describes kite-borne sonde measurements performed by personnel from the NPS during the Roughness and Evaporation Duct (RED) Experiment. The goal of RED was to understand and model the factors affecting the transmission of radio frequency (RF) and Electro-Optical (EO) transmissions over a rough ocean surface. The key aspect was RF and EO wave transmission between the R/P Flip and shore stations. Because these radio and optical transmissions were strongly affected by the vertical gradients of temperature and specific humidity, it was important to obtain accurate measurements of these properties, particularly near the surface along the transmission paths. Of particular interest, were the characteristics (especially the top) of the "evaporation duct", a low level feature affecting RF transmissions that is caused by a decrease in humidity immediately above the ocean surface. Typically, the evaporation duct height is estimated with bulk methods based on values of sea surface temperature and single level values of airflow wind speed, temperature and humidity near the surface. For RED it was deemed necessary to directly measure temperature and humidity profiles, along the path. To accomplish this, standard Vaisala RS-80 rawinsondes were deployed from kites tethered to the R/V Wailoa, a small (35 foot) research vessel with a low profile. The kites were continuously raised and lowered between 1 and 140 meters above the surface, allowing several profiles with a vertical resolution of 0.1 mb (1 meter). At the start of each profile, the kite string was spooled out at a speed that allowed the sonde package to skim just above the surface for a distance of at least 50 to 150 meters from the Wailoa. By only using data collected beyond 50 meters from the ship, ship contamination effects on temperature and humidity profiles were minimized. In most cases, measurements were performed all along the length of the RF path, a process that lasted about 2 hours. After along-path profile transects were completed, the sonde was balloon launched to obtain profiles through the entire troposphere, describing RF elevated trapping layers if present. A preliminary look at the first measurements revealed that the method successfully characterized an evaporation duct that extended up to approximately 10 meters. This paper examines the kite measurements with particular focus on determining: 1. The high-resolution characteristics of the evaporation duct and other low level atmospheric features. 2. The spatial variations in atmospheric features along the Rf and EO paths. 3. The comparison with bulk measurements of evaporation duct from the Wailoa, Flip, buoys and shore stations. 4. The comparison with direct measurements from Flip and research aircraft.

EVALUATION OF EVAPORATION DUCT MODEL PERFORMANCE USING AREPS

P. Frederickson*, K. Davidson, Naval Postgraduate School, Monterey, CA
J. Stapleton, D. Shanklin, R. Wiss, T. Nguyen, E. Burgess, C. Weeks, Naval Surface Warfare Center, Dahlgren Division, Dahlgren, VA
W. Thornton, T. Brown, Lockheed Martin Tactical Systems, Dahlgren, VA

Near-ocean surface radar propagation assessments from the Advanced Refractive Effects Prediction System (AREPS) using different evaporation duct models were evaluated through comparison with actual radar propagation measurements. The performance of two different evaporation duct models were compared; the Jeske-Paulus (JP) model, which is currently incorporated within AREPS, and the Naval Postgraduate School (NPS) model, which was developed for the shipboard MORIAH/SMOOS(R) system. Meteorological data from the NPS buoy 7 km offshore were used to run the evaporation duct models and obtain near-surface refractivity profiles, which were then input to run AREPS. The resulting AREPS coverage diagrams were then compared to actual propagation measurements.

The propagation measurements used in this study were obtained off Wallops Island, Virginia in April-May 2000 with the Microwave Propagation Measurement System II (MPMS II), designed and operated by the Naval Surface Warfare Center, Dahlgren Division. The MPMS system consisted of a small boat fitted with S-, C- and X-band transmitters that traversed vertically up and down a mast and a shore receiver station with antennas mounted on a fixed mast. As the boat transmitted back to the shore station from varying heights as it traveled away from the coast, a close approximation to a height versus range propagation coverage diagram was directly measured that could be compared to an AREPS-produced diagram.

Only data obtained under evaporation duct-dominated propagation conditions were examined in this study. It was found that in unstable conditions (air cooler than the ocean surface) the NPS model consistently performed better than the JP model, with rms errors of less then 4 dB generally being observed out to 20 nmi range. In unstable conditions the JP model overestimated the evaporation duct height. In stable conditions (air warmer than the ocean surface) the NPS model performed better than the JP model out to about 15 nmi, and at greater ranges the JP model agreed better with the propagation measurements. This study indicates that accurate propagation assessments in evaporative ducting-dominated conditions are possible when horizontal refractivity variations are not too great and high quality meteorological data are available.

NON-LINE OF SIGHT PROPAGATION OVER MOUNTAINOUS TERRAIN

K.Pelman, G.Young
The Pennsylvania State University
Department of Meteorology
503 Walker Building
University Park, Pa 16802
S.A.Fast
The Pennsylvania State University
Applied Research Laboratory
P.O. Box 30
State College, PA 16801

The MM5 mesoscale weather model was used to model phenomena responsible for non-line of sight propagation over mountainous terrain. During the night, microwave beams have been observed to take non-line of sight paths over mountain crests. These paths permitted detection of a transmitter in one valley by a receiver in an adjacent valley, despite an intervening ridge. The implications of this occurrence for radar include both clutter enhancement when terrain masking fails due to ducting and counter-detection of the radar even when it was thought to have been masked by the terrain. In this paper, we try to understand the meteorological causes of these nocturnal ducts by modeling the terrain induced flows and their impact on the refractivity field.

In order to accomplish this task, MM5 was used to obtain the diurnal flow fields that cause the diurnal refractivity fields. MM5 produced the expected nocturnal ducts over the ridge crests during many nights, generally under similar meteorological conditions. These ducts are caused by the breaking of mountain waves and are around 15 M-units strong with a thickness of about 150 meters. The strength of the duct might be reduced and the thickness blurred, however, by the weather model's finite vertical resolution.

This type of duct can trap frequencies of around 200 MHZ and higher (wavelengths on the order of 1 meter or less), with a critical angle of around 5.5 degrees. The curved duct, however, reduces the angle between the beam and the duct, making it easier for an electromagnetic beam to become trapped. To provide the range-dependant refractivity profiles necessary to accurately predict signal loss, MM5 output was ingested into a propagation model. Results from propagation model output will illustrate the effects of curved nocturnal radar ducts on electromagnetic propagation.

PROBABILITY DISTRIBUTIONS OF PATH-LOSS IN AN URBAN MICROCELLULAR LOS ENVIRONMENTS UNDER ROAD TRAFFIC CONDITIONS.

H. Shimizu*, H. Masui, M. Ishii, K. Sakawa
YRP Key Tech. Labs. Co., Ltd.
Yokosuka, 239-0847, Japan
T. Kobayashi
Tokyo Denki University
Chiyodaku, Tokyo, 101-8457, Japan
M. Abo, C. Nagasawa
Tokyo Metropolitan University
Hachioji, Tokyo, 192-0397,Japan

We have developed a system for measuring line-of-sight (LOS) centerline blocking. Here, we report its use in measuring the path loss when the LOS centerline is blocked in LOS propagation in an urban environment with low base station antenna height.

On the transmission side, an array of semiconductor lasers emit red light modulated with a 10-kHz square wave. On the receiving side, the direct current component of the signal received by an optical detector is blocked and the signal is detected by a lock-in amplifier to suppress the noise of sunlight and artificial light. The use of a rubidium oscillator on both the transmitting and receiving sides allows independent synchronization between the transmitter and receiver, thus making it possible to measure LOS centerline blocking between transmitting and receiving antennas that are far apart.

The measurement was carried out in a heavily-developed area in metropolitan Tokyo. The probability distributions of path loss and the LOS centerline blockage were measured simultaneously. An 8.45 GHz continuous wave signal was transmitted from a point approximately 200 m away on the road along a line of sight that was about 27 m wide. A vertically-polarized half-wavelength dipole antennas were used for transmission and reception. The laser beam emitted from the transmitting antenna position in the direction of the receiving antenna position is measured at the receiving antenna position, so that the LOS is off when a vehicle is blocking the laser beam and on when there is no blocking. The measurement was performed in a high traffic volume time period and in a low traffic volume period.

The cumulative distribution of path loss is shown plotted on Rayleigh probability paper. The plot is nearly linear, indicating a Rayleigh distribution. Even in a LOS section, the path loss probability is found to follow a Rayleigh distribution.

MICROWAVE PATH-LOSS CHARACTERISTICS WITH HIGH BASE STATION ANTENNA IN AN URBAN AREA

K. Sakawa*, H. Shimizu, M. Ishii, H. Masui
YRP Key Tech Labs Co., Ltd.
YRP Center, Ichibankan, 6F
3-4 Hikari-no-oka, Yokosuka
239-0847, Japan
T. Kobayashi
Tokyo Denki University
2-2 Kanda-nishiki-cho, Chiyodaku, Tokyo
101-8457, Japan

In parallel with increased demand for mobile communications, a need has arisen for wireless systems that can deliver high-speed and high-quality communications. In this regard, the 2-GHz band has been selected for use by the 3rd-generation IMT-2000 system, while the microwave band is the leading candidate for the succeeding 4th-generation system that is to provide wireless communications at even higher capacities and speeds. Much research has been reported on propagation characteristics in the microwave band.

In particular, we see many reports of work that is concerned with the propagation characteristics of the configuration in which, assuming the use of microcells to increase system capacity, the installation height of the base station antenna is lower than the surrounding buildings. This street microcell system with low antenna height, however, is not the only system that should be considered. For example, use of a microwave band in conjunction with high antenna height can be an effective means of decreasing the handover processing load at switches and reducing the number of station installation. It is therefore important that the propagation characteristics of this kind of system also be understood.

In this study, we measured microwave path-loss characteristics in an urban area in Japan within an environment where base-station antenna height is sufficiently higher than that of peripheral buildings.

Frequency characteristics for urban path loss in the microwave band were found to observe 21Log(f), nearly the same as conventional characteristics in the UHF band. When applying this behavior to the Sakagami model developed for UHF use and employing mobile-station antenna-height compensation of the Okumura-Hata model, estimated and measured values agreed well. In addition, on attempting to make the same comparison with regard to measured results in an urban environment of a different scale, good agreement was again obtained.

FORWARD AND INVERSE ANALYSES OF GPS RADIO OCCULTATIONS IN THE NEUTRAL ATMOSPHERE

C.O. Ao, G.A. Hajj, S.S. Leroy, B.A. Iijima, M. de la Torre Juarez, A.J. Mannucci
Jet Propulsion Laboratory
California Institute of Technology
4800 Oak Grove Drive, Pasadena, CA 91109, USA

Radio occultation measurements using Global Positioning System (GPS) satellites as transmitters and low Earth orbiting (LEO) satellites as receivers have proven to be successful at probing the refractivity structure of the Earth's atmosphere. It is known, however, that the sharply varying refractivity existing in the moist, lower troposphere presents significant algorithmic and data-processing challenges to the current retrieval techniques. One limitation in the existing algorithms is the reliance on the assumption of spherically symmetric atmosphere (at least locally). Thus better forward and inverse modeling of wave propagation through a non-spherically symmetric atmosphere in the context of radio occultation needs to be developed and examined.

We carry out forward simulations of wave propagation through the neutral atmosphere using the phase screen model. In the phase screen model, the atmosphere is represented by single or multiple screens which act to introduce a phase delay to the incident wave. In general, the phase delay can vary two-dimensionally across the screen. Outside the screens, the wave propagates as in vacuum. While multiple phase screens can be used to rigorously model the extended atmosphere, employing a large number of such screens would incur significant computational cost. We show that the far-field diffraction pattern generated by a given refractivity profile can be accurately reproduced with a single phase screen, provided that the phase delay introduced by the screen is properly computed. The single phase screen method allows for simple and computationally efficient modeling of a non-spherically symmetric atmosphere, with possibly sharp gradients in the vertical and horizontal directions perpendicular to the raypath. The forward simulation results are presented in terms of the ray's bending angles, and comparisons are made with the standard geometric optics solution which assumes a spherically symmetric atmosphere.

We investigate the inversion of the forward simulation data to obtain the refractivity structure of the atmosphere. The inversion is performed using the Abel transform combined with a backpropagation algorithm which translates the field pattern from the distant observation plane to one closer to the occultation. We assess the effectiveness of the Abel inversion on different backpropagated planes and study how the presence of horizontal refractivity gradients could give rise to errors in the inverted vertical profile. Finally, we apply the backpropagation algorithm to the new radio occultation data obtained with CHAMP and SAC-C and present retrieval results.

TECHNIQUES TO IMPROVE IMAGING THROUGH DISCRETE SCATTERING MEDIA

S. Jaruwatanadilok*, A. Ishimaru, Y. Kuga
Department of Electrical Engineering
Box 352500
Univeristy of Washington, Seattle
Washington, 98195

Imaging through random media is an important problem with many applications including optical remote sensing and bio-optics. As the optical depth gets larger, the imaging resolution and contrast deteriorates because of the effect of scattering. In this paper, we will investigate the applications of Radiative Transfer Equation (RTE) in optical imaging. It is believed that the more of the incoherent component we remove, the better the image quality we achieve. There are techniques that we propose to reduce the effect from the incoherent component. In particular, we study off-axis intensity subtraction (OAIS) and cross-polarization intensity subtraction (CPIS) imaging techniques based on the fact that off-axis and cross-polarization contains most of the incoherent component. We show the effectiveness of these techniques in this paper. Also, we investigate a new imaging technique using freqency modulation waves, i.e., the photon density waves. We analyze the intensity and polarization characteristics of the photon density waves with different modulation frequencies. We solve the RTE for linearly and circularly polarized waves using the discrete ordinates method. Using the numerical solutions to the RTE, we will show the conditions in which OAIS and CPIS are most effective. Moreover, continuous photon density waves exhibit a narrow angular spectrum with a lower level of incoherent component compared to regular continuous waves. Also, the shape of pulse photon density waves shows less effect of multiple scattering of the random media. These findings establish the possibility of using photon density waves for improved imaging. Furthermore, we apply these techniques to numerical simulations of a cross image and show that they consideraly improve the quality of images in terms of contrast.

Session F3, 8:55-Fri.

SATELLITE AND AIRBORNE REMOTE SENSING

Chairperson: S. Sekelsky and J. Piepmeier

AIRBORNE CONICAL SCANNING MILLIMETER-WAVE IMAGING RADIOMETER

J.R. Piepmeier, P. Racette, J. Wang
NASA Goddard Space Flight Center
Greenbelt, MD 20771, USA

The airborne Conical Scanning Millimeter-wave Imaging Radiometer (CoSMIR) will provide measurements for calibration and validation (cal/val) of the high-frequency channels of the DMSP Special Sensor Microwave Imager/Sounder (SSMIS). The SSMIS is a next-generation orbiting microwave imager/sounder, a series of which are designed to monitor the Earth's environment for the next decade. The sensor combines the capability of the currently existing Special Sensor Microwave/Imager (SSM/I) (at 19-85 GHz) and Special Sensor Microwave/Temperature-2 (SSM/T-2) (at 91-183 GHz) and covers a wide frequency range of 19-183 GHz. Instead of imaging using cross-track scanning like the SSM/T-2 or the Advanced Microwave Sounding Unit-B (AMSU-B), the new sensor scans conically at $\sim$54°incidence angle for all frequency channels. In the past, the Millimeter-wave Imaging Radiometer (MIR) was used for airborne cal/val efforts of the aforementioned sounding instruments. The MIR, however, is a cross-track scanning instrument with rotating polarization basis and is not well suited for SSMIS cal/val studies. On the other hand, the new CoSMIR instrument is conical scanning, providing the constant incidence-angle and polarization-basis observations needed for comparison to the next generation spaceborne radiometers (i.e., DMSP SSMIS and NPOESS CMIS).

Designed to fly aboard the NASA ER-2 high-altitude research aircraft, the CoSMIR consists of four radiometers operating at 50 (3 channels), 92, 150, and 183 (3 channels) GHz. The radiometers are housed in a cylinder that is mounted in an elevation-under-azimuth gimbals such that constant incident-angle conical scanning is the normal mode of operation. (This scanning configuration is similar to the NOAA PSR aircraft instrument.) Two calibration targets rotate with the azimuth axis such that the radiometer scanhead needs to be rotated only in the elevation axis to complete a two-look calibration sequence – a unique feature of CoSMIR that allow high raster efficiency. Two embedded computers are co-located with the radiometers and calibration targets for data acquisition. The computers are networked to third computer, the control and archival system. The scanning motion of the gimbals is achieved using a programmable two-axis closed-loop DC brushless servo-motor system. All the data collected by the archival system is stored on solid-state disk.

PRECIPITATION-RATE RETRIEVALS AT 15- AND 50-KM RESOLUTION USING AMSU PASSIVE MICROWAVE DATA

F.W. Chen*, D.H. Staelin
Research Laboratory of Electronics
Massachusetts Institute of Technology
Cambridge, MA 02139-4307, USA

Prior instantaneous precipitation-rate retrievals using neural networks operating on five limb-corrected NOAA-15 Satellite AMSU channels near 53 and 183 GHz yielded promising agreement with coincident NEXRAD 3-GHz radar observations up to 20 mm/hr (D. H. Staelin and F. W. Chen, *IEEE TGARS*, **38**, 2322-32, 2000). That earlier work, based on four early NOAA-15 summer and fall satellite orbits, has been superceded by this study of 21 orbits distributed over an entire year. In addition, the 50-km resolution data obtained near 53 GHz has been converted to equivalent 15-km data based on precipitation morphology evident near 183 GHz, permitting rain rates up to 200 mm/hr to be retrieved. Finally, all but the two upper stratospheric AMSU channels are now utilized.

One performance metric is the rms error between AMSU and NEXRAD retrievals smoothed to match AMSU beamwidths. Those 2353 precipitating pixels not used to train the 15-km neural network were partitioned into six NEXRAD rain-rate categories: 1-2, 2-4, 4-8, 8-16, 16-32, and >32 mm/hr. The rms discrepancies between these 15-km resolution AMSU and NEXRAD retrievals are 1.6, 2.0, 3.3, 7.7, 14, and 39 mm/hr for the six categories, respectively. When the 15-km retrievals are smoothed to 50-km resolution the rms discrepancies for the same six categories are 1.1, 1.7, 2.9, 6.4, 12, and 23 mm/hr, respectively, for 1494 precipitating 50-km pixels. For light rain (0.5-1 mm/hr) the 50-km rms discrepancy is 0.84 mm/hr. It is not clear how much improvement can be obtained in this metric, for these discrepancies are also arguably approaching the intrinsic accuracy of NEXRAD itself.

Another metric tests whether either sensor sees heavy rain when the other does not. For this same set of 2353 precipitating 15-km pixels, none of the 88 pixels for which AMSU retrieved over 31 mm/hr were observed by NEXRAD to be raining below 10 mm/hr. Similarly, none of the 114 pixels for which NEXRAD observed over 35 mm/hr were seen by AMSU to be raining below 3 mm/hr.

A final metric involves sensitivity to snowfall. At 2305 UTC on March 5, 2001 a major storm that left two feet of snow in parts of New England was imaged by ASMU; the same retrieval algorithm yielded up to 11.5 mm/hr precipitation. When AMSU passed over New England 4.5 hours earlier and 8 hours later it saw almost no precipitation, which was also consistent with ground observations

RETRIEVAL OF STRATUS MICROPHYSICAL PARAMETERS USING MILLIMETER-WAVE RADAR AND VISIBLE OPTICAL DEPTH

R. T. Austin*, G. L. Stephens
Department of Atmospheric Science
Colorado State University
Fort Collins, CO 80523-1371, USA

The performance of a recently developed retrieval of stratus cloud microphysics (Austin and Stephens, *J. Geophys. Res.*, in press) is investigated. The algorithm uses measurements of millimeter-wave radar reflectivity and (optionally) visible optical depth to retrieve geometrical mean radius as a function of height and a column value for the particle number density (if visible optical depth information is available). Using this information, parameters such as effective radius and liquid water content may be derived.

The retrieval assumes a lognormal distribution of cloud droplets having no significant drizzle:

$$N(r) = \frac{N_T}{\sqrt{2\pi}\sigma_{log} r} \exp\left[\frac{-\ln^2(r/r_g)}{2\sigma_{log}^2}\right] \quad (1)$$

The number density is assumed to be constant in height, and a value is prescribed for the width parameter σ_{log}.

The retrieval is formulated in an estimation theory framework, allowing the inclusion of *a priori* information and requiring explicit specification of input uncertainties. It provides quantitative measures of uncertainty in the retrieved quantities and the relative influence of the measurements and *a priori* information. The retrieval design was driven by the requirements of the upcoming CloudSat mission, which will orbit a 94 GHz Cloud Profiling Radar on a satellite scheduled for launch in 2004.

In this presentation, we describe the application of the retrieval to data from recent aircraft measurement campaigns. We discuss comparisons between the retrieved parameters and *in situ* measurements, finding that agreement is generally good in regions deemed to be free of drizzle. We examine the influence of and sensitivity to *a priori* information and its specified uncertainties, and quantify the benefit gained by the addition of visible optical depth to the retrieval process. We also comment on extensions of the algorithm to the drizzle case and associated retrievals of light precipitation.

AIRBORNE MILLIMETER-WAVE CLOUD RADAR CALIBRATION BY INTERCOMPARING CLOUD OBSERVATION WITH A GROUND-BASED CLOUD RADAR

Li, L., Sekelsky, S.M., Bergada, M.
Microwave Remote Sensing Laboratory
University of Massachusetts
Amherst, MA 01002
Sadowy, G.A.
NASA Jet Propulsion Laboratory
Pasadena, CA

Millimeter-wave cloud radars operating at 95 GHz (W-band) and 35 GHz (Ka-band) have become fundamental tools for cloud research. During the past decade, a few W-band cloud radars have been developed and flown. Meanwhile, the NASA CloudSat program will launch the first spaceborne 94 GHz (W-band) cloud radar for measuring vertical cloud distribution on a global scale.

Because of the extreme portability the delicate nature of W-band components calibration integrity is crucial for cloud radar systems. Regular external calibrations are necessary to ensure the quality of the data collected using these radars. This is straight-forward for ground-based radars but challenging for airborne systems due to the strict limitation of radar beam pointing angle and the motion of the aircraft. During the past years, different calibration and inter-comparison approaches have been carried out for the 95 GHz airborne cloud radar (ACR), which was jointly developed by the University of Massachusetts (UMass) at Amherst and NASA JPL as the prototype of the NASA CloudSat cloud profile radar (CPR). These approaches include side-by-side inter-comparison from the ground along with the ground-based UMass cloud profiling radar system (CPRS) and co-located simultaneous cloud observation when the aircraft flying over the CPRS during field experiments. By observing the same cloud volumes, calibration results were transferred from the pre-calibrated CPRS to ACR.

Co-located and side-by-side inter-comparison were performed during the Summer 1998 DC-8 Cloud Radar Experiment at New Ibera, LA, during the Cloud IOP 2000/ARESE II experiment at the DOE ARM SGP CART site and during the summer of 1998 at the University of Massachusetts at Amherst. ACR calibration result was further validated using a trihedral corner reflector. Data analysis shows that co-located or side-by-side inter-comparison are the efficient and accuracy ways to calibrate the airborne radar using a pre-calibrated ground-based system. This technique will be refined and used for the pre-launch calibration of the CloudSat radar.

PR-2AS: A DUAL-POLARIZATION DUAL-FREQUENCY AIRBORNE PRECIPITATION RADAR

G. Sadowy, A. Berkun, S.L. Durden, E. Im
Jet Propulsion Laboratory
4800 Oak Grove Drive
Pasadena, CA, 91109, USA

A dual-frequency (13.8 and 35.6 GHz) airborne precipitation radar has been developed by NASA / Jet Propulsion Laboratory. This new system serves as a technology test bed supporting the development of a Second Generation Spaceborne Precipitation Radar (PR-2) and also provides data useful for development of dual-frequency, dual-polarization rain rate retrievals.

In addition to supporting development of an advanced spaceborne precipitation radar concept, the PR-2 Airborne Simulator (PR-2AS) is a unique and capable science instrument in its own right. The PR-2AS serves as a successor to JPL's Airborne Rain Mapping Radar (ARMAR) which has flown aboard NASA's DC-8 Airborne Laboratory during the TOGA-COARE, CAMEX and KWAJEX experiments. Like ARMAR, PR-2AS utilizes a down-looking cross-track scanner to capture three-dimensional measurements of precipitation. However, unlike ARMAR, PR-2AS operates simultaneously at two frequencies with two receiver polarizations, all utilizing a common antenna which has been designed to yield matched sample volumes. Use of a dual-frequency, dual polarization feed horn with matched beams simplifies and improves the accuracy of dual-frequency based rain rate retrievals.

In order to avoid the use of very high peak power transmitters, linear frequency modulated (LFM) chirp waveforms are transmitted. These waveforms are then compressed in time to achieve the desired range resolution. Suppression of range compression sidelobes is critical since range sidelobes from the surface return can obscure weak near-surface precipitation echoes. Real-time digital waveform generation and pulse compression yields range sidelobe suppression of greater than 60 dB while achieving orders of magnitude reduction in output data rate.

This paper introduces the PR-2AS instrument and it's capabilities and highlights these innovations. To illustrate the utility of the PR-2AS for science investigations we also present dual frequency / dual polarization data collected during the recent CAMEX4 experiment.

DEVELOPMENT OF A COMPACT MILLIMETER-WAVE PULSE COMPRESSION RADAR

L. Li, J.I. Roman-Nieves*,S.M. Sekelsky
Microwave Remote Sensing Lab
University of Massachusetts
Amherst, MA 01003, USA

The need to measure high altitude clouds over large areas has motivated the development of airborne millimeter-wave radars. Millimeter-wave radars have been used increasingly for cloud studies because they offer greater resolution and increased sensitivity versus microwave frequency radars. The first airborne solid state pulsed Compact Millimeter wave Radar (CMR) was developed at the University of Massachusetts in 1998, with funding from the U.S. Department of Energy Atmospheric Radiation Measurement (DOE-ARM) Program. It was designed to fly on high altitude aircraft such as the DOE Altus Unmanned Aerospace Vehicle (UAV) and the NASA ER-2.

The CMR design was optimized to reduce size, weight, and power consumption in comparison with previous airborne cloud radars. The small size and low prime power consumption are required for UAV operation. In addition, CMR uses a solid-state trasmitter that have not high voltage and can operate unpressurized at high altitude. Other important aspects of its design include the utilization of a W-band low noise amplifier and incorporation of a compact folded less antenna. Internal calibration circuitry was also developed to increase the precision of the system. High speed data processing is performed in real time with an FPGA board assisted by a host computer, and pulse pair data was collected in a local storage device. The prototype CMR was tested in a both a ground-based configuration and on the low altitude DOE Twin Otter aircraft during an experiment in Monterey, CA.

The next generation CMR is currently under development. It will use pulse compression to improve sensitivity to clouds. This method has the advantage that it offers the increased detection capability of long pulse radars and also the range resolution of narrow pulse radars. The solid state pulse transmitter will be replaced with an array of low power diode amplifiers, making the system more reliable by increasing the number of signal sources.

AN ADVANCED MULTI-FREQUENCY RADAR FOR ATMOSPHERIC RESEARCH

N. Majurec*, S. Sekelsky, L. Li, D. Schaubert
Microwave Remote Sensing Laboratory
University of Massachusetts, Amherst
Amherst, MA 01003, USA

An Advanced Multi-Frequency Radar (AMFR) system for studying clouds and precipitation is presented. This portable radar will consist of three polarimetric Doppler subsystems operating at Ku-band (13.8 GHz), Ka-band (33 GHz) and W-band (95 GHz), a programmable scanning pedestal and a unique single aperture antenna that will generate co-located matched beams at each wavelength. This combination of wavelengths allows measurement of a wide range of atmospheric targets including weakly reflecting clouds and precipitation. AMFR reflectivity and Doppler data will provide unique measurements of particle size, phase, and liquid or ice mass content that are not available from single-wavelength radar data. Demonstrations of multi-wavelength radar (CPRS UMass) have shown that such information is contained in the measurements of signal extinction and scattering differences, which results from non-Rayleigh scattering effects. The spectrum of polarization measurements over the three radar bands may also provide better estimates of ice particle shape. Although the existent double band radar systems are very capable, the addition of a third lower frequency channel is crucial for eliminating ambiguities due to extinction at millimeter-wavelengths, and for probing deeper into precipitation while scanning.

The Ku-band radar subsystem design features two 100kW magnetrons that transmit V and H polarized pulses and a low noise figure receiver. Like the CPRS subsystems, the Ku-band radar will be fully polarimetric and capable of collecting Doppler measurements. A digital automatic frequency control (AFC) loop will be used to tune the receiver to the magnetron frequency. Because the magnetrons are oscillators and have a random start-up phase, a phase correction must be applied to each transmitted pulse. Instead of the traditional analog coherent oscillator (COHO) technique we will make this correction digitally. Development of a new high duty cycle FM chirp pulse compression transmitter and the employment of a W-band low noise amplifier will improve overall sensitivity at W-band by 13 dB to 20 dB, depending on the level of pulse compression achieved, resulting in the most sensitive W-band radar built to date. These enhancements will allow for better detection of clouds and deeper penetration into precipitation at low elevation angles. A new data system for three radar subsystems will be developed. The data system will be implemented using a stand-alone processing card consisting of two 65 MHz digitizers, two Xilinx TM Field Programmable Gate Array-based (FPGA) signal processors and a customized I/O daughter board.

HIGH-RESOLUTION RAIN RATE IMAGERY OBSERVED USING THE NOAA POLARIMETRIC SCANNING RADIOMETER.

Klein*,M., Yevgrafov,A., Leuskiy,V., Serke,D.
CIRES, University of Colorado/NOAA Environmental Technology Laboratory
Boulder, CO 80305, USA
Gasiewski, A.J.
NOAA Environmental Technology Laboratory
R/E/ET1,325 Broadway
Boulder, CO 80305, USA
Corbella, I.
Universitat Politcnica de Catalunya
08034 Barcelona, Spain

Microwave brightness imagery obtained using the NOAA Polarimetric Scanning Radiometer (PSR/A) during the NASA CAMEX-3 experiment offers a unique high-resolution perspective of clouds, rain, water vapor fields, and sea state during hurricane conditions. The uniqueness of this data lies in the broad spectral range of the observed bands, the full (fore and aft) conical scanning mode (providing two looks at the same scene), the high spatial resolution (1-2.5 km), and polarimetric sensitivity. The PSR/A radiometers operate at the atmospheric window frequencies of 10.7, 18.7, 37 and 89 GHz, with one channel at 21.5 GHz on the wing of the 22.235 GHz water absorption line. All channels are sensitive to both vertical and horizontal polarization. CAMEX-3 flights occurred under different atmospheric conditions ranging from clear sky to severe tropical convection, and included hurricane rainband and eyewall overpasses.

An emission-based nonlinear statistical retrieval algorithm, similar to that described in [Skofronick-Jackson, Gasiewski, IEEE Trans. Geosci. Remote Sensing, July 1995.], for rain rate retrieval was developed. The PSR/A 10.7 GHz channels with horizontal and vertical polarization are used because of their mostly monotonic response to rain rate.

The algorithm was developed using brightness temperatures (TB) statistics for hydrometeor profiles computed using Microwave Radiative Transfer (MRT) model [Gasiewski, Staelin, Radio Sci., 1990.] and the MM5 numerical weather prediction model. The MM5 model was initialized to simulate hurricane Opal at landfall on the Gulf of Mexico coast on October 4, 1995. Modeled TB values compared satisfactorily with data observed by Defense Meteorological Satellite Program (DMSP) satellites.

The PSR retrieved rain rate will be compared to the TRMM Microwave Imager (TMI) rain rate for the coincident observations during the CAMEX-3 experiment.

Session F4, 13:35-Fri.

REMOTE SENSING OF THE OCEAN SURFACE

Chairpersons: V. Zavorotny and E. Westwater

HURRICANE DIRECTIONAL WAVE SPECTRUM SPATIAL VARIATION IN THE OPEN OCEAN AND AT LANDFALL

E.J. Walsh*, C.W. Wright, D. Vandemark, W.B. Krabill
NASA/GSFC/Wallops Flight Facility, VA 23337 USA
A.W. Garcia, U.S. Army Engineer Research and Development Center, Vicksburg, MS, USA
S.H. Houston, National Weather Service Forecast Office, CPHC/NOAA, Honolulu, Hawaii
S.T. Murillo, M.D. Powell, P.G. Black, F.D. Marks, NOAA AOML, Hurricane Research Division, Miami, FL, USA
E.J. Walsh currently on assignment at NOAA Environmental Technology Lab, Boulder, CO, USA

On 24 August 1998, the NASA Scanning Radar Altimeter flew aboard a NOAA WP-3D hurricane research aircraft to document the sea surface directional wave spectrum spatial variation when Hurricane Bonnie was in open water east of the Bahamas. Two days later, the SRA documented the wave field spatial variation in the region between Charleston, SC, and Cape Hatteras, NC, as Bonnie made landfall near Wilmington, NC. Bonnie was moving faster prior to landfall (9.5 m/s) than when it was encountered in the open ocean (5 m/s) and the maximum wind speed was lower (39 m/s) than during the first flight (46 m/s). The open ocean wave height spatial variation indicated that Hurricane Bonnie would have produced waves of 11 m significant wave height on the shore northeast of Wilmington had it not been for the continental shelf. The gradual shoaling distributed the wave energy dissipation process so the wavelength and wave height were reduced gradually as the shore was approached. The wave height 5 km from shore was about 4 m. Despite the dramatic differences in wave height caused by shoaling and the differences in the wind field and forward speed of the hurricane, there was a remarkable agreement in the wave propagation directions for the various wave components on the two days. This suggests that, in spite of its complexity, the directional wave spectrum in the vicinity of a hurricane may be well behaved and lend itself to be modeled by a few parameters, such as the maximum wind speed, the radii of the maximum and gale force winds, and recent movement.

COMPARISON OF MEASURED LGA MICROWAVE BACKSCATTERING FROM BREAKING WAVE CRESTS WITH NUMERICAL CALCULATIONS

*West, J. C., Oklahoma State University, Stillwater
Sletten, M. A., Naval Research Laboratory, Washington, D.C.
Duncan, J. H., University of Maryland, College Park

In previously reported work (S.-J. Ja *et al. Radio Science*, 2002, in press), a computational electromagnetic code has been used to find the time-dependent LGA backscattering from several series of measured profiles representing the measured displacements of the crests of breaking waves generated in a wave tank. Additional experiments have been performed at the University of Maryland wave tank where the radar backscatter from the wave crest was measured simultaneously with the optical measurement of the crest profile. Both the radar system and the optical measurement were mounted on an instrument carriage that moved with the wave crest, providing continuous backscatter and profile measurements throughout the breaking process. This has allowed the direct comparison of the measured and numerically calculated scattered signals. The numerical calculations were performed using an electromagnetic technique that expands the moment method using the geometrical theory of diffraction. The finite conductivity of the water was treated using impedance boundary conditions at the interface.

The experimental and numerical signals show many common features. When viewing a weakly spilling breaker, both the vertically (VV) and horizontally (HH) polarized backscattering signals increase as the wave steepen and a bulge forms on the front of the crest. After the bulge collapses and breaking begins, turbulent eddies are shed from the crest. The mean level of the VV backscatter remains approximately constant during this time, while the HH backscatter decreases continuously after the onset of breaking. Both the experimental and numerical signals show relative maxima as turbulent eddies move across the crest, although the numerical results are more sensitive to the finest structure of the eddies. This is most likely because these features are limited in azimuthal extent ("short-crested"). The major difference between the signals is the HH-to-VV polarization ratios, which are significantly higher in the experimental signal. This demonstrates the importance of multi-path interference in "sea spike" events, which is not yet represented in the numerical calculations. When a plunging breaker was illuminated, the scattered signals were marked by a reduction in the VV backscattering during the formation of the breaker jet while the HH signal continued to increase. This represents an experimental demonstration of a sea-spike event resulting from single scattering from the jet that was first identified in numerical calculations (J. C. West, *Proc. IGARSS 2000*, Honolulu, 3120-3122).

RADAR INVESTIGATIONS OF BREAKING WATER WAVES AT LOW GRAZING ANGLES WITH SIMULTANEOUS HIGH-SPEED OPTICAL IMAGERY

M.A. Sletten, Code 7255, Naval Research Laboratory, Washington DC 20375
J.H. Duncan, University of Maryland, College Park MD
J.C. West, Oklahoma State University, Stillwater OK

Radar scattering experiments were recently carried out at the wavetank facility at the University of Maryland-College Park. Spilling and plunging breakers with a water wavelength of approximately 80 cm were generated by means of a chirped wave packet, and were then imaged with a high-speed camera in conjunction with a laser sheet. Simultaneously, the radar backscatter generated by the breakers at a nominal grazing angle of 12 degrees was measured by an ultrawideband, dual-polarized radar with a range resolution of approximately 4 cm and usable frequency content in the 6-12 GHz band. In addition to providing both quantitative profiles of the evolving water surface and the corresponding ultra-high resolution radar backscatter, this experimental setup also included a moving instrument carriage that allowed the sensors to follow the breakers throughout their entire evolution.

An analysis of the results shows that for the spilling breaker, over 90 percent of the horizontally polarized (HH) energy scattered back to the radar is generated during the initial stage of breaking by the small bulge near the wave crest. For vertical polarization (VV), the initial breaking stage produces about 50 percent of the backscattered energy. The Doppler velocity associated with this energy is slightly higher than that of the phase speed of the dominant wave in the water wave packet. For VV, the remainder of the backscattered energy is generated by the turbulent, post-breaking surface, and in fact a close correlation is observed between increases in the VV backscatter amplitude and the shedding of turbulent cells of vorticity after the wave breaks. The Doppler velocity associated with this VV energy steadily decays from a velocity near that of the dominant wave phase speed down to a velocity close to that of the wave orbital motion. For the plunging breaker, the initial feature on the crest, an overturning jet, generates 30 to 40 percent of the total backscattered energy for both HH and VV. Initial Doppler velocities are again slightly higher than the dominant wave phase speed, particularly for HH polarization, and the spread in measured velocities is higher than for the spilling case.

Polarization ratios (HH/VV) near 10 dB are observed during the initial breaking stage of the spiller and near 20 dB in the case of the plunger. Numerical simulations of the backscatter that use the measured profiles as inputs show that these large polarization ratios are due only in part to multipath scatter off the front face of the wave.

AIRBORNE KA-BAND POLARIMETRIC MEASUREMENTS DURING THE SHOALING WAVES EXPERIMENT

V. Irisov*
Zel Technologies, LLC
NOAA/Environmental Technology Laboratory
L. Fedor
CIRES
University of Colorado
NOAA/Environmental Technology Laboratory
V. Leuski
CIRES
University of Colorado
NOAA/Environmental Technology Laboratory
B. Patten
NOAA/Environmental Technology Laboratory

The Shoaling Wave experiment was conducted in November-December 1999 off the coast of North Carolina. It involved numerous ship, aircraft, and buoy measurements of the atmospheric and oceanic parameters in an area of steadily increasing water depth. Smooth sea-bottom topography is well-suited for the purposes of sea wave transformation study.

The NOAA Environmental Technology Laboratory installed and operated three microwave radiometers on a CIRPAS (Center for Interdisciplinary Remotely-Piloted Aircraft Studies) Twin Otter aircraft: a 37 GHz (Ka-band) cross-track scanning polarimeter, a 60 GHz scanning radiometer, and a dual-frequency 23/31 GHz zenith/nadir looking radiometer.

Now we present the results obtained by the cross-track scanning Ka-band polarimeter. The radiometer measured the intensity of the microwave radiation at three linear polarizations: -45 deg., 0 deg., and 45 deg., which allowed us to retrieve the first three Stokes parameters at various incidence angles. Scanning was produced by a 45 deg. mirror controlled by a stepping motor. Ka-band polarimeter was able to observe sky and ocean radiation almost from zenith to nadir. It provided an opportunity to use tip-cal calibration technique during a flight.

Beside calibration the atmospheric part of the scans was used for compensation for downwelling radiation from the clouds. As a result an absolute calibration of the order of 1 K was achieved. Wind dependence of the brightness temperature at vertical and horizontal polarizations was obtained for nadir incidence angles from 17 deg. up to 80 deg. During the experiment wind speed varied from 2 to 14 m/s. Parabolic approximations of the brightness temperature wind dependence were derived for a variety of incidence angles.

PASSIVE POLARIMETRIC MEASUREMENTS OF FOAM AND ROUGHNESS EFFECTS ON MICROWAVE EMISSIVITY

S.C. Reising*, K.A. Horgan, E.J. Knapp
113 Knowles Engineering Bldg., Univ. of Massachusetts
Amherst, MA 01003-4410, USA
W.E. Asher
APL, Univ. of Washington, Seattle, WA 98105-6698, USA
L.A. Rose, K.M. St. Germain, P.W. Gaiser, D.J. Dowgiallo
Naval Research Laboratory 7223, Washington DC 20375, USA

Accurate retrieval of ocean wind speed and direction from spaceborne microwave radiometers requires knowledge of how changes in surface properties affect microwave emissivity. Foam caused by whitecaps on the ocean surface dramatically increases the sea surface emission. In addition, wind roughening is a key mechanism allowing spaceborne microwave radiometers to remotely sense wind speed and direction. Near-surface measurements are needed to improve quantitative knowledge of the effect of changing surface conditions, including foam and roughness, on microwave emissivity.

This paper presents results from three near-surface measurement campaigns completed during 2000-01. First, in May 2000, two polarimetric radiometers operating at 10.8 and 37 GHz were deployed at the Naval Research Laboratory's Chesapeake Bay Detachment (CBD) to measure foam emissivity. A foam generator was used to create a stable foam layer on the flat water surface of the bay, covering 95% of the radiometers' fields of view. The brightness temperatures of the sea surface (with and without foam) and of the downwelling radiation were measured at 10.8 (X-band) and 37 GHz (Ka-band). Microphysical measurements were used to characterize the foam thickness, bubble size distribution and void fraction of the foam, important parameters for initializing electromagnetic models of the microwave emissivity of foam.

Second, we present results from coordinated radiometric and video observations during the Fluxes, Air-Sea Interaction, and Remote Sensing (FAIRS) experiment, conducted from the U.S. Navy's R/P FLIP, off the coast of California during September and October 2000. Two polarimetric radiometers were deployed with boresighted video to observe the ocean surface for wind speeds of up to 15 m/s with concomitant large-scale breaking waves. These radiometric data of dynamic breaking waves demonstrate that the emission depends upon the time dynamics of wave breaking and decay as well as on the viewing angle. Third, we present preliminary results from Wind and Salinity Experiment, WISE 2000, on the Casablanca oil platform in the Mediterranean Sea, 40 km offshore from Tarragona, Spain. A 37 GHz (Ka-band) polarimetric radiometer measured sea surface and sky emission for wind speeds up to 12 m/s, at incidence angles from 35° to 65°.

TWO-SCALE SCATTERING MODEL APPLICATION TO RADAR "SEA-SPIKES" AND POLARIZATION RATIO

Fuks,I.M., Smirnov, A.V.,
ZelTech, LLC/NOAA, Environmental Technology Laboratories, Boulder, CO

Many studies shows that at low grazing angles there are appeared the pulsed enhancements mostly at horizontal polarization. These enhancements, known as "sea-spikes", are observed with a narrow polar diagram, producing the spikes, and in narrow space-time bands. We suggest that under low grazing angles, and in cross-wind environment, it might be realized such radar geometrical condition when very steep surfaces result in the polarization inversion.

Following the main idea of two-scale scattering model, we introduce the large-scale (compare to the radar wavelength λ) plane facets on the sea surface, covered by the small-scale Bragg-scattering ripples. The scattering cross sections σ^0_{HH} and σ^0_{VV} in the Cartesian frame of reference, where axis Oz is directed to zenith and xOz is the plane of incidence, can be expressed as follows:

$$\begin{aligned} \sigma^0_{HH} &= \alpha^2\sigma_{hh} + \beta^2\sigma_{vv},\ \sigma^0_{VV} = \alpha^2\sigma_{vv} + \beta^2\sigma_{hh}, \\ \alpha &= \frac{\cos\psi_0\cos\gamma - \sin\psi_0\sin\gamma\cos\varphi}{\sin\theta},\ \beta = \frac{\sin\gamma\sin\varphi}{\sin\theta}. \end{aligned}$$

where θ is an angle between wave vector $\mathbf{k}$ $(-k\cos\psi_0, 0, -k\sin\psi_0)$ and vector $\mathbf{N}$ $(\sin\gamma\cos\varphi, \sin\gamma\sin\varphi, \cos\gamma)$ normal to the facet, and σ_{hh} and σ_{vv} are the radar backscattering cross sections in the local reference frame . From these equations follows that for small grazing angles ψ_0, the positive "sea-spikes" of σ^0_{HH} are caused by the steep facets with normal $\mathbf{N}$ located in the plane perpendicular to the plane of incidence ($\varphi \simeq \pi/2$), and they are accompanied by the negative "sea-spikes" of σ^0_{VV}. For polarization ratio $K^{HH}_{VV} = \sigma^0_{HH}/\sigma^0_{VV}$ it follows:

$$K^{HH}_{VV}(\psi_0) = \frac{K^{hh}_{vv}(\theta) + \omega}{1 + \omega\cdot K^{hh}_{vv}(\theta)},\ \omega = \left(\frac{\sin\gamma\sin\varphi}{\cos\psi_0\cos\gamma - \sin\psi_0\sin\gamma\cos\varphi}\right)^2,$$

where $K^{hh}_{vv}(\theta) = \sigma_{hh}/\sigma_{vv}$ is the polarization ratio in local reference frame. It is seen that for cross-wind direction ($\varphi \simeq \pm\pi/2$) can exceed essentially that one for the up/down wind direction ($\varphi = 0, \pi$).

In such consideration, even "sea-spikes" are result of resonant, Bragg scattering on the steep surfaces of waves carrier the small-scale perturbations. The effect was found in the data from the Coastal Ocean Probing Experiment (COPE) and was confirmed from other earlier published experiments.

EFFECTS OF SLOPE MODULATION ON THE POLARIZATION DEPENDENT SCATTER CROSS SECTIONS OF RANDOM ROUGH SURFACES-STATIONARY TWO-SCALE FULL WAVE APPROACH

Bahar, E., *Crittenden, P., EE, MS, CEO, Univ. of Nebraska, Lincoln

Using the small height/slope perturbation solution, it is shown that the vertically and horizontally polarized backscatter cross sections of random rough surfaces have a significantly different dependence upon the incident angle. Thus, for highly conducting surfaces, the ratio of the two cross sections σ^{PP} (P=Vertical, Horizontal) is $\frac{\sigma^{VV}}{\sigma^{HH}} = \left|\frac{1+sin^2\theta}{cos^2\theta}\right|^2$. As the incident angle θ approaches 90^o, this ratio becomes very large. The corresponding expressions for the physical optics solutions are polarization independent. The physical optics and perturbation solution for the backscatter cross sections are in agreement only for normal incidences (specular scatter).

Ample experimental data, however, indicates that the backscatter cross section $\sigma^{PP}(P = VorH)$ can be of the same order of magnitude and also significantly larger than the values predicted by both physical optics and perturbation theory.

A unified full wave approach is used to express the backscatter cross sections as weighted sums of two cross sections. One is associated with the larger scale surface cross section, mulitiplied by the magnitude squared of the smaller scale surface height characteristic function. The second is the cross section associated with the smaller scale surface height, modulated by the slopes of the larger scale surface. When the composite rough surface is characterized by a continuous surface height spectral density function, it becomes necessary to judiciously separate the smaller scale surface from the larger scale surface. It is shown that this can be done reliably using the full wave approach by seeking stationary solutions to the cross sections over a wide range of mean square values for the small (or large) scale surface heights. These stationary values for the polarization dependent backscatter cross sections can be practially equal and also significantly larger than the corresponding physical optics and perturbation results.

BACKSCATTER CROSS SECTIONS FOR A SUPERPOSITION OF PEARSON-MOSKOVITZ RANDOM ROUGH SURFACE EXPRESSED AS A STATIONARY WEIGHTED SUM OF TWO CROSS SECTIONS

*Crittenden, P., Bahar, E., MS, EE, CEO, Univ. of Nebraska, Lincoln

Superpositions of two Pearson-Moskovitz surface height spectral density functions are used to characterize composite random rough sea surfaces. Using a unified full wave approach, the backscatter cross sections of the random rough surfaces are expressed as weighted sums of two cross sections. The first, associated with the larger scale component of the surface is reduced by a factor related to the smaller surface height characteristic function. The second, associated with the smaller scale component of the surface accounts for slope modulation by the larger scale surface. Unlike the conventional hybrid perturbation/physical optics solutions, the unified full wave approach is not restricted by the small Releigh parameter ($\beta = 4k_0^2 h_s^2 << 1$, where k_0 is the free space wave number and h_s^2 is the mean square height of the small scale surface).

The total surface height spectral density function is expressed as a sum of larger and smaller scale surface spectral density functions (without specifying a discrete spatial wave number for spectral decomposition) and the ratio of the mean square height of the small scale surface and the total surface h_s^2/h^2 can be varied from zero to unity. Thus, in the limits, the total composite surface is regarded as a large scale surface (associated with the physical optics solution) or as a small scale surface (associated with the original full wave solution). It is shown that the unified full wave solutions for the scatter cross sections are stationary over a very wide range of values for h_s^2/h^2 and the results are not significantly dependent on spectral decomposition of the composite rough surface.

Session G1, 13:35-Wed.

RADAR TECHNIQUES

Chairperson: J. Foster

PROPOSAL FOR THE DETERMINATION OF A RELATIONSHIP BETWEEN SE SPECTRA AND THEIR ANGULAR DIRSTRIBUTION

LaHoz,C.
The Auroral Observatory, PO Box 952
9001 Tromsø, Norway
Hagfors,T.,Rietveld,M.
MPAe, Max Planck Strasse 2
37191 Katlenburg Lindau, Germany
Isham,B.
EISCAT
9027 Ramfjordbotn, Norway

With strong irradiation of the ionosphere with electromagnetic waves the various modes in the magnetoionic plasma interact nonlinearly creating E.M. waves escaping from the ionosphere. These waves have been termed Stimulated Electromagnetic Emission or SEE for short. The frequency spectra of the radiation has been studied in great detail, and a number of characteristic spectral features have been identified and related to particular processes in the ionosphere. Great importance is associated with the separation in frequency between the pump and harmonics of the local electron gyro-frequency, and the spectral properties and the amount of induced anomalous absorption are both affected by this separation. Waves created in the ionosphere of non-electromagnetic nature do not propagate away from the ionosphere and can in some cases be observed by the electron density fluctuations associated with them. These density fluctuations are sometimes referred to as plasma turbulence, sometimes as parametric decay. The association of these density fluctuations and the properties of the SEE phenomenon is by no means simple, and not well understood.

Plasma density fluctuations have been the subject of scattering observations at EISCAT with antennas scanning a number of positions corresponding to different angles between the wave propagation direction and the geomagnetic field and a preference of some phenomena for the field aligned direction was identified. Other phenomena such as heater-excited artificial aurora and the generation of field aligned irregularities seem to also show a preference for the field aligned positions. In view of this evidence of angular structure in heater-induced disturbances it is of interest to investigate experimentally whether similar angular structure is present in the various spectral features the SEE signals and to compare the results with radar observations of plasma turbulence. To this end we propose and describe a simple two element interferometer experiment, and if available, some experimental data.

ANOMALOUS ION LINE SPECTRA ASSOCIATED WITH ENHANCED PLASMA LINES OBSERVED DURING AURORAL PRECIPITATION

B. Isham*
EISCAT Scientific Association, Norway

C. La Hoz
University of Tromsø, Norway

M. T. Rietveld
EISCAT Scientific Association, Norway
Max-Planck-Institute for Aeronomy, Germany

T. Grydeland
University of Tromsø, Norway

F. Forme
CETP/UVSQ/IPSL, Velizy, France

Anomalous incoherent scatter echoes are radar echoes from the F or upper E regions whose ion line spectral shape departs from that corresponding to thermal equilibrium. The scattered power is enhanced and the spectra can be symmetric or asymmetric with one or the other shoulder more enhanced. Several theories have been proposed which can be divided into two classes: (1) direct electron or ion beam instabilities that distort and enhance the ion line and (2) a beam-enhanced Langmuir wave which becomes the pump for a parametric decay into enhanced daughter Langmuir and ion acoustic waves; the beam-enhanced pump and the enhanced daughter waves may be observed as non-thermally enhanced incoherent scatter ion and plasma lines. Direct beam instabilities fail to explain one or another characteristic of the observations, for example they may require large currents or enhance only one ion line shoulder, contrary to observations showing enhancements of either or both shoulders, or both shoulders with a central peak. On the other hand, parametric instability mechanisms appear better positioned to explain most if not all of the observations. Since they also produce enhancements of the plasma lines, a decisive test is whether the anomalous ion line echoes are accompanied by enhanced plasma lines. Parametric instabilities, or Langmuir turbulence, can also explain the enhanced central ion line peak. Here we present recent measurements made with the EISCAT VHF (224 MHz) radar in northern Scandinavia of anomalous ion line spectra accompanied by strong plasma line enhancements. These measurements provide important evidence in support of the parametric decay instability, or, more generally, of natural Langmuir turbulence in the aurora.

ELIMINATION OF LARGE INTERFERERS FROM PULSE RADAR AND OTHER SPREAD SPECTRUM DATA

Bibl,K.*,Cheney,G.P.
Center for Atmospheric Research
University of Massachusetts-Lowell
600 Suffolk St.
Lowell, MA 01854

Although Spread Spectrum Systems are designed to minimize disturbance by coherent interference, they are sometimes overwhelmed by interference which easily can be larger than 40 dB above the wanted pulse signal. Years of studies have led to the development of a new spectrum analysis method, called the Iterative Spectrum Analysis. By a simple calculation, the exact frequency and then the exact amplitude and phase of the largest spectral line in the spectrum is determined from the complex amplitudes of adjacent spectrum lines. The corresponding complex sine wave is subtracted in the time domain and a new spectrum created. This process is repeated until the data are sufficiently cleaned. Iterative Spectrum Analysis can reduce even a large number of coherent interferers by at least 20 dB without affecting the broadband signals significantly. On the contrary, the method unveils the correct amplitude and phase which is corrupted by the interference.

Interference elimination by punching out lines of large amplitudes in the spectrum is a well known and often patented method. But if the actual frequency is in between the sampled Doppler frequencies, the residual tail can be up to 30 maximum amplitude and cover and modify a large range of the pulse spectrum.

Although requiring a significant amount of computing effort, a safe method has been found to decrease interference by at least 20 dB, even in cases of substantial multiple interference with strong modulation without a carrier. But because of the substantial increase in Digital Signal Processing power, it is possible to pre-process a multitude of data in real time.

A computer program has been developed to pre-clean the raw data for the whole of each pulse period independently before the standard pulse compression and spectrum analysis of each range and highly interfered actual data have been cleaned successfully.

MILLSTONE HILL E REGION COHERENT SCATTER EXPERIMENTS: NEW PERSPECTIVES ON THE MID-LATITUDE POLARIZATION JET ELECTRIC FIELD AND ITS VARIABILITY

P. J. Erickson, J. C. Foster, F. D. Lind
Atmospheric Sciences Group
MIT Haystack Observatory
Westford, MA 01886 USA

The Millstone Hill 440 MHz UHF radar facility with its 46 meter steerable antenna, megawatt-class transmitter, and -170 dBW receiver sensitivity can detect not only weak incoherent scatter returns from the background ionosphere, but also intense 34 cm irregularities from northward directions where aspect angles are nearly perpendicular to the geomagnetic field. Whenever ambient electric fields exceed the Farley-Buneman two-stream irregularity threshold of 15-20 mV/m, geomagnetic field topology allows reception of coherent backscatter over 2-4 degrees of geomagnetic latitude.

Millstone Hill has been pursuing studies of the characteristics of E region mid-latitude irregularities and the interrelationship of backscatter cross-section, phase velocity, and electric field strength for more than a decade [*e.g. St. Maurice et al, JGR, 94, 6771-6798, 1989; Foster and Tetenbaum, JGR, 96, 1251-1260, 1990*]. Recent experiments have led to the significant discovery of a linear relation between backscattered power and driving electric field amplitude at 34 cm wavelength [*Foster and Erickson, GRL, 27, 3177-3180, 2000*]. This fact can be combined with enhancements in radar system technology, allowing one-second temporal and one-kilometer spatial resolution, to produce very detailed information on the electric field in the mid-latitude sub-auroral ionosphere. In particular, the fine-scale structure in the vicinity of the polarization jet and SAID (sub-auroral ion drift) exhibits dramatic variability. Observations show uniform electric fields which rapidly transition into superimposed multiple instances of narrow (0.1 degree), intense (~60 mV/m), SAID configuration fields having lifetimes as short as 1.5 minutes and equatorward gradients as large as 4 mV/m per km [*Erickson et al, Rad. Sci., in press, 2001*].

We present an overview of Millstone Hill coherent backscatter capabilities and discuss the insights gained into the highly complex nature of the mid-latitude polarization jet and SAID region. In particular, new rapid scanning modes allow imaging of the entire coherent irregularity backscatter sensitivity region on minute time scales, while fixed-position experiments allow simultaneous E region coherent echo and F region background electric field determinations. We present examples of polarization jet structure obtained with these observational modes, and describe future plans for enhanced experiments with the new MIDAS-W workstation based radar system.

MEASURING THE COMPLETE INCOHERENT SCATTER SPECTRUM AT ARECIBO

Sulzer, M.P., Gonzalez, S.A.
Arecibo Observatory
HC 3 Box 53995
Arecibo PR 00612
Behnke, R.A.
National Science Foundation

The purpose of the work described here is to make significant improvements in the measurements of parameters determining the incoherent scatter spectrum in the topside of the Arecibo ionosphere. Under different conditions the spectrum is best described as a continuous function of frequency or a set of discrete components. The latter description is appropriate in the F region where most useful component is the low frequency ion line, while the much weaker high frequency plasma line is useful only when enhanced by photo-electrons. The third component is the extremely weak and infrequently measured gyro line. The first description becomes appropriate for low electron number densities when the electrostatic plasma resonance becomes weak compared to the thermal spreading force. In the limit of very small density the spectrum is Gaussian and contains information only about the electron temperature, but at higher densities when the ion line is present but the plasma resonance is still broad, the shape of the spectrum contains the usual information in the ion line and the high frequency portion contributes additional information about the density and electron temperature.

Our first measurements during the July 2000 Bastille day storm and the recovery period demonstrated the practicality of these measurements given adequate data acquisition and computational facilities. These facilities improve each year, and soon these measurements will become as routine as ion line measurements alone. Therefore it is important that we verify the usefulness of the data by comparisons to the theory. The result from the measurements of last summer is that the data do not agree with theory.

Since then we have made additional measurements under normal ionospheric conditions using different data acquisition equipment. These spectra are in agreement with the earlier ones, and so the disagreement with theory is still unexplained. We also have made measurements of the ion and gyro lines in the lower F region. These latter measurements are in agreement with theory, and thus our only problem is with the weak transition spectra in the topside.

THE HAARP VHF RADAR

Djuth, F.T.*
Geospace Research, Inc.
El Segundo, CA 90245, USA

In May 2001, a new VHF radar system was installed at the HF Active Auroral Research Program (HAARP) site in Gakona, Alaska. The purpose of the radar is to monitor naturally occurring phenomena in the atmosphere/ionosphere above HAARP as well as modifications to the ionosphere brought about by the HAARP high-power, high-frequency modification facility. The radar transmitter is capable of operating from 135 to 143 MHz. However, from a practical standpoint, the radar is typically tuned between 139.0 MHz and 140.5 MHz. The bandwidth available for transmission is limited by the matching network of the co-linear, coaxial dipole antenna, known frequency bands containing interfering signals, and the frequency range assigned for radar operations. The maximum and minimum pulse widths are 2 milliseconds and 0.5 microseconds, respectively, and the maximum duty cycle is 10 %. Each of these three parameters is checked on a pulse to pulse basis as part of an autonomous protection system. As currently configured, the radar employs sixteen transmitter modules to generate between 32 and 40 kW peak power. Eight transmitters are assigned to each quadrant of the antenna, and the pulse phase of each quadrant is computer-controlled. Circulators are used as a buffer between the transmitter and the transmit-receive switches, and serve as an effective means of dumping transmitter power to a load bank in the event that the antenna and/or the transmission lines are damaged while the radar is in operation. The radar receiver has four channels and employs analog circuitry to mix the radar signals down to an intermediate frequency (IF) band of 10 MHz +6/-8 MHz. Each of the four IF channels is digitized at 40 megasamples per second with 12-bit resolution. Digital downconverting receivers having multiple channels are used to filter and decode radar signals. Range-gated, raw-voltage data is stored on a hard disk drive, and a range-time-intensity plot of the radar backscatter is shown in real time. In the future, the radar will be operated in a stand-alone mode, and the results will be available in real-time on the Internet. To date, the radar has been used to monitor Polar Mesosphere Summer Echoes and interesting new phenomena related to auroral particle precipitation. The wide variety of techniques available with this new system is described in the presentation along with details of the radar architecture.

32-BIT COMPLEMENTARY AND STAGGERED PULSE CODES

K. Bibl*, G P.Cheney
Center for Atmospheric Research
University of Massachusetts-Lowell
600 Suffolk St.
Lowell, MA 01854

Binary multi-chip codes are used for many coherent Radar applications. Very often Barker Codes are chosen because they have minimum leakage for single pulses. But when the expected Doppler frequencies are not too high (Doppler periods larger than the pulse period), then complementary pulse pairs can be used. They have even lower leakage under those conditions. There are still substantial limitations for those complementary codes: leakage is only small if the whole system , including the transmitter power amplifier, is linear; the receiver bandwidth, matched to the chip-width of the transmitter, will produce different amplitudes, dependent on how often the chips change their phase; also there is the problem of cross-talk between adjacent pulses. From 40 different 16-chip complementary pulse pairs, a pulse pair has been found which has the distinct minimum cross-correlation of 4 or less when one is moved incrementally over the other, while the auto-correlation is 3 or less. These two phase codes are interlaced with each other while the second one is shifted by +90 degrees. Then the complement is formed where the second code is shifted by -90 degrees. Thus a 32-bit complementary pulse pair is formed where each pulse has a maximum of 32 and no leakage in the real part of its auto-correlation, but a complementary leakage of 5 or less in its imaginary part. These leakages cancel each other if the Doppler is small. This 32-chip complex complementary code with one-half chip-size (to keep the total pulse length the same) has substantial advantages compared with the 16-chip code: 1) It narrows the received signal by almost a factor of two in spite of the same receiver bandwidth. 2) It improves the signal/noise by about 2 dB and often much more for coherent interferers. 3) Each of the 32-chip pulses has a leakage of 5/32 instead of 3/16 and a cross-talk of 6/32 instead of 4/16. 4) Although the resulting amplitude is 1 dB below the signal from the 16-chip code because of the frequent switching, its amplitude over the whole pulse changes only by 1 dB while the amplitude of the 16-chip code, dependent on the receiver bandwidth, changes by more than 3 dB. Staggered Pulse Codes have the property that very short and long ranges can be monitored simultaneously. For them, similar advantages can be achieved when each chip of the staggered pulse code is split into two and a quasi-random + or - 90 degree phase-shift is applied to one of the two halves.

PASSIVE INCOHERENT SCATTER RADAR

F.D. Lind
MIT Haystack Observatory
Route 40
Westford, MA 01886, USA
J.D. Sahr
Department of Electrical Engineering
University of Washington
Seattle, WA 98195-2500, USA

Passive radar is a technique for exploiting transmitters of opportunity to make radar observations. The application of this technique to the observation of coherent scatter from E-region irregularities has recently been demonstrated using the Manastash Ridge Radar and FM radio signals. Although the cross-section for incoherent scatter is many orders of magnitude smaller than that of coherent scatter targets we evaluate the feasibility of passive incoherent scatter radar. We demonstrate that for a wideband digital beamforming passive radar it is possible to achieve positive signal to noise ratio incoherent scatter observations. This can be done using FM radio or Digital Television broadcasts for reasonable integration times and resolutions. We compare the performance of this technique to currently operational incoherent scatter radars and highlight the benefits of the new approach. We show that passive incoherent scatter radars should be able to perform as well as or better than current incoherent scatter radar designs. These radars would also have the fundamental advantage of always being active due to the CW nature of many transmitters of opportunity. Passive incoherent scatter radars should also have relatively low construction and operations costs compared to active systems. We also discuss the difficulties of this approach including clutter limitation, site selection, data management, and the extraordinary computational burden of the data processing. Finally, we discuss the Low Frequency Array (LOFAR) and its potential application as a passive radar for the demonstration of passive incoherent scatter. This system is a newly proposed radio telescope that will be sensitive to signals in the 10-240 MHz range. It will consist of 13,000 dipole antennas clustered in approximately 100 stations and distributed over an area of 400km.

MEASURING F REGION ION AND ELECTRON TEMPERATURES AT JICAMARCA USING INCOHERENT SCATTER RADAR: RESULTS AND THEORY INCLUDING COULOMB COLLISIONS

*Sulzer, M.P., Aponte, N., Gonzalez, S.A.
Arecibo Observatory
HC 3 Box 53995
Arecibo, PR 00612

The measurement of ion and electron temperatures is one of the basic functions of the incoherent scatter radar. We describe the technique for measuring these temperatures at Jicamarca using our new library of functions including the effects of Coulomb collisions. We also review the theory needed to generate the library and summarize measurements confirming the new technique.

Measurements made during almost the last forty years at Jicamarca have been questioned because the results often show that the apparent electron temperatures are less than the apparent ion temperatures. This violates the physics of the region: energy flows from the electrons to the ions during the day, and equilibrium exists at night. The problem resulted from the omission of the effects of electron-ion and electron-electron collisions in the equations for the incoherent scatter spectrum.

A numerical solution including the effects of the collisions gives spectra which imply equal temperatures when expected. The collisional effect is far greater than simple models such as Langevin's equation or the BGK approximation imply when observations are made looking vertically, or nearly so, with the Jicamarca radar. It is necessary to include the effects of both types of collisions with high accuracy since the resulting effect is dependent upon the interaction between the two and is unlike either alone.

The numerical simulations show the following results: First, the rapid decrease of the collisional coefficients with increasing electron speed plays a very important role in the resulting IS spectral shape. Second, electron-ion collisions, affecting the direction, but not significantly affecting the speed of the electrons, would alter only the central part of the IS spectrum. Third, the inclusion of electron-electron collisions, which affect both direction and speed, alters the spectrum more than one might expect based on the relatively small size of the coefficients.

HIGH LATITUDE IONOSPHERIC TOMOGRAPHY

G.S. Bust*,T.L. Gaussiran II, C. Coker, D.S. Coco
Applied Research Laboratories
The University of Texas at Austin
Austin, TX 78713, USA

Applied Research Laboratories, The University of Texas at Austin, deployed a four receiver ionospheric tomography array to Greenland in September of 2000, and have now collected more than a years worth of data. In addition, in collaboration with Northwest Research Associates and the Geophysical Institute, University of Alaska Fairbanks, we have been collecting data from a six receiver tomography array in Alaska since October 2000.

We will present results based upon our analysis of tomographic inversions obtained from selected data sets for both the Greenland and Alaska arrays. The first results from the Greenland array will focus upon comparisons between tomography inversions and results from the Sondestrom incoherent scatter radar (ISR). The objective of comparing tomography results to the ISR is to develop a quantitative understanding of the accuracy of the tomographic inversions in a high latitude environment. Validation results for both the F-region and the E-region of the ionosphere are presented.

The second set of results we will present will focus on the high latitude ionospheric structure and dynamics inferred from the tomographic inversions of electron density. The presented results will include imaging F-region structures and the response of the Greenland ionosphere to the ionospheric storm on March 31 - April 1 2001. We will also present results cross-comparing the Alaska and Greenland arrays, and the ionospheric response of both arrays during the March 31- April 1 storm.

In addition ot the above results, we will present intial results from two tomographic world days. The international tomographic research community has agreed to make September 19-20 2001 and December 12-13 2001 tomographic world days. For these days the tomogrpahic community will collect data, process and perform inversions on their data in a timely fashion. We will present initial results from at least the first world day.

RADAR OBSERVATION OF TOPSIDE DENSITY AS A PROXY FOR IONOSPHERIC TEC

J. C. Foster*, P. J. Erickson
Atmospheric Sciences Group
MIT Haystack Observatory
Westford, MA 01886
A. J. Coster
MIT Lincoln Laboratory
Lexington, MA

North-South elevation scans with the Millstone Hill incoherent scatter radar provide ionospheric plasma density latitude/altitude observations of the mid-latitude ionosphere between 35 and 65 invariant latitude and altitudes between 150 km and 800 km. The Millstone Hill radar has been in operation through three solar cycles (since 1979 using the fully steerable 150-foot diameter antenna) and these long-term operations have built up a database of radar elevation scans which sample a span of 15 - 25 latitude with better than 1 latitude resolution and 35 km altitude resolution. F-region total electron content (TEC), can be determined by integrating the electron concentration between altitudes 150 km to 800 km at each degree of latitude. GPS observations of TEC made with good (30-s) time resolution from a grid of observing sites across the continental United States have been used to construct two-dimensional maps of TEC during the major disturbances (e.g. July 15/16, 2000). Plasma advection from lower latitudes brings a swath of storm-enhanced density (SED) [Foster, J. Geophys. Res., 98, 1675-1689, 1993] with total electron content (TEC) 100 TEC units into the region immediately equatorward of the trough during such conditions. Communications and navigation systems relying on trans-ionospheric propagation must be able to compensate for the effects of such sharp gradients in total electron content in the Northeastern American sector. In our initial study of SED, it was noted that this important feature could be identified and monitored in the topside ionosphere by examining the mid-latitude plasma density data at constant altitude. Recent work by Su et al. [GRL, 28, 111-113, 2001]has indicated that ionospheric SED maps to detached plasmaspheric regions in the magnetosphere and that the single-altitude radar observations can be used to identify and monitor these large-scale field-aligned TEC structures. In this paper we examine the observed relationship among total line-of-sight TEC observed by GPS, F-region TEC derived from the radar elevation scans, and topside density at constant altitude from single-point radar observations. Our objective is to establish a basis for using the historical database of topside plasma observations as a proxy for TEC in the important mid-latitude magnetosphere-ionosphere coupling region during disturbed conditions.

Session G2, 13:55-Thurs.

DATA ASSIMILATION

Chairperson: D. Anderson

IONOSPHERIC TOMOGRAPHY AND DATA ASSIMILATION MODELS

R. W. Schunk*, L. Scherliess, J. J. Sojka
Utah State University
Center for Atmospheric and Space Sciences
4405 Old Main Hill, SER 246
Logan, UT 84322-4405 USA

Ionospheric weather disturbances can have detrimental effects on a variety of civilian and military systems and operations. They can affect over-the-horizon (OTH) radars, HF communications, surveying and navigation systems, surveillance, spacecraft charging, power grids, pipelines, and the FAAs Wide-Area Augmentation System (WAAS). In an effort to mitigate the adverse effects of the ionosphere on these systems/operations, a major effort is being devoted to developing improved specification and forecast models. An approach that has recently gained prominence is a data assimilation technique that is based on a Kalman filter and a physics-based ionospheric model. The filter provides an efficient means for assimilating different data types into a time-dependent, physics-based, numerical model, taking into account the uncertainties in both the model and data. Some of the data to be assimilated include in situ density measurements from satellites, ionosonde electron density profiles, occultation data, ground-based GPS TECs, TECs between ground stations and LEO satellites with radio beacons, and line-of-sight UV emissions from selected satellites. However, an important aspect of a data assimilation model is the need to acquire high-resolution measurements of weather features, and ionospheric tomography is a powerful way of obtaining 2-dimensional (usually altitude versus latitude) images of ionospheric variations at selected locations. Currently, tomography chains exist in the United States, South America, Europe, Russia, Greenland, and Asia. Although tomography is relatively new to our field, this technique has already been successful in reconstructing several different ionospheric density structures, including the main trough, boundary blobs, traveling ionospheric disturbances, and the Appleton anomaly. The current status of tomography and data assimilation methods will be reviewed.

DEVELOPMENT OF A PHYSICS-BASED REDUCED STATE KALMAN FILTER FOR THE IONOSPHERE IN GAIM

L. Scherliess*, R. W. Schunk, J. J. Sojka, D. C. Thompson
Utah State University
Center for Atmospheric and Space Sciences
4405 Old Main Hill, SER 246
Logan, UT 84322-4405 USA

A physics-based data assimilation model of the ionosphere is under development as the central part of a DoD MURI funded program called GAIM (Global Assimilation of Ionospheric Measurements). With the significant increase in the number of ionospheric observations that will become available over the next decade, this model will provide a powerful tool towards an improved specification and forecasting of the global ionosphere, with an unprecedented accuracy and reliability. The goal of this effort will be specifications and forecasts on spatial grids that can be global, regional, or local (50 km x 50 km). The specification/forecast will be in the form of 3-dimensional electron density distributions from 90 km to geosynchronous altitudes (35,000 km). The main data assimilation in GAIM will be performed by a Kalman filter.

In this paper we present a practical method for the implementation of a Kalman filter using a new physics-based ionosphere/plasmasphere model (IPM). This model currently includes 5 ion species (O_2^+, N_2^+, NO^+, O^+, and H^+) and covers the low and mid latitudes from 90 km to about 20,000 km altitude. A Kalman filter based on approximations of the state error covariance matrix is developed, employing a reduction of the model dimension and a linearization of the physical model for the propagation of the error covariance matrix. These approximations lead to a dramatic reduction in the computational requirements. To develop and evaluate the performance of the algorithm we have used an Observation System Simulation Experiment (OSSE). In this paper, we will initially present the physics-based ionosphere/plasmasphere model (IPM) used in GAIM, and demonstrate its use in the reduced state Kalman filter. Initial results of the filter in one longitudinal plane using synthetic measurements will also be presented.

VALIDATION OF A GLOBAL IONOSPHERIC DATA ASSIMILATION MODEL

B. Wilson*
JET PROPULSION LABORATORY
California Institute of Technology
4800 Oak Grove Dr.
Pasadena, CA 91109
G. Hajj, C. Wang, X. Pi, I.G. Rosen
Dept. of Mathematics
University of Southern California
Los Angeles, CA 90089-1113

A fully 3-dimensional Global Assimilative Ionosphere Model (GAIM) is currently being developed by a joint University of Southern California and JPL team as part of a DOD effort funded by a Multidisciplinary University Research Initiative (MURI). GAIM uses a first-principles ionospheric physics model (forward model) and Kalman filtering or a 4DVAR technique to not only solve for densities on a 3D grid but also estimate key driving forces which are inputs to the theoretical model, such as the ExB drift, neutral winds, and production terms. The driving forces are estimated by using the adjoint equation to compute the required partial derivatives, thereby greatly reducing the computational demands compared to other techniques. For estimation of the grid densities, GAIM uses an approximate Kalman filter implementation in which the portions of the covariance matrix that are retained (the off-diagonal elements) are determined by assumed but physical correlation lengths in the ionosphere. By selecting how sparse or full the covariance matrix is over repeated Kalman filter runs, one can fully investigate the tradeoff between estimation accuracy and computational speed.

Although GAIM will ultimately use multiple datatypes and many data sources, one can perform a first test of quantitative accuracy by ingesting GPS-derived TEC observations from ground and space-based receivers and then comparing the retrieved density field to independent ionospheric observations. A series of such GAIM retrievals will be presented and validated by comparisons to: vertical TEC data from the TOPEX altimeter, slant TEC data from ground GPS sites that were not included in the assimilation runs, and global ionosonde data (F0F2, HMF2, and bottom-side profiles where available). By presenting animated movies of the GAIM densities and vertical TEC maps, and their errors computed as differences from the independent observations, we will characterize the reasonableness and physicality of the climatology derived from the GAIM forward model and the quantitative accuracy of the ionospheric weather specification provided by the assimilation retrievals.

DETERMINING A 'BREAK-EVEN' POINT FOR KALMAN DATA ASSIMILATION IN THE IONOSPHERE

J. J. Sojka*, R. W. Schunk, L. Scherliess, D. C. Thompson
Utah State University
Center for Atmospheric and Space Sciences
4405 Old Main Hill, SER 246
Logan, UT 84322-4405 USA

Although data assimilation modeling is still in its infancy in the ionospheric field, the determination of a break-even return is worthy of discussion. In this context, break-even is defined as: under what conditions will an assimilation model of the ionosphere provide equivalent, and then superior specification and possibly forecast, results to what is currently available? This question is closely related to the availability and quantity of measurements that can be made available in real-time. This paper will discuss the break-even point by using a Kalman data assimilation model for traveling ionospheric disturbances (TID). The model will enable the issues of data quantity and quality to be explored while still being able to determine how present-day techniques of identifying a TID would perform.

TIDs will be launched from the auroral region equatorward, traveling at a constant speed. This permits making a one-dimensional model assumption, with the velocity as a free parameter. The USA east-coast longitude sector will be simulated with an initial selection of ionosonde stations that correspond to actual observatories. A TID is assumed to be a coherent structure on top of the normal ionospheric F-layer and, hence, is modeled as a perturbation in F-layer density with noise associated with an observational capability. Hence, the simulated observations contain 20% to over 100% noise. In the study, the number of stations and the TID amplitude-to-noise level will be parameters that are varied; the objective being to find a minimum requirement on the number of stations, which will also be dependent upon noise level, that are required to ensure that the Kalman filter 1-D TID model can correctly identify the TID. This, in turn, is compared to what present-day identification schemes, mainly visual inspection such as an expert system, require.

DATA ASSIMILATION WITH DATA FROM SSUSI AND GUVI - WHAT UV IMAGERS CAN CONTRIBUTE

Paxton, L. J., Morrison, D., Zhang, Y. Kil, H. Wolven, B., Meng, C-I.
JHU/APL
11100 Johns Hopkins Rd.
Laurel, MD 20723

The Special Sensor Ultraviolet Spectrographic Imager (SSUSI) is set to launch on the DMSP F16 spacecraft in the Fall of 2001. In the same timeframe the Global Ultraviolet Imager (GUVI) on the NASA TIMED spacecraft will launch. These two instruments are far ultraviolet imagers that image the dayglow, nightglow, and aurora in 5 colors. These colors are the HI 121.6 nm line, OI 130.4 nm, OI 135.6 nm line, and two N_2 Lyman-Birge-Hopfield bands (140-150 nm and 165-180 nm). From these five color bands the SSUSI and GUVI science data algorithms produce environmental data records (EDRs). These EDRs from the SSUSI instrument are set to be assimilated by the Parameterized Real-time Ionospheric Specification Model (PRISM). The SSUSI instrument provides a wide variety of ionospheric parameters at high spatial resolution. These include NmF2, HmF2, and TEC on both the dayside and the nightside on a global basis. In addition, in the auroral region, NmE and HmE as well as Eo effective and Q effective are produced. Both of the auroral boundary location (poleward and equatorward) are provided. Both SSUSI and GUVI will provide O/N_2 ratios on the dayside disk as well as N_2, O_2, and O neutral density profiles in the dayside limb and a proxy for the solar EUV flux shortward of 40 nm. In this paper we will discuss how this data will be used by PRISM and how the data from GUVI and SSUSI can be used as inputs by other assimilative models to provide near real-time ionospheric and neutral atmospheric specification.

USING VARIOUS KALMAN FILTERING TECHNIQUES FOR NEUTRAL COMPOSITION FORECASTING

Minter, C.F., Fuller-Rowell, T.J., Codrescu, M.V.
Cooperative Institute for Research in Environmental Sciences
University of Colorado, Boulder

To determine the propagation parameters of high-frequency radio, an accurate forecast of the ionosphere is desirable. Until recently, obtaining a real-time and precise description of neutral atmospheric composition has acquired less consideration in comparison to other parameters such as ionospheric and neutral density. However, forecasting the ionosphere, especially during geomagnetic storm times, is strongly dependent on perturbations in the neutral composition. Because of this coupling between the ionosphere and neutral atmospheric chemistry, accurate knowledge of the neutral composition is critical in forecasting the ionosphere. The more accurate description of the neutral atmospheric composition is then used to supplement input parameters for ionospheric modeling.

In the research presented here, data assimilation techniques are applied to more accurately determine the neutral atmospheric species. The neutral atmospheric species are measured using remote sensing airglow data from polar orbiting spacecraft. Data is assimilated and noise from this data is reduced using filtering techniques in combination with a state propagation model. Methods for ingesting satellite data, predicting the state of the neutral atmosphere in the future, and filtering the data are investigated and then used simultaneously, utilizing the benefits of each, to reproduce the neutral atmospheric composition.

Since data assimilation techniques have enormous computational requirements for global forecasting, a significant amount of study is required to decrease the computation time while not decreasing accuracy. In this presentation, various methods are tested and compared in speed and accuracy in recreating a simulated data set and are documented as a benchmark for data assimilation of the neutral atmospheric composition as well as for other similar global systems.

APPLICATION OF EMPIRICAL ORTHGONAL FUNCTIONS (EOF) TO A DATA ASSIMILATION PROCEDURE

Tomoko Matsuo, Arthur D. Richmond
NCAR-HAO, PO Box 3000, Boulder, CO 80307, USA

In this study we characterize dominant modes of the high-latitude electric field variability as a set of two-dimensional empirical orthogonal functions (EOFs), based on a sequential non-linear regression analysis of the electric field derived from plasma drift measurements during the Dynamics Explorer-2 (DE-2) satellite mission (1981-1983). Together with the mean fields, 11 EOFs are capable of representing 68% of the squared electric field, leaving only a fairly random component as a residue. While such mathematically independent EOFs do not necessarily represent physically independent modes of variability, each of the first two EOFs is actually related to a widely known physically prominent effect on the convection patterns. The variability associated with the interplanetary magnetic field (IMF) B_Y component emerges as the primary mode, and the IMF B_Z effect emerges as the secondary mode. The tertiary mode reflects variability in the cusp region, but is not significantly correlated with the IMF.

Adapted to the dominant modes of the variability in the system, EOFs are ideal basis functions for data assimilation procedures. Not only do EOFs take account of the spatial coherence of the variability on large scales, so that even a data void area can be well constrained by using them as basis functions, but the use of EOFs also reduces the required number of basis functions and makes the corresponding background error covariance decoupled (diagonalized). In this paper we discuss application of the obtained EOFs to data assimilation using the Assimilative Mapping of Ionospheric Electrodynamics (AMIE) developed by Richmond and Kamide (*J. Geophys. Res.*, **93**, 5741-5759, 1988).

WEB-BASED EMPIRICAL MODELS OF THE IONOSPHERE AND THERMOSPHERE USING INCOHERENT SCATTER RADAR DATA

J.M. Holt*, S. Zhang
MIT Haystack Observatory
Westford, MA 01886

Improved specifications and predictions of the ionosphere/thermosphere (IT) system are an important objective of the National Space Weather Program. As a contribution toward meeting this objective, we have developed several empirical models of the average behavior and variability of key parameters which characterize the IT system. These models will be valuable in several ways to space weather studies and systems. Incoherent scatter radar data are available only a few days a month due to budgetary restrictions, but the models will always be available to provide a climatological representation of the state of the ionosphere and its variability for any set of conditions. The models covers a wide range of latitudes and altitudes and thus are useful for validation of global theoretical and empirical models. They will also be used in investigations of specific scientific problems, such as storm-time density gradients and enhancements. Preliminary model results are now available over the World Wide Web (http://www.openmadrigal.org) for user-specified input parameters.

The models are based on Millstone Hill incoherent scatter radar data from 1977 to the present. They include a local model of the E and F-region ionosphere over Millstone Hill; a regional model of basic and derived F-region scalar parameters as measured from Millstone Hill, including electron density, electron and ion temperature; and a model of the E×B plasma drifts and corresponding electrostatic potential patterns. The scalar models are keyed to solar and geomagnetic indices chosen by multiple regression, so that deviations of actual data from the model represent the remaining day-to-day variability due to such causes as tidal forcings, gravity waves and uncertainties in the solar EUV flux. The electric field model is keyed to the interplanetary magnetic field. It represents the average response to solar wind induced changes in the magnetospheric convection, thus providing a baseline from which more variable effects of substorms, storms and disturbed neutral winds (the disturbance dynamo) can be isolated.

Session G3, 13:35-Fri.

GPS AND THE IONOSPHERE

Chairperson: A.J. Coster

THE DESCENT OF SOLAR CYCLE 23

J. M. Kunches
NOAA Space Environment Center
Boulder, CO 80305, USA

Solar Cycle 23 is now in its post-maximum phase. The month of sunspot maximum was April 2000, with an associated smoothed sunspot number of 120.7. Periods of significant activity have occurred in the past two years, and additional, though less-frequent, major events are anticipated during the next few years. GPS operations may be affected to varying degrees when space weather is disturbed. Both amplitude and phase scintillation conditions may prove troublesome in maintaining lock on the GPS signal. TEC variability, especially apparent during geomagnetic storms, may impact the ability of models used by single frequency GPS users to estimate the pseudorange error. These strong geomagnetic storms may still occur in the descending phase of the solar cycle, if past solar cycles can offer any guidance. Episodes of strong solar x-ray flares and solar proton events will become increasingly scarce as the solar cycle winds down. In general, these conditions are less problematic for GPS applications than are the severe geomagnetic storm events. A more chronic condition will occur during the post- maximum phase. The magnitude of the Extreme Ultraviolet solar emissions will dim gradually over time, resulting in smaller TEC values in the dayside ionosphere, and, in general, a more benign background ionosphere to be affected by the pulses of space weather. The less EUV flux coupled with a generally lower level of space weather events, means the promise of a more regular ionosphere and relative calm for GPS users. A summary of activity to date will be presented and a speculation of what's ahead for the remainder of Cycle 23 will be given.

BENEFITS OF GPS MODERNIZATION TO THE ATMOSPHERIC SCIENCE COMMUNITY

A. J. Van Dierendonck
AJ Systems/GPS Silicon Valley
1131 Seena Avenue
Los Altos, CA 94024-4925
Anthea Coster
MIT Lincoln Laboratory
Millstone Hill Radar
244 Wood Street
Lexington, MA 02420-9108

In March 1998, two major enhancements to the Global Positioning System directed at civilian users worldwide were announced. These were a second civil code on L2 and a third civil signal (later designated at L5 in 1999) for safety of life services. Since that time, the details of modernization have been largely worked out. The task of designing the new coding on L5 was assigned to representatives of the civil community by the GPS Joint Program Office (JPO) via the Department of Transportation (DOT). The civilian representatives met on the RTCA Special Committee SC-159, Working Group 1, for close to two years to develop the L5 codes. The result is a new signal that is more resistant to interference and that performs considerably better in low signal-to-noise environments. The complete modernized GPS signal structure includes the addition of the military's earth coverage and spot beam M-Codes on L1 and L2, the addition of the civil C/A (and/or R/C code) on L2, and the introduction of the entirely new civil frequency and code at L5.

Aside from the obvious advantages of the increased signal power proposed for all signals, it is the new civilian codes that will primarily benefit the atmospheric community. All existing geodetic receivers will perform without disruption as nothing will change on the current L2 P/Y Code and L1 C/A and P/Y Codes. However, new receivers using new codes will perform significantly better. This paper will detail the specific benefits of these codes in estimating atmospheric parameters such as precipitable water vapor and the total electron content (TEC). It will also detail some of the current problems for GPS receivers in scintillation environments, and describe how the new signals will alleviate those problems.

This work is partially sponsored by the Air Force under Air Force Contract AF19628-00-C-0002 Opinions, interpretations, conclusions, and recommendations are those of the author and are not necessarily endorsed by the United States Air Force.

GLOBAL IONOSPHERE MAPS AND RELATED PRODUCTS GENERATED BY THE CODE ANALYSIS CENTER OF THE IGS

S. Schaer
Astronomical Institute
University of Berne
Switzerland

CODE, the Center for Orbit Determination in Europe, acts as one of currently five so-called ionosphere associate analysis centers of the International GPS Service (IGS) which produce global total electron content (TEC) maps on a regular basis. These maps are derived from data of the IGS tracking network, the primary product of the IGS. At CODE, a final, a rapid, and a predicted TEC map product are generated. The data format to provide the TEC information is the IONosphere map EXchange (IONEX) format as adopted by the IGS. GPS-based IONEX files may also contain estimates for P1–P2 code biases of the current GPS satellite constellation, which are obtained as a by-product of the TEC determination.

We are able to present a unique, uninterrupted time series of global TEC data, meanwhile covering seven years. Some remarkable results of our ionospheric analyses could be retrieved due to the fact that we make use of a spherical harmonics expansion (referring to a solar-geomagnetic frame) to represent the global TEC distribution. The demonstration of a significant lunar impact on the Earth's TEC distribution may be considered as one highlight of these analyses.

We give an overview of the ionosphere products regularly generated by the CODE analysis center: global as well as site-specific TEC maps, P1–P2 code bias values, but also values for satellite-related P1–C1 code biases which may become relevant for single-frequency GPS users. Time series of particular TEC parameters and results concerning the two types of code biases are shown. Finally, CODE's latest ionosphere product, improved "Klobuchar-style" ionospheric coefficients, a result of a "compression" of our global IONEX data, is introduced.

VALIDATION OF GLOBAL IONOSPHERIC TOTAL ELECTRON CONTENT MAPPING USING A MULTI-SHELL APPROACH

Komjathy A., Runge T., Wilson B., Mannucci A., Reyes M.
Jet Propulsion Laboratory
California Institute of Technology
4800 Oak Grove Drive, M/S 238-600
Pasadena, CA 91109

Dual-frequency transmissions from GPS satellites have been used for many years to measure and map ionospheric total electron content (TEC) on global scales. Global Ionospheric Mapping (GIM) software developed at the NASA Jet Propulsion Laboratoty (JPL) uses observations from about 100 GPS sites, an extended shell model, and Kalman filtering to compute global maps of vertical TEC with 15-minute time resolution and about 5-degree spatial resolution. Recently, the GIM algorithms have been enhanced to solve for parameters on a multi-shell grid, instead of using a single grid at a fixed ionospheric centroid height. Such multi-parameter models are designed to improve the accuracy of slant TEC retrievals and the ability to calibrate slant TEC measurements for arbitrary propagation paths. The extra parameters allow GIM to better model horizontal gradients and variations in peak height, while still retaining a simple, constrained fitting model as compared to a full tomographic density solution which is vastly underdetermined using only ground GPS data.

We will present two methods to validate the multi-shell approach: missing site and missing satellite tests. The missing site approach uses a global network of dual-frequency GPS stations but excludes a handful as validation sites. The line-of-sight TEC at these "missing" sites is predicted, using the GIM coefficients along with estimated satellite and receiver differential biases, and then validated against the actual line-of-sight TEC observations. A similar approach can be used for individual GPS satellite tracks in which line-of-sight TEC is predicted using only data from other GPS satellites and then validated against the observations. A series of comparisons using several days of data will be presented using both the conventional single-layer and the new multi-shell approaches. It is expected that the multi-shell approach will provide better slant TEC accuracy at low elevation angles along with more consistent bias solutions. Several versions of the multi-shell approach which use shells at different altitudes will be examined to see which one yields the best slant TEC prediction accuracy.

MONITORING IONOSPHERIC RESPONSE TO GEOMAGNETIC STORMS OVER THE SOUTH AMERICAN SECTOR USING GPS TOTAL ELECTRON CONTENT MEASUREMENTS

M. Fedrizzi*, INPE-DAE, Brazil
Visiting Grad. Student, GRL, Univ. New Brunswick, Canada
R. B. Langley, M. C. Santos, GRL, Univ. New Brunswick, Canada
A. Komjathy, Jet Propulsion Laboratory, USA
E. R. de Paula, I. J. Kantor, INPE-DAE, Brazil
W. D. Gonzalez, INPE-DGE, Brazil

Despite the fact that much has been learned about physical, dynamical and chemical processes that drive ionospheric storms, understanding the effects of geomagnetic storms on the neutral and ionized upper atmosphere is still one of the most challenging topics remaining in the physics of this atmospheric region. In order to investigate the magnetospheric and ionospheric-thermospheric coupling processes, many researchers are taking advantage of the dispersive nature of the ionosphere to compute total electron content (TEC) from Global Positioning System (GPS) dual-frequency data. Currently, there are a large number of GPS receivers in continuous operation. However, these stations are unevenly distributed, being situated mostly in the Northern Hemisphere. The relatively smaller number of GPS receivers located in the Southern Hemisphere and, consequently, the reduced number of available TEC measurements, cause ionospheric modelling to be less accurate in this region. In this paper, GPS data from the Brazilian Network for Continuous Monitoring by GPS (RBMC) have been used along with data from the International GPS Service (IGS) network to investigate the response of the ionosphere over the South American region during geomagnetic storms. For this study, we are using the University of New Brunswick (UNB) Ionospheric Modelling Technique, which uses a spatial linear approximation of the vertical TEC above each station using stochastic parameters in a Kalman filter estimation to describe the local time and geomagnetic latitude dependence of the TEC. The utilisation of the RBMC GPS data to monitor the ionosphere over the South American sector will provide more accurate and representative regional and global ionospheric models and help us to obtain a better understanding of the physics and dynamics of the low-latitude and equatorial ionosphere during geomagnetically disturbed periods.

IONOSPHERIC REMOTE SENSING WITH THE IONOSPHERIC OCCULTATION EXPERIMENT (IOX): FIRST RESULTS

Paul R Straus*
The Aerospace Corporation
Mail Stop M2/259
PO Box 92957
Los Angeles, CA 90009

The Ionospheric Occultation Experiment (IOX) is a dual-frequency GPS receiver with a single Earth-limb viewing antenna. Ionospheric remote sensing is possible during occultation events in which the line of sight to a GPS satellite being tracked by IOX sets through the Earth's limb. IOX is one of four experiments to be flown as part of the United States Air Force Space Test Program's PICOSat mission, with launch anticipated in early September of 2001. PICOSat will be placed into a 68 degree inclination, 800 km altitude orbit, enabling IOX to make ionospheric measurements at all local times under near-solar maximum conditions over the course of its mission. The IOX instrument will be described together with initial observations obtained from this mission. Plans for data analysis and scientific studies will be discussed. These include (1) cross-validation of UV ionospheric remote sensing techniques through comparisons with data from sensors on TIMED and DMSP F16 (both of which are also expected to launch sometime late in 2001); (2) potential observations of equatorial scintillations using an occultation sensor; (3) evaluation of aspects of the occultation data relevant to space weather prediction or assimilation into ionospheric specification models; and (4) detailed analysis of ionospheric structures through enhanced ionospheric tomography. Enhanced ionospheric tomography evaluations are possible through a combination of IOX data with ground-based observations of a dual-frequency beacon that is one of the other three experiments on PICOSat. Ground-based receiver chains will provide information on horizontal structures which can be combined with occultation measurements of vertical structure to provide a more complete picture of the local ionosphere than is possible with beacon measurements alone, as has been done on previous missions.

TOTAL ELECTRON CONTENT VARIABILITY AT SOUTHERN LATITUDES OVER BRAZIL USING GPS SIGNALS.

Mendes da Costa, A.*
Space Geophysics Division
National Institute for Space Research
Sao Jose dos Campos, SP 12901-970. Brazil
Fonseca Junior, E.S.
Geodetic and Topography Laboratory
Univ. of Sao Paulo
Sao Paulo, SP 05424-970, Brazil
Vilas Boas, J.W
Astrophysics Division
National Institute for Space Research
Sao Jose dos Campos, SP 12901-970, Brazil

Some specific characteristics of ionospheric total electron content (TEC) obtained through GPS propagation signals received in Presidente Prudente - Brazil (22 07S; 51 22W) from 1997 to 2001 are described. TEC daily hourly averages during four and a half consecutive years are analyzed and the diurnal, seasonal and solar activity variations are discussed. The effects of the South Atlantic Magnetic Anomaly (SAMA) in the ray-paths are discussed using TEC values measured at different GPS stations of the Brazilian GPS Continuous Monitoring Network. This is a geodetic reference network composed at present, by thirteen stations, two of them take part in the International GPS Service (IGS). All the data have been processed with the 4.2 version of the BERNESE software developed by the University of Bern (Switzerland). This software is specially addressed to the development of permanent networks, to a quick development of GPS small surveys in L1 and in L2, to the combination of different types of receivers and simulations. To study the ionosphere, two distinct models are used to describe the its deterministic component: a local model based in the bidimensional expansion of Taylors series and a global or regional model based in the spherics harmonics expansion. TEC measurements seem to show a high efficiency in detecting moderate to intense geomagnetic storms, as well as the ionization produced by specific meteor showers. The relative importance of the protonosphere contribution to the total ionization is also investigated. Finally, an attempt is made to study the latitudinal behavior of TEC over Brazil and the results are compared to TEC values measured at different southern longitudes.

UNDERSTANDING THE EFFECTS THE PLASMASPHERE HAS ON IONOSPHERIC STUDIES UNDERTAKEN WITH GPS TEC MEASUREMENTS

P.A. Webb*
NAS/NRC/Goddard Space Flight Center
Greenbelt, Maryland 20771, USA
E.A. Essex
Cooperative Research Centre for Satellite Systems
Department of Physics, La Trobe University
Bundoora, Victoria 3086, Australia

The plasmasphere is formed from the flow of topside ionospheric plasma up the Earth's closed magnetic field lines, which are located at low and mid geomagnetic latitudes. When studying the ionosphere using Total Electron Content (TEC) derived from Global Position System (GPS) signals, the overlying plasmasphere is often disregarded. For example, in ionospheric studies a mean ionospheric height around 400 km is used when converting slant TEC to vertical TEC, such as when using the single thin shell approximation to the ionosphere. The justification for this approach is that the electron densities in the plasmasphere are several orders of magnitude lower than in the ionosphere and will, therefore, make only a small contribution to the TEC. However, TEC measurements depend on the integral of the plasma density along the ray path between the GPS satellite and the GPS receiver. Because the GPS satellites orbit at an altitude of 20,200 km the plasmaspheric contribution to the TEC measurement can, at times, be of a similar magnitude to the ionospheric contribution. In this case the assumption of a mean ionospheric height of 400 km can be in error and, consequently, the resulting vertical TECs may be incorrect.

The Global Plasmasphere Ionosphere Density (GPID) model has been developed to model the global scale evolution of the electron densities in the plasmasphere. Combined with the most recent version of the International Reference Ionosphere (IRI2001), GPID can calculate the electron densities along any arbitrary ray path, from which the TEC can be determined. Using GPID it is possible to investigate the effects that the plasmasphere has on the calculation of TEC derived from GPS signals. This presentation will demonstrate several examples of these effects, and will show when excluding the plasmasphere from an analysis will most likely produce significant error. Further, GPID can be used to predict the TEC obtained from ionospheric occultations undertaken by GPS receivers on Low Earth Orbit (LEO) satellites. Examples of these occultations will be shown, as well as comparisons to direct TEC plasmaspheric observations also obtained from GPS-equipped LEO satellites.

MEASUREING IONOSPHERIC SCINTILLATION EFFECTS AND TEC USING GPS SIGNALS

A. J. Van Dierendonck
GPS Silicon Valley
Los Altos, CA 94024-4925

Over the last few years, GPS receivers have been used as a means for measuring ionospheric scintillation effects on a global basis. This was not widely possible during the last solar activity peak. Some of the GPS receivers have the capability to sample wide bandwidth signal phase and amplitude at relative high rates (50 Hz). The importance of the wide bandwidth is that scintillation parameters, such as spectral content, can be computed, not just the effects of the scintillation on GPS receiver performance.

The majority of the current wide bandwidth monitoring is being done using a commercial off-the-shelf NovAtel GPS receiver implemented with special software – the GSV4000 GPS Ionospheric Scintillation Monitor (GISM) and redecessor prototype units. Now, GPS Silicon Valley customers have fielded the new GSV4004 GPS Ionospheric Scintillation and TEC Monitor (GISTM) receiver. This receiver, a NovAtel EURO4 dual-frequency receiver with special firmware, comprises the major component of a GPS signal monitor, specifically configured to measure amplitude and phase scintillation from the L1 frequency GPS signals, and ionospheric TEC from the L1 and L2 frequency GPS signals. This scintillation and TEC monitoring receiver is housed in a NovAtel GPStation4E housing along with a low-phase noise oscillator, and provides true amplitude, single frequency carrier phase measurements and TEC measurements from up to 11 GPS satellites. It will also track one SBAS (WAAS, EGNOS or MSAS) satellite, providing L1 measurements and data, instead of the 12th GPS satellite. The unit comes with complete software that allows the automatic measurement and computation of all major scintillation parameters and TEC. A variety of antennae, with or without choke rings and cables, are available as options.

In this paper, the wide bandwidth monitoring capabilities of these receivers will be described and performance test results will be presented. This is followed by the presentation of data collection from a selection of recorded scintillation events.

EQUATORIAL SCINTILLATION CLIMATOLOGY: IMPLICATIONS FOR GPS NAVIGATION AND SATELLITE COMMUNICATIONS

K. M. Groves, S. Basu, J. M. Quinn, H. Kuenzler
Air Force Research Laboratory
Space Weather Center of Excellence
Hanscom AFB, MA, 01731, USA
W. J. McNeil, R. C. Caton
Radex, Inc., 3 Preston Ct., Bedford, MA, USA

The routine occurrence of equatorial post-sunset Spread F and radio wave scintillation is a well-known phenomenon. VHF and GPS scintillation observations over the past five years at a number of low-latitude stations permit us to quantify the spatial and temporal climatology of strong scintillations as well as to study their effect on GPS navigation and satellite communication systems. Observations in the VHF band have shown that the entire region encompassed within 15 to 20 degrees of the magnetic equator experiences severe scintillation activity caused by electron density irregularities associated with large-scale plasma bubbles. The occurrence frequency and intensity of this activity has a strong dependence on solar flux and consequently exhibits a dramatic solar cycle variation. For example, the occurrence frequency of strong VHF scintillation decreases by a factor of 2-3 as the solar cycle varies from maximum to minimum. At L-band frequencies the relative variation is even more severe as strong scintillation is essentially absent at solar minimum. Moreover, L-band scintillation shows a marked meridional dependence correlated with variations in electron density from the magnetic equator to the anomaly regions at approximately 15 degrees magnetic latitude. The results indicate that significant impacts on GPS navigation may be limited to anomaly regions around the solar maximum period. It is also shown that the offset between the geographic and geomagnetic equators combined with the GPS constellation geometry render certain longitude sectors more vulnerable to impacts on GPS positioning accuracy. VHF satellite communications systems may be impacted throughout the solar cycle and across the entire equatorial belt. When scintillation activity is characterized by the S4 parameter (the normalized standard deviation of the signal intensity) alone, VHF scintillations appears to show little meridional variation within the equatorial region. However, when additional parameters of the signal fluctuations, such as the intensity decorrelation time, are examined, the nature of VHF scintillations is found to exhibit significant differences with latitude. Specifically, fluctuations near the anomaly are found to have much shorter decorrelation times, and presumably reduced coherent bandwidths, than occur at the magnetic equator. These results may impact the design of future communication systems that seek to mitigate scintillation effects through frequency or time diversity strategies.

GPS PROXY MODEL FOR REAL-TIME UHF SATCOM SCINTILLATION MAPS FROM THE SCINTILLATION NETWORK DECISION AID (SCINDA)

R.G. Caton*, W.J. McNeil
Radex, Inc.
3 Preston Ct.
Bedford, MA 01730
K.M. Groves, S. Basu
Air Force Research Laboratory
Hanscom AFB, MA 01731

In order to increase the region of coverage and provide a more reliable situational awareness of scintillation impacts on users of space-based communication/navigation systems, L-Band scintillation measurements from GPS satellites are ingested, in real-time, to the Scintillation Network Decision Aid (SCINDA) model.

SCINDA is a real-time, data driven communication outage forecast and alert system developed by Air Force Research Laboratory, at Hanscom AFB and made operational through a joint effort between the US Air Force and US Navy. UHF and L-Band scintillation parameters are measured, modeled, and propagated in time to provide a regional specification of the scintillation environment in an effort to mitigate the impacts on the satellite communication (SATCOM) community.

In previous implementations of the SCINDA model, while data collected on links to various geosynchronous satellites were used to produce a graphical representation of the "plume" structures responsible for the observed scintillation, GPS scintillation data were limited to being displayed as spheres at the 300 Km ionospheric penetration point and colored to indicate the level activity on a given link at a given time. With their three-dimensional representation, the modeled "plumes", based on the geosynchronous data, could then be mapped to the ground from the location of a selected satellite location producing a "Scintillation Specification Map" detailing "outage" regions on the globe. In an effort to provide UHF SATCOM users with a more consistent estimation of scintillation impacts on their systems, GPS sensors, measuring S4 at L-Band frequency are now used as a supplement to the stationary UHF links dramatically increasing the region coverage at each individual station, particularly those located outside the anomaly crest regions.

In this talk, we will present results from our validation effort of the GPS proxy model and demonstrate its usefulness as an adjunct to the SCINDA model in producing nowcast and forecast UHF scintillation products that are useful in providing the most accurate specifications available.

REGIONAL GPS MAPPING OF STORM ENHANCED DENSITY

Anthea J. Coster
M.I.T. Lincoln Laboratory, Millstone Hill Radar
244 Wood Street, Lexington, MA 02420-9108
John C. Foster, P.J. Erickson
M.I.T. Haystack Observatory
Off Route 40, Westford, MA 01886
F. J. Rich
Air Force Research Laboratory
Hanscom Air Force Base, Lexington, MA

During geomagnetic disturbances, intense storm-time electric fields of magnetospheric origin extend across mid-latitudes and redistribute the ionospheric plasma through advection across both latitude and local time. Strong increases and sharp spatial gradients in total electron content (TEC) characterize the ionospheric storm response, and these features can significantly impact Global Positioning System (GPS) performance. Sharp gradients in TEC are also difficult to model, and their presence can degrade radar metric accuracy in satellite tracking. TEC measurements from GPS receivers scattered throughout the eastern and southeastern parts of the U.S., including a few located in the Caribbean, are used to monitor the ionospheric response to several geomagnetic storms. A time history of TEC perturbations in two dimensions has been constructed using the GPS data. The data typically show plasma advection from the lower latitudes bringing in storm-enhanced density (SED) [Foster, J. Geophys. Res., 98, 1675-1689, 1993] with total electron content (TEC) 100 TEC units coming into the region immediately equatorward of the trough. This plasma is transported to higher latitudes and to earlier local times - approaching the noon meridian. Additional maps of the storm-induced ionospheric perturbations observed with the Millstone Hill incoherent scatter radar, spanning the mid-latitude ionosphere between 35 and 65 invariant latitude, further support the GPS observations. In-situ DMSP satellite observations of electric fields and particle precipitation are used to study the structure and dynamics of solar-induced geomagnetic storms. This paper specifically analyzes the TEC enhancements from both major (Kp values greater than 7) and minor geomagnetic storms (Kp values greater than 4). These storms are compared in terms of impact and strength of the storm enhanced density observed.

This work is sponsored by the Air Force under Air Force Contract AF19628-00-C-0002 Opinions, interpretations, conclusions, and recommendations are those of the author and are not necessarily endorsed by the United States Air Force.

Session G4, 13:35-Sat.

IONOSPHERE GENERAL TOPICS

Chairperson: B. Wright

EFFECTS OF HF HEATER-PRODUCED IONOSPHERIC STRUCTURES ON THE DUCTING OF VLF TRANSMISSIONS

M.J. Starks*
Space Vehicles Directorate
Air Force Research Laboratory
Hanscom AFB, MA 01731

Comprehensive three-dimensional ray tracing studies show that local ionospheric density perturbations caused by the HF heater at Arecibo can significantly affect the amount of power from up-going 28.5 kHz VLF transmissions that is coupled into plasmaspheric ducts on nearby magnetic field lines. The formation of large density depletions perturbs the ray paths of up-going VLF and may enhance or reduce the total amount of power in a local duct by up to 18 dB. Small perturbations at ionospheric heights are magnified as rays propagate toward plasmaspheric ducts, thereby altering the L-shell distribution of ducted power. The effect is highly dependent on duct location, and altitude variations in the duct entrances of as little as 40 km may determine whether ducted power is enhanced or reduced.

This effect has immediate consequences for experimental efforts. The natural cross-L drift of plasmaspheric ducts has been measured at tens of m/s, and a duct may drift in altitude by tens of km in less than one hour. This motion can slowly move a duct from a region of enhanced power flux to one of reduced flux. The effects on the power distribution are also highly dependent on the extent of the density depletion created by the heater. This in turn is partially controlled by the drift of ionospheric plasma over the heater beam. The complex interplay of these factors may therefore explain the difficulty in obtaining consistent experimental observations of heater-enhanced or heater-suppressed local VLF ducting from day to day, or even from hour to hour.

The ray tracing studies also show that meridional irregularity sheets produced by the HF heater affect ducted power to a lesser extent by guiding upgoing VLF rays in the ionosphere and subsequently randomizing their group velocity vectors.

The enhancement of available VLF energy in the lower ionosphere due to scattering from heater-produced bottom-side irregularities strongly affects the magnitudes of both mechanisms.

USING TOMOGRAPHY RECEIVERS FOR SCINTILLATION IN GREENLAND

C. Coker, G.S. Bust, T.L. Gaussiran II
Center for Ionospheric Research
Applied Research Laboratories
University of Texas at Austin
Austin, TX 78713-8029 USA

The capabilities and results of using the Coherent Ionospheric Doppler Receiver (CIDR) for observing ionospheric scintillation are presented. Measurement capabilities of the receiver were verified on the bench in Austin, Texas, by simulating phase scintillation. Specifically, the Doppler and phase error measurements from 150 and 400 MHz signals are examined. Data from a chain of CIDR tomography receivers along the West Coast of Greenland are examined, with emphasis placed on the January 2001 scintillation campaign time frame and other selected dates. The utility of phase scintillation measurements from individual and differential frequencies is examined. Periods of increased scintillation activity were observed during periods of increased magnetic activity.

As the low-earth orbiting satellites pass over an individual station, small scale spatial structures can be observed in the F-region over a large geographic region ($\sim$15 degrees of latitude). From Sondrestrom during magnetically quiet periods, the field of view includes the auroral zone as well as portions of the polar cap and mid latitude ionosphere. During disturbed periods the oval expands towards the equator, so that the field of view is primarily in the polar cap with the auroral zone to the south. Scintillation was observed in the polar cap and auroral zone from Sondrestrom. The chain of receivers in Greenland provides for multiple look-angles through the same (or nearly the same) ionospheric structure generating the scintillation, allowing for studies of isotropy. The chain also expands the coverage area, providing for studies of the spatial distribution of scintillation, in the polar cap under disturbed conditions.

QUANTIFYING SPREAD F BY DIGITAL IONOSONDES

J.W. Wright, NGDC, NOAA and CIRES, Boulder CO, USA
N.A. Zabotin, Rostov State Univ., Rostov on Don, Russia

The width of frequency-spreading (df/f) on ionograms has been shown (by comparison with OGO-6 Satellite observations) to be proportional to dN/N near the F-region peak. Thus even classical analog ionograms using logarithmic frequency scales were direct-reading for this important parameter.

Despite the common term "frequency spreading", Spread F is always and fundamentally range spreading: the phenomenon occurs when multiple scattering, aided by refraction, produces a multiplicity of echoes (or "glints") along the range axis. What distinguishes classical "frequency spreading" from classical "range spreading" is the extent of frequency- (and temporal-) correlation within this fundamental range spreading. When spread-echo range is highly correlated over a broad frequency bandwidth, the result is commonly called "range spreading"; conversely, narrow correlation bandwidths in frequency lead to the common term "frequency spreading". This perspective permits a digital ionosonde to recognize spread echo automatically, and, if wanted, in real time. We quantify Spread F (more generally, "spread echo") by two simple steps:

(a) Construct a count of closely-spaced echoes resulting from individual pulses (or "pulsets", by the dynasonde) in bins of constant width in d(log(f)) disposed near the classical penetration frequencies foE, foF2, fxF2, etc.;

(b) Compute the weighted mean and weighted variance of d(log(f)), using the bin counts as weights. Twice the resulting variance is an estimate of the standard deviation, 2delta(log(f)) 2df/f dN/N. The weighted means convert to mean plasma frequencies (e.g., 'sfoF2', sfoE, the 's' signifying "spread") and are arguably a better representation of the layer peak plasma frequencies than the conventional parameters (e.g. foF2, foE) in spread echo conditions.

Data sequences from three Dynasonde installations illustrate application of automated spread echo quantification in the auroral, mid-latitude and equatorial ionospheres. The existence of "Spread E" is itself a new and potentially important feature, not previously discussed in ionogram literature. The equatorial case receives special consideration because some implicit assumptions of the method may not apply there.

Spread F quantification joins a suite of diagnostic methods by which the digital ionosonde can monitor irregularity parameters over scales ranging from 10's of meters to thousands of kilometers, and intensities dN/N from 0.1 to 100 percent. We compare, in particular, our spread F results with those of the "Phase Structure Function" of another paper presented here.

DYNAMICS OF IONOSPHERIC IRREGULARITY SPECTRA FROM DYNASONDE ECHO STRUCTURE FUNCTIONS

N.A. Zabotin
Rostov State Univ.
Rostov on Don, Russia
J.W. Wright
NGDC, NOAA and CIRES
Boulder CO, USA

In modern HF pulse sounding using research ionosondes the phase and amplitude of each echo are measured precisely and frequently; the 'same echo' can be identified from one time to the next. Thus, such values form continuous temporal series permitting comprehensive statistical processing. The most informative tool for these analyses is the Structure Function (SF), which is defined as the square of the difference of a random function, averaged over all pairs of points a certain distance (or 'lag', τ) apart. It can be used to express both temporal echo parameter variations and spatial ionospheric electron density irregularities.

A theoretical relation between structure functions of phase variations and small-scale ionospheric irregularities has been obtained for a model of frozen irregularities moving with a drift velocity, on the assumption that the irregularity spectrum is described by a power law. A remarkable property of the SF behavior in the small-lag regime is its log-log-linear character: it is well approximated by a linear dependence, $\log(\mathrm{SF}) = SIA + SIB \log(\tau)$. Structure indices *SIA* and *SIB* are related by the theory to the irregularity spectrum parameters. Dynasonde B-mode allows us to define a rudimentary structure function (RSF), containing only a few initial lags, but these are sufficient to determine *SIA* and *SIB*. Thus standard dynasonde ionograms, rather than dedicated time-series, become a practical resource for irregularity diagnostics. Details of this method are presented in *Radio Science*, **36**, 757, 2001.

In the present paper we apply this approach to dynasonde data obtained in three main latitudinal regions, at Huancayo (equatorial CONDOR campaign of 1983), at Bear Lake Utah (mid-latitude), and at Tromso (EISCAT auroral-latitude observatory). The method reveals basic characteristics of these geophysical regions. By obtaining physical properties of small-scale ionospheric irregularities we may follow the dynamics of the irregularity spatial spectrum. We expand this approach by investigation of echo amplitudes, and discover the same log-log-linear behavior of the amplitude SF with strong diurnal variations of corresponding structure indices. The diagnostic consequences of this effect are to be considered.

INFLUENCE OF MAGNETIC DECLINATION ON THE LOW LATITUDE IONOSPHERE: DIGISONDE STUDIES AT FORTALEZA, SAO LUIS AND JICAMARCA FOR A MAGNETICALLY DISTURBED PERIOD

F. Bertoni*, CNPq (Brazil) funded doctoral student at UML
(1)Instituto Nacional de Pesquisas Espaciais, S.J. Campos, Brazil
B. Reinisch
(2)Center for Atmospheric Research, University of Massachusetts Lowell
I. Batista, M. Abdu
(1)Instituto Nacional de Pesquisas Espaciais, S.J. Campos, Brazil

Digital ionosondes are providing a large amount of data all over the world. Many stations around the globe use the Digisonde DPS-4 (Reinisch et al., Radio Sci., 32, 4, pp. 1681-1694, 1997) or the DGS256 since they are versatile systems that offer the possibility of auto-scaling ionogram data in real time. Ionospheric drift analysis software for post-processing software is also available (Scali et al. Radio Sci., 30, 5, pp. 1481-1498, 1995).

In February 2001, a new DPS started operation in Fortaleza (3.8°S, 38°W), Brazil; Fortaleza is ~10°south of the magnetic equator. In June of the same year, the DPS in Jicamarca (12°S, 77°W), Peru, resumed operation, and since September 1994 there is a DGS256 operating at Sao Luis (2.3°S, 44°W), Brazil. The magnetic declinations are very different, resulting in interesting ionospheric behavior at these stations. In Fortaleza and Sao Luis the declination is about 20°W and in Jicamarca, 2°E. Batista et al. (J. Geophys. Res., 91, A11, 12,055-12,064, 1986) studied the differences between the magnetic characteristics at Fortaleza and Huancayo, Peru. The authors pointed out the influence of magnetic declination on the F-layer. They used the Δ h′ F/Δ t method (Abdu et al., J. Geophys. Res., 86, pp. 11,443-11,446, 1981) in order to determine the vertical drift at nighttime.

It is well known that magnetic storms can inhibit or stimulate the occurrence of equatorial spread-F. The inhibition or stimulation can be caused by different mechanisms. Electric fields, mapped from high to low latitudes, can influence the F-Layer dynamo electric fields and, consequently, the $\mathbf{E}\times\mathbf{B}$ vertical drift. This affects the pre-reversal peak height behavior. This paper analyzes ionogram and drift data obtained with these Digisondes during a magnetically disturbed day on 17 August 2001.

REFLECTION HEIGHTS OF LF RADIO WAVES IN THE IONOSPHERIC D-REGION

R. Michael Jones
CIRES
University of Colorado
Boulder, CO 80309-0216, USA

In using radio wave reflection coefficients measured at various frequencies f and angles of incidence i_0 to estimate ionospheric profiles, it helps to arrange those measurements according to their relative reflection heights. (See NOAA Tech. Memo. ERL WPL-29, 1977, PB2763878, and the errata at http://cires.colorado.edu/people/jones.mike/pubs/errata4.htm.) We use the notation here that $X = f_N^2/f^2 = r_0 c^2 N/(\pi f^2)$ is the normalized electron density, $Y = f_H/f$ is the normalized gyrofrequency, and $Z = \nu/\omega$ is the normalized collision frequency, where f_N is the plasma frequency, r_0 is the classical electron radius, c is the free-space speed of light, and $\omega = 2\pi f$. At LF and VLF (3-300 kHz), the approximation $Y \gg 1$ is always valid.

Whenever the radio waves reflect below the height h_1 (65-70 km in mid-latitudes) where the collision frequency equals the gyro frequency (i.e., where $Z = Y$), then we can neglect the effect of the Earth's magnetic field on the propagation. In that case, the reflection height is that height where $X = Z\cos^2 i_0$. This is the height where $2r_0 c^2 N/\nu = f\cos^2 i_0$, showing that reflection height increases with $f\cos^2 i_0$ for that case. This case occurs only during the daytime, when the electron density is large enough.

When $f\cos^2 i_0$ is larger than $2r_0 c^2 N(h_1)/\nu(h_1)$, the wave will reflect above the height h_1, so that the effect of the Earth's magnetic field must be taken into account. For frequencies less than the collision frequency (i.e., $Z > 1$), only the extraordinary wave has a significant reflection coefficient, and reflection occurs at the height where $X = Y(1 - \sin^2 i_0 \cos^2\psi)^{1/2}\cos i_0$, where ψ is the angle of the wave with the magnetic meridian. This is the height where $r_0 c^2 N/(\pi f_H) = f(1 - \sin^2 i_0 \cos^2\psi)^{1/2}\cos i_0$, showing that reflection height increases with $f(1-\sin^2 i_0 \cos^2\psi)^{1/2}\cos i_0$. This corresponds to $f\cos^2 i_0$ for propagation in the magnetic meridian (North-South), and to $f\cos i_0$ for propagation normal to the magnetic meridian (East-West).

For frequencies greater than the collision frequency (i.e., $Z < 1$), only partial reflection of the ordinary wave occurs at LF, and then only for nighttime profiles. The height of the partial reflection is the height where $X = \cos^2 i_0/(1-\sin^2 i_0 \cos^2\psi)$. This is the height where $f_N = (r_0 c^2 N/\pi)^{1/2} = f\cos i_0(1 - \sin^2 i_0 \cos^2\psi)^{-1/2}$.

D-REGION ELECTRON-DENSITY PROFILES FROM LF REFLECTION-COEFFICIENT MEASUREMENTS

R. Michael Jones
CIRES
University of Colorado
Boulder, CO 80309-0216

For radio waves that reflect below the height where the collision frequency equals the gyrofrequency (about 65 km in midlatitudes), the effect of the Earth's magnetic field can be neglected, and the reflection coefficient depends on the conductivity profile $f_r(h) \equiv 2\pi f_N^2(h)/\nu(h) = 2r_0c^2N(h)/\nu(h)$, where c is the free-space speed of light and r_0 is the classical electron radius. A phase integral calculation (which is very accurate for horizontal polarization, but only approximate for vertical polarization) shows that the log of the reflection coefficient times the cosine of the angle of incidence is a function of the wave frequency times the square of the cosine of the angle of incidence.

$$\ln R\cos i_0 = -2i\omega\cos^2 i_0/c\int_0^{h_r}[1 - iX/(Z\cos^2 i_0)]^{1/2}dh + .5i\pi\cos i_0,$$

where $\omega = 2\pi f$ is the wave frequency. For a monotonic $N(h)/\nu(h)$ profile,

$$\ln R\cos i_0 = -4\pi iF/c\int_0^{-iF}(1 - if_r/F)^{1/2}(dh/df_r)df_r + .5i\pi\cos i_0,$$

where $F = f\cos^2 i_0$, and $f_r(h)$ or $h(f_r)$ gives the monotonic profile. For a smooth profile, the real part can be approximated by a real integral to give

$$\ln|R|\cos i_0 \approx -\frac{\pi^2}{c}\int_0^{f\cos^2 i_0}(1 - \frac{f_r}{f\cos^2 i_0})^{-1/2}(dh/df_r)f_r df_r.$$

This is an Abel integral, which can be inverted to give

$$h = -\frac{c}{\pi^3}\int^{2r_0c^2N/\nu}\frac{1}{y^2}\int_0^y\left(\frac{F}{y-F}\right)^{1/2}\frac{d(\log|R|\cos i_0)}{dF}dFdy,$$

which gives the shape of the profile, but not it's vertical displacement. For $f\cos^2 i_0 < 2r_0c^2N(h_1)/\omega_H$, we can neglect the effect of the Earth's magnetic field, where h_1 is the height where the collision frequency ν equals the gyrofrequency ω_H. For $f\cos^2 i_0$ greater than that, the propagation is more complicated. Calculated and measured reflection coefficients show that the transition can be easily recognized (NOAA Tech. Memo. ERL WPL-29, 1977. PB2763878. errata at http://cires.colorado.edu/people/jones.mike/pubs/errata4.htm). These formulas are very accurate for horizontal polarization. They are approximate for vertical polarization.

LOW-LATITUDE NIGHTTIME ELECTRON DENSITY DISTRIBUTION FROM ULTRAVIOLET LIMB OBSERVATIONS

Thonnard, S.E., McDonald, S.E., Dymond, K.F., Budzien, S.A., McCoy, R.P.
Space Science Division
Naval Research Lab
Washington, DC 20375, USA

At night, the distribution of the O I 1356-Angstrom emission can be used to infer variations in the electron density in the upper atmosphere. Using a limb-scanning remote sensing technique, observations of this major nightglow emission can be used to determine the vertical electron density distribution. At low latitudes, the dominant variation in the 1356-Angstrom nightglow is due to the equatorial anomaly. These arc shape structures follow the magnetic dip equator and vary in intensity, height, and spatial separation.

In February 1999, the Air Force Space Test Program launched the Advanced Research and Global Observation Satellite (ARGOS) in an 830km altitude, near-polar sun-synchronous orbit with a 2:30pm ascending node local time. The ARGOS satellite contains several instruments that monitor the upper atmosphere of the Earth. One instrument, the Low Resolution Airglow and Aurora Spectrograph (LORAAS) is a prototype of a series of sensors that will be flown by the Defense Meteorological Satellite Program (DMSP) over the next decade. The LORAAS instrument has collected numerous spectra of Earth's airglow in the extreme ultraviolet and far ultraviolet regimes (800 - 1700 Angstroms). Limb scans, atmospheric radiance profiles, in the satellite's orbital plane are collected every ninety seconds. The intensity profiles associated with the equatorial anomaly were measured by LORAAS and interpreted using analysis techniques developed for the DMSP. Additionally, a pseudo-tomographic technique was used to invert series of intensity profiles to specify the vertical and latitudinal electron density distribution about the anomaly region.

These analysis techniques have been applied to an entire month, October 2000, of LORAAS observations to determine the variability of the tropical arcs. The analysis results yield altitude verses latitude cross-sections of the nighttime ionosphere. From these ionospheric cross-sections, the separation and relative electron density distribution of the northern and southern anomaly crests were obtained. More than 85

REAL TIME SOLAR RADIO BACKGROUND/BURST EFFECTS (SORBE) PRODUCT UNDER DEVELOPMENT

S. Quigley*
Air Force Research Laboratory
AFRL/VSBX c/o SMC Det 11/CIT
Peterson AFB, CO 80914-2902

The Air Force Research Laboratory (AFRL) and Detachment 11 of the Space Missile Systems Center (SMC) have combined efforts to design, develop, test, and implement new graphical products for Air Force space weather operations. The newest product under development addresses the effect of background and event-level solar radio output on operational DoD systems. Strong bursts of radio wave emissions given off by the sun during solar events can detrimentally affect radar and satellite communication systems that have operational receiving geometries within the field of view of the sun. For some systems, even the background radiation from the sun can produce effects. The radio frequency interference (RFI) of interest occurs on VHF, UHF, and SHF frequency bands, usually lasting several minutes during a solar flare. While such effects are limited in time and area (typically a few degrees in viewing angle), they can be quite severe in magnitude. The result can be significant lack in a radar systems ability to detect and/or track an object, and loss of a communication systems ability to receive satellite signals. Such negative effects on key systems has resulted in a requirement for an operational product that details the problem in real-time. To develop the product, several factors must be taken into account. The operating parameters of the observing solar radio telescopes (RSTN and SRBL systems for the USAF) must be known these include observed frequencies, sensitivities, and interpolation curves. In addition, some operating parameters of the affected radar and satellite communications systems must be known these include specific systems threshold levels, bandwidth and range responses, and side-lobe specifications. A brief statistical and anecdotal history of solar radio burst events is presented, along with an overview of the current operational product under development at the joint SMC-AFRL Rapid Prototyping Center.

CHARGED AEROSOL COLLECTION INSIDE PMSE'S BY A MAGNETICALLY SHIELDED ROCKET PROBE

B. Smiley, M. Horanyi, S. Robertson
Dept. of Physics
University of Colorado at Boulder
Boulder, CO 80309, US

A charged aerosol detector was flown during the MIDAS/SOLSTICE rocket campaign in June 2001 over Andoya, Norway. The probe is a graphite collection surface with a permanent magnet underneath to deflect electrons and light ions. This probe was first used on a sounding rocket over White Sands, NM in 1998, where it measured a thin positively charged layer 500 m thick at an altitude of 86.5 km, followed by a broad negatively charged layer which extended a few kilometers lower [Geophys. Res. Lett. 27, 3825 (2000)]. The flights aboard the two MIDAS payloads were the second use of the probes.

The first MIDAS launch was into a triple layered PMSE that extended from 82 to 90 km. On both upleg and downleg, the detector saw finely detailed positive charge structures within the PMSE. These uniquely shaped layers were completely correlated with simultaneously collected positive ion data. On downleg, the probe measured a thin burst of negatively charged particles at 83 km.

The second MIDAS flight was fired into a very strong single-layered PMSE. On downleg, thin bursts of negative charge were seen from 87 km to 83 km. Also, a single thick layer of negative charge was measured at 82 km. This layer had a very sharp upper boundary and extended downward over the next km.

During both flights the probe also measured a smooth, positively charged background which was well correlated with the positive ion probe. Also seen was a photoelectron signal due to solar UV. Cloud cover prevented lidar support for either launch. This work was funded by NASA.

Session G/H1, 8:55-Wed.

METEOR PHYSICS

Chairperson: J. Mathews

METEOR HEAD ECHO MEASUREMENTS WITH THE SONDRESTROM RADAR

C.J. Heinselman, J. Jørgensen
Center for Geospace Studies
SRI International
333 Ravenswood Ave.
Menlo Park, CA 94025

The Sondrestrom Incoherent Scatter Radar (ISR) routinely measures the natural high-latitude ionosphere. In addition to solar UV produced ionization, it regularly measures the influence of auroral precipitation on the ionospheric electron density profiles as well as the formation and dynamics of sporadic layers of metal ions in the E region. The material supporting these sporadic E layers comes from metal atoms released during meteoroid ablation. Especially at high latitudes, metal ions undergo significant transport as they are driven by the large magnetospherically generated electric fields. Previous high- latitude sporadic E studies have concentrated on this electric field driver but they have been only partly successful in describing the observed characteristics of the layers. A full description of the metal atom evolution must consider both the distribution of the source of the material and this transport.

Recent software upgrades to the data acquisition system of the Sondrestrom ISR allow the recording of unprocessed samples from individual radar pulses. This capability has been used to support several measurement campaigns directed toward meteor head echo detection and characterization. The system's nominal operating frequency is 1.29 GHz - significantly higher than that used in the bulk of previously reported measurements. It also operates in a high latitude environment, which affects the properties of the upper atmospheric environment into which the meteoroids ablate.

Initial analysis of a subset of the measurements shows, among other things, a relatively broad distribution of meteoroid velocities. Measurements have now been made from several different meteor showers. The characteristics of the meteor head echoes from these showers will be compared. Data will also be presented from non-shower periods and the characteristics contrasted with those from shower periods.

SCATTERING CHARACTERISTICS OF METEOR HEAD ECHOES COLLECTED USING ALTAIR

S. Close*, S. Hunt, A. Coster
MIT Lincoln Laboratory
Lexington, MA
M. Oppenheim, L. Dyrud
Boston University, Center for Space Physics
Boston, MA

Meteor data were collected using radar and optical sensors at the Kwajalein Missile Range (KMR) during the peak of the Leonid 1998 storm. These data contain the only simultaneous observations of meteors using seven frequencies (VHF, UHF, L-, S-, C-, Ka- and W-band) as well as optics. The primary sensor was the ARPA Long-Range Tracking and Instrumentation Radar (ALTAIR), due to its VHF and UHF operating frequencies. ALTAIR is highly calibrated and has interferometry (angle) and polarization capabilities, which gives the true position and shape of the meteor. During the peak of the 1998 storm, ALTAIR detected approximately one head echo every two seconds, as well as numerous specular and non-specular ionization trails. This paper contains analysis of the scattering characteristics of the VHF and UHF head echoes and supports the theory that the head echo scattering mechanism is consistent with an overdense object. First, we present results that indicate that most head echoes have trajectories that are inconsistent with current "down-the-beam" theories and vary between 0 and 80 degrees from ALTAIR boresight. Next we examined the normalized polarization ratios of the head echoes by utilizing both the LC and RC returned signal at VHF and UHF. These data show a mean distribution that is consistent with a sphere-like return that is dependent upon maximum RCS but independent of aspect angle or altitude. An in-depth examination of the RCS data revealed that the RCS scales with the velocity and altitude. The RCS dependence on wavelength was determined, as well as an upper RCS cutoff that scales with the mean free path to wavelength ratio. Finally, we present the first three-frequency detection (VHF, UHF and L-band) of a head echo/non-specular trail pair.

Prepared for the Department of the Army under Air Force Contract F19628-00-C-0002. Opinions, interpretations, conclusions, and recommendations are those of the authors and are not necessarily endorsed by the United States Air Force or Army

METEOR VELOCITY DETERMINATION USING THE ADVANCED RESEARCH PROJECT AGENCY LONG RANGE TRACKING AND INSTRUMENTATION RADAR

Hunt, S.M.,Close, S.
MIT Lincoln Laboratory
Brown, P.
University of Western Ontario
Oppenheim, M., Dyrud, L.,
Boston University

Abstract. During 1998-1999, the Leonid and Perseid meteor shower activity was observed using radar and optical sensors at the Kwajalein Missile Range (KMR). Due to its large aperature, high-power and simultaneous operating frequencies (UHF-160 MHz, VHF-422 MHz), the ARPA Long-Range Tracking and Instrumentation Radar (ALTAIR) is the KMR sensor best suited for detecting micro-meteors. ALTAIR transmits right-circular (RC) polarized energy and measures left-circular (LC) sum, RC sum, LC azimuth angle difference, and LC elevation angle difference receiver signal response. Meteor head echo detection rates as great as one per second were recorded and equate to a minimum detectable visual magnitude of +11 [Brown, 2001]. While collecting the meteor data using ALTAIR required no radar system modification, the task of reducing and calibrating the recorded data to support the analysis of meteor parameters is newly developed. This paper provides an overview of the techniques used to determine the meteor head echo position and velocity using ALTAIR data. The relative number of meteors encountering the atmosphere at UHF and VHF as a function of range rate and true velocity are presented. The ALTAIR head echo number distributions are corrected for the radar's tendency to detect faster-moving meteors (radar head echo ionization) and are normalized to ALTAIR's minimum detectable mass. These data present the corrected observational head echo velocity results and provide atmospheric velocity distributions for meteoroids at a constant mass limit.

Prepared for the Department of Army under Air Force Contract F19628-00-C-0002. Opinions, interpretations, conclusions, and recommendations are those of the authors and are not necessarily endorsed by the United States Department of Defense.

THE LINEAR PLASMA THEORY OF METEOR TRAILS AND IMPLICATIONS FOR RADAR MEASUREMENTS

M. Oppenheim*, L. Dyrud
Center for Space Physics
Boston University
725 Comm. Ave., Boston MA 02215
S. Close, S. Hunt
MIT Lincoln Labs and
Center for Space Physics

Radars probing the atmosphere between 75 and 130 km frequently receive echoes from plasma trails left by ablating micron-sized meteors. These echoes have proven useful in characterizing meteors and in estimating wind velocities and temperatures. Two distinct types of radar echoes return from meteor trails. First, strong "specular" echoes occur when the radar pointing direction lies perpendicular to the meteoroid's trajectory. Second, weaker "non-specular" echoes are measured by large-aperture radars when not pointing perpendicular to the trail's orientation.

In two earlier papers[a], we used simulations to show that non-specular echoes can easily result from the gradient–drift/Farley–Buneman (GDFB) instability which rapidly develops into plasma turbulence. We also discussed the mechanism whereby this instability causes rapid anomalous diffusion.

This paper further develops the plasma physics of meteor trail irregularities and compares the results with simulations and observational data. This study helps us use radar data to better understand the composition of meteor trails and their interactions with the surrounding atmosphere. In particular, we can evaluate: (1) the criterion for the onset of the instability as a function of altitude, atmospheric temperature, and meteor trail composition and density; (2) the nature of the instability and the resulting waves; (3) the range of unstable wavelengths both perpendicular and oblique to the geomagnetic field; and (4) the growth rates at each wavelength. This analysis should enable us to better use meteor radar data to characterize meteors and the upper atmosphere.

[a]M. Oppenheim, A. vom Endt and L. Dyrud, Electrodynamics of meteor trail evolution in the equatorial E-region ionosphere, GRL, 2000, 3173 and
L. Dyrud and M. Oppenheim and A. vom Endt, The anomalous diffusion of meteor trails, GRL, 2002, 2775

RADIO SCIENCE ISSUES SURROUNDING HF/VHF/UHF RADAR METEOR STUDIES

J. D. Mathews
Communications Space Sciences Laboratory
Penn State University
University Park, PA 16802-2707

Classical meteor radars depend on coherent (Fresnel) scattering from a meteor trail oriented perpendicular to the radar wave-vector at closest approach to the radar. Meteor trails viewed in this manner are described as classical radar meteors with under/over-dense trails. While meteor head-echoes are rarely seen with classical low-power, wide-beam meteor radars, they are essentially always seen by large aperture (narrow-beam), high-power VHF/UHF radars. We discuss the expected radar scattering cross-sections (RCSs) of head- versus trail-echoes and how equilibrium concepts such as plasma frequency are of limited use in describing the results. Particular attention is given to the frequency dependence of the RCS and how the frequency dependence may yield considerable new information regarding the plasma distribution in the coma surrounding the meteoroid. As the head-echo is directly associated with the meteoroid, instantaneous (single-pulse) Doppler observations are possible. In the case of classical trail-echoes, the time evolution of the RCS as a function of frequency may provide new information on the plasma diffusion rate and thus on atmospheric density and temperature. Information from the time evolution of the trail must however be considered in light of new results showing that the trail rapidly B-field-aligns in a manner apparently driven by plasma instabilities that develop in 10-100 msec after trail deposition. It is in the context of instability-driven B-field alignment of the trails that we discuss anomalous trail-echoes. The anomalous trail-echo is a range-spread, chaotic (non-classical) trail-echo derived from a meteor that travels at an arbitrary angle relative to the radar wave-vector. We present theoretical simulations illustrating these concepts.

MEASURING ALTITUDE PROFILES OF DIFFUSION FROM NON-SPECULAR METEOR TRAILS

Dyrud, L.P., Oppenheim, M.M. , Close S., Hunt, S.
Center for Space Physics
Boston University

Recent observations demonstrate that sensitive radars, such as Altair, Arecibo, EISCAT, Jicamarca and MU, are capable of detecting a 'new' type of meteor trail. These large aperture radars detect plasma generated from direct meteor entry (head echos) which are often followed by non-specular trail reflections over an extended range. We demonstrate a technique that uses non-specular meteor trail observations to obtain instantaneous altitudinal profiles of diffusion rate.

The exponential decay of traditional, specular meteor trails has, for decades, been used to characterize the the diffusion rate of the meteor trails based on the following power relationship, $P(t) = P(0)exp\frac{32\pi^2 Dt}{\lambda^2}$. Measurements of diffusion are then used to derive neutral mesosphere temperatures. However, trail reflections from a specular trail yield a diffusion coefficient for a single altitude, or depending on trail orientation, return the diffusion averaged over the altitude spanned by the trail and beam intersection. Since individual non-specular trails are observed over 2-8 km range, they have the potential to yield diffusion rates over their entire observation range not just one altitude.

We demonstrate a technique for measuring diffusion profiles from non-specular trail observations, and discuss the advantages and caveats for this technique. Finally, we apply our findings to the issue of anomalous trail diffusion perpendicular to $\vec{B}$ [*Dyrud* et al., *Geophys. Res. Lett.*, **31** ,2775, 2001]. This technique is ideally suited for studying geomagnetic influence on trail diffusion, because high power radars include interferometry information from the head echo, yielding trail orientation to $\vec{B}$ within a few degrees. With this technique we can more accurately access any effect of inhibited cross-field diffusion. The initial cases studied from the ALTAIR radar data show that the meteor trail diffusion rate vs altitude is better represented by a uniform diffusion rate than a rate inhibited by slow cross field diffusion.

ELECTRON BEAMS FROM SPACE: ANOTHER KIND OF METEOR

Raymond A. Greenwald
Johns Hopkins University
Applied Physics Laboratory
Jan J. Sojka
Center for Atmospheric and Space Sciences
Utah State University
Joe E. Borovsky
Los Alamos National Laboratory

In many instances, we are interested in relating phenomena observed in the Earth's magnetosphere with those observed in the conjugate ionosphere. Unfortunately, we have no way of doing this with any degree of precision. As a consequence, there has been an endless series of arguments on the connectivitiy of ionospheric phenomena with processes observed in the magnetosphere and our scientific understanding of magnetosphere-ionosphere coupling has been limited. In this paper, we consider a new method for finding and tracking the precise location of the ionospheric footprint of a magnetospheric spacecraft. Specifically, we consider the ionization products of a pulsed energetic electron beam emanating from the spacecraft along the magnetic field and impinging on the ionosphere. For nominal currents and pulse durations, this beam will produce overdense ionization patches in the conjugate D and lower-E regions that can be readily detected with the HF radars of the SuperDARN network. Very strong signal responses (40-60 dB above the radar noise level) will be observed for periods ranging from 1-2 seconds following each beam pulse. The detection of these signatures is quite similar to the detection of meteor echoes, although the signature decay for meteor echoes is through diffusion, whereas the decay for these echoes is through the slower process of recombination. This difference is due to the relative cross sections of a meteor and the electrom beam at ionospheric altitudes. By injecting a series of electron beam pulses every 1-2 minutes, it should be possible to track the ionospheric footprint of the spacecraft over many hours of universal and local time. Other possible side benefits of this approach include regular observations of meteor winds across extended longitude sectors and controlled observations of recombination rates at D-layer altitudes.

LEONID METEOR SPECTRA FROM 110 NM TO 900 NM AS OBSERVED FROM THE MSX SATELLITE

Morrison, D., Carbary, J., Romick, G.
Johns Hopkins Applied Physics Lab.
11100 Johns Hopkins Rd.
Laurel, MD 20723

Spectra were recorded during the Leonid Meteor shower on November 18, 1999 by the five Spectrographic Imagers on board the DoD Ballistic Missile Defense Organization Mid-Course Space Experiment Satellite (MSX). These are among the first complete spectra from the far ultraviolet (110 nm) to the near infrared (900 nm) ever obtained of a meteor entering the atmosphere. The spacecraft was pointed at a tangent altitude of 100 km with the tangent point at 37.24N and 78.15E at 00:23:36.2 UT. The slits (1° in length) were oriented parallel to the earth limb with the meteor passing downward through the center. The meteor spectra appear in one 0.5 second integration frame on two of the five spectrographic imagers. On three spectrographic imagers covering the wavelength range from 164 nm to 589 nm spectral enhancements appear in two successive frames at some wavelengths and four frames in other wavelengths. The spectra show enhanced OI and NI lines in the near infrared and far ultraviolet and the 557.7 nm OI line (decays in 4 frames) indicative of high speed, high temperature and high altitude meteors. The spectra are rich in atomic neutral and some ion lines of Fe, Ca, Mg, O and N with the most intense emissions occurring in the wavelength intervals between 230 nm and 290 nm. Molecular bands of NO, O_2, N_2, CO, OH if present are very weak compared to the line emissions. This presentation will discuss the various emissions and their relative intensities and the implications on the composition of the meteor and atmospheric excitation.

Session G/H2, 8:35-Fri.

LIGHTNING EFFECTS IN THE IONOSPHERE I

Chairperson: S. Cummer

STUDIES OF LIGHTNING AND LIGHTNING INDUCED IONOSPHERIC EFFECTS AT ARECIBO OBSERVATORY

V.P. Pasko, J.D. Mathews
CSSL Laboratory, The Pennsylvania State University, University Park, PA16802
M. Stanley
Department of Physics, New Mexico Tech, Socorro, NM 87801
U. S. Inan, T. Wood
STAR Laboratory, Stanford University, Stanford, CA 94305
S. Gonzalez, Q. Zhou, M. Sulzer, C. Tepley
Arecibo Observatory, Arecibo, PR 00612

In August-September 2001 an experimental campaign has been conducted in Puerto Rico to perform correlative studies of lightning and lightning-induced ionospheric effects using the Arecibo Observatory (AO) UHF radar, a VHF radio interferometer, a VLF receiver and a low light video camera. In order to thoroughly study the 40-100 km atmosphere/ionosphere and lightning at lower altitudes at unprecedented resolution, we have recorded all data from each UHF radar pulse allowing utilization of well established short-integration time incoherent scatter radar (ISR) techniques at UHF as well as a search for various non-thermal scattering processes and the sorting/averaging of data in non-traditional manners such as into bins depending on the radial range of the lightning discharge from AO. AO offers by far the most sensitive radar for these studies. In addition, we have measured lightning properties, location and time of occurrence (with 1 microsecond resolution) using 274 MHz New Mexico Tech interferometer system complemented by a flat plate antenna allowing detection of the electrostatic field change and polarity of cloud to ground lightning strikes. We have also monitored lightning-associated lower ionospheric disturbances by recording a subionospherically propagating 40.75 kHz VLF signal from NAU transmitter (Aguadilla, Puerto Rico) and performed broadband recordings of lightning sferics using a VLF receiver of Stanford University deployed on Vieques Island. The observational program has been complemented by video recordings of lightning and large scale luminous phenomena above thunderstorms (i.e., sprites) using a SONY CCD camera equipped with GEN III intensifier. On September 3, 2001 several sprite events have been observed between 01 and 03 UT over Haiti/Dominican Republic thunderstorms. In this talk we will provide description of the experiment and will report results of preliminary analysis of the collected data. This program has been supported by Small Grants for Exploratory Research (SGER) program of National Science Foundation. The GEN III intensifier has been provided by ITT Night Vision Industries.

DE-2 EVIDENCE OF LIGHTING INDUCED IONOSPHERIC MODIFICATION

C.F. Keating
Department of Physics
University of South Dakota
414 E Clark St
Vermillion, SD 57069 USA

Classical theory states that a shielding layer will develop between thunderstorms and the ionosphere. This shielding layer prevents any electric field effects from the storm system reaching the ionosphere or, at most, resulting in minor modification to the electric field in only the lowest regions of the ionosphere. But, what we see is that there is a discrepancy between theory and experimental evidence. Existing theories do not satisfactorily explain well-documented phenomena such as upward lightning or gamma-ray and x-ray bursts associated with thunderstorms. Researchers consistently report surprising results that do not fit the theory. This is an indication of how little we know and understand about the global electric circuit. While there is experimental evidence to support the classical thought, there is also experimental evidence that is contrary to those same theories. Additionally, there are consistent reports of observations that cannot be explained using current theories. Observations appear to show that upward lightning creates narrow paths with a high conductivity that act as conduits between the upper levels of thunderstorms and the ionosphere. These paths would make it possible for thunderstorms generated electric fields to penetrate and modify the ionosphere to much higher altitudes than previously theorized. The experimental evidence supports our contention that current theories are inadequate to explain all aspects of thunderstorm-ionosphere connection. The question remains: Do thunderstorm-generated electrical events result in modification of the middle ionosphere, or not? We will present preliminary results of our campaign to examine data collected by instruments on the Dynamics Explorer-2 (DE-2) satellite for evidence of ionospheric modification.

SPACE-BORNE OBSERVATIONS OF INTENSE GAMMA-RAY FLASHES

Fishman, G.J.
Space Science Department SD50
National Space Science andTechnology Center
Huntsville, AL 35812

Intense millisecond flashes of MeV photons have been observed with space-borne detectors. These flashes must originate at altitudes above at least 30 km, in order to be observable by orbiting detectors. At least 70 events have been detected by the Burst and Transient Source Experiment (BATSE) aboard the Compton Gamma-Ray Observatory (CGRO) during its nine year lifetime. The most likely origin of these high energy photons is bremsstrahlung from electrons, produced by a rare type of high altitude electrical discharge above thunderstorm regions. As a discharge phenomenon above thunderstorms, they are likely related to jets and sprites. A detailed description of the observations will be presented.

Intense millisecond flashes of MeV photons have been observed with space-borne detectors. These flashes must originate at altitudes above at least 30 km, in order to be observable by orbiting detectors. At least 70 events have been detected by the Burst and Transient Source Experiment (BATSE) aboard the Compton Gamma-Ray Observatory (CGRO) during its nine year lifetime. The most likely origin of these high energy photons is bremsstrahlung from electrons, produced by a rare type of high altitude electrical discharge above thunderstorm regions. As a discharge phenomenon above thunderstorms, they are likely related to jets and sprites. A detailed description of the observations will be presented.

Intense millisecond flashes of MeV photons have been observed with space-borne detectors. These flashes must originate at altitudes above at least 30 km, in order to be observable by orbiting detectors. At least 70 events have been detected by the Burst and Transient Source Experiment (BATSE) aboard the Compton Gamma-Ray Observatory (CGRO) during its nine year lifetime. The most likely origin of these high energy photons is bremsstrahlung from electrons, produced by a rare type of high altitude electrical discharge above thunderstorm regions. As a discharge phenomenon above thunderstorms, they are likely related to jets and sprites. A detailed description of the observations will be presented.

TERRESTRIAL GAMMA RAY FLASHES AND ENERGETIC ELECTRON PRECIPITATION PRODUCED BY A CYCLONIC THUNDERSTORM IN CENTRAL AUSTRALIA

Inan, U. S., STAR Laboratory, Stanford University, Stanford, CA
Fishman, G. J. , NASA/MSFC, Huntsville, AL
Blake, J. B., The Aerospace Corp, Los Angeles, CA
Christian, H. J. ,NASA/MSFC, Huntsville, AL
Bortnik, J., STAR Laboratory, Stanford University, Stanford, CA

An unusual sequence of Terrestrial Gamma-ray Flashes (TGFs) were observed by the BATSE/CGRO instrument on March 1, 2000 as CGRO passed over an intense and long enduring cyclonic thunderstorm in northeastern and central Australia. The TGF event consisted of seven bursts each of < 1 ms duration and separated by ≈ 2 ms in time, with the peak intensity of successive bursts increasing and then decreasing with time. Analysis of data from the Lightning Imaging Sensor (LIS) on the TRMM satellite documented the lightning rate and other characteristics of the thunderstorm which had an extent in the north-east direction of ≈ 400 km and persisted for nearly a day, exhibiting high flash rates. Although no lightning or sferics data was available at the precise time of the TGF event, the intensity of the storm and the fact that the TGF was observed while CGRO was overhead (with BATSE detectors viewing nadir direction showing the largest intensities) the storm center are consistent with a causative association. Analysis of energetic particle data from the low altitude SAMPEX satellite indicates that this same storm produced significant precipitation of energetic (> 1 MeV) electrons from the Earth's inner radiation belts, as evidenced by a distinctive peak of enhanced electron flux in the drift loss cone observed at L=2.25, poleward displaced with respect to the thunderstorm as predicted for electron precipitation induced by non-ducted obliquely propagating whistler waves injected by lightning discharges. SAMPEX detectors sensitive to energies > 30 keV and > 500 keV exhibited even broader peaks, indicating that the precipitation induced by this thunderstorm encompassed a broad region of L-shells ranging from L=1.5 to 2.4, much like that predicted by recent ray tracing analyses. In this paper, we report the characteristics of the singular TGF event and examine SAMPEX data from similar orbits on successive days to document the association of the drift loss cone enhancements with lightning discharges occurring within the cyclonic thunderstorm. We interpret the data in the context of recent ray tracing analyses to determine the expected L-dependence of the whistler-induced precipitation for direct comparison with satellite data. One of the implications of observations of TGFs at high altitudes above thunderstorms is the associated production of energetic runaway electrons beams, driven upward by intense quasi-static thundercloud fields. Such electrons beams have been predicted to produce optical emissions, ionization changes and gamma-rays in geomagnetically conjugate regions. Experiments are currently underway to search for such conjugate effects.

MID-LATITUDE SPORADIC E, THUNDERSTORMS AND LIGHTNING: CAUSAL CONNECTIONS?

J.W. Wright, STP/NGDC/NOAA and CIRES, Boulder

Sporadic E ('Es') at mid-latitudes is well established as resulting from advection of long-lived (metallic, meteoric) ions into thin layers near convergent nulls of magnetic field-aligned ion velocity induced by wind shear. Electric fields may contribute to, modify and sometimes even dominate this convergence. On ionograms, where details of vertical structure are exaggerated by radio group retardation, Es is distinctive by its "thin-layer" appearance. It can exceed the background (photochemical) E-layer peak plasma frequency (foE) by large factors, and display highly variable spatial and temporal activity. Ionosondes are particularly sensitive to (frequency-dependent) conditions of total internal reflection; it is not uncommon that Es 'blankets' observations of the overlying F-region below a frequency 'fbEs', while echoes from the same reflection height extend to much higher radio frequencies ('foEs'). Moderate Sporadic E (with fbEs foEs foE) is more ubiquitous than intense events, and may not require a significant meteoric-ion inventory.

Intense Es displays a local-summer maximum, of cause not confidently known although the thermospheric tidal wind system probably contributes a basic framework.

Anecdotal evidence for an association of Sporadic E with thunderstorms is abundant in radio amateur discussions and publications on the WWWeb. Often Es enhancements, rather confidently inferred from incidents of VHF (and higher frequency) propagation, are claimed to be associated with particular storms and locations, and even with particular lightning strokes.

In this paper, I examine the seasonal incidence of intense Es at a few mid-latitude ionospheric observatories in relation to the incidence of lightning. The focus is on seasonal patterns, rather than on individual events. There is a clear, general correspondence between the spring onset and autumn finale of the two phenomena, as summarized for 42 years of Boulder ionosonde observations. Data kindly made available by the National Lightning Detection Network (NLDN, Global Atmospherics Inc.), as summarized at NASA/MSFC, provide a more extensive basis for this comparison. I hope by these results to provoke some discussion of the existence and directions of causality among thunderstorms, lightning, and Sporadic E.

METEOROLOGICAL AND ELECTRICAL CHARACTERISTICS OF HIGH PLAINS SPRITE- PRODUCING STORMS

Lyons, W.A., Nelson, T.E.
FMA Research, Inc, Fort Collins, CO
Price., C.
Tel Aviv University, Ramat Aviv, Israel
S. Cummer
Duke University, Durham, NC
Williams, E.R.
MIT/Lincoln Lab, Lexington, MA
Stanley, M.A.
New Mexico Tech, Socorro, NM

After a decade of research, a general conceptual model of the meteorological characteristics of the storms which produce sprites had arisen. Also various assertions as to the characteristics of the unusual positive cloud-to-ground (+CG) lightning which yielded sprites had been made. Two recent field programs have allowed the collection of data which can begin to test these conceptual models. The summer 2000 Severe Thunderstorm Electrification and Precipitation Study (STEPS), as well as the 1999 NASA Stratospheric Sprites Balloon campaign, have provided numerous excellent case studies. A wide variety of remote sensing tools were employed to investigate TLE-producing storms over the High Plains. These included several types of low-light video systems deployed at Yucca Ridge, the National Lightning Detection Network (NLDN), the NOAA NEXRAD radar network, GOES 8, the New Mexico Tech Lightning Mapping Array and several ELF transient recording sites distributed worldwide. Detailed analyses of MCS over the STEPS network revealed the sprite-producing +CGs tended to cluster near but not coincident with the coldest cloud tops. Two methods of calculating the charge moments of the TLE-parent +CGs confirmed that large values (averaging some 1000 C*km) are an apparent requirement for sprites. Detailed analysis of the radar echo evolution for sprite-producing storms show that with a few exceptions, the most consistent sprite producers are large (great than 20,000 sq. km.) with expansive stratiform precipitation regions. Continued analysis of the large MCS of 18 August 1999 show sprite-producing +CGs tend to congregate below the colder portions of the storms cloud shield within stratiform precipitation areas with relatively low radar reflectivities (25 - 40 dBZ). Five halos were associated with CGs by the NLDN. All five were associated with ELF slow-tails recorded at about 1000 km range. A new hybrid ELF/VLF technique used receivers in Israel to monitor sprite-related ELF transients originating in Nebraska, a range of 11 Mm. The conceptual models of sprite storms and lightning appear to be largely confirmed.

ROUND-THE-WORLD DETECTION OF AUSTRALIAN SPRITE LIGHTNING BY SCHUMANN RESONANCE METHODS

E. Williams, R. Boldi, A. Patel, MIT, Cambridge
R. Dowden, C. Rodger, LF*EM Research Ltd, New Zealand
Z. Kawasaki, Electrical Engineering, Osaka University, Japan
Y. Hobara, LPCE/CNRS, Orleans, France
M. Hayakawa, University of Electro-Communications, Tokyo, Japan

The first documentation of sprites over the Australian continent occurred on November 26, 1997*. Video cameras (with image intensifiers) positioned near Darwin, Australia in the Top End captured about 70 sprites over a mesoscale convective system 200-300 km to the southwest. Examination of the ELF archive of electromagnetic transients recorded in West Greenwich, Rhode Island has revealed ten events which line up in time with the sprite video images. These events have been geolocated by the wave impedance/magnetic bearing method over the Australian continent. The initial electric field excursions of all events indicate positive polarity, suggesting large positive ground flashes, and consistent with many earlier observations elsewhere. The computed vertical charge moments, based on the assumption that the duration of the lightning/sprite current is short in comparison with the time for light to propagate around the world,are inexcess of 700 C-km, the threshold for conventional dielectric breakdown at an assumed sprite initiation altitude of 75 km. This moment threshold is based on the method outlined by C.T.R. Wilson but includes the effect of the ionosphere and a realistic profile of atmospheric density. This collecion of events is of particular interest from the standpoint of single-station mapping because they are all close to the Rhode Island antipode near Perth,Australia. Details of the electromagnetic waveforms and their interpretation will be discussed in comparison with the video imagery. The optical characteristics of those sprites in the same storm which were not geolocatable from Rhode Island will be compared in details with the stronger events that were located. *(Hardman et. al., of Geophysical Research, **26**,105, D, 4689 – 4697, 2000)

STATISTICS OF TLE TYPES AND PROPERTIES OBSERVED DURING THE 1999 SPRTIES BALLOON CAMPAIGN

L. Bhusal, E.A. Bering, III*, J.R. Benbrook, J.A. Garrett, A.M.P. Paredes, Physics Dept., Univ. of Houston, Houston
Moudry, D.R., E.M. Wescott, D.D. Sentman, H. C. Stenbaek-Nielsen, Geophysical Inst., UAF, Fairbanks
Lyons, WA, FMA Research, Ft. Collins

Historically, the process of sprites or Transient Luminous Event (TLE) detection has required an alert human observer to notice them on a low light level TV (LLTV) monitor, either in real time or playback. The payloads of the 1999 Sprite Balloon Campaign have all sky uplooking photometers not sensitive to events below the balloons. We have used the photometer data to find more TLE's that were missed, by checking it at the times reported by the National Lightning Detection Network (NLDN). During Flight 1 (07/06/99) we surveyed 3 hours of data, containing 1652 strokes. We found 56 TLE's, 7 associated with +CG's and 49 with -CG's. During flight 3 (08/21/99), we surveyed 2 hours of data, containing 1017 strokes with 104 TLE's, 28 associated with +CG's and 76 with -CG's. During Flight 3, ground observation was possible. So far we have identified 26 sprites, sometimes mixed with other TLE phenomena, 28 stand-alone sprite halos, and 7 elves. Some of these events were not associated with NLDN events. Since most of the unidentified balloon-observed events were associated with -CG's, we suggest that most of them were sprite halos. There was enough time delay between the CG strokes and the light pulses to rule out elves. All of these events produced an electric field pulse with a decay time that was consistent with charge deposition in the mesosphere. By assuming a simple dynamic dipole model, we can solve for the dipole moment of the sprtie itself. For the +CG TLE's we have found a 100 C-km threshold value of the charge moment of the TLE itself. We do not find a similar threshold for -CG's. It was also found that all CG strokes deposit some charge in the mesosphere.

MESOSPHERIC ENERGY INPUT OWING TO SPRITES AND OTHER TLE'S AND THE POSSIBLE EFFECTS THEREOF

E. A. Bering, III*, J.R. Benbrook, L. Bhusal, J.A. Garrett, A.M.P. Jackson, Physics Dept., Univ. of Houston, Houston
D.D. Sentman, D.R. Moudry, E.M. Wescott, H.C. Stenbaek-Nielsen, Geophysical Inst., UAF, Fairbanks
W.A. Lyons, FMA Research, YRFS, Ft. Collins

This paper discusses the chemistry and energy balance implications of the results of the 1999 Sprites Balloon Campaign. Flight 3 of the campaign flew from Ottumwa, Iowa at 00:39:32 UTC to 11:12:00 UTC on 08/21/99. 68 transient luminous events were observed. A sprite at 0955:36.980 UTC on 21 August 1999 produced a vertical electric field perturbation of 0.275 V/m that was similar in time profile to the light emission. There was also a positive azimuthal magnetic pulse of 3 nT. These data suggest that the sprite itself carried an upward current of 6-11 kA, and that the light emission was the result of the deposition of -7 C of charge near 75-78 km altitude. The deposition of this much charge also deposited 50-100 MJ of electrostatic potential energy in the mesosphere. All of the other 23 sprites observed by the balloon payload show similar signatures. No published model predicts the signatures observed in these data. Further investigation has discovered that virtually all cloud to ground (CG) lighting strokes were followed 2-6 ms later by a delayed ELF pulse 2-4 ms long produced by D-region polarization and mesospheric charge deposition. Sprite halos produced by -CG's were 4-7 times as common as +CG events, which means that published event rates based on ground observations of spritea rates are serious underestimates. Sprites or halos occurred when the deposited charge moment was large enough to produce an electric field in the mesosphere that exceeded 65 V/m. The quantitative impact of these observations on our understanding of the chemistry and energy balance of the mesosphere will be discussed.

DIFFUSE AND STREAMER REGIONS OF SPRITES

Victor P. Pasko*
CSSL Lab., Penn State University, University Park, PA 16802
Hans C. Stenbaek-Nielsen
Geophysical Institute, University of Alaska Fairbanks, AK 99775

Sprites are luminous features appearing at mesospheric/lower ionospheric altitudes above thunderstorms [e.g., Sentman et al., GRL, 22, 1205, 1995]. The theoretical analysis of Pasko et al. [GRL, 25, 2123, 1998] indicates existence of three distinct altitude regions in sprites: (1) The upper diffuse region; (2) The intermediate transition region; and (3) The lower streamer region. Sprites indeed often exhibit an amorphous non structured glow at their tops which converts to highly structured breakdown regions at lower altitudes [e.g., Stanley et al., GRL, 26, 3201,1999; Gerken et al., GRL, 27, 2637, 2000; Stenbaek-Nielsen et al., GRL, 27, 3829, 2000; Barrington-Leigh et al., JGR, 106, 1741, 2001; Wescott et al., JGR, 106, 10467, 2001]. The unique feature of the sprite imaging data reported by Stenbaek-Nielsen et al. [2000] is that all observations were consistently performed with full gain of the intensified CCD imager. As a result most, if not all, sprite events substantially saturated the imager at onset. However, subsequent frames provided unprecedented recordings of temporal development of low light sprite features. In particular, the absolute majority of the recorded events clearly demonstrate and allow accurate measurement of the transition altitude between the upper diffuse and the lower streamer regions discussed in [Pasko et al., 1998].

We report here results of comparison of model results of Pasko et al. [1998] and high-speed observations of Stenbaek-Nielsen et al. [2000] in terms of the transition boundary between the diffuse and streamer regions of sprites. The analysis of 25 events indicated the mean transition altitude 78 km with standard deviation 4 km. The measured standard deviation appeared to be in excellent agreement with the mean 25 km offset of the horizontal position of sprites from the underlying parent lightning stroke measured by Wescott et al. [2001]. The transition altitude is a sensitive function of the ambient parameters at the mesospheric and lower ionospheric altitudes (i.e., the electron number density profile). The reported measurements are compared with fifteen model profiles of the ambient conductivity at sprite altitudes compiled from existing models and literature on this subject. For the electron density profiles, in particular, the best fit between the model and observations has been achieved for profiles calculated using IRI-95 model and the night time electron density profile of Wait and Spies [Tech. Note 300, NBS, Boulder, CO, Dec. 30, 1964] (see also [Inan, GRL, 17, 729, 1990]), which also produced the best fit between the high speed video observations of halos and model results reported recently by Barrington-Leigh et al. [2001].

Session G/H3, 13:15-Fri.

LIGHTNING EFFECTS IN THE IONOSPHERE: II

Chairperson: S. Cummer

SPRITE CURRENTS DURING THE SUMMER OF 2000

S.A. Cummer, W. Hu
Electrical and Computer Engineering Department
Duke University
Durham, NC 27708
W.A. Lyons, T.E. Nelson
FMA Research, Inc.
Fort Collins, CO

We have systematically analyzed a large number of sprite producing lightning discharges in the summer of 2000 using continuous extremely low frequency (ELF) magnetic field recordings at Duke University during the STEPS campaign. In analyzing many hundreds of sprites on many different days, we find that clear sprite current pulses (short ELF pulses that are temporally linked to the sprite and therefore originate in high altitude currents) occur in only 9% of sprites. This rate varies significantly from day to day, however, with some days approaching 50% and other days containing no sprite current pulses. This variability could originate either in the forcing from lightning below or in the mesospheric and ionospheric conditions at sprite altitudes. We closely examine the characteristics of lightning that does and does not generate sprite currents to determine whether forcing from below is responsible for this difference.

Sprite current is driven by lightning-generated mesospheric electric fields in regions of breakdown-enhanced electrical conductivity [Pasko et al., GRL, 18, 3493, 1998] and therefore contains information about the magnitude of the high altitude electric field. This field is also closely linked to lightning charge moment change in the thunderstorm below, which can be independently measured from the lightning ELF radiation. We use a combination of numerical simulations and data to investigate the quantitative relationship of sprite current and lightning current and to determine whether the lightning and sprite current observations are self-consistent.

Lastly, the evidence that these secondary pulses originate in sprite and not lightning currents is overwhelming but still indirect. We propose a ground-based measurement that could unambiguously demonstrate that the source current for these pulses flows at high altitudes.

NON-SPECTRAL MEASUREMENTS OF IONIZATION PROCESSES IN SPRITES

Christopher P. Barrington-Leigh
Space Sciences Lab
University of California
Berkeley, CA 94720-7450

An electric field imposed on a weakly ionized gas containing electronegative species such as O_2 may lead to either an increase in electron density (through electron impact ionization) or to a decrease in electron density as a result of dissociative attachment of electrons (such as $e^- + O_2 \rightarrow O^- + O$). The conductivity may also increase or decrease accordingly in an applied electric field. Pasko *et al.*, (*GRL*, **25**, 2123-6, 1998) described how the atmospheric density (i.e., altitude), ambient conductivity, and the rise time of the external electric field determine whether ionization or attachment processes dominate in an ambient atmosphere, and how this determines whether (and where) narrow corona streamers are likely to form in sprites. Because the conductivity is itself affected by ionization and attachment processes, the behaviour of the electron density is strongly (and nonlinearly) dependent on its initial conditions (past history) and on the temporal profile of the imposed electric field.

Experimental interest in the energetics of sprites has been directed in large part towards spectral measurements of optically-emitting regions. Nevertheless, such results are still scarce. Several non-spectral (but primarily optical) observations have recently been used to help to understand what is going on in terms of electron and ion densities. These measurements, mentioned below, are discussed in light of available models.

(1) The observed dendritic structure in sprites is clear evidence of a highly localized inhomogeneity in ionization processes, and agrees well with theoretical descriptions of corona streamers at mesospheric altitude. (2) The curvature observed in sprite halos is evidence of strong space charge formation and can be used in comparison with models to constrain the electron density enhancement at 70–80 km. (3) The recently reported exponential relaxation of optical emissions in bright sprites can be explained in terms of macroscopic and microscopic models and suggests that free electrons may become highly depleted in sprite streamer channels. (4) Lightning currents which cause sprite halos may, if slow to decay, end up depleting available electrons near the VLF reflection height rather than leaving a density enhancement. This could have relevance for early/fast VLF pertubations. It may be concluded that ion conductivity and the depletion of electron density are often as prevalent an effect in sprites as electron density enhancement.

BLUE SPRITE IMAGERY: CHARACTERISTICS AND ASSOCIATED THUNDERSTORM ENERGETICS

M.J. Taylor, R.M. Dial
Center for Atmospheric and Space Science and Physics Department
Utah State University
Logan, UT 84322
S.A. Cummer
Electrical and Computer Engineering Department
Duke University
Durham, NC 27708
M. Fuellekrug
Institut fur Meteorologie und Geophysik
Universitt Frankfurt
D-60323 Frankfurt
W.A. Lyons
FMA Research, Inc.
Fort Collins, CO

Multi-spectral measurements of sprite signatures were made during two summer campaigns at Yucca Ridge, CO during 1998 and 2000. For the first campaign three co-aligned intensified video cameras were used to investigate the red (N2 1 PG), blue (combination of N2+ 1 NEG and N2 2 PG), and white-light signatures. These data revealed a preponderance for red N2 1PG emission associated with positive cloud-to-ground discharges but only a limited number (¡ 10) of events with significant blue emission were recorded. During summer 2000 blue sprite signatures were investigated using an intensified CCD camera fitted with the same blue filter as the 1998 measurements. Once again only a limited number of events with significant blue emission were recorded but the higher quality of the data revealed clear structure throughout the body of the sprites. In this presentation we utilize a unique set of high time resolution, multi-station ultra low frequency (ULF) magnetic field measurements that were made during the summer of 1998. These sensors are sufficiently sensitive to detect long continuing currents that contributed substantially to the initiation of many of these sprites. The ULF data are analyzed to fully characterize the lightning responsible for the observed sprite events and to investigate any fundamental differences between the lightning responsible for occasional blue sprite signatures. Initial analysis indicates that the blue sprites are generated in response to larger charge moment changes than those without the blue signature, but the difference does not appear to be as straightforward as the presence or lack of sprite current.

SPECTRAL PROPERTIES OF BLUE JETS AND BLUE STARTERS

Victor P. Pasko*, and Jeremy J. George
CSSL Lab., Penn State University, University Park, PA 16802

Blue jets and blue starters are narrowly collimated beams of blue light that propagate upwards from the tops of thunderclouds [Wescott et al., GRL, 22, 1209, 1995; 23, 2153, 1996]. The jets appear to propagate upward at speeds of about 100 km/s and reach terminal altitudes of 40-50 km [Wescott et al., 1995], while the starters protrude upward to a maximum 25.5 km in altitude [Wescott et al., 1996]. Blue jets and blue starters have been captured by black and white and color video cameras, allowing to make some important suggestions about optical bands responsible for the observed blue color of jets and starters [e.g., Wescott et al., 1995]. However, no wavelength resolved optical spectra of blue jets and blue starters have been obtained to date.

We report here results from a new three-dimensional fractal model, which closely resemble the characteristics of blue jets and blue starters observed by Wescott et al. [1995; 1996] in terms of their altitude extents, transverse dimensions and conical structure. The main physical concept of our model is based on the recent suggestion by Petrov and Petrova [Tech. Phys., 44, 472, 1999] that blue jets correspond qualitatively to the development of the streamer zone of a positive leader and therefore should be filled with a branching structure of streamer channels. The model simulates the propagation of branching streamer channels constituting blue jets and starters as a three dimensional growth of fractal trees in a self-consistent electric field created by thundercloud charges. The model is based on a phenomenological probabilistic approach proposed in [Niemeyer et al., IEEE Trans. Electr. Insul., 24, 309, 1989] and is a straightforward expansion of the previously developed two-dimensional version [Pasko et al., GRL, 27, 497, 2000].

The fractal model allows accurate determination of the macroscopic electric fields in regions of space occupied by streamers. Our results indicate that for a variety of input parameters these fields are very close (within several %) to the minimum electric field required for propagation of positive streamers in air E_{cr}^{+} [Pasko et al., 2000, and references therein] and generally are not sufficient to excite any observable optical emissions. Our conclusion therefore is that the observed optical luminosity in blue jets and starters comes from large electric fields existing in narrow regions of space around tips of small scale corona streamers constituting them. We performed a survey of publications on emission spectroscopy of corona discharges in air at different pressures, including those corresponding to the altitude range of blue jets and starters. In our talk we will report results of comparisons between these measurements and our model predictions, which provide additional supporting evidence for the mechanism of blue jets and blue starters based on streamer coronas.

EARLY/FAST DISTURBANCES OF THE LOWER IONOSPHERE

Moore, R.C., STAR Lab, Stanford University
Barrington-Leigh, C.P., Space Sciences Lab, U.C. Berkeley
Inan, U.S., STAR Lab, Stanford University

Early/Fast disturbances of subionospheric Very Low Frequency (VLF) signals constitute the earliest experimental evidence indicating a direct impulsive coupling of energy produced by lightning discharges to the overlying mesosphere and lower ionosphere. Although the discovery of early/fast perturbations significantly precedes that of the more spectacular luminous phenomena known as sprites and elves, the physical mechanism responsible for creating the early/fast disturbance is still not quantitatively understood. Previous models have been used to represent accurately the scattering pattern of the early/fast disturbance [e.g., Johnson et al., 1999], but have not yet reproduced the absolute magnitudes of the observed VLF signal perturbations. It has recently been suggested [Barrington-Leigh, 2001] that early/fast events may be associated with the so-called sprite halos, which involve substantial ionization changes at 70-85 km altitudes. In this paper, we quantitatively assess this possibility, using a model which incorporates both the quasi-electrostatic (QE) field and the electromagnetic pulse (EMP) released by powerful lightning discharges [Barrington-Leigh et al, 2001] to determine the ionospheric conductivity changes together with recent experimental measurements of early/fast events and model calculations of VLF propagation and scattering. Early/Fast events are captured by the Stanford Holographic Array for Ionospheric and Lightning research (HAIL) system, consisting of nine closely-spaced ($\sim$65 km) VLF receivers, while the propagation and scattering calculations are carried out using a 3-dimensional version of the Long Wave Propagation Code (LWPC) [Lev-Tov et al., 1995]. Results indicate that the scattering pattern of the modeled disturbance is consistent with that of Johnson et al. [1999] and in addition that the modeled conductivity changes provide for significantly larger absolute magnitudes of the observed VLF signal perturbations. In this paper, we analyze several Early/fast events, including an event observed with the HAIL array in association with a positive lightning stroke occurring at 06:22:23.559 UT on 29 October, 2000. This and other events during this period were detected by many of the HAIL receivers, allowing for accurate determination of the scattering pattern of the disturbance. We present results for several different ambient ionospheric conditions.

Session G/H4, 8:35-Sat.

REMOTE SENSING FROM SPACE

Chairperson: B. Reinisch

IMPROVING GPS/MET IONOSPHERIC ELECTRON DENSITY PROFILES USING AN "COMPENSATED" ABEL INVERSION METHOD

L.-C. Tsai
CSRSR
National Central University
Chung-Li, Taiwan 320, R.O.C.

In 1993 the University Corporation for Atmospheric Research organized a proof- of-concept experiment on a LEO satellite (the MicroLab-1 satellite) at a nearly circular orbit of ~735 km altitude and ~70° inclination angle to receive GPS signals and demonstrate active limb sounding of the Earth's atmosphere and ionosphere by radio occultation technique. The main objectives of this GPS-LEO occultation mission were numerical weather prediction and long-term monitoring of the Earth's climate and thus it was termed the Global Positioning System/Meteorology (GPS/MET) program. However, GPS/MET has also been able to sound the ionosphere from the orbit altitude to the Earth's surface and provide high vertical resolution profiles of ionospheric electron density through the Abel inversion of ray-path bending angle or TEC measurements. These retrieval processes generally assume spherical symmetry of electron density distribution at the locality of occultations and use the Abel integral transform to invert the data. It is obvious that this assumption of spherical symmetry in the ionosphere is almost never true. We have pointed that due to the effect of the spherical symmetry assumption utilized for the Abel inversion, an even asymmetry at the equatorial anomaly would likely cause the Abel inversion to systematically under-estimate the electron density near the north and/or south crests of equatorial fountain features. In this paper, we have approached a compensation procedure for measured TEC values through several close-up occultation observations. The compensated TEC values are further used to yield to electron densities through the Abel integral transform. In order to assess the accuracy of the GPS/MET ionospheric electron density retrievals, coincidences of ionosonde data with GPS/MET occultations have been examined. The retrieved electron density profiles from GPS/MET TEC observations have been compared with ionogram auto-scaling and inversion results derived from the Chung-Li digisonde (24.6°N, 121.0°E) and the Bear-Lake dynasonde (41.9°N, 111.4°W).

FIXED-FREQUENCY OBSERVATIONS OF ISIS-2 SOUNDER-STIMULATED PLASMA RESONANCES AND EMISSIONS

R.F. Benson
Goddard Space Flight Center
Greenbelt, MD 20771, USA

Ionspheric topside sounders and magnetospheric radio sounders routinely stimulate local plasma resonances. A proper classification of these resonances can be used to accurately deduce (to within a few percent) both the *in situ* electron density and the magnetic field strength even in very tenuous plasmas where the former is difficult to measure. Based on many decades of research with ionospheric topside sounders by many investigators, most of the observed resonances have one of two causes: the reception of (1) coherent sounder-generated electrostatic waves of low group velocity or (2) non-coherent plasma emissions stimulated by the sounder pulse. Those observed at the electron plasma frequency f_{pe}, the harmonics of the electron cyclotron frequency f_{ce}, and at the upper-hybrid frequency f_{uh} (where $f_{uh}^2 = f_{pe}^2 + f_{ce}^2$) have been attributed to (1) above. Those observed between the f_{ce} harmonics and below f_{pe}, designated as the Dn resonances, have been attributed to (2) above. Those observed between the f_{ce} harmonics and above f_{pe}, designated as the Qn resonances, have usually been attributed to (1) above (D. B Muldrew, *J. Geophys. Res.*, **77**, 1794-1801, 1972) but evidence has been presented that a contribution from (2) above is also involved (R.F. Benson, *Radio Science*, **17**, 1637-1659, 1982). Both the Dn and the Qn resonances have been related to magnetospheric banded emissions (R. F. Benson et al., *J. Geophys. Res.*, **106**, 13,179-13,190, 2001).

An investigation of ISIS-2 ionograms corresponding to fixed-frequency operation has provided additional evidence to support the claim that the Qn resonances contain elements of both the reception of coherent sounder-generated waves and sounder-stimulated non-coherent plasma emissions. The data were identified from some 300,000 ISIS-II digital topside-sounder ionograms, publicly available from the National Space Science Data Center, Goddard Space Flight Center, making use of the search page at http://nssdc.gsfc.nasa.gov/space/isis.html.

ELECTRON DENSITY PROFILES IN THE MAGNETOSPHERE FROM IMAGE/RPI PLASMAGRAMS

B. Reinisch, X. Huang, P. Song, I. Galkin
Center for Atmospheric Research
University of Massachusetts, Lowell, MA
R. Benson, S. Fung, J. Green
NASA Goddard Space Flight Center, Greenbelt, MD

The Radio Plasma Imager (RPI) on IMAGE conducts echo radio sounding experiments producing plasmagrams that display echo amplitudes as function of virtual range and frequency. These plasmagrams show different type of echo traces resulting from X, O and Z mode wave propagation, and the identification of the wave modes requires careful analysis. Angle of arrival measurements together with the echo trace characteristics reveal two classes of echoes, direct and field-aligned propagation (FAP) echoes. In this paper we describe the technique of inverting the FAP traces into electron density profiles. These profiles represent the density distribution along the field line that intersects the spacecraft. In many instances, RPI receives FAP echoes from the local as well as the conjugate hemisphere. This allows the calculation of the complete density distribution from one ionosphere to the conjugate one, beginning at altitudes of $\sim$0.5 or 1 R_E. Once a profile has been calculated, in general from the X trace, it is possible to validate the analysis by calculating the expected Z and O traces and compare the calculated traces with the measured ones. We found excellent agreement assuring the accuracy of the profiles. By applying this technique to different time periods, we were able to assess the effect of CME's on the magnetosphere.

During the March 31, 2001 event the solar pressure was more than 40 times greater than normal with a sustained southward interplanetary magnetic field, conditions for a major magnetic storm. The Kp index went up to near 9. During the event, the IMAGE orbit was near the noon-midnight meridian monitoring the magnetospheric responses at local noon and midnight. The RPI sounding measurements show that the total content of the plasma changed dramatically during the event. The dayside density dropped significantly during the storm and we also observed the refilling process after the storm. There is potential evidence for an increased density on the nightside during the event, which may be the result of the higher solar wind density. Quantitative assessment of the density variations during the event and the refilling process afterward will be presented.

PLASMA DISTRIBUTION AS A FUNCTION OF LATITUDE AND L-SHELL IN THE PLASMASPHERE: AN RPI CASE STUDY

X. Huang*, B. Reinisch, P. Song, G. Sales, G. Khmyrov, A. Kozlov
Center for Atmospheric Research
University of Massachusetts, Lowell, MA

In the past it has been difficult to assess the plasma density (N_e) distribution along magnetic field lines with in-situ measurements because it is rare to have a few satellites along the same field line. It is also challenging to derive the distribution from theory because the existence of field-aligned flow makes a static approximation invalid. The new sounder observations by the radio plasma imager (RPI) on IMAGE [Burch et al., EOS Trans. American Geophys. Union, 82, 241-145, 2001], make it possible to measure the entire field-aligned profile within the time it takes to step through the frequencies that cover the plasma frequencies from the satellite location to the ends of the field line in the topside ionosphere [Reinisch et al., Geophys. Res. Lttrs, in press, 2001]. This takes approximately 10 s, i.e., the measurement is made almost instantaneously. A special profile inversion technique inverts the field-aligned propagation echo traces to profiles along the field line. Each profile is validated by recalculating the echo traces for different wave modes using the derived profile. This paper discusses the application of the new technique to one IMAGE pass in the morning sector when the sequence of plasmagrams shows clearly defined echo traces. A case study shows a sequence of eight consecutive profiles while IMAGE changed position from L=2.22 to L=3.23. Soundings were made every two minutes. Each sounding provides a complete hemisphere-to-hemisphere density profile. By piecing together these profiles along different L shells we were able to construct two-dimensional density distributions as a function of latitude and L-shell.

MODELING COMPARISONS TO PLASMA OBSERVATIONS OBTAINED FROM RPI/IMAGE

P.A. Webb*
NAS/NRC/Goddard Space Flight Center
Greenbelt, Maryland 20771
USA
R.F. Benson
Goddard Space Flight Center
Greenbelt, Maryland 20771
USA
B.W. Reinisch
University of Massachusetts Lowell
Lowell, Massachusetts 01854
USA

NASA's Imager for Magnetopause-to-Aurora Global Exploration (IMAGE) satellite (J. L. Burch,*EOS, Trans. AGU*, **82**, 241 and 245, 2001) is currently in a highly inclined elliptical orbit that takes it between altitudes of 1000 km and seven Earth radii. During each 14.2 hour orbit IMAGE's instruments have the opportunity to observe the plasma distribution from the topside ionosphere to beyond the plasmapause. One such instrument carried by IMAGE is the Radio Plasma Imager (RPI) (B. W. Reinisch et al., *Geophys. Res. Lett.*, **28**, 1167-1170, 2001). Using the RPI, the local electron density can be separately calculated from observed plasma resonances and the plasma spectrograms. An electron density profile for each orbit can be obtained by calculating the electron density at different points along the orbit, which can then be compared to the predictions of plasmaspheric electron density models.

Several static empirical models of the plasmasphere have been published. Two such models are the Carpenter and Anderson ISEE/whistler based model (D. L. Carpenter and R. R. Anderson,*J. Geophys. Res.*, **97**, 1097-1108, 1992), and the GCPM model (D. L. Gallagher et al.,*J. Geophys. Res.*, **105**, 18819-18833, 2000). The theoretical based Global Plasmasphere Ionosphere Density (GPID) model has recently been developed by the first author to simulate the global scale evolution of the number densities of the ions and electrons in the plasmasphere. Combined with the latest version of the International Reference Ionosphere (IRI), GPID can model the dynamic emptying caused by geomagnetic storms and the following refilling of the plasmasphere.

The accuracy of the empirical models and the theoretical GPID model will be ascertained by comparing their predictions with the electron densities derived from the RPI by conducting these comparisons across a variety of geomagnetic L-shells and various geomagnetic storm conditions.

AND COMPARISON TO SHARP EDGES IN IMAGE EUV IMAGES

J. Goldstein, T. Huegerich, P.H. Reiff
Dept Phys and Astron, Rice University
Houston, TX 77005, USA
B.R. Sandel, T. Forrester
Lunar and Planetary Lab, University of Arizona
Tucson, AZ 85721, USA
D.L. Gallagher
NASA MSFC
Huntsville, AL 35812, USA
B.W. Reinisch
Center for Atmosph Res, U. Mass, Lowell
Lowell, MA, USA

Remote-sensing of the plasmasphere is routinely accomplished by the extreme ultraviolet imager (EUV) on the Imager for Magnetopause-to-Aurora Global Exploration (IMAGE) satellite. In EUV images, the plasmapause is assumed to be the 'He^+ edge,' i.e., the sharp edge where the brightness of 30.4 nm He^+ emissions drops drastically. This assumption can be tested with the help of dynamic spectrograms recorded by the Radio Plasma Imager (RPI) in passive receiving mode. The RPI dynamic spectrograms provide in situ measurements of the electron number density; one can identify the plasmapause by determining these values along the IMAGE orbit. During each IMAGE orbit, RPI in situ plasmaspheric electron density data are deduced while IMAGE is at low magnetic latitudes, and EUV remote-sensing images of the plasmasphere are obtained when IMAGE is at higher magnetic latitudes, and outside the plasmasphere. The RPI and EUV instruments therefore provide two different and complementary measurements of the plasmapause location that can be compared with each other. In this study it was assumed that any density gradient in the RPI data that was sufficiently steep would show up in EUV data as a sharp He^+ edge. Steep density gradients were identified in RPI dynamic spectrograms from over two hundred IMAGE passes through the plasmasphere, providing over three hundred plasmapause radial (L) locations. Corresponding He^+ edges were selected from EUV images, and mapped to the magnetic equator, where their radial (L) locations can be determined. We show the results of a comparison between the radial locations of the RPI density gradients and the radial locations of the EUV He^+ edges, and determine that the correlation between the two types of measurement is good, justifying the assumption that the He^+ edge is the plasmapause.

RELATIVE POWER LEVELS OF MULTIPLE RPI/IMAGE FIELD-ALIGNED MAGNETOSPHERIC ECHOES

R.F. Benson, S.F. Fung, J.L. Green
Goddard Space Flight Center
Greenbelt, MD 20771, USA
B.W. Reinisch
University of Massachusetts, Lowell
Lowell, MA 01854, USA

The Radio Plasma Imager (RPI) (B. W. Reinisch et al., *Geophys. Res Lett.*, **28**, 1167-1170, 2001) on the Imager for Magnetopause-to-Aurora Global Exploration (IMAGE) satellite (J. L. Burch,*EOS, Trans. AGU*, **82**,241 and 245, 2001) often detects discrete long-range echoes when IMAGE is located in the general vicinity of the plasmapause. The long time delays indicate that these echoes, which extend over a few hundred kilohertz up to at least 600 kHz, do not correspond to signal returns from the nearby plasmapause. Some echoes include traces that do not extend toward zero virtual range. These "floating" traces often have an "epsilon" shape similar to those observed at low altitudes in the topside ionosphere by ISIS 1 when it was immersed within equatorial plasma bubbles. The ISIS 1 observations were interpreted in terms of ducted propagation along field-aligned electron-density irregularities (FAI) that were maintained from one hemisphere to the other (P. L. Dyson and R. F. Benson, *Geophys. Res Lett.*, **5**, 795-798, 1978) following the earlier work based on Alouette 1 observations at higher (1,000 km) altitude (D. B. Muldrew, *J. Geophys. Res.*, **68**, 5355-5370, 1963).

An investigation of the relative power levels of these magnetospheric epsilon signatures was carried out in order to determine the degree of signal loss between the various echo components (which are attributed to different magnetospheric path lengths). At each frequency, the power level corresponding to the signal received on the x dipole antenna (the same one used for transmission) for each echo component was recorded. The results indicate that the path length of the signal is not a major contributor to differences observed in the received power among the echo components. Thus the magnetospheric "epsilon" shaped echoes appear to be due to nearly loss-free propagation along FAI that are maintained from one hemisphere to the other in the vicinity of the plasmapause in a manner similar to their ionospheric counterparts.

WAVE POLARIZATION OF FIELD-ALIGNED PROPAGATING MODES USING IMAGE/RPI

G. Sales*, X. Huang, B. Reinisch, I. Galkin
Center for Atmospheric Research
University of Massachusetts, Lowell, MA
R. Benson, P. Webb
NASA Goddard Space Flight Center, Greenbelt, MD

Field-aligned propagation (FAP) modes have been observed extensively during the lifetime of the IMAGE/RPI satellite project. Both direction-of-arrival and time delay measurements have supported the hypothesis that these modes are directed along the geomagnetic field lines from the satellite down to altitudes where reflection back to the satellite occurs. The plasmagram inversion technique, developed at UMLCAR, has determined that these "guided" modes have, primarily, extraordinary polarization. With the orthogonal antenna system on the IMAGE satellite, used first to determine the arrival angle, it is now also possible to analyze the polarization of the arriving waves over a range of frequencies. From the measured amplitude and phase on the three antennas we can reconstruct the polarization ellipse at the satellite.

We have selected one of the many sequences of plasmagrams to analyze the polarization characteristics of these FAPs. These FAP modes are predominately observed for $2 < L < 5$ with a median value of $L = 3$. Of these, approximately 40and the median is between two and three plasmagrams. On Aug. 25, 2000 as IMAGE/RPI approached the plasmasphere, at $L = 4.75$, a sequence of three plasmagrams recorded these field aligned propagation modes over a period of 8 minutes. The sequence ended at $L = 4.45$, a significant travel distance for the satellite from the beginning to the end. We discuss the extensive passive and active calibration analyses that were required to determine the correct arrival-angles for these modes. Building on the success in the arrival-angle analysis we turned our attention to the polarization characteristics of the FAP modes. The RPI plasmagram is used to determine the local electron gyro frequency and the local plasma frequency. Combining these with the arrival-angle measurements and with the received amplitude and phase on the antenna system we can determine the received polarization as a function of frequency and time.

Session H1, 13:35-Wed.

WAVE-PARTICLE INTERACTION

Chairperson: C. Kletzing

MICROWAVE PROPAGATION AND REFLECTION FROM TURBULENT FLUCTUATIONS IN FUSION PLASMAS

R. Nazikian
Princeton Plasma Physics Laboratory
Princeton, NJ 08540

Microwave reflectometry (the reflection of electromagnetic waves from a plasma cutoff) is now routinely used for probing the structure of magnetohydrodynamic and turbulent fluctuations with unprecedented spatial resolution in the core of high temperature fusion plasmas. The quantitative interpretation of such measurements has been a major objective of the fusion plasma community for the last decade and dramatic progress has recently been made in the simulation and laboratory testing of the method and its capability for measuring the correlation properties of plasma turbulence. The simultaneous propagation of multiple frequency microwaves into plasma has allowed the spatial correlation properties of the turbulence to be infered along the direction of wave propagation, while the strength of the scattered waves at the receiver has been used to infer the magnitude of the irregularities. The ever increasing need for more refined measurements has recently led to new efforts aimed at imaging turbulent fluctuations near the reflecting layer. This objective is particularly challenging given the strong curvature of the background plasma and the limited access for the necessary large aperture optics. Work in the early 60s on radio wave reflection from the ionospheric indicated that the conditions necessary for imaging fluctuations may be satisfied during quiescent periods. The modern method of numerical back projection has been applied to existing microwave measurements on fusion devices. Such analysis indicates that imaging may well be feasible in fusion plasmas during quiescent periods where the turbulent scale length significantly exceeds the free space wavelength of the probe beam. Conditions specific to the core of fusion plasma such as the small amplitude of density fluctions (less than 1%) and the uniformity of the background plasma has been of central importance to the quantitative interpretation of the microwave reflection measurements. This contrasts with the very deep irregularities which often occur in the ionosphere, leading to strong perturbations on the reflected waves. Future developments and new applications of the method in fusion science will be discussed.

LOW FREQUENCY OSCILLATIONS IN A PLASMA WITH SPATIALLY VARIABLE FIELD-ALIGNED FLOW

G. Ganguli
Plasma Physics Division
Naval Research Laboratory
Washington DC 20375 USA

The effects of a transverse gradient in the plasma flow velocity parallel to the ambient magnetic field (Vz) are analyzed. It is shown that a transverse velocity gradient in the parallel ion flow, even in small magnitude (i.e., dVz/dx is much smaller than the ion gyrofrequency), can increase the parallel phase speed of the ion acoustic waves sufficiently to degrade the ion Landau resonance and escape strong ion Landau damping. This results in a significantly lower threshold current for the current driven ion acoustic instability, which can fall below that of the current driven ion cyclotron instability. This also enables the ion acoustic waves to be generated when the ion temperature equals or exceeds the electron temperature. In addition, an ion flow gradient can also lower the threshold for the current driven ion cyclotron instability by reducing the ion cyclotron damping. But more importantly, for a sufficient magnitude, the flow gradient can give rise to a new class of ion cyclotron waves via inverse cyclotron damping. A broadband wave spectrum with multiple cyclotron harmonics is possible. A combination of the multiple cyclotron harmonic waves can result in spiky parallel electric field structures with their peaks separated by an ion cyclotron time. Nonlinear evolution of the waves results in substantial ion heating and cross-field transport, which can affect the meso-scale transport properties. Self-consistent electron flux intensifies with wave growth and indicates modulation at the wave frequency. Spatial gradient in the parallel electron flow is also considered but it is found that they play a minimal role in the low frequency regime. The relevance of these results to natural plasma environments will be discussed.

* This work is supported by the Office of the Naval Research

LABORATORY STUDY OF THE EFFECT OF A MAGNETIC FIELD ALIGNED PLASMA FLOW WITH A TRANSVERSE VELOCITY GRADIENT ON THE EXCITATION OF CURRENT-DRIVEN ION ACOUSTIC AND ION CYCLOTRON WAVES

Agrimson, E. P., D'Angelo, N., Merlino*, R. L.
Department of Physics and Astronomy
The University of Iowa
Iowa City, IA 52242

The effect of a magnetic field aligned plasma flow with a transverse velocity gradient (parallel velocity shear) on the excitation of current-driven ion-acoustic and ion-cyclotron waves was investigated experimentally in a double-ended Q machine. In the absence of parallel velocity shear, the electron drift velocity associated with the parallel current was insufficient to excite ion acoustic waves in our plasma having equal electron and ion temperatures. However, when a sufficient plasma flow with transverse shear was present, current-driven ion acoustic waves were observed [E. P. Agrimson, N. D'Angelo and R. L. Merlino, Phys. Rev. Lett. 86, 5282 (2001)]. This result is in agreement with the theoretical prediction that parallel velocity shear substantially reduces the critical electron drift velocity needed to produce the ion-acoustic instability [V. V. Gavrishchaka, S.B. Ganguli, and G. I. Ganguli, Phys. Rev. Lett. 80, 728 (1998)]. Recently a similar investigation of the effect of parallel velocity shear on the excitation of electrostatic ion-cyclotron (EIC) waves was undertaken. Electrostatic ion-cyclotron waves are known to be readily excited in a single-ended Q machine plasma by drawing an electron current along the magnetic field to a small (at least a few ion gyroradii in diameter) disk electrode immersed in the plasma [see, e.g., J. J. Rasmussen and R. W. Schrittwieser, IEEE Trans. Plasma Sci. 19, 457 (1991)]. However, it seems now that this method of exciting the EIC instability also inevitably involves the presence of parallel velocity shear. We have attempted to systematically study the effects of parallel velocity shear and current and found that under the conditions in which the current is present but the shear is eliminated, the EIC waves are not excited. These results appear to be in general agreement with the theoretical predictions of Gavrishchaka et al. [Phys. Rev. Lett. 85, 4285 (2000)].

Supported by NSF

A KINETIC TREATMENT OF A PERPENDICULAR GRADIENT IN MAGNETIC-FIELD-ALIGNED FLOW IN A THERMALLY ANISOTROPIC PLASMA

Robert S. Spangler, Jr., Earl E. Scime
Department of Physics
West Virginia University
Morgantown, WVa 26501
Gurudas I. Ganguli
Code 6794
Naval Research Laboratory
Washington D.C. 20375-5000

The linearized dispersion relation describing waves in a plasma having a uniform magnetic field, uniform density, and an inhomogeneous parallel (to the magnetic field) flow [G. Ganguli, M.J. Keskinen, H. Romero, R. Heelis, T. Moore, and C. Pollock, J. Geophys. Res., 99, 8873, 1994.] is generalized to include thermal anisotropy, a key feature existing in many space and laboratory plasmas. The effects of thermal anisotropy on the ion acoustic mode and the ion cyclotron mode are examined. The growth rate of the ion acoustic mode is shown to increase with the perpendicular to parallel ion temperature ratio, and the real frequency at which the maximum growth rate occurs is shown to upshift significantly. The angle that an ion acoustic wave propagates is also shown to depend on the ion temperature ratio. The growth rate for the ion cyclotron mode is shown to increase with the perpendicular to parallel ion temperature ratio in the presence of inhomogeneous flow, and the real frequency is not significantly affected. Also presented is a generalized calculation of perturbed distribution functions [Sarfaty, M., S. DeSouza Machado, F. Skiff, Phys. Plasma, 3, 4316, (1996); Skiff, F., IEEE Transactions of Plasma Science, 20, 701, (1992).] to include an inhomogeneous field-aligned flow. Without shear, the first order perturbed distribution as a function of the parallel velocity is independent of the orientation of the wavevector in the plane perpendicular to the background magnetic field. A method of determining the wavevector components present in a plasma with inhomogeneous field-aligned flow is presented. The results are applicable to the FAST mission.

GROUND BASED OBSERVATIONS OF FLICKERING AURORA

McHarg, M.G., US Air Force Academy, CO *
Stenbaek-Nielsen, Geophysical Institute, University of Alaska, Fairbanks

The exact mechanisms for auroral electron acceleration are not fully understood. A comparison of experimentally determined arc thicknesses with 22 different theoretical predictions of arc thicknesses shows very poor agreement (Borovsky, *J. Geophys. Res*, 1993). Of the possible theories examined by Borovsky approximately a third would have temporal fluctuations of the auroral intensity associated with them. Ground based narrow field TV and high speed photometry offer a unique perspective on the spatial and temporal scales of the aurora. Narrow field TV data are used to evaluate the spatial extent, and variations in auroral morphology. A high-speed photometer bore-sighted to narrow field TV is used to explore the fast intensity fluctuations of the auroral light. We observe auroral intensity fluctuations at frequencies above the Nyquist frequency of the TV camera in flickering aurora. We present data that shows a band limited tone of $\approx$ 50 Hertz, that decreases in frequency to $\approx$ 30 Hertz in approximately 3 minutes. Immediately following the band limited tone becomes broad band up to $\approx$ 50 Hertz, followed by a narrow band tone at $\approx$7 Hertz. This narrow band 7-Hertz tone is seen in the narrow filed TV camera as flickering aurora.A possible interpretation of the observed data in terms of a wave particle modulation of the primary electrons causing the auroral light is presented. Possible sources of thewave field are electromagnetic ion cyclotron waves (Temerin et al. *J. Geophys. Res* 1986), and inhomogeneous energy density driven (IEDD) waves (Ganguli et al. , *J. Geophys. Res* 1994, Ganguli in *Cross Scale Coupling in Space Plasma*, Geophysical Monograph No. 93, 1995 and Gavrishchaka et al. *Phys. Plasmas* 1996). While ground based high spatial and temporal resolution observations alone can not alone determine the modulation mechanism of auroral electrons they represent an important contribution to the remote sensing of space plasmas.

GYRORESONANT INTERACTIONS OF LIGHTNING-INDUCED WHISTLERS AND RADIATION BELT ELECTRONS

Inan, U. S.
Space, Telecommunications and Radioscience Laboratory
Stanford University
Stanford, California 94305

Whistler waves injected into the magnetosphere by lightning discharges have long been to interact in cyclotron resonance with radiation belt electrons, leading to amplification of the waves, triggering of emissions, and precipitation of the particles out of their trapped orbits. Lightning-induced Electron Precipitation (LEP) bursts have been directly observed in the bounce-loss-cone on satellite based detectors, allowing for detailed comparison with theoretical predictions. LEP bursts in the bounce loss cone have also been extensively detected from the ground via the associated D region ionization, with individual LEP bursts unambiguously associated with causative lightning discharges. Such measurements indicate that tens to hundreds of LEP events may be produced by a single thunderstorm. However, until mid 1999, the spatial extent of the LEP regions was not known. Formerly, LEP events were thought to be produced *only by ducted* whistlers, which propagate within (and thus affect only the electrons within) filamentary ducts < 400 km at the equator. Uncertainties in the number and size of ducts made it difficult to estimate global consequences of the LEP phenomenon. Two exciting set of new observations now indicate that obliquely propagating non-ducted whistler waves, which permeate much larger regions of the magnetosphere, may regularly precipitate radiation belt electrons over L-shells ranging from the vicinity of the plasmapause to L=1.5. Ground-based VLF imaging has revealed that individual lightning flashes can precipitate significant energetic electron flux over an ionospheric region of $\approx$2000 km horizontal extent, and the SAMPEX spacecraft observed thousands of cases of enhanced fluxes of > 150 keV electrons in the *drift loss cone* (see below) throughout the inner belt and slot regions, typically confined to narrow L-shell intervals, and often associated with thunderstorm activity. The L-dependence of precipitation fluxes observed on SAMPEX are remarkably consistent with predictions of ray tracing analyses for specific locations of active thunderstorms which inject non-ducted whistler waves over a large range of L-shells. Whistler-electron interactions in the inner radiation belt and slot regions may or may not involve amplification of the injected waves and triggering of emissions. However, in the outer radiation belt and in the vicinity of the plasmapause whistlers are commonly known to trigger long enduring bursts of emissions, which in turn precipitate energetic electrons.

DISPERSIVE ALFVEN WAVES: NONLINEAR AND KINETIC EFFECTS

R. Rankin*, J.C. Samson, V.T. Tikhonchuk, J. Wanliss
Department of Physics
University of Alberta

The auroral accelerator contains localized field-aligned potential drops capable of energizing electrons to many keV. One possible explanation involves excitation of dispersive Alfvén field line resonances (FLRs) that lead to inverted-V electron precipitation and density cavities depleted of current carrying electrons. We present results of two-fluid modeling of nightside FLRs on stretched geomagnetic field lines, and discuss the various saturation mechanisms affecting the scale and spatial structure of the excited waves. We classify various nonlinearities affecting the evolution of FLRs, and discuss the need for a kinetic treatment of parallel electron dynamics: The bounce time of electrons on geomagnetic field lines is much smaller than the wave period of observed mHz FLRs, implying that the electron dynamics is very non-local along the field line. The two-fluid MHD formalism therefore breaks down.

Accounting for the mirror force, and solving the Vlasov equation for parallel electron motion, we show that in the auroral accelerator, the Alfvén wave conductivity is much smaller than predicted by two-fluid theory. The large parallel Alfvén wave current and low conductivity lead to very enhanced parallel electric fields, on the order of mV/m. Accounting for hot magnetospheric and cold ionospheric plasma populations, we show that the characteristic electron energy in the accelerator is comparable to the quasistatic potential associated with the density and temperature gradient along the field line. Finally, we compare the results of our model with observations, and indicate how auroral MPA data can be used to infer the stretching of nightside field lines that is necessary to explain the low frequencies of observed FLRs.

CHORUS EMISSIONS FROM THE MAGNETOSPHERE

R.A. Helliwell, Stanford University, Stanford, CA

Chorus emissions are narrowband variable frequency whistler-mode (WM) waves that usually appear in groups, generally called chorus. The individual elements or chorus can be triggered by whistlers, WM echoes of previous chorus elements and by signals (e.g. dot-dash Morse code) from ground-based Vlf stations. Chorus may also arise in a band of WM noise called mid-latitude hiss. A coherent-wave instability (CWI) has been postulated to explain triggered chorus and the amplification of the triggering wave (Helliwell, 1967, JGR, 72(19), 4773; Helliwell and Inan, 1982, JGR, 87, 3537). Vlf wave injection experiments to study the CWI were performed at Siple Station, Antarctica, in the period 1973-1988 (Helliwell, 1988, Rev. of Geophysics, 26(3), 551). One of the most interesting and successful experiments was aimed at generating chorus by injecting artificial hiss. The transmitter signal consisted of a contiguous series of 100 ten-ms pulses at frequencies randomly distributed within a 400 Hz band, typical of a band of natural hiss. This sequence was repeated every second to determine the temporal variation of any correlation between this hiss and chorus emissions. The results showed clearly that certain constellations of 10 ms pulses produced growth and sometimes triggering of discrete chorus elements that continued to grow well above the frequency band of the artificial hiss (Helliwell et al., 1986, JGR, 91, 4381). Other related Siple Station experiments are reviewed elsewhere (Helliwell, 1988, Rev. of Geophysics, 26(3), 551; Helliwell et al, 1990, GRL, 17(5), 599). On the theoretical aspects of the CWI, there are challenging problems resulting from the complexity of the computations required. However some progress has been made in computer simulation of the CWI by limiting the parallel velocity of the resonant electrons to a small range around resonance for a constant frequency input signal. The simulation results predict a characteristic advance in phase with growth of the applied signal, due to the effect of the inhomogeneity (Carlson et al, 1990, JGR, 95, 15,073), which agrees well with the experimental measurement at the conjugate point of the phase of applied signals from the Siple II transmitter (Paschal and Helliwell, 1984, JGR, 89(A4), 1667). In general, the predictions of the CWI are in good agreement with the experiments.

THE ROLE OF ELECTRON DENSITY INHOMOGENEITIES IN IONOSPHERIC RADIO EMISSION

J. LaBelle
Department of Physics and Astronomy
Dartmouth College
Hanover, NH 03755 USA

Mounting evidence suggests that density structure in the source region strongly influences the frequency and time structure of radio waves emitted from ionospheric plasmas. Because the auroral ionosphere contains significant electron density structures over a wide range of spatial scales, as well as highly non-thermal particle distributions for generation of plasma waves, natural auroral radio emissions provide some of the best examples of the role of electron density inhomogeneities in ionospheric radio emission. Here we review two recent examples: Structured Langmuir waves generated by auroral electrons where $f_{pe} > f_{ce}$ in the F-region; and the fine structure of auroral roar emissions. The former phenomenon, called "HF Chirps," consists of multiplet narrow band waves just above the plasma frequency observed with sounding rockets and satellites. These may arise because density cavities of the appropriate spatial scales trap the Langmuir waves and impose a discrete frequency structure on them, which is retained by waves which escape the trapped condition and propagate in the ionosphere, usually for only short distances before they are damped. Another candidate example is the auroral roar emission, a relatively narrow band emission ($\delta f/f \sim 0.1$) that occurs near two and three times the ionospheric electron cyclotron frequency, characterized by fine structure consisting of narrowband (as narrow as 6 Hz) discrete features or multiplets whose frequency rises or falls with time. Evidence suggests that the auroral roar emission originates as upper hybrid waves generated where the upper hybrid frequency matches cyclotron harmonics in the F-region auroral ionosphere, and that these electrostatic waves mode-convert to L-mode and propagate to ground level. Possibly, electron density enhancements of the appropriate spatial scale in the source region trap these upper hybrid waves and impose a discrete frequency structure on them, which is retained by the escaping mode-converted radiation. If these models of auroral radio wave generation are accurate, they point to a more significant role for electron density structure determining emitted wave characteristics than has been previously appreciated.

STIMULATED EMISSIONS AND RADAR SCATTER FROM PULSED RF-IONOSPHERE INTERACTIONS AT HAARP

Sheerin*, J. P., J. P. Mills, Physics and Astronomy, Eastern Michigan Univ., Ypsilanti, MI
Groves, K. M.,AFRL Hanscom, MA
Bristow, W. A., Geophysical Inst., U.Alaska-Fairbanks
Pau, J., A. Y. Wong, Physics and Astronomy, UCLA
Ramos, C., ECE Dept., Cornell

High power HF radiowave pulses launched from ground-based transmitters interact with overdense quies-cent ionospheric plasma to produce strong turbulence effects. These effects are evident in the ion and plasma lines detected by diagnostic radars. Several spatial and temporal signatures in the backscattered plasma lines show reproducible evidence of strong turbulence effects at many scales. Complementary to radar probe diagnostics are stimulated electromagnetic emissions (SEE) which propagate to HF receivers on the ground. Many experiments using SEE receivers have been performed using relatively long (seconds) HF pulses. Long HF pulses are sufficient to produce irregularities and turbulence at several scales incorporating many effects. Effects which dominate for short HF pulses of interest may be masked by turbulence which develops on larger scales for longer HF pulses.

We report a series of experiments performed at HAARP (Gakona, Alaska) using both radar and SEE diagnostics for a wide range of HF pulse widths down to ten mil-liseconds and several HF amplitude modulation frequencies of interest in the ELF range. Using short HF pulses, we are able to discriminate, characterize, and compare prompt SEE spectra over the timescales of typical radar features. The SuperDARN-Kodiak radar reveals the growth of striations for longer HF pulsewidths. The SEE spectra taken during with short, low duty cycle HF pulses may be compared to models of SEE generation mechanisms. SEE spectra were also recorded using HF modulations in ELF range of interest and in the E-region ionosphere. We present the results of numerical simulations modeling the development of strong short-scale turbulence and mesoscale irregularities for comparison with these experiments.

ION HEATING IN THE EARTH'S MAGNETOSPHERE DURING SUBSTORM AND STORM-TIME

E.E. Scime*,A.M. Keese
Department of Physics, West Virginia University
C.J., Pollock
Southwest Research Institute, San Antonio, TX

In this study, energetic neutral atom (ENA) images from the Medium Energy Neutral Atom (MENA) imager on the Imager for Magnetopause-to-Aurora Global Exploration (IMAGE)observatory are analyzed. In the MENA imager, incident ENAs create secondary electrons at a carbon foil and then strike a detector that records their position and time of impact. The electrons are used to determine the trajectory and time-of-flight of the ENA. Unique gold transmission gratings are used to eliminate the intense background ultraviolet light due to the Earth's geocorona. Trajectory information and the spacecraft spin enable two-dimensional ENA images to be constructed. The time between the electron and ENA pulses provides an energy measurement if the ENAs are assumed to be hydrogen. Using the energy spectrum of the MENA neutral flux data, images of the plasma ion temperature are created based on estimates of the peak line-of-sight ion temperature. The geomagnetic activity of the magnetosphere in the images ranges from mildly active to stormy. We find that the remotely measured ion temperatures agree with local, in-situ, ion temperature measurements in the inner magnetosphere. We also find an asymmetry in the ion temperature when comparing the dusk and dawn sectors late in storm intervals; the dawn sector of the magnetosphere appears to be colder. Single particle drifts suggest a simple explanation for the observed asymmetry. Westward drifts due to the gradient and curvature in the local geomagnetic field dominate transport of higher energy ions from the night side. Transport of the lower energy ions is dominated by E x B drift in the background convection field. For typical background convection field strengths, the cross over between these two regimes should occur in the range of a few keV. Thus a bifurcation in energy, with higher energy ions executing gradient and curvature drifts through the dusk side and lower energy ions executing convective drift through the dawn side, would lead to observations of larger ion temperatures on the dusk side and lower temperatures on the dawn side.

Session H2, 13:35-Thurs.

LABORATORY EXPERIMENTS AND SPACECRAFT - PLASMA INTERACTIONS

Chairperson: W.E. Amatucci

DUST PARTICLES DETECTED IN THE OUTER SOLAR SYSTEM BY THE VOYAGER 1 AND 2 PLASMA WAVE INSTRUMENTS

D.A. Gurnett*, A.M. Persoon, W.S. Kurth, L.J. Granroth
Dept. of Physics and Astronomy
University of Iowa
Iowa City, IA 52242,USA

During the Voyager 1 and 2 flybys of the outer planets, it was discovered that the plasma wave instrument could detect small micron-sized particles striking the spacecraft. When a micron-sized particle strikes the spacecraft, the particle is vaporized by the kinetic energy of the collision, thereby producing a small cloud of plasma that expands rapidly away from the impact site. As the plasma cloud sweeps over the plasma wave electric antenna, it produces a voltage pulse. By counting the number of pulses per unit time, the impact rate and number density of the impacting particles can be determined. The particle mass can also be estimated from the amplitude of the voltage pulse.

In this paper we report on measurements of dust impacts detected to heliocentric radial distances of 83.4 AU (astronomical units) for Voyager 1 and 66.0 AU for Voyager 2. For both spacecraft the impact rate has been nearly constant, independent of heliocentric radial distance, at a rate of about 4 impacts per hour for Voyager 1, and about 5 impacts per hour for Voyager 2. The small difference may be due to the fact that Voyager 1 is farther from the ecliptic plane than Voyager 2. The average number density is about 2×10^{-8} m^{-3}. The mass of the impacting particles is difficult to estimate, but is believed to be on the order of 10^{-10} to 10^{-11}g. The absence of strong latitudinal or radial gradients suggest that the particles probably do not originate from planetary rings, moons, or asteroids. Most likely they are of interstellar origin, or possibly from an object orbiting the Sun at great distances, such as comets or Kuiper belt objects.

PARTICLE TRANSPORT IN RF AND DC GLOW DISCHARGE COMPLEX PLASMAS IMPLICATIONS FOR LABORATORY AND MICROGRAVITY STUDIES

E. Thomas
Physics Department
Auburn University
Auburn University, AL 36849 USA
NRL - DUPLEX Team
Naval Research Laboratory
Washington, DC, USA
MPE - Complex Plasma Group
Max Planck Institute for Extraterrestrial Physics
Garching, Germany

Complex (or dusty) plasma research involves the study of the interactions between charged microparticles and plasma in which the microparticles are suspended. Over the past fifteen years, the investigation of these plasma systems has evolved from the characterization of contaminants in industrial processing plasmas to a significant experimental and theoretical scientific research enterprise that currently involves several dozen laboratories around the world.

Much of this effort has focused on strongly coupled phenomena, e.g, the plasma crystal state [H. Thomas, Morfill, Nature, 379, 29 (1996)], or on collective modes, e.g., the dust acoustic waves [Barkan, et. al, Phys. Plasmas, 2, 3563 (1995)] in these systems. Recently, through the use of new optical diagnostic techniques, e.g., particle image velocimetry (PIV) [E. Thomas, Phys. Plasmas, 6, 2672 (1999)] and laser flashing, it is now possible to perform detailed measurements of two dimensional particle transport in complex plasmas. These transport measurements have been used to identify a variety of phenomena in complex plasmas including: the closed transport of the microparticles in suspended clouds and the characterization of possible nonlinear effects in dust acoustic waves. Additionally, these measurements are used in the reconstruction of potential structures in the plasma.

This talk will highlight recent measurements of microparticle transport in both rf-generated and dc-generated glow discharge plasmas. Emphasis will be placed on characterizing similar phenomena that are observed in both systems. Of particular interest are experiments that characterize the motion of individual microparticles approaching boundary layers in both types of complex plasmas systems. Finally, a brief discussion of the relevance of the laboratory results to microgravity phenomena will be given.

GROUND-BASED MEASUREMENTS SIMULATING SPACE ENVIRONMENT INTERACTION OF MATERIALS AND SEE SPACECRAFT CHARGING MATERIALS DATABASE FOR SPACECRAFT CHARGING MODELING

J.R. Dennison
Physics Department
Utah State University
Logan, UT 84322-4415, USA
C.D. Thomson
W.-Y. Chang
Jason Kite
Neal NIckles
R. E. Davies

Materials used for spacecraft and space structures are subject to severe environmental effects including high vacuum conditions, hot and cold extremes temperature, strongly oxidizing atomic oxygen environments, and high fluxes of energetic electrons, ions, neutrals and photons. Instrumentation developed at Utah State University through funding from the AFOSR and NASA Space Environments and Effects Program is designed to simulate, at least to some level, all of these conditions and to study spacecraft-plasma, charged particle, and photon interactions with spacecraft surfaces. Specifically, the chamber provides controlled neutral environments, controlled temperatures, electron fluxes, ion fluxes, photon fluxes, and a wide array of neutral and charged particle and photon detectors. In principle, these capabilities can be used simultaneously, allowing study of synergistic effects. Extensive surface science characterization capabilities are also available to fully characterize the samples in situ. The facilities are particularly well suited to study electron emission as related to spacecraft charging, including electron-induced secondary and backscattered yields, spectra, and angular resolved measurements as a function of incident energy, species and angle, plus ion-induced electron yields and photoelectron yields. Measurements are ongoing to characterize an wide array of spacecraft materials by determining all parameters required for the materials database used in NASCAP spacecraft charging modeling codes. We present here: (i) a description of our instrumentation and specifics of the experimental and analysis methods used; (ii) an overview of the SEE Spacecraft Charging Materials Database, including materials studied and planned for testing in the near future; and (iii) applications of our studies on effects of contamination and surface charging and the use of angle-resolved electron emission spectra to improve modeling of spacecraft charging.

RECENT DEVELOPMENTS OF THE PLASMA IMPEDANCE PROBE TECHNIQUE AT UTAH STATE UNIVERSITY

J. D. Ward*, C. M. Swenson, C. M. Furse, C. Fish
Department of Electrical and Computer Engineering
Utah State University

The electrical impedance of an antenna exposed to the space environment is dependent upon the parameters of the space plasma in which it is immersed (electron density, collision frequencies, external magnetic field, temperature). This effect was first observed by (J. E. Jackson *J. Geophys. Res.*, 64(8), 1074-1075, 1959). Since that time probes have been built and flown to deduce parameters of the space environment based upon this effect. The technique has primarily been used to measure electron density in the Earth's ionosphere by *in situ* measurements on sounding rockets and satellites. It has a significant advantage over Langmuir methods in that it is insensitive to vehicle potential and probe surface contamination.

Proper data analysis requires an accurate theory for the impedance of an antenna immersed in a magnetized plasma. The problem has been solved for electrically short antennas under a quasi-static approximation. The current distribution on the surface of the antenna is assumed and the dielectric tensor for a two component fluid model of a cold plasma is used. It provides a relatively simple expression for the impedance which can be used for data analysis (K. G. Balmain *IEEE Trans. Antennas Propagat.*, AP-17(3), 389-392, 1969).

Utah State University is developing a three dimensional FDTD simulation of an antenna in an ionospheric plasma. This model is based on a fluid description of a warm, colisional, magnitized plasma. These simulation results have been compared to the quasistatic closed form solutions of Balmain. The validated simulation is used to analize geometers with non-standard current distributions, that are imposible thru analytical methods, namely microstrip antennas. These geometries are being explored to simplify the mechanical integration of the impedance probe antenna onto spacecraft.

Utah State University has also developed new instrumentation for plasma frequency and impedance probes based on modern electronic devices. The combined instrument can track the plasma resonance while providing a impedance profile simultaneously. These new instruments will be flying on the NASA CODA rocket in January, 2002, the NASA E-Winds rockets in Fall of 2002 and the NASA/Air Force ION-F satellites in 2003. The additional information provided by these new instruments can be used to extend the diagnostics beyond simple electron density measurements. The goal is to combine improved measurement capability with the FDTD simulation to obtain electron temperature and collision frequency.

MITIGATION OF SPACECRAFT CHARGING FOR THE PURPOSE OF CONDUCTING PLASMA MEASUREMENTS

C.J. Pollock
Southwest Research Institute
6220 Culebra Road
San Antonio, TX 78238
T.E. Moore
Laboratory for Extraterrestrial Physics
Mail Code 692
NASA/Goddard Space Flight Center
Greenbelt, MD 20771

Spacecraft typically float at some electric potential different from that of the plasma in which they are immersed. The value of this potential is determined by the balance of electric currents contributed by photo- and secondary electron emission, and the absorption of plasma electrons and ions. In the vicinity of Earth, spacecraft floating potentials can range from some tens of volts positive under solar illumination in low plasma density regions (such as Earths high altitude magnetospheric polar cap), to thousands of volts negative in eclipse, when immersed in hot plasma. In the low altitude ionosphere, spacecraft typically float at up to 1 Volt negative. The effect of spacecraft charging on local plasma measurements may be important if the magnitude of the floating potential is a significant fraction of the energy-per-charge targeted in the plasma measurements. We will present an overview of techniques used to mitigate the effects of spacecraft charging on plasma measurements. These fall into two categories: spacecraft neutralization, and plasma instrument aperture biasing. Further, we will present examples of plasma measurements that have been modified or actually enabled by these techniques. One important example is the Plasma Source Instrument (PSI), which has routinely enabled the observation of terrestrial polar wind outflow by the Thermal Ion Dynamics Experiment (TIDE) on NASAs Polar satellite. The PSI produces Xe^{+} plasma that establishes a low impedance electrical connection between the satellite and the ambient plasma, thereby reliably reducing the spacecraft potential in regions of polar wind outflow from several tens of volts to the order of $+1$ volt.

PROPERTIES OF THE AURORAL ZONE IONOSPHERE INFERRED USING PLASMA CONTACTOR DATA FROM THE INTERNATIONAL SPACE STATION

S.L. Koontz, E.A. Bering, III*+, NASA/JSC, Houston
+ Also at Physics Dept., Univ. of Houston, Houston
D.S. Evans, SEL, NOAA, Boulder
I. Katzddag, B. Gardner, SAIC, San Diego
now at JPL, Pasadena
R.M. Suggs, J.I. Minow, NASA/MSFC, Huntsville
P.J. Dalton, D.C. Ferguson, G.B. Hillard, NASA/GRC, Cleveland
J.L. Counts, H. Barsamian, J. Kern, R. Mikatarian, Boeing, Canoga Park and Houston

Comparison of the auroral electron precipitation maps produced by the NOAA POES satellite constellation with the flight path of the International Space Station (ISS) reveals that ISS regularly passes through the southern auroral oval south of Australia. During the first few months of 2001, ISS configuration and flight attitude were such that tensioning rods on the space station solar array masts could collect current from the ionosphere in the same way as a bare wire antenna or electrodynamic tether. The ISS has two plasma contactors that emit the electron currents needed to balance electron collection by surfaces such as the lattice of bare rods on the solar array masts. During this period, these electron currents exceeded 0.1 A at times. The largest currents were observed in the auroral oval south of Australia, often after orbital sunset. On the space station, the solar array 40 m long masts each have over 400 m of stainless steel tensioning rods. When subject to orbital $\mathbf{v} \times \mathbf{B} \cdot \mathbf{l}$ induced potentials, the rods collect substantial currents from the ionosphere. Models of the mast collection processes based upon J. R. Sanmartin's bare wire collection theory have been incorporated into computer codes that integrate models of the station geometry, orbital motion, earth's magnetic field, and ionosphere to obtain plasma contactor emission currents. During the period being analyzed, the station flew in an orientation such that the masts were perpendicular to the orbital velocity vector, and parallel to the earth's surface. Maximum $\mathbf{v} \times \mathbf{B} \cdot \mathbf{l}$ potentials are generated near the magnetic poles. The current drawn by the masts is linearly proportional to the plasma density. The plasma contactor emission current can be converted to an estimate of plasma density. These measurements show that the plasma density in the nighttime auroral ionosphere is frequently several times that predicted by the International Reference Ionosphere (IRI)-90 and IRI-2001 models. We will discuss how the observations order themselves with geomagnetic activity. We will compare the peak densities with auroral energy inputs inferred from electron precipitation monitors on the NOAA-15 and NOAA-16 spacecraft.

MEASUREMENTS OF SHEAR ALFVÉN WAVE DISPERSION FOR FINITE PERPENDICULAR WAVE NUMBER

C. A. Kletzing, S. R. Bounds
Department of Physics and Astronomy
203 Van Allen Hall
University of Iowa
Iowa City, IA, 52245
W. Gekelman, C. Mitchell
Department of Physics
University of California Los Angeles
1000 Veteran Avenue, Suite 15-70
Los Angeles, CA, 90095-1696

Shear Alfvén waves are thought to play a significant role in several regions of near-Earth space including the plasma sheet, magnetopause, and auroral zone. The interesting physics occurs when the waves have narrow perpendicular structure. Two limiting cases are usually considered: 1) the inertial case ($V_{th} < V_A$) for which the perpendicular length scale is set by the electron skin depth and 2) the kinetic the case ($v_{th} > v_A$) for which the key perpendicular scale is the ion acoustic gyroradius. Although the dispersion relation for these waves has been derived by several authors, direct experimental measurements to verify the dispersion relation have been few. We present an experimental determination of the shear Alfvén wave dispersion relation as a function of perpendicular wave number made at the LArge Plasma Device at UCLA as part of space and laboratory physics collaboration. The dispersion relation comparison is derived from measurements of the parallel phase velocity of shear Alfvén waves. The phase velocity is determined by timing wave peak travel times between two fixed locations. Examples of the waveforms and the cross-correlation technique used to find the phase velocity will be presented. The measurements are for a case which lies between the inertial and kinetic limit cases, providing a test of different forms of the dispersion relation. The measured wave dispersion is compared with both fluid and fully kinetic dispersion relations, which shows that although the fluid dispersion relation gives the correct basic form of the dispersion relation variation with perpendicular wave number, good agreement between data and theory requires the use of the kinetic dispersion relation with finite frequency corrections.

ION JOULE HEATING IN LABORATORY SIMULATIONS OF SPACE PLASMA PROCESSES*

Walker, D.N., W.E. Amatucci, G.I. Ganguli, R.F. Fernsler
Plasma Physics Division
Naval Research Laboratory
Washington, DC 20375, USA

As a part of a laboratory-based experimental effort we demonstrated the ability to control the magnitude and direction of the electric field (or the sign of potential change) in space in a simulated ionospheric environment. We are able to produce ion heating in this environment as a function of ion-neutral collision frequency consistent with the calculated Joule heating rate. Ultimately we wish to fully characterize the effect of electric field structure on the heating by varying the localization of the fields (e.g., creating multiply-peaked potential distributions, varying the scale size of the field) and by allowing the potentials to have a time-dependent amplitude. In space, this implies multiple localized structuring and in time it implies a frequency variation from the ELF range to the ion plasma frequency. In results presented here, we have increased the data sample and varied the spatial size of the fields. In a few instances we have produced doubly-peaked potential profiles. Consistent with earlier results, we have been able to demonstrate a peak in the ion temperature as a function of collision frequency. New results shown in this data indicate that for approximately constant pressure and electric field, the normalized ion temperature increases with the scale size of the electric field region but the data suggests a limit to this increase (for a given scale size). We base this conclusion on using the frequency-width-at-half-maximum (fwhm) of the electric field region as a marker of the spatial scale size which we designate as L_E. We will present analysis of data which depends on scale size comparisons among L_E, the mean free path for ion neutral collisions and the ion gyroradius.

* Work supported by ONR

LABORATORY MEASUREMENTS OF ION DRIFTS AND DENSITY PERTURBATIONS ASSOCIATED WITH LARGE AMPLITUDE SHEAR ALFVÉN WAVES

Palmer, N.E., Gekelman, W.N.
Dept. of Physics, UCLA
Los Angeles, CA 90095, USA

Measurements from spacecraft such as Freja, FAST, and Polar have stimulated discussion of the importance of Alfvén waves in auroral processes. Alfvén waves have been observed in the ionosphere in connection with narrow field-aligned density striations and accelerated electron fluxes, and the component of the wave electric field along $\mathbf{B}$ (i.e., $E_{\|}$) is one possible acceleration mechanism. Recent experiments in the Large Plasma Device at UCLA have studied in detail the ion drifts and density perturbations associated with large amplitude ($B_{wave}/B_0 \sim 10^{-3}$) shear Alfvén waves launched from an inductive loop antenna in an argon plasma. Two-dimensional laser-induced fluorescence (LIF) was used to make direct time-resolved measurements of the ion drifts and temperature in four cross-sectional planes along the path of the wave. At the frequency of the wave ($0.8\omega_{ci}$) the LIF data are a superposition of the $\mathbf{E} \times \mathbf{B}$ and polarization drift signals, but the two drifts can be distinguished by their phase relation to $\mathbf{B}_{\text{wave}}$. Correlated measurements of $\partial\mathbf{B}/\partial t$ at the same spatial positions as the LIF measurements allow us to compute $\mathbf{E}_{\perp}$ from the drifts, and then estimate $E_{\|}$ from the appropriate dispersion relation. For the conditions of this experiment with $B_0 = 1200$ G and $n = 1.4 \times 10^{12}$ cm^{-3}, the maximum wave fields measured were $B_{wave} = 0.66$ G, $E_{\perp} = 25$ V/m, and $E_{\|} \approx 0.5$ V/m ($E_{\|}/E_{\perp} \approx 1/50$). At lower frequencies the LIF data exhibit ion flows that can be related to plasma density perturbations ($\delta n/n \sim 0.1$) measured with Langmuir probe techniques. The four planes of measurements all together reveal the comprehensive structure and propagation of the wave as well as a detailed description of the ion motion.

ON THE ROLE OF LOWER HYBRID COLLAPSE IN THE AURORAL IONOSPHERE

Schuck, P. W.
NRC Postdoctoral Fellow
Schuck, P. W., Ganguli, G. I.
Naval Research Laboratory
4555 Overlook Ave., SW
Washington, DC, 20375-5320
Kintner, P. M.
Cornell University
Ithaca, NY, 14853

Very low frequency (VLF) hiss comprised of quasi-electrostatic whistler waves is the most ubiquitous emission observed in the auroral ionosphere. This emission exhibits a sharp lower cutoff at the local lower hybrid resonance $\omega = \omega_i/\sqrt{1+\omega_e^2/\Omega_e^2}$ where ω_i and ω_e are the ion and electron plasma frequencies and Ω_e is the electron cyclotron frequency. Frequently large amplitude VLF wave are observed to be localized in small scale density depletions of a few to tens of percent and 20-100 m in diameter. This phenomena, termed Lower hybrid solitary structures (LHSS), is associated with ion heating at altitudes accessible to sounding rockets.

The correlation between large amplitude electric fields and density depletions motivated several attempts to explain the observations via a soliton collapse process using the Musher-Sturman equations [V. D. Shapiro *et al.* Phys. Fluids. B **9**, 3148, 1993]. Statistical analysis of the LHSS observed by the Freja satellite have not supported the collapse theories because of large discrepancies between theoretical predictions and the observed structure widths, density depletion depths, electric field strengths, and pertinent time-scales [H. L. Pecseli *et al.*, J. Geophys. Res. **101**, 5299, 1996].

Recently, *Robinson* has attempted to reconcile these discrepancies with a theory of strong lower hybrid turbulence based on the *nucleation cycle* [P. A. Robinson, *et al.*, Phys. Plasmas **3**, 133, 1996; P. A. Robinson, Adv. Space Res. **23**, 1679, 1999]. According to this scenario, the auroral plasma consists of wave packets of localized, coherent lower hybrid states trapped in density depletions which are embedded in a background of low-level, incoherent turbulence. The nucleation cycle predicts the statistical properties of strong turbulence as a whole (the incoherent and coherent) in contrast to theories which focus on the collapse of a single, isolated, coherent wave packet.

We examine the statistical properties of the lower hybrid turbulence observed by the TOPAZ III sounding rocket. This experiment observed several thousand LHSS during the 20 minute flight. We conclude the collapse plays little to no role in the dynamics of LHSS observed in the auroral ionosphere.

SPACE CHAMBER INVESTIGATION OF MAGNETOSPHERIC BOUNDARY LAYER DYNAMICS

M. M. Balkey,* W. E. Amatucci, G. Ganguli, D. N. Walker
Plasma Physics Division
Naval Research Laboratory

Laboratory experiments have been conducted to simulate the dynamics of magnetospheric boundary layers. During periods of high solar activity these regions, such as the plasma sheet boundary layer and the magnetopause, can become severely compressed. At times, these boundary layers are compressed to scale lengths on the order of and smaller than the ion gyroradius. Under these conditions, a steep density gradient is formed along with static transverse (to $\mathbf{B}$) electric field structures. Since the scale size of the electric field structure is smaller than an ion gyroradius, the ions do not experience a fully developed $\mathbf{E} \times \mathbf{B}$ drift while the electrons experience the usual $\mathbf{E} \times \mathbf{B}$ drift. This leads to a sheared cross magnetic field electron flow with respect to the ions. Theoretical analysis indicates that this plasma condition is unstable to the electron-ion-hybrid (EIH) instability in the lower hybrid frequency range (Ganguli et al. it Phys. Fluids, **31**, 2753, 1988). The NRL Space Physics Simulation Chamber (SPSC) experiments reported here demonstrate the characteristics of waves associated with stressed boundary layers. Electric fields with scale length as small as $\sim 0.25\rho_i$ have been created using a novel technique in which two interpenetrating plasmas have independently controllable plasma potentials. Under these conditions, the onset of an instability in the lower hybrid frequency range has been observed with mode characteristics that are similar to those expected for the EIH Instability (Romero et al. *Geophys. Res. Lett.*, **17**, 2313, 1990). The SPSC experiment shows that waves propagate transverse to $\mathbf{B}$ and mode frequencies both above and below the lower hybrid frequency have been observed. We present experimental results showing the transverse electric field structure and the associated wave characteristics.

*Work supported by the Office of Naval Research.

Session H3, 13:35-Sat.

WAVES IN DUSTY PLASMAS

Chairpersons: R.L. Merlino

CROSS-FIELD INSTABILITIES IN COLLISIONAL DUSTY PLASMAS

M. Rosenberg
Department of Electrical and Computer Engineering
University of California, San Diego
La Jolla, CA 92093-0407

Dusty plasmas (ionized gases containing micron to sub-micron sized charged dust grains) occur in many space and astrophysical environments and in various laboratory plasma devices. The presence of charged, massive dust grains in a plasma can both modify the behavior of standard ion waves and instabilities and lead to the appearance of new very low frequency dust waves and instabilities. In this talk, some recent work on instabilities in weakly ionized, collisional dusty plasmas is discussed with attention given to dusty plasmas in the Earth's upper mesosphere or lower E region [e.g. dusty meteor trails, polar mesosphere summer echo (PMSE) regions]. Instabilities driven by particle drifts across the magnetic field are considered.

First, the effect of charged dust on the Farley-Buneman (two-stream) instability is discussed for plasma parameters representative of the lower E region at $\sim 90 - 100$ km (Rosenberg, *IEEE Trans. Plasma Sci.*, **29**, 261-266, 2001). While the presence of negatively charged dust can lower the critical electron drift for instability at lower altitudes, it can increase the critical drift at higher altitudes; the presence of positively charged dust can have the opposite effect.

Next, a low frequency Hall current instability in the dust acoustic frequency regime is discussed for dusty plasmas in the lower E region (Rosenberg and Shukla, *J. Geophys. Res.*, **105**, 23135-39, 2000). For certain plasma and dust parameters (e.g., the presence of a sufficient density of dust grains with large positive charge), the critical electron $\mathbf{E} \times \mathbf{B}$ drift for instability may be $\lesssim$ the ion thermal speed.

Finally, the above analyses are extended to consider the effects of diamagnetic drifts associated with plasma density gradients due to the presence of localized regions of charged dust. Applications to dusty meteor trails, PMSE, and collisional dusty plasmas in the laboratory are discussed.

AN OVERVIEW OF DROPPS: A PROGRAM TO STUDY THE POLAR SUMMER MESOSPHERE WITH ROCKET, LIDAR AND RADAR MEASUREMENTS

R. A. Goldberg*
Laboratory for Extraterrestrial Physics
Code 690
NASA Goddard Space Flight Center
Greenbelt, MD 20771

DROPPS is an acronym for The Distribution and Role of Particles in the Polar Summer Mesosphere. During July, 1999, two sequences of rockets were launched from Andya Rocket Range, Norway. The purpose was to investigate the polar summer mesosphere, particularly polar mesospheric summer echoes (PMSE) and their possible relationship to noctilucent clouds (NLC). ALOMAR Lidar and the ALWIN MST Radar were used to continuously monitor the mesosphere for NLCs and PMSEs. EISCAT VHF radar provided information about PMSEs downstream from the launch site. Sequence 1 was launched during the night of 5-6 July into a strong PMSE display with a weak NLC at the base of the PMSE. Sequence 2 was launched on the early morning of 14 July into a strong NLC, but unexpectedly with no PMSE evident. Of note was the observed presence of negatively charged particulates or aerosols within the PMSE region, which also contained an electron "biteout" that could be indicative of scavenging. The PMSE layer contained electrodynamic turbulence or irregularities, which was less evident within the observed NLCs. Spectral plots of the A.C. electric field during the first flight show higher frequencies generated within the NLC region than in the PMSE region, although the particle size within the NLC was somewhat larger. Meteorological data from the MET payloads show a wind shear which could have generated neutral turbulence within the PMSE on the first night, but which was absent on the second. Finally, the electron density during Sequence 2 was significantly lower than during Sequence 1, which could help explain the absence of a PMSE observation during the second sequence. Implications regarding the origin of PMSEs and their relationship to NLCs are discussed.

SOME THOUGHTS ON MICROMETEOROIDS [illegible]Y PLASMAS

J. D. Mathews
Communications and Space Sciences Laboratory
Penn State University
University Park, PA 16802-2707

Nanometer through 100 micron sized) charged particles are important plasma processes in the upper atmosphere as well as in the solar and local galactic environments. Recent VHF and UHF radar observations of micrometeors at Arecibo Observatory have yielded important information regarding various properties of these particles. Our current understanding of the process of micrometeoroid interaction with the atmosphere and the resultant generation of the "plamsa coma" that gives rise to the radar "head-echo" is reviewed. Also reviewed are the new estimates of the whole earth mass flux over a particle mass range of $\sim 10^{-5} - 10^{2}$ μgm and the evidence for terminal impulsive destruction of these particles rather than gradual ablation. The impulsive destruction of these particles is likely a significant source of nanometer "smoke" particles in the upper atmosphere and also offers an explanation of the so-called Calcium anomaly in the meteor zone. These smoke particles are almost certainly very important to the formation of high-latitude noctilucent clouds (NLCs) and to the radar visible Polar Mesospheric Summer Echoes (PMSEs).

The orbital properties of these particles as determined by the radar observations are also reviewed. In particular, particle charging effects in addition to radiation pressure and Poynting-Robertson drag cause the particle orbit to rapidly "forget" their origins. However, a stream of interstellar particles apparently produced in the Geminga pulsar progenitor supernova has been identified. We note the importance of understanding particle charging processes and the dependence on the materials involved. We also note the question of cosmic ray induced permanent charging of these

USTY WAKES: EFFECTS OF CHARGED DUST ON WAKE DYNAMICS

L.J Gelinas, M.C. Kelley
Cornell University
Ithaca, NY
M.F. Larsen
Clemson University
Clemson, SC
C.L. Siefring, P.A. Bernhardt
Naval Research Laboratory
Washington, DC

Recent observations of artificial aurora associated with mesospheri
TMA (trimethyl aluminum) releases suggest that dusty plasma effects could
be responsible for the auroral-type emissions (Gelinas et al., 2001). Observa-
tions of artificial aurora associated with a TMA release began several years
ago when a small amount of kerosene was added to the TMA payload dur-
ing the loading process. The aurora develops 10 to 20 km below the rocket,
projected down along the magnetic field line that the rocket is crossing. and
persists for several minutes. Electric field strengths on the order of several
V/m may can excite airglow emissions, mimicking 'natural' aurora, and the
fairly long lifetime of the process leads us to believe that a slowly-diffusing
ast-contaminated wake may be responsible for this electric field generation.

Plasma ions are depleted in the wake of a supersonic rocket payload
g through the ionosphere, leaving behind a net negative charge, since
rmal electrons are undisturbed. In an electron-ion plasma this charge
e is quickly neutralized by motion of the electrons out of the charged
enging neutral dust particles to the wake can significantly chang
mics, effectively changing the times scales over which the
e is neutralized. These persistent electric fields in the wake
ersonic "dusty" objects may be responsible for the auroral-
ved in the TMA aurora, either by particle acceleration
We discuss the ways in which dust particles, both charged and
ke dynamics of supersonic objects in the Earth's meso-
the production of artificial aurora.

TRAPPED IONS AROUND A DUST GRAIN IN PLASMA: EFFECT ON SHIELDING AND GRAIN CHARGING

Martin Lampe, Gurudas Ganguli, Glenn Joyce
Naval Research Laboratory, Washington, DC 20375-5346
Valeriy Gavrishchaka
SAIC, McLean, VA 22102

The problem of electrostatic shielding around a small spherical collector immersed in plasma, and the related problem of electron and ion flow to the collector, date to the origins of plasma physics. The earliest work by Langmuir[1] was motivated by probe theory, subsequent work was also directed toward spacecraft charging, and recently there has been considerable interest in connection with the physics of "dust grains" in plasma. Theoretical analyses of these problems have generally been based on the assumption that collisions can be neglected, since the mean free path is typically long compared to the Debye shielding lambda. However, investigators beginning with Bernstein[2] have speculated that negative-energy trapped ions, created by occasional collisions, might be important. We have performed an analytic calculation of the density of both trapped and untrapped ions, self-consistent with a calculation of the potential.[3] We show that under typical conditions for dust grains immersed in a discharge plasma, trapped ions dominate the shielding cloud in steady state, even in the limit of very long mean free path. In fact, the density of trapped ions in steady state is independent of the mean free path, as pointed out by Goree.[3] The problem depends mainly on two dimensionless parameters, t=Tn/Te and u=a/lambda, where Tn is the neutral molecule temperature, Te is the electron temperature, and a is the grain radius. The trapped ion density near the grain can be many times larger than the untrapped density in the regime u**2 much less than t much less than 1, and as a result the shielded potential is different from the results of orbital motion limited theory. Collisions also increase the ion current to the grain. Although this effect is proportional to the collision frequency, the proportionality constant is very large, and trapped ions dominate the ion current even when the collision frequency is quite small. As a result, the negative floating potential of the grain, and the charge on the grain, can be suppressed by a factor as large as two to three. These analytic results appear to be in general agreement with a recent Monte Carlo calculation by Zobnin, et al.[5]
Supported by Office of Naval Research and NASA
1. H. Mott-Smith and I. Langmuir, Phys. Rev. 28, 27 (1926).
2. I. Bernstein and I. Rabinowitz, Phys. Fluids 2,112(1959).
3. M. Lampe, et al, Phys. Rev. Lett. 86, 5278-5281 (2001).
4. J. Goree, Phys. Rev. Lett. 69, 277 (1992).
5. A. V. Zobnin, et al, JETP 91, 483 (2000).

EXPERIMENTAL EVIDENCE FOR DEBYE SHIELDING OF DUST BY ORBITING IONS

Z. Sternovsky,* S. Robertson
Department of Physics
University of Colorado
Boulder, CO 80309-0390, USA
D. Kingrey
Department of Physics
Cornell University
Ithaca, NY 14853

Theoretical and numerical models [Lampe et al., PRL 86, 5278 (2001); Goree, PRL 69, 277 (1992)] have shown that the Debye shielding cloud around negatively charged dust particles may contain a large fraction of trapped ions. In a search for these ions, we have modified an experiment in which the charge on dust particles is measured in a Faraday cup after they have fallen through a plasma in a DP plasma device [PRL 75, 838 (1995)]. The particles are silicon dioxide less than 0.15 mm in diameter and the plasma density is adjusted for a 1 mm Debye length for ions from charge exchange collisions. The pressure of argon is adjusted to give many of these collisions in the time of flight. A bias voltage on the entrance tube to the cup is used to locally remove the sheath at the wall. An electric field between the entrance tube and the Faraday cup may or may not be applied to remove the orbiting ions. The grain charging potential is about -10 V. The charge deposited in the cup by grains 0.14 mm in diameter is made 20 percent more negative by the application of a 100 V/cm electric field (pointing away from the cup) which is consistent with the removal of about 10*5 orbiting ions. The reversal of the polarity of the electric field draws ions into the cup and the measured charge is the same as with no field. The charge on 0.08 mm grains is more negative by 40 percent, which is consistent with the smaller fraction of orbits which would intersect the smaller grains. Further experiments are in progress. This research is supported by the U.S. Department of Energy.

H3.7

ROTATING TOROIDAL DUST CLOUDS IN THE NRL LARGE VOLUME DUSTY PLASMA EXPERIMENT: INITIAL OBSERVATIONS AND PARTICLE VELOCITY ANALYSIS*

*dcci**
W. Physics Division, Code 6755
Research Laboratory
Washington, DC 20375
Thomas, Jr., C.S. Compton, B.J. Christy
sics Department
burn University
Auburn, AL 36849

cently, experiments on the physics of dusty plasmas have begun in the
esearch Laboratory's newly constructed Large Volume Dusty Plasma
iment (DUPLEX). This chamber has been constructed using transpar-
polycarbonate walls, allowing for nearly 360 degree visibility of its large
ume plasma. The DUPLEX plasma is an argon dc glow discharge operated
t pressures ranging from 50 to 250 mtorr and voltages ranging from 500 to
1000 V. The dust grains are 1 micron alumina particles located on the dis-
charge cathode, which become charged and levitated in the plasma. Large
volume toroidal dust cloud structures that rotate in both the azimuthal (i.e.,
about the cylindrical axis) and poloidal (i.e., about the toroidal axis) direc-
tions have been observed to spontaneously form within the system. These
structures have been investigated in a recent collaborative effort between the
Naval Research Laboratory and Auburn University. The shape and rotation
characteristics of the structures are found to depend sensitively on character-
istics of the background plasma such as the neutral pressure and discharge
voltage. We present detailed analysis of the spatially resolved motion of the
dust grains suspended in the argon plasma. Spatially resolved two-dimension
measurements of the rotational velocities of the particles are made using
Auburn University Particle Image Velocimetry(PIV) laser system [E. The
Jr., *Phys. Plasmas*, **6**, 2672 (1999)]. Examples illustrating the morpholo
mation of central voids, particle transport, and disruption of the clou
presented. Analysis of a number of variables, including the radial a
velocities and angular accelerations of the dust grains will be desc

*Work supported by the Office of Naval Research and the
ence Foundation.

H3.8

Session J1, 13:35-Wed.

NEW MILLIMETER AND SUBMILLIMETER WAVELENGTH ARRAYS

Chairperson: J. Mangum

THE SUBMILLIMETER ARRAY PROJECT

J.M. Moran
Harvard-Smithsonian Center for Astrophysics
Cambridge, MA 02138, USA

The Submilllimeter Array is a joint project of the Smithsonian Astrophysical Observatory and the Academia Sinica Institute for Astronomy and Astrophysics (Taiwan). The Array will consist of eight 6-m antennas, which are moveable among 24 pads near the summit of Mauna Kea in Hawaii. Baselines will range from 8 to 500 meters. The array will cover all bands in the region from 180 to 900 GHz.

The status of the Array as of September 1, 2001, is as follows: Four antennas (six baselines) are operating at 230 and 345 GHz with a total bandwidth of about 360 MHz and a resolution of about 0.5 MHz. Five pads are available, which provide baseline spacings from about 17 to 75 meters. Two of these antennas are equipped with 650 GHz receivers. Another antenna, the first of two from ASIAA, is undergoing preliminary tests on Mauna Kea. Another is in an advanced stage of assembly on the mountain.

The final two antennas are scheduled for deployment in January and June, 2002. The hardware for the digital portion of the hybrid correlator is complete, and is being brought on line incrementally. Full bandwidth capability will not be achieved until the end of 2002.

The reflector for each antenna has 72 machined aluminum panels mounted on a backup structure of carbon fiber tubes. The reflector surfaces are being adjusted by holography with the use of an artificial beacon at 230 GHz with measurements acquired in interferometric mode through the correlator. One reflector has been adjusted to the design goal of 12 microns rms.

Data at 345 GHz is being acquired on several sources that have both continuum and CO emission for testing purposes. These include the late type stars CRL 618 and CRL 2688, the star forming region AFGL 5142 and the planets. SgrA* is also being monitored. These results and other test measurements will be described in this talk. The current status of the instrument is described on the project web site: http://sma-www.harvard.edu.

THE SUNYAEV-ZEL'DOVICH ARRAY

Carlstrom, J.E., for the SZA collaboration
University of Chicago

The Sunyaev-Zel'dovich Effect (SZE) is a small spectral distortion of the Cosmic Microwave Background (CMB) induced by the scattering of the CMB photons off the hot, ionized, atmospheres of galaxy clusters. SZE measurements can be used to make independent determinations of several cosmological parameters including the Hubble constant and the matter density of the Universe. Only recently has high quality imaging of the SZE toward selected massive clusters been possible. The advances have been possible due to new techniques and instrumentation. The focus is now shifting from SZE observations of x-ray detected galaxy clusters to conducting large scale surveys for clusters through their SZE. SZE surveys should provide large samples of galaxy clusters with a simple and well defined selection criteria. A powerful and unique aspect of SZE surveys is that the cluster detection limit is a mass threshold with essentially no redshift dependence. The large number clusters and clean selection criteria of the SZE surveys will enable large improvements to the Hubble constant and other cosmological parameters. More importantly, the surveys will allow us to probe directly the evolution of structure in the universe, which in turn will allow us to set constraints on the underlying cosmology.

The Sunyaev-Zel'dovich Array (SZA) is a designed to conduct deep SZE cluster surveys over tens of square degrees. The SZA builds upon the success of the OVRO/BIMA SZE imaging system, in which low-noise cm-wave receivers are mounted on the mm-wave telescopes during the summer months. The SZA consists of eight 3.5 m telescopes with low-noise HEMT amplifier based receivers operating at Ka band (26 - 36 GHz) and W band (85 - 115 GHz). A version of the COBRA digital correlator will be use to provide 8 GHz of instantaneous bandwidth. The SZE will be located at the Owens Valley Radio Observatory. The SZA will also be used for a fraction of the time with the six 10.4 m OVRO telescopes to form a novel heterogeneous array.

AMIBA - A TECHNICAL OVERVIEW

R. N. Martin*
ASIAA - Hawaii Operations
82 Pu'uhonu Place, Suite 210
Hilo, HI 96720-2010 USA

K. Y. Lo
ASIAA
P.O. Box 23-141
Taipei 106, TAIWAN

As part of a 4-year Cosmology and Particle Astrophysics (CosPA) Research Excellence Initiative in Taiwan, AMiBA (a 19-element dual-channel 85-105 GHz interferometer array) is being specifically built to search for high redshift clusters of galaxies via the Sunyaev-Zeldovich Effect(SZE). In addition, AMiBA will have full polarization capabilities, in order to probe the polarization properties of the Cosmic Microwave Background. AMiBA, to be sited in Hawaii, will reach a sensitivity of 1 mJy or 7 K in 1 hour. The project involves extensive international scientific and technical collaborations. Researchers from Academia Sinica Institute of Astronomy and Astrophysics (ASIAA), National Taiwan University (NTU), Australia Telescope National Facility (ATNF), Canadian Institute of Theoretical Astrophysics (CITA), University of Toronto, Carnegie Mellon University, University of Pennsylvania, and Bristol University are collaborators in the AMiBA project. The construction of AMiBA is scheduled to begin on site in 2002. The AMiBA facility will start operations in early 2004.

There are three principal science goals for AMiBA: (1) a survey for high z clusters via the SZE; (2) in search of the missing baryons in large scale structures via the SZE; and (3) the polarization of the CMB.

The AMiBA telescope is a platform array of 19 elements. Each element is a dual polarization, cooled receiver package with a dish attached to the top for optics. Two dish sizes, 0.32 m and 1.18 m are being constructed for AMiBA. The dishes are interchangeable for mounting on the receiver packages. The entire array of elements is connected together via an analog cross correlator which provides for the full polarization correlation products.

To evaluate many of the designs involved in the AMiBA project, a prototype system is being developed first. The prototype will consist of two receiver packages on a simple mount. The prototype will be assembled and begin testing in the first quarter of 2002.

COMBINED ARRAY FOR MILLIMETER ASTRONOMY

A. J. Beasley, D. P. Woody
CARMA/OVRO
Big Pine, CA 93513, USA

The Combined Array for Millimeter Astronomy, CARMA, will combine the two existing US millimeter arrays, the BIMA Hatcreek array and the Caltech OVRO array on a new high-altitude site in the mountains east of the Owens Valley Radio Observatory. The CARMA consortium consists of four universities: the California Institute of Technology, the University of California at Berkeley, the University of Illinois and the University of Maryland. CARMA will be a heterogeneous array of six 10m antennas and nine 6m antennas. There are several potential sites, ranging in altitude from 7,200 to 8,200 ft. altitude, all with access to 2-3km baselines.

The 225 GHz opacity at the new sites is a factor of two lower than the 4,000 ft. valley floor, consistent with a 2km scale height for atmospheric water vapor. The wide field imaging and point source sensitivity of CARMA will be more than double that of the existing instruments. The 105 baselines and two different antenna sizes will dramatically improve the image quality on all size scales. An array of eight 3.5m antennas will also be built at the CARMA site for Sunyaev Zel'dovich effect observations. This array can be incorporated into CARMA for complete imaging of very wide fields.

The telescopes will continue to operate in the 3mm and 1mm bands with 4GHz of IF bandwidth and dual polarization capability for both bands. The COBRA correlator being developed for OVRO will be expanded to handle the increased number of baselines from CARMA while still providing 8GHz of processed bandwidth, 4GHz from each of two polarizations. Tropospheric phase correction using multi-channel 22GHz radiometers will be an important part of maximizing the science output from CARMA.

MILLIMETER WAVELENGTH CAPABILITIES OF THE EVLA

P.J. Napier
PO Box 0
Socorro NM 87801

The goal of the Very Large Array Expansion (EVLA) Project is to improve the frequency coverage, sensitivity and resolution of the VLA radiotelescope. In the first phase of the project, which has now begun, new receivers and a much wider bandwidth correlator will provide a significant new observing capability in the long-millimeter-wavelength bands. The three highest frequency bands of the EVLA suite of receivers will be 18.0-26.5 GHz, 26.5-40.0 GHz and 40.0-50.0 GHz. The system temperatures and antenna aperture efficiencies for these bands will be 54K, 0.52; 45K, 0.39; 66K, 0.34; respectively. The 66K system temperature for the highest frequency band will only be achieved in the lower end of the band where atmospheric absorption is lowest. The 26.5-40 GHz band will be available by 2009 and the other two bands are already available.

The new correlator, which will be available in 2009, will allow processing of 8 GHz of continuum bandwidth for each of the two circular polarizations provided by the receivers. The sensitivity will be such that phase and pointing calibrators will be available within a degree or two of any point on the sky. This will allow phase coherence to be achieved on even the longest VLA baselines by rapidly (15 seconds of time) switching between a phase calibrator and a target source. Another approach to phase calibration that is being studied is the use of the 18.0-26.5 GHz receiver as a water-vapor radiometer. Antenna pointing to an accuracy of 3 arc.sec., a twentieth of a beamwidth at 50 GHz, will be possible by offset pointing from a nearby pointing calibrator.

The performance and design goals and current design status of the EVLA Project will be reviewed during the talk.

ALMA SITE AND CONFIGURATIONS

Simon J. E. Radford
National Radio Astronomy Observatory
949 North Cherry Avenue
Tucson, Arizona 85721

The international Atacama Large Millimeter Array will be constructed on the high (5050 m) plateau southwest of Cerro Chajnantor, Chile, about 40 km east of the village of San Pedro de Atacama. Measurements since 1995 have demonstrated this is a premier site for observations at millimeter and submillimeter wavelengths, with exceptional atmospheric conditions, i. e., transparency and stability. The entire area has been declared a "scientific preserve" by decree of the Chilean government. The 225 GHz and 350 μm atmospheric transparency is better more often at Chajnantor than at Mauna Kea. The first quartile zenith transparencies at Chajnantor and the South Pole are roughly equal.

The ALMA will consist of sixty four antennas, each 12 m diameter. These antennas are transportable so the array can be reconfigured to provide a variety of observational capabilities. Instead of discrete configurations, the ALMA will use a flexible reconfiguration scheme. By moving a few antennas, the array size can be increased or decreased slightly in a self-similar manner. In operation, the array will be reconfigured continuously, cycling from the smallest to the largest configuration and back with a schedule adjusted to meet scientific demand. The ALMA configurations have a total of 250 antenna stations and span a 100:1 dynamic range from 150 m to 14 km diameter. Design goals depend on the configuration size. The smallest configuration is designed for maximum surface brightness sensitivity, the intermediate configurations, about 250 m to 3 km diameter, are designed for high quality imaging with Gaussian synthesized beam shapes that minimize sidelobes and reconstruction errors, and the largest configuration is designed for maximum resolution.

The NRAO is a facility of the National Science Foundation operated under cooperative agreement by Associated Universities, Inc.

ALMA 12 METER PROTOTYPE ANTENNAS

Jeffrey S. Kingsley*
National Radio Astronomy Observatory
Dr. Torben Andersen
European Southern Observatory / Lund
Dr. Ukita Nobuharu
Nobeyama Radio Observatory

The Atacama Large Millimeter Array (ALMA) project has procured three high performance prototype antennas for evaluation. These revolutionary telescopes will operate at millimeter and submillimeter wavelengths to comprise an array of individual antennas each 12 meters in diameter that work together to make precision images of astronomical objects. The goal of the ALMA Project is an array of 64 antennas that can be positioned as needed over an area 10 kilometers in diameter so as to give the array a zoom-lens capability.

Specifications for these antennas are very demanding, that include subarcsecond pointing with high surface accuracy and stringent path length stability. A unique specification of the antennas is the fast switch capabilities that can change antenna position by 1.5 degrees in one second with an accuracy of 3 arcseconds rms. A fast-switching capability is imposed by the need to rapidly and repeatedly calibrate the phase of the array. The antennas make extensive use of carbon fiber reinforced plastic (CFRP) technology in order to maintain a stable parabolic surface in the harsh thermal and wind environment characteristics of the ALMA site at 5,000 meters elevation in the Andes mountains of northern Chile. Advance metrology systems are also incorporated in to the designs in order to meet the pointing requirements. These unenclosed antennas must be transportable for reconfiguration with the ability to perform full solar observations.

The prototype type antennas will be delivered to the NRAO VLA site in New Mexico for testing and evaluation in 2002 and 2003. A selection will be made in 2004 for production of the antennas that will be manufactured and sent to the ALMA site in Chile to compose the array. The design and construction of these antennas have been optimized for quantity production and to operate at the high altitude site. The current status of the 12-meter prototype antennas and designs will be reviewed.

ALMA RECEIVER DEVELOPMENT

J. M. Payne*
National Radio Astronomy Observatory

The proposed receivers for ALMA are a significant advancement on any receivers produced so far for radio astronomical millimeter and submillimeter wave spectroscopy. To realize the very best noise performance superconducting devices must be used which require cooling to 4 degrees Kelvin. Also, to achieve the optimum performance single mode waveguide with corrugated horns must be used which leads to sub division of the required frequency coverage into 10 separate bands. These bands cover all of the atmospherically-accessible windows from 30 to 900 GHz as follows: Band 1, 31.3-45 GHz; Band 2, 67-90 GHz; Band 3, 89-116 GHz; Band 4, 125-163 GHz; Band 5, 163-211 GHz; Band 6, 211-275 GHz; Band 7, 275-370 GHz; Band 8, 385-500 GHz; Band 9, 602-720 GHz; Band 10, 787-950 GHz. Each band will allow for simultaneous reception of two orthogonal polarizations, will perform at a receiver noise temperature of between 6 and 10 times the quantum limit of h*nu/k over 80 percent of the band, and will have an IF bandwidth of 8 GHz per polarization. The design will also allow for the inclusion of a water vapour radiometer using the 183 GHz line for phase correction.

The receiver concept used is that of cartridges, with each cartridge containing a dual polarization receiver covering a specific band of frequencies. This concept lends itself well to the collaborative nature of the project in which one member of the collaboration may be responsible for a certain frequency band. The complete receiver will consist of 10 cartridges mounted in a single Dewar with a single closed cycle refrigerator cooling all the cartridges. The progress on the design of the receivers will be described and mention will be made of the proposed calibration system and possibilities for the LO system.

DESIGN AND STATUS OF THE ALMA BASELINE CORRELATOR

Webber*, J.C., Escoffier, R.P., Broadwell, C.M, Greenberg, J.H.
National Radio Astronomy Observatory
2015 Ivy Road, Suite 219
Charlottesville, VA 22903

The design and status of the baseline correlator being designed by the NRAO for the ALMA radio astronomy observatory are presented here. This correlator will process the output of the 64 antennas that are to comprise the main array of the ALMA observatory with a bandwidth of 16 GHz per antenna.

The NRAO, in cooperation with other North American, European, and Japanese scientific agencies, is at present developing the ALMA radio astronomy array. The array is to consist of 64 twelve-meter diameter antennas. The finished instrument is to be used for observing astronomical sources at millimeter and submillimeter wavelengths and will be located at a 5000 meter altitude site in the Atacama desert of Chile.

A lag (XF) architecture has been selected for the ALMA correlator working at a system clock rate of 125 MHz. Antenna-based electronics in the correlator include 4-Gsample/sec 3-bit digitizers, digital FIR filters for bandwidth selection working at an equivalent 4 GHz clock rate, delay lines, and signal conditioning logic to packetize the output of the high speed digitizers in order to drive lower speed correlator circuits.

A custom application specific integrated circuit (ASIC) has been designed for use in measuring the cross- and auto-correlation coefficients in the array. Each correlator ASIC has 4096 lags including 20 bits of integration and 16 bits of results secondary storage. Prototype units of this ASIC are at present being made at a silicon foundry.

Prototype logic cards for the correlator have been made and evaluated successfully during the last year. These logic cards include the FIR filter card, the data packetizer card, and a long term accumulator card. A correlator card that holds 64 of the correlator ASICs has been designed and is at present in prototype fabrication. All cards tested so far have demonstrated acceptable functional and speed characteristics.

*The National Radio Astronomy Observatory is operated by Associated Universities, Inc. under cooperative agreement with the National Science Foundation.

Session J2, 13:55-Thurs.

NEXT GENERATION VLBI DATA TRANSMISSION SYSTEMS

Chairperson: J. Romney

THE S3 WIDE BANDWIDTH VLBI DATA RECORD-PLAYBACK SYSTEM AND CONSIDERATION FOR THE FUTURE OF WIDE BANDWIDTH VLBI DATA RECORD-PLAYBACK SYSTEMS

Dr. Wayne Cannon
Department of Physics Astronomy
York University
4700 Keele Street
NorthYork, Ontario M3J 1P3
P. Newby, G. Feil, A. Novikov, B. Feir
Centre for Research in Earth and Space Technology (CRESTech)
Space Geodynamics Laboratory
4850 Keele Street, 1st Floor
North York, Ontario M3J 3K1

Future scientific applications of VLBI are being planned for the coming decade that will require sensitivities significantly higher than the VLBI systems of the present day for which rountine use is usually carried out at data rates in the range of 128 Mbit/sec to 256 Mbit/sec. Such applications include space VLBI missions such as VSOP-II in which planning is under way to carry out high dynamic range VLBI observations on baseline lengths ranging up to approximately 40,000 km and for which data rates in the range of 1024 Mbit/sec to 2048 Mbit/sec are being contemplated. The "S3" VLBI data record-playback system under development at the Space Geodynamics Laboratory, based on an array of digital video tape transports, will provide user data rates of 1024 Mbit/sec to 2048 Mbit/sec. Depending on configuration, unattended operation for as long as 130 hours at 1024 Mbit/sec or 65 hours at 2048 Mbit/sec is achievable in the S3 system using robotic tape changers. This will permit unattended operation at rates as high as 2048 Mbit/sec from 5:00 PM on a Friday until 8:00 AM on a Monday.

For time horizons as long as two decades and beyond it is envisaged that future space VLBI missions may require VLBI data rates in the range 4096 Mbit/sec to 8192 Mbit/sec. Such wide bandwidth data recording systems may possibly be constructed from arrays of advanced design magnetic video tape recorders designed to serve the needs of the high definition TV market or possibly constructed from arrays of advanced design magnetic disc drives. This paper attempts to provide a comparison, from a VLBI perspective, of the strengths and weaknesses of these two possible future technical options.

MARK 5 DISC-BASED VLBI DATA SYSTEM

A. R. Whitney
MIT Haystack Observatory
Westford, MA 01886

The Mark 5 system is being developed as the first high-data-rate VLBI data system based on magnetic-disc technology. Incorporating primarily low-cost PC-based components, the Mark 5 system will support data rates up to 1024 Mbps recording to an array of up to 16 inexpensive removable IDE discs. An initial demonstration system has been used to record data at 576 Mbps, with correlation on a Mark 4 correlator at Haystack Observatory.

With the continuing fall in disc prices, IDE discs are already becoming competitive with the cost of Mark 4/VLBA tape, with the expectation that prices will continue to fall to a level below 1/GB with capacities expanding to hundreds of GB per disc.

Besides recording and playing from disc, the Mark 5 system will be fully e-VLBI compatible, utilizing standard Gigabit Ethernet connections. For real-time e-VLBI usage, data may be either directly transmitted or received; for quasi-real-time usage, e-VLBI data may be buffered through the disc array. A demonstration e-VLBI experiment, supported by DARPA, using the Mark 5 system is planned between Haystack Observatory and NASA/GSFC in 3Q 2002.

A development effort is now underway at Haystack Observatory, with support from BKG, EVN, KVN, MPI, NASA, NRAO and USNO to fully develop the Mark 5 system. The development plan is highly attentive to compatibility requirements with existing Mark 4 and VLBA data-acquisition and correlator systems, with prototype deployment of 12 systems expected in spring 2002. A fully VSI-compliant Mark 5 system is expected to be available in late 2003, along with the necessary adapter interfaces required to utilize the VSI Mark 5 system with existing Mark 4 and VLBA data-acquisition and correlator systems.

EVN APPROACHES TO NEXT GENERATION VLBI DATA TRANSMISSION SYSTEMS

*S.M. Parsley, S.V. Pogrebenko
JIVE, Postbus 2, 7990 AA Dwingeloo, Netherlands.

The European VLBI Network (EVN) is a consortium of 10 radio astronomical institutes. It combines radio telescopes in Europe and beyond into a coherent instrument with the highest angular resolution possible today. The current EVN operation uses magnetic tape to transport data from the telescopes to the central data processor at JIVE, in the Netherlands.

The overall system, including the JIVE correlator, was designed to operate at a data rate of 1 Gbps per station. Limitations of the tape technology however have restricted this to 256 Mbps for regular operation and impose a practical upper limit of 512 Mbps. Even this has been achieved only by the use of highly customized, laboratory grade recorders. Based on recent developments of worldwide optical fiber networks and high performance hard disks two possible options are considered to push the operational data rate of the EVN to 1 Gbps and beyond:

1. Use of worldwide optical fiber network infrastructure for real time or near real time operation.

2. Use of Terabyte scale hard disk arrays for traditional record transport playback operation.

Both options have many features in common since they are based on commodity equipment and services. Currently several pilot projects are under consideration in the EVN in order to exploit these possibilities:

1. e-EVN pilot project aimed to connect 4 EVN station to the JIVE correlator using pan-European optical fiber networks for 1 Gbps real time operation.

2. Smaller scale project to connect only two stations, Westerbork and Jodrell Bank, with limited (256 Mbps) data rate.

3. Transatlantic VLBI data transfer in cooperation with our US colleagues.

4. PC/disk based recording/play back units for traditional VLBI data pipeline operation.

Within the scope of these pilot projects PC/disk units are considered to be common elements of both applications because such platforms can allow us to have sufficient data throughput and buffering capacity to satisfy operational demands of both networked and transportable media approaches.

RECENT VLBI ACTIVITIES AT CRL

T. Kondo, Y. Koyama, J. Nakajima, M. Sekido, R. Ichikawa, E. Kawai, H. Okubo, H. Osaki, M. Kimura
Kashima Space Research Center
Communications Research Laboratory
893-1 Hirai, Kashima
Ibaraki 314-0012, JAPAN
T. Yoshino, J. Amagai, H. Kiuchi, F. Takahashi
Communications Research Laboratory
4-2-1 Nukuikita, Koganei
Tokyo 184-8795, JAPAN

Communications Research Laboratory (CRL) CRL has participated in IVS (International VLBI Service for Geodesy and Astrometry) as one of Technology Development Centers. We have published the CRL TDC newsletter biannually to inform the VLBI community of our current activities. The newsletter is also available through the homepage (*http://www.crl.go.jp/ka/radioastro/tdc/index.html*). Current hot topics are "Gigabit VLBI System", "Internet VLBI", and "VLBI Standard Interface".

The developments of the gigabit VLBI system has been finished. Geodetic VLBI experiments have been performed using this system. Data quality and the estimation errors comparable to the K-4 VLBI system have been attained. Some survey observations of weak radio sources have been also carried out. We have also successfully achieved real-time VLBI at data rate of 1 gigabit per second using this system and high-speed communications network in collaboration with NAOJ, ISAS and Nippon Telegraph and Telephone Corp. (NTT). The experiment was conducted on June 23, 2001, using the Kashima 34m antenna and Usuda 64m antenna.

A new real-time VLBI system using IP (Internet protocol) technology has been developed since 1999 to reduce network-cost and to expand connection sites of network. We call this system "IP-VLBI" or "Internet VLBI". We have been developing the PC-base IP-VLBI system consisting of a PCI-bus sampler board and PC software to make real-time data transmission, reception and correlation.

We have been contributing to establish the VLBI standard interface (VSI) with a technology coordinator of IVS. Specifications of VSI hardware (VSI-H) Ver1.0 was opened to public in August, 2000. It is available through the VSI homepage (*http://dopey.haystack.edu/vsi/*) or Japanese VSI homepage (*http://www2.crl.go.jp/ka/radioastro/tdc/ivs/vsi/*). We have been adapting VSI-H to gigabit VLBI system, S2-K4 copying system, and VSI-based K4 data acquisition system.

OPTICAL FIBRE LINKS IN E-MERLIN

R.E. Spencer*, B. Anderson, R. McCool
University of Manchester
Jodrell Bank Observatory
Macclesfield, Cheshire, UK

The only feasible way of achieving major increases in sensitivity for existing radio astronomy synthesis arrays is by increasing bandwidth. Receivers are approaching their quantum limit, and in any case the atmosphere limits their performance. Increasing the collecting area is expensive. The extremely wide bandwidths or data rates available for optical fibre signal transmission suggests that fibre links could be useful, and indeed their particularly low loss of makes fibre the technology of choice.

Studies at Jodrell Bank of both analogue and digital transmission of GHz bandwidth radio astronomy signals on optical fibres have shown that digital data transmision gives superior performance for links exceeding a few km in length. The proposed upgrade to MERLIN (to produce e-MERLIN) will replace the existing narrow band (28 MHz) analogue microwave links with optical fibres carrying digital data at 30 Gbits/sec.

The radio astronomy IF signals will consist of 2 x 1.5 GHz channels (for 2 polarisations), sampled at the Nyquist rate and 4 bit digitised. An 8–10 bit conversion takes place before external modulation of the laser optical signal. 3 lasers will be used per telescope, each externally modulated at 10 Gbits/sec. The optical signals will be multiplexed onto a single fibre (using wavelength division multiplexing). The total length of fibre in the array will exceed 400 km, with the longest link being over 100 km. Erbium doped fibre amplifiers will be required to give adequate signal to noise and low error rates. The full system and design goals will be described in the paper.

In addition the fibre link may be required for cohering local oscillator signals, our development work in this area and estimated phase stability performance will also be discussed.

THE FUTURE OF VLBI DATA TRANSMISSION AT THE NRAO

R.C. Walker
National Radio Astronomy Observatory
Socorro, NM 87801, USA

The National Radio Astronomy Observatory (NRAO) operates the Very Long Baseline Array (VLBA), which is a full time VLBI instrument that includes 10 antennas and a 20 station correlator. It also operates the Green Bank Telescope (GBT) and Very Large Array (VLA), both of which participate in VLBI. Among these various instruments, the NRAO has approximately 50 VLBI record or playback units. The current systems are expensive to operate and are old technology that will not be maintainable much longer. They also limit the bandwidth, and hence the sensitivity of VLBI observations. For these reasons, the NRAO is considering alternatives for future VLBI data transmission systems. In the near term, this is likely to be a new recording system such as the Mark V being developed at Haystack Observatory. But real-time data transmission over fiber optics would have great operational advantages and is being explored.

In the longer term, the future data transmission system at NRAO will be influenced by the possibility of integrating the VLBA with the Expanded VLA (EVLA). That upgrade is designed to expand the capabilities of the VLA by a factor of 10 in many dimensions. Two major components of the project are a new correlator and approximately 8 new antennas. The correlator, which is being contributed by Canada, is capable of processing VLBI data. The new antennas, referred to as the New Mexico Array (NMA), extend the resolution of the VLA by a factor of 10 and fill the gap in UV spacing between the VLA and the VLBA. An integrated VLA/NMA/VLBA would cover all baselines from 25 m to 8600 km, allowing the choice of resolution to be based entirely on the scientific needs of a project. The NMA will have the same 16 GHz bandwidth capability as the rest of the EVLA, requiring a data transmission system with a capacity of 96 or 128 Gbps, depending on the number of bits per sample. Full integration of the VLBA and EVLA would require similar connections to the VLBA antennas, although some lesser bandwidth options would also be interesting. The details of how such connections will be made to the NMA, let alone the VLBA, are yet to be determined. Any feedback, especially from the communications industry, on how to obtain such bandwidths in an affordable manner would be appreciated.

Session J3, 8:35-Fri.

NEW VLBI TECHNIQUES AND SCIENCE RESULTS

Chairperson: M. Reid

SPACE VLBI WITH VSOP

P.G. Edwards*
ISAS, Sagamihara, Kanagawa, Japan

Very Long Baseline Interferometry (VLBI) is a powerful technique for high angular resolution radio imaging. The feasibility of improving resolution by having a radio-telescope in orbit — 'space VLBI' — was demonstrated in the 1980s, paving the way for the development of the HALCA satellite by Japan's Institute of Space and Astronautical Science (ISAS). The satellite is the orbital element of the VLBI Space Observatory Programme (VSOP), a large international collaboration of space agencies and ground observatories which have combined resources to create the first dedicated space VLBI mission.

HALCA was launched from the Kagoshima Space Center in February 1997. HALCA's elliptical orbit has a period of 6.3 hours, with a perigee height above the Earth's surface of 560 km, and an apogee height of 21,400 km, thus enabling imaging VLBI observations on baselines over three times longer than those achievable on Earth. HALCA is supported by a network of five dedicated tracking stations, in Japan, Australia, Europe and the USA. The tracking station being used transmits a 15.3 GHz reference tone to the satellite, and HALCA transmits the science data in real-time at a rate of 128 mega-bits per second to the tracking station at 14.2 GHz.

Radio telescopes from the Very Long Baseline Array, the European VLBI Network, the Asia-Pacific Telescope, and other unaffiliated telescopes are combined to form ground arrays for VSOP observations, depending on the source position and the requirements of the observation. Scientific observations are carried out in the 1.6 GHz and 5.0 GHz observing bands. To the end of August, 2001, over 650 VSOP observations had been made: 73% for projects selected by international peer-review from proposals submitted by the astronomical community, and 22% for a mission-led, systematic survey of active galactic nuclei, with the remainder being for engineering purposes.

Among the key science results from the mission to date have been brightness temperature distributions for active galactic nuclei well in excess of the nominal inverse Compton limit, magnetic field orientations revealed by dual polarization studies, the ability to make high resolution detections of absorption features at low frequencies, the surprisingly low interstellar scattering inferred from VSOP observations of a galactic OH maser, high linear resolution studies of the nearby galaxy M87, and a considerably improved means of studying the spectral index distributions of sources. In this presentation, the HALCA satellite and VSOP mission will be described, results from VSOP observations presented, and plans for the future briefly outlined.

VLBI OBSERVATIONS OF LINE AND CONTINUUM ABSORPTION

Peck, A. B.*
Harvard CfA & MPIfR, Bonn
60 Garden St., MS 78
Cambridge, MA 02138, USA

One of the most important problems in the study of active galactic nuclei is understanding the detailed geometry, physics, and evolution of the central engines and their environments. The leading models describing the central few parsecs of these sources involve an accretion disk and circumnuclear torus of gas and dust around a central black hole. The orientation of this structure relative to our vantage point determines whether or not the central engine is obscured. Much of the circumnuclear torus is thought be comprised of neutral atomic gas, and the fraction of ionized gas is expected to be around 10%. This means that such a structure should be detectable by imaging HI absorption with very high angular resolution toward bright inner radio jets and also using multi-frequency observations which allow us to image free-free absorption toward the central engine.

The milliarcsecond scale angular resolution, fine spectral resolution and high sensitivity of the current VLBI networks make these techniques ideal for searching for circumnuclear tori in a variety of radio sources, ranging in size and radio power from Seyferts to the very young Compact Symmetric Objects, to older, larger Fanaroff-Riley type 2 galaxies.

I present a summary of some of the recent evidence for circumnuclear tori in galaxies which exhibit radio axes close to the plane of the sky, resulting in a segment of a disk or torus crossing our line of sight to the core and inner radio jets. Understanding the distribution and kinematics of the gas detected toward the central parsecs of these sources provides an important test of the torus model and of unified schemes for active galactic nuclei.

AN OCTAVE HIGHER: VLBI POLARIMETRY AT 86 GHZ

Attridge, J.M., MIT Haystack Observatory, Westford, MA

VLBI revolutionized radio astronomy by uncovering previously concealed features in a variety of radio sources. For example, early theoretical models describing the structure and evolution of jets from the cores of AGNs were transformed by VLBI as evidence mounted for jet asymmetries, beaming, superluminal motion, and bulk relativistic motion. VLBI polarization (VLBP) observations add another critical observable by providing information about the structure and evolution of the magnetic fields in synchrotron and masing sources. Magnetized plasma between observer and source alters the polarized emission, and therefore VLBP also affords a means to study the physical conditions of the media in or around radio sources.

Linear polarization in continuum sources is diminished due to cancellation within tangled magnetic fields and the effects of Faraday rotation. VLBP observations at 86 GHz, possible with the CMVA and now the VLBA, should be less affected by Faraday rotation and opacity, for these effects are reduced at high frequencies. In addition, 86 GHz VLBP probes structures with higher angular resolution than previously attainable.

The challenges of 86 GHz VLBI are numerous. Coherence times at 86 GHz are only $\sim$ 10 seconds, limiting solution intervals in many tasks, yet 86 GHz data are lower in SNR than 43 GHz data. Wind loading significantly affects the pointing accuracy of many 86 GHz antennas. Some 86 GHz dishes are equipped with non-standard feed systems that compound the difficulties associated with standard polarization calibration approaches.

Typically, strong AGNs are used for polarization calibration of both other AGNs and masers. Currently, there is no known calibrator by which to register absolute electric vector position angles (EVPAs) at 86 GHz. Linear polarization in masers around AGB stars can approach 100% in some isolated features, and is often aligned tangentially to the maser ring (e.g. A. J. Kemball & P. J. Diamond, *ApJL*, **481**, L111-L114). It is possible that polarized masers may provide EVPA calibration for 86 GHz, either alone or in combination with observations of AGNs.

Observations of 3C 273 and 3C 279 taken in April 2000 with the CMVA have resulted in the first reported VLBP images at 86 GHz (J. M. Attridge, *ApJL*, **553**, L31-L34, 2001). The images reveal the EVPAs of 3C 273 and 3C 279 to be orthogonal to each other. The cores of both 3C 273 and 3C 279 continue to display low levels of fractional polarization at 86 GHz, challenging the expectation that Faraday depolarization decreases at high frequencies. In fact, the core of 3C 273 is unpolarized to a limit of 1%; if this is attributed to Faraday depolarization alone, the dispersion of rotation measure in the core of 3C 273 is >90000 rad m^{-2}.

CIRCULAR POLARIZATION OF SAGITTARIUS A* AND OTHER ACTIVE GALACTIC NUCLEI

G.C. Bower
Radio Astronomy Laboratory
UC Berkeley

In the last few years there has been renewed interest in the circular polarization (CP) at radio wavelengths of active galactic nuclei (AGN), ranging from extremely low luminosity AGN, such as Sagittarius A* (Sgr A*), to extremely powerful AGN at cosmological distances, such as 3C 279. New observations of CP variability and spectra have been used to infer the presence of electron-positron jets, low energy electrons, stable magnetic fields, and extremely compact regions. In a handful of sources, CP dominates linear polarization (LP). The similarities and differences between the CP properties of AGN classes may provide important clues to the nature of jets.

The discovery of CP in Sgr A* has added a significant new constraint for theory. The CP is apparently composed of a high and low frequency components. The low frequency component is only mildly variable with a fixed mean of -0.3% over the past 20 years. The high frequency component, observed from 8.4 to 43 GHz, is strongly variable on timescales of days, going from $< 0.1\%$ to $\sim -1\%$. Similar CP properties have also been observed in the low luminosity AGN, M81. Both M81 and Sgr A* exhibit no LP over the observed ranges.

Three new surveys for AGN have been performed recently: two of high luminosity AGN and one of low luminosity AGN. These are the first of their kind in nearly two decades. Detection rates for high and low luminosity AGN are $\sim 50\%$ and $\sim 10\%$, respectively, suggesting that different emission and/or wave propagation physics is at work. Very long baseline interferometric (VLBI) imaging of the high luminosity AGN finds nearly all of the CP to be located in the core. There is no correlation between LP and CP among high luminosity AGN. A particularly interesting source among the high luminosity AGN is PKS 1519-273, which shows strongly variable CP at levels as high as $\sim -4\%$.

These discoveries have been the result of the application of careful observational technique in connected element interferometry and VLBI. For interferometers with circularly polarized feeds, CP is the small difference between the parallel hand intensities. It is very sensitive to calibration uncertainties. We describe observing techniques and a model for VLA measurements of CP that includes the effects of beam squint, gain errors, polarization leakage and receiver nonlinearities. It fits remarkably well with observed errors.

VLBI OBSERVATIONS OF THE POLARIZATION OF H2O MASERS

T. H. Troland
Department of Physics and Astronomy
University of Kentucky
Lexington, KY 40506 USA
A. P. Sarma
Department of Astronomy
University of Illinois
Urbana, IL 61801 USA

It has long been recognized that magnetic fields are likely to play a key role in the dynamics of star formation. However, measurements of field strengths in star-forming regions, via the radio-frequency Zeeman effect, are difficult. Most existing measurements suffer from two important limitations. They sample relatively low density gas (less than 10^5 cm^{-3}), and they suffer from poor spatial resolution. Therefore, they do not reveal magnetic field strengths in the densest regions and on the smallest scales that are most intimately associated with the star-formation process.

The 22 GHz H_2O maser transitions, originating from star-forming regions, offer an opportunity to study magnetic fields at high density and on small spatial scales. Circular polarization in the maser radiation can be related to line-of-sight field strengths via the Zeeman effect. The masers are believed to operate at high density (10^9 cm^{-3}). The individual maser spots are small (of order 1 au or 10^{13}cm), and they occur in groups. Therefore, very high spatial resolution observations with the Very Long Baseline Array (VLBA) can reveal field strengths in multiple maser spots, effectively mapping out the magnetic field over regions of a few 10's of au.

We present results for an initial set of VLBA observations of H_2O maser spots in the massive star-forming region W3 IRS5. We observed circular polarization from four maser spots in a 100 by 100 mas (230 by 230 au) field. We estimate line-of sight field strengths for these spots in the range -14 to -42 mG. The relative coherence of the field over this size scale is expected if the masers arise in an outflow region where the field is entrained in moving gas. Moreover, field strengths of this order are expected if the field-strength-gas density scaling relationship, found at lower densities, is applied to the locales of the H_2O masers.

FULL-POLARIZATION VLBI OBSERVATIONS OF HYDROXYL MASERS

V.L. Fish, M.J. Reid, A.L. Argon
Harvard-Smithsonian Center for Astrophysics
60 Garden St.
Cambridge, MA 02138, USA

Hydroxyl masers are useful tracers of conditions surrounding the ultra-compact HII (UCHII) regions associated with high-mass stars in their infancy. Their high brightness allow them to be seen at the high resolution offered by VLBI techniques. Since maser spots typically move at a projected rate of a few milliarcseconds per year, multiepoch proper motion studies can be completed in a few years. E. E. Bloemhof, M. J. Reid, and J. M. Moran (*ApJ*, **397**, 500-519, 1992) showed that OH masers are seen in expansion from the UCHII.

Hydroxyl masers often exist in right- and left-circular polarized pairs at offset velocities, suggesting Zeeman splitting. Since the splitting coefficients are large in the ground-state $^2\Pi_{3/2}, J = \frac{3}{2}$ transitions, local magnetic fields as weak as a few $\times 100\mu$G can be identified. Additionally, the sense of the velocity splitting between Zeeman components gives the line-of-sight direction of the local magnetic field. This gives constraints on the magnetic field morphology surrounding the UCHII. While the exact role that magnetic fields play in high-mass star formation is unknown, it is clear that they are important. The magnetic pressure inferred from OH Zeeman measurements is comparable to the gravitational pressure (and much larger than the thermal pressure in the region).

The full, three-dimensional orientation of the magnetic field could in principle be determined if the π components were detected as well. Unlike the abundant circularly-polarized σ components, a π component would be highly linearly polarized with almost no circular polarization. However, no such component has been observed. If Faraday rotation is responsible for destroying coherent amplification of π components, this may provide a constraint on the local electron density.

We are in the process of observing about 20 UCHIIs with VLBI in order to map the magnetic field structure around them and to search for π components. Preliminary results from this survey will be presented.

VLBI OBSERVATIONS OF OH (1720 MHZ) MASERS

Brogan, C.L.*, Claussen, M., Goss, W.M.
National Radio Astronomy Observatory
Socorro

Supernovae have a profound effect on the morphology, kinematics, and metallicity of galaxies. The impact of supernova shocks on surrounding molecular clouds is also thought to trigger new generations of star formation. A critical ingredient in such interactions and, indeed, all aspects of supernova remnant (SNR) evolution are magnetic fields. OH (1720 MHz) masers have been found in $\sim$ 20 SNRs, or 10% of the known SNRs in our Galaxy. In recent years, these masers have been recognized as signposts for the interaction of SNRs with molecular gas. In addition to tracing SNR/molecular cloud interactions, the OH (1720 MHz) maser line also provides a unique opportunity to measure the strength of the post-shock magnetic field via Zeeman splitting. Indeed, the Zeeman effect in these masers provide the only currently known means to directly measure the magnetic field strengths in SNRs. A limited number of previous high resolution observations have indicated that these masers are unusually large compared to H II region masers, with sizes ranging from 50 to 180 mas. It is currently unclear whether the large sizes observed previously are intrinsic to SNR–OH masers or if interstellar scattering is responsible. In addition, there are some indications that the observed magnetic field values vary with resolution. Recent results from efforts to both detect the magnetic fields over many spatial scales and resolve the maser spot sizes of OH (1720 MHz) masers toward several SNRs using the VLBA and MERLIN will be presented. These observations have yielded magnetic field detections between 0.5 and 2.5 mG and large maser spot sizes of about 10^{15} cm. Some of the implications from these data including the resulting magnetic pressures, and brightness temperatures will also be discussed.

HIGH PRECISION PULSAR ASTROMETRY WITH THE NRAO VLBA

W. F. Brisken
NRAO
PO Box O
Socorrom NM 87801, USA

The NRAO Very Long Baseline Array was used to measure the proper motions and parallaxes of eight nearby pulsars to sub-milliarcsecond accuracy. Different gradients in the ionosphere strength above each station that change on timescales of about one minute required the development and use of a new technique to measure the ionospheric electron content and remove its effects from the interferometer data.

Dual frequency astrometry has been common practice to geodecists for quite some time, mainly using receivers at about 2.5 and 8 GHz. Delay measurements made at the two frequencies could be used to measure the excess delay caused by the ionosphere. This technique has been used primarily for geodesy (determining VLBI station positions and monitoring the tectonic motions of the earth) and for establishing the international celestial reference frame. Most of the sources used in such observations are bright quasars.

This dual frequency approach will not work for pulsars because of their very low brightness at 8 GHz. The 1.5 GHz band is usually chosen for pulsar astrometry since it is usually a good compromise between the falling flux density and increasing resolution with increased frequency. The VLBA allows observations in the 1.4 to 1.7 GHz range with 8 independently tunable 16 MHz bands. Phase measurements made at each of the bands allow the measurement of the ionosphere strength. This method is restricted to pulsars that are bright enough for an ionosphere solution to be obtained within about 30 seconds. The signal-to-noise of these measurements was increased by utilizing pulsar gating.

PROPER MOTIONS IN THE LOCAL GROUP

Brunthaler, A., Falcke, H. Henkel, C
Max-Planck-Institut fuer Radioastronomie
Auf dem Huegel 69
53121 Bonn
Germany
Reid, M., Greenhill, L.
Harvard Smithsonian Center for Astrophysics, MS42
60, Garden Street
Cambridge, MA 02138

Key and still largely missing parameters for measuring the mass content and distribution of the Local Group are the proper motion vectors of its member galaxies. The problem when trying to derive the gravitational potential of the Local Group is that usually only radial velocities are known, and hence statistical approaches have to be used. The expected proper motions for galaxies within the Local Group, ranging from 20 to 100 μas/yr, are detectable with VLBI using the phase-referencing technique. We present first epoch phase-referencing observations of bright masers in IC10 and M33 with respect to background quasars.

In our first group of observations, we observed the H2O masers in IC10 three times over a period of two month to check the accuracy of the relative positions. The relative positions were obtained by modeling the interferometer phase data for the maser sources referenced to the background quasars. The two quasars are separated by 1 and 0.25 degrees on the sky from the IC10 masers. The model allowed for a relative position shift for each source and a single vertical atmospheric delay error in the correlator model for each antenna. The rms of the relative positions for the three observations is only 0.01 mas which is approximately the expected position error due to thermal noise.

Further observations will allow us to detect extragalactic proper motions out to a distance of 800 kpc within $\sim$ 1 year. These observations will constrain dynamical models for the Local Group and the mass and dark matter halo of Andromeda and the Milky Way.

Also, we present a method to measure the distance to M33, ultimately to better than about 5% accuracy. This will allow re-calibration of the extragalactic distance scale based on Cepheids. The method is to measure the relative proper motions of two H_2O maser sources on opposite sides of M33. The measured angular rotation rate, coupled with other measurements of the inclination and rotation speed of the galaxy, yields a direct distance measurement.

Session J4, 13:35-Fri.

HARDWARE AND SOFTWARE COMPLEXITIES OF LARGE-N ARRAYS AND PROPOSED SOLUTIONS

Chairperson: J. Tarter and B. Carlson

OPTIMIZATION OF AN ARRAY CONFIGURATION WITH LARGE NUMBER OF ANTENNAS MINIMIZING SIDE LOBES.

L.R. Kogan
National Radio Astronomy Observatory
Socorro, NM 87801, USA

The result of optimization of the array configuration for the number of antennas 200, 500 has been given. Different metrics of the of the configuration quality are compared. The arguments in favor of the minimum side lobe metric are provided. The minimization of the worst side lobe at the given circle at the sky is chosen as a criterion of the optimization. The optimization is based on the algorithm published by L.Kogan at *IEEE Transaction on AP* **48**, No 7, 1075-1078, 2000. The algorithm is coded at AIPS as task CONFI. The task CONFI as well as the simulation task UVCON have been modified increasing the number of antennas up to 1000.
The less area of optimization the deeper can side lobes be suppressed. By the nature the side lobes can be separated at the two classes: near side lobes and grating side lobes. Grating side lobes can be very large reaching at the extreme case of even UV distribution 100%. The near side lobes spread from the main synthesize lobe to $\sim \sqrt{N}$ of $\frac{\lambda}{D}$, where N is number of antennas at the array; D is its size. The two sets of configurations for the number of antennas 200 and 500 have been designed optimizing the near and grating side lobes. The found configurations give the worst near side lobes ~ 0.0008, and ~ 0.0003 for the number of antennas 200 and 500 at the diameter of the circle at the sky equaled 20 synthesized beam. The relevant side lobes at the diameter of the circle at the sky equaled 100 synthesized beam (including grating side lobes) are 0.014 and 0.010 for the number of antennas 200 and 500. An example of simulation is given using M51 as a model at $\lambda = 21cm$ and size of the array 400km with 200 antennas at the array. The dynamic range $\sim 10^4$ has been achieved.

ON USING ADAPTIVE ESTIMATION TO MINIMIZE THE NUMBER OF SAMPLES NEEDED TODEVELOP A PATTERN TO A SPECIFIED UNCERTAINTY

E.K. Miller
3225 Calle Celestial
Santa Fe, NM 87506-1213

Computing far-field patterns in electromagnetics, although generally not as computationally expensive as solving for the current induced on an object, can none-the-less at times dominate the overall computer time associated with some problems and models. This can especially be the case in determining the monostatic radar cross section of large objects, since the current distribution must be obtained for each incidence angle. Similarly, when using physical optics to determine the radaition pattern of a large reflector antenna, the computer time is dominated by evaluation of the far field. In addition, when employing the point sampling and linear interpolation of the far field that is most often used to develop the pattern, it can be necessary to sample very finely in angle to avoid missing fine, but important, details in the pattern such as nulls, increasing the computer cost proportionately.

A procedure based on model-based parameter estimation is described that greatly reduces the number of samples that are needed while developing an easily computed, continuous representation of the pattern. It employs windowed, overlapping fitting models whose parameters are adaptively estimated from sparsely sampled far-field values, the sampled angles being successively selected where the maximum difference occurs in the overlapping models. The fitting models themselves employ either discrete-source approximations to the radiating currents or Fourier models of the far field. The model-based procedure permits the maximum acceptable uncertainty in the estimate of the pattern to be specified, which furthermore can be adjusted, if desired, to accommodate changing levels in the pattern. For the cases investigated, as few as 1.5 to 2 samples per far-field lobe are found to be sufficient to develop an estimate for a radiation pattern that is accurate to 0.1 dB, and 2.5 samples per lobe for a simple scatterer. In general, however, it appears that the required sampling density is determined by the rank of the field over the observation window, which in turn is a function of both the aperture size and the spatial behavior of the source distribution within that aperture.

THE ANTENNA CONFIGURATION OF THE ALLEN TELESCOPE ARRAY

D.C.-J. Bock
Radio Astronomy Laboratory
University of California at Berkeley
Berkeley, CA 94720, USA

The Allen Telescope Array (ATA) is a next-generation large-N telescope which will capitalize on the relative decrease of electronics in the cost of new instruments. It will maximize collecting area within the available budget by using many small antennas instead of fewer larger ones. The cost optimization has led to a choice of 350 6.1-m offset Gregorian antennas.

The ATA will have several characteristics unique to interferometers of comparable collecting area, including a wide field of view, broad instantaneous frequency coverage, and a multi-beaming capability which will enable the instrument to be used for several simultaneous programs. The ATA configuration design needs to keep antenna shadowing and connectivity costs to a reasonable level. The wide variety of geological conditions and foundation costs must be considered in the optimization. Within these constraints, imaging performance drives the configuration design. The basic capabilities of the ATA will make it a premier instrument for large area surveys and imaging extended structure, so the configuration has been optimized to provide excellent imaging fidelity. The synthesized beam has sidelobes which are below 1% within the antenna primary beam. The antennas baselines will be in the range 11 to 700 m, for a high spatial dynamic range and a naturally-weighted synthesized beam of $78''(\nu/1.4\,\mathrm{GHz})^{-1}$. The irregular nature of the final configuration ensures low far sidelobes (0.3% rms), desirable for RFI rejection. Although more compact designs (comparable to the proposed VLA E-array) would enhance sensitivity at the shortest spacings, mosaicing with the ATA's wide field of view will make imaging very extended structure efficient, even while preserving reasonable angular resolution.

In this paper I will present the ATA configuration, describing the site characterization and configuration design process.

THE ATA ELEMENT

D.R. DeBoer*, J.W. Dreher
SETI Institute
2035 Landings Drive
Mountain View, CA 94043
G. Engargiola, M.C. Fleming, J.B. Lugten, W.J. Welch
Radio Astronomy Laboratory
University of California
Berkeley, CA 94720
S. Weinreb
Jet Propulsion Laboratory
4800 Oak Grove Drive
Pasadena, California 91109

As one of the primary components that gets multiplied by N, design of the individual array element is a key factor in any array design. For a predetermined net collecting area, in fact, the collection area of a single element determines the value of N and hence the scale of all subsequent components. The Allen Telescope Array (ATA) element will consist of a small parabolic antenna equipped with a single wide-band feed, cryogenic low-noise amplifiers (LNA), fiber-optic RF links, and commodity electronics. The initial desired net geometric collection area will be one hectare (10^4 m^2), so $N \approx 1.3\times10^4/D^2$, where D is the projected diameter of the parabola.

The antenna is an offset Gregorian with a projected diameter of 6.10 m and a 2.4 m subreflector arranged to satisfy the on-axis cross-polarization nulling constraint. This antenna size dictates using about 350 antennas to yield the desired net area. A dual polarization, log-periodic feed with a bandwidth of about 0.5 ? 11.5 GHz will be used in conjunction with two wide-band, cryogenic LNA?s of the same bandwidth. This entire bandwidth will then be transmitted back to the central lab for further processing via two RF fiber-optic links (one per polarization). The cryogenics will consist of a small dewar that actually fits up inside the feed, as will the pulse-tube refrigerator (PTR) and compressor.

The element controller will be an internet-ready microprocessor and communications will be via TCP/IP. Likely this processor will be a native Java Virtual Machine with sufficient processing capability to handle all pointing and house-keeping tasks. It will communicate via a standard protocol to a daughter board with sufficient I/O to monitor the state of the element.

SIGNAL PROCESSING FOR THE ALLEN TELESCOPE ARRAY

L. R. D'Addario, SETI Institute, Mountain View, CA

The Allen Telescope Array (ATA) will include 350 antennas of 6.1 m diameter and have continuous frequency coverage from 0.5 to 11.2 GHz. This makes it the largest-N radio telescope so far. The need for low-cost processing of its many wide band signals has produced significant technical challenges.

The ATA is a privately-funded project of the SETI Institute in collaboration with the Radio Astronomy Laboratory of UC Berkeley. It will be the first instrument available full time for SETI searches, and it will simultaneously be used for a wide variety of astronomical research. This is possible through the use of multiple independently-tuned signal channels and multiple back-end detectors, along with the fact that the single-dish beam includes several SETI target stars for nearly any direction in the sky.

This paper describes the details of the signal processing required between the antennas and the detectors. For SETI and for some point-source astronomy (e.g., pulsars), the antennas are configured as a phased array, generating up to 16 simultaneous electronically-steered beams within the primary beam. For astronomical imaging, the antennas are configured as a Fourier synthesis array, where a correlator computes the cross-power spectrum for each pair (61,425 baselines). In all cases, common equipment performs the necessary delay and phase tracking and amplitude scaling; this is done in specialized digital hardware. Up to four dual-polarization channels can be processed, each tunable to a different frequency within the RF range, and each having about 100 MHz bandwidth. For each such channel, up to four separate "beams" can be formed, each tracking a different sky position, and each connected to a separate back end. Because of the large number of antennas, it is possible to create beams with nulls in the directions of several interfering sources while maintaining high SNR in the direction of the desired source.

The major design challenges included (a) cost, since the goal is to achieve a construction cost of less than 25 M$US for the entire array (including antennas, monitor/control, and all common electronics, but not including back ends); (b) signal interconnections, since aggregate data rates of up to 7 Tb/s are needed between subsystems; and (c) flexibility, to support a wide range of scientific uses and various interference mitigation methods.

The ATA project is now in its detailed design phase. Prototypes of the antennas and electronics are due to be completed late in 2002, at which time a subset of the array with the first few antennas will be in operation. The full array is currently scheduled to be completed in 2005.

THE ATA IMAGER

W.L. Urry
University of California - Berkeley
Radio Astronomy Dept.
601 Campbell Hall
Berkeley CA 94720-3411

The Allen Telescope Array of 350 6-meter antennas will provide four independently tuned groups of four output ports from each antenna for a total of 16 signal ports. Each output port will have 8-bit quantization and independent tracking of delay and phase. Emerging from each output port will be two polarizations of 100 MHz bandwidth extracted from the .5 - 11.2 GHz RF band of the telescope front end. Four independently tuned groups of three ports will be dedicated to beam forming for a total of 12 beams that can be independently targeted. Each beam may support a different "back-end" so that a SETI search or a pulsar experiment may take place simultaneously. The remaining four independently tuned 100 MHz ports will be dedicated to an imaging "back-end." An imaging "back-end" is described.

The imager will rely on an FX correlator architecture. The dual polarization signal from each antenna will be separated into 1024 frequency channels. All correlations for each channel will be measured. The classic approach of using a fast Fourier transform as a filterbank has always led to severe sidelobe levels or channel overlap depending upon the windowing used at the input to the FFT. A polyphase technique enables the input window to the FFT to be extended well beyond the length of the transform resulting in a filterbank with excellent channel separation and sidelobe characteristics. From the polyphase filterbanks, the signals will proceed to a bank of correlators. Each correlator computes all 61425 baselines for each of the frequency channels. A serious problem exists in getting the signals from the polyphase filterbanks to the correlators. Each channel of the 350 antennas must be multiplied with the corresponding channel in all of the 349 other antennas. Only half of these multiplications are redundant. The innovation of a memoryless corner turner solves this signal distribution problem. The corner turner converts the 350 streams of 1024 frequency channels into 350 streams of antennas of 3 frequency channels each. Each correlator sees a sequential stream of all of the antennas and a simple architecture is described that can easily compute all of the baselines as the data enters one antenna at a time.

HIGH DYNAMIC RANGE RADIO SYNTHESIS IMAGING WITH TIME VARIABLE PRIMARY BEAMS

T.J. Cornwell
NRAO
PO Box 0
Socorro, NM 87801, USA

High dynamic range imaging with radio synthesis arrays is possible using self-calibration algorithms in which the calibration of the array is determined from the observation of the source, rather than from observations of an external calibration source. For the very highest dynamic range, the array setup (bandpasses, nominal pointing, etc) is determined as well as possible, and kept as stable as possible. In such cases, the effect of time variations in the setup are second order rather than first order. However, if the setup is allowed to vary, the variations can have a first order effect, with disastrous consequences for the dynamic range. This is well known for millimeter synthesis arrays, and has led to very precise antenna pointing and surface requirements for the Altacama Large Millimeter Array. It also holds for other radio synthesis arrays, such as the Square Kilometer Array. For SKA, the primary beam is envisaged as being time-variable for two reasons: to allow nulling of bright sources, and by virtue of the use of banks of small elements synthesized into large equivalent antennas. A time variable primary beam due to either of these causes will hinder the acheivement of the very high dynamic range imaging expected of the SKA. The extension of self-calibration to allow determination of the time-variable primary beam is theoretically possible and has been advocated as a solution for this problem. However, as yet, no image-plane self-calibration algorithm has been demonstrated. To settle this point, simulations of such effects are necessary, together with the development of algorithms aimed at such an extended self-calibration.

LARGE-N POSSIBILITIES WITH THE EVLA CORRELATOR

B.R. Carlson*
Dominion Radio Astrophysical Observatory
Herzberg Institute of Astrophysics
National Research Council of Canada
Penticton, B.C., Canada
P.E. Dewdney
Dominion Radio Astrophysical Observatory
Herzberg Institute of Astrophysics
National Research Council of Canada
Penticton, B.C., Canada

A new correlator is being developed for the Expanded Very Large Array (EVLA). This correlator will offer wide bandwidths, flexible digital subbanding, and thousands of spectral channels per baseline. Additionally, the correlator design allows dynamic tradeoffs between bandwidth, number of antennas, and number of beams on the sky that may be attractive for a 1st generation SKA correlator, particularly if the EVLA is used as a test-bed for SKA technologies and if the EVLA evolves into the SKA. For the EVLA, the correlator offers 16 GHz of bandwidth per antenna with 16384 spectral channels per baseline in wide-band modes and up to 256k spectral channels per cross-product at narrower bandwidths. The design allows up to 8, 2 GHz wide-band beams to be placed anywhere on the sky, and within each of those beams, up to 16 sub-band beams within 0.5 deg of the wide-band delay center (depending on basline). Thus, up to 128 beams at 128 MHz bandwidth each can be deployed. If the station bandwidth and maximum number of beams is reduced, then more stations–up to a factor of 4–can be processed without changing the correlator's internal configuration. Using current technology, a factor of 4 increase in the number of stations reduces the bandwidth per station to 1 GHz and the number of spectral channels per baseline to 1024. However, Moore's law improvements can be effectively employed to increase the bandwidth to 4 GHz per station with as many spectral channels per baseline as technology permits with only a "re-spin" of the correlator board. This is an attractive upgrade path that retains the bulk of the hardware and software infrastructure, significantly reducing the cost and development time of an upgrade.

A SIX BILLION CHANNEL MULTIBEAM SPECTROMETER FOR SETI

D. Werthimer*, P. Demorest, J. Cobb, E. Korpela, M. Lebofsky
Space Sciences Laboratory
University of California
Berkeley, CA 94720-7450
M. Davis
Seti Institute
2035 Landings Drive
Mountain View, CA 94043-0818
C. Dick
Xilinx Inc.
2100 Logic Dr.
San Jose, CA 95154
T. Dillon
Dillon Engineering
9825 West 50th St. Suite 202
Edina, MN 55424

We describe our design for a six billion channel multi-beam spectrometer, SERENDIP V. The instrument will be used to conduct a piggyback SETI sky survey in conjunction with the upcoming seven beam receiver at Arecibo.

The system analyzes fourteen 300 MHz bandwidth signals from seven beams and two polarizations simultaneously. Each channel is 0.74 Hz wide, yielding a total instantaneous bandwidth coverage of 4.2 GHz in a 1.5 second integration time. The instrument is modular and can be easily re-configured for different receivers and telescopes. For example, the system can be configured to process a pair of 2.1 GHz bandwidth signals, or it can be configured to process fourteen 300 MHz bandwidth signals (7 beams with two polarizations or 14 beams with one polarization).

The instrument uses a polyphase filter bank to sub-divide each of the 300 MHz bands into 1.56 MHz sub-bands. The polyphase filter bank provides > 80 dB out of band rejection, keeping strong RFI from contaminating adjacent sub-bands. FFT boards further divide the sub-bands into 0.67 Hz channels. Each FFT board computes a 2^{22} point FFT on 64 sub-bands. A bank of post processors calculate power spectra at octave spaced resolutions, combine polarizations, smooth the baseline, and search for signals above the threshold. All signal processing is implemented in Xilinx field programmable gate arrays.

Portions of this design will be directly applicable to the development of technologies and instrumentation required for observatories that are in the planning or development stages such as the Allen Telescope Array and the Square Kilometer Array.

STATUS AND PERFORMANCE OF THE GREEN BANK TELESCOPE

Minter, A.H., Maddalena, R.J., Balser, D.S., Ghigo, F.D., Langston, G.I.
NRAO
PO Box 2
Green Bank, WV 24944 USA

The Robert C. Byrd Green Bank Telescope (GBT) has unique capabilities including an unprecedented design and start-of-the art receivers and backends. The most distinguishing features include an offset geometry which provides a 100-m projected clear aperture, an active surface, a closed-loop metrology system for maintaining surface accuracy and pointing, receivers that will cover 100 MHz to 115 GHz, and a new 256k-channel, 800 MHz bandwidth spectrometer. First light was achieved on August 22 2000 with observations at a frequency of 403 MHz of the extragalactic radio source 1140+223 and the pulsar PSR B1133+16 and commissioning started in February 2001. We have essentially completed the first phase of commissioning, delivering a telescope capable of observations up to 15 GHz. Telescope efficiencies, pointing, focus tracking, spillover, and beam shapes are all close to or match what was expected a priori. For example, measurements at 2 GHz indicate the telescope has a pointing rms of well under 8", the expected aperture efficiency of 70first side lobe level of -30 dB, essentially no detectable spillover, and a system temperature at zenith of 18 K. In an early call for shared-risk observations, 80 observing proposals were submitted and 24 were accepted. Four experiments have been run at the time this abstract was submitted with the majority of the remaining observations scheduled to be completed by the end of 2001. We have had successful bi-static radar observations with Arecibo, fringes from test VLBI experiments, and pulsar searches. In this talk we will give the current status of commissioning, summarize the GBT's performance, and review some of the results from early science.

Index

E

F

G

H

I

J

K

L

M

N

O

P

Q

R

S

T

U

V

W

Y

Z